LUND UNIVERSITY

Validating the existence of the supercraton Vaalbara in the Mesoarchaean to Palaeoproterozoic

Gumsley, Ashley

2017

Document Version:
Publisher's PDF, also known as Version of record

Link to publication

Citation for published version (APA):
Gumsley, A. (2017). *Validating the existence of the supercraton Vaalbara in the Mesoarchaean to Palaeoproterozoic*. [Doctoral Thesis (compilation), Department of Geology]. Lund University, Faculty of Science, Department of Geology, Lithosphere and Biosphere Science.

Total number of authors:
1

LUND UNIVERSITY

PO Box 117
221 00 Lund
+46 46-222 00 00

LITHOLUND THESES 30

Validating the existence of the supercraton Vaalbara in the Mesoarchaean to Palaeoproterozoic

ASHLEY GUMSLEY
LITHOSPHERE AND BIOSPHERE SCIENCE | DEPARTMENT OF GEOLOGY | LUND UNIVERSITY 2017

LITHOLUND THESES 30

Validating the existence of the supercraton Vaalbara in the Mesoarchaean to Palaeoproterozoic

Ashley Gumsley

LUND UNIVERSITY

Lithosphere and Biosphere Science
Department of Geology

DOCTORAL DISSERTATION
by due permission of the Faculty of Science, Lund University, Sweden.
To be defended in Pangea, Department of Geology, Sölvegatan 12, Lund,
on the 22nd of September 2017 at 13:15.

Faculty opponent
Professor Richard Hanson
Texas Christian University

Front cover: Waterfall following a NE-trending mafic dyke on the southeasternmost terrane of the Kaapvaal Craton.

Back cover: The author standing on the shore of the Morskie Oko lake in the Tatra mountains of Poland and Slovakia.

Lithosphere and Biosphere Science
Department of Geology
Faculty of Science

ISBN 978-91-87847-32-5 (print)

ISBN 978-91-87847-33-2 (pdf)

ISSN 1651-6648

Printed in Sweden by Media-Tryck, Lund University, Lund 2017

Organization

LUND UNIVERSITY
Department of Geology
Sölvegatan 12
SE-223 62 Lund
Sweden

Author: Ashley Gumsley

Document name

DOCTORAL DISSERTATION

Date of issue: 22 September 2017

Sponsoring organization: –

Title: Validating the existence of the supercraton Vaalbara in the Mesoarchaean to Palaeoproterozoic

Abstract

In this thesis, the longevity and continuity of the Vaalbara supercraton is addressed in six papers aimed at placing new temporal and spatial constraints on the supercraton in the Mesoarchean to Paleoproterozoic. It has been speculated since the 1960's that the Kaapvaal Craton in southern Africa, together with the Pilbara Craton in Western Australia existed as a single landmass during the Precambrian – the Vaalbara supercraton. Many studies have demonstrated the geological similarities between the cratons, particularly in terms of their Mesoarchean to Paleoproterozoic unconformity-bounded sequences. These unconformity-bounded sequences have continuously been refined and developed, especially since the 1990's. The first main stratigraphic similarities lie in the volcanic and sedimentary successions found in the Neoarchean Fortescue Group and Ventersdorp Supergroup basins on the Pilbara and Kaapvaal cratons, respectively, along with other associated basins. The unconformably overlying Hammersley (and Turee Creek) Group and Transvaal Supergroup on the Pilbara and Kaapvaal cratons, respectively, also show many stratigraphic similarities, and both host world-class deposits of hydrothermally-upgraded iron formations. However, no marker beds or precise age matches have yet been made, especially in the extensive Mesoarchean to Paleoproterozoic mafic dyke swarms and sill provinces present in each craton from the time interval discussed in this thesis. Regardless, the geological discussions has been aided by geochronological and paleomagnetic studies, which have both credited and discredited the existence of the Pilbara and Kaapvaal cratons as nearest neighbours for the time interval between ca. 2.87 Ga and ca. 2.65 Ga.

In this thesis, the so-called magmatic barcode record of large igneous provinces (LIPs), which are extensive and short-lived volcanic events, of the Kaapvaal Craton is presented together with that of the Pilbara Craton in conjunction with previous geochronological and paleomagnetic studies. This magmatic barcode record refines temporal, and through paleomagnetism, spatial constraints, and invalidates the existence of Vaalbara as a distinct continuous supercraton. Magmatic and paleomagnetic linkages between the 2.99-2.98 Ga Usushwana Complex on the Kaapvaal Craton and the ca. 2.87 Ga Millindinna Complex on the Pilbara Craton are shown to be incorrect with new ages for the Usushwana Complex and Badplaas dyke swarm presented in Gumsley et al. (2015). Extensive mafic dyke swarms associated with Neoarchean Fortescue volcanism on the Pilbara Craton and Ventersdorp volcanism on the Kaapvaal Craton also show less similarities from new paleomagnetic and geochronological constraints. These constraints are presented in Gumsley et al. (2016) and Evans et al. (2017) for the newly identified White Mfolozi and Black Range mafic dyke swarms, respectively, on the Kaapvaal and Pilbara cratons. Gumsley et al. (2017) and Kampmann et al. (2015) also present a new LIP, the Ongeluk, on the Kaapvaal Craton which has not been identified on the Pilbara Craton. This new LIP is composed of the Ongeluk Formation in the Transvaal Supergroup on the western margin of the Kaapvaal Craton, as well as the Westerberg Sill Province and a north-trending mafic dyke swarm. The Ongeluk LIP appears to break some of the stratigraphic comparison between the upper Transvaal Supergroup on the Kaapvaal Craton and the Turee Creek Group on the Pilbara Craton. In addition, a new late Paleoproterozoic mafic dyke swarm, the Tsineng swarm, is presented for the western Kaapvaal Craton in Alebouyeh Semami et al. (2016), which is correlated with Hartley Formation volcanism in the Olifantshoek Supergroup. This magmatic event may also define a new LIP on the western Kaapvaal Craton. This mafic dyke swarm and its associated volcanism has also not been documented on the Pilbara Craton.

Instead, it is proposed that the Pilbara and Kaapvaal cratons were part of a much larger continent or supercontinent in the Neoarchean to Paleoproterozoic. This large crustal block likely included the Wyoming, Superior and Hearne cratons of North America, together with the Kola-Karelia Craton located between Russia and Finland, as well as possibly the Singhbhum Craton of India and the Samartia terrane of Russia and Ukraine. This continent or supercontinent, termed 'Supervaalbara' here, allows for the Kaapvaal and Pilbara cratons to share many geological similarities without being nearest neighbours, along possibly the same passive margin. The geological evolution of all these cratons is very similar, particularly in the Paleoproterozoic, and which may have been driven by global processes. These global processes may include true polar wander, the submergence and subsequent remergence of continents with sea-level rise and fall, as well as atmospheric oxygenation and global glaciation. Paleomagnetic studies provide further continuity supporting the existence of Supervaalbara, which appears geologically distinct from the Rae family of cratons, suggesting perhaps two different continents in the early Paleoproterozoic before the assembly of the supercontinent Columbia (Nuna) in the late Paleoproterozoic.

Key words: Vaalbara, Kaapvaal Craton, Pilbara Craton, U-Pb geochronology, paleomagnetism, supercontinent, large igneous province, dyke swarm, sill province

Classification system and/or index terms (if any): –

Supplementary bibliographical information: –

Language: English

ISSN and key title: 1651-6648 LITHOLUND THESES

ISBN: 978-91-87847-32-5

Recipient's notes: –

Number of pages 130

Price: –

Security classification: –

Signature: 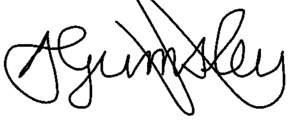

Date: 11 August 2017

KOCHAM CIE

Contents

List of papers

This dissertation is based on six appended papers, which are listed below. Papers I and II have been reproduced with permission from Elsevier. Papers III, IV and VI have been reproduced with permission from the Taylor & Francis Group. Paper V has been reproduced with permission from the Proceedings of the National Academy of Sciences of the United States of America.

Paper I:

Gumsley, A., Olsson, J., Söderlund, U., de Kock, M., Hofmann, A., Klausen, M., 2015: Precise U-Pb baddeleyite age dating of the Usushwana Complex, southern Africa–Implications for the Mesoarchaean magmatic and sedimentological evolution of the Pongola Supergroup, Kaapvaal Craton. *Precambrian Research* **267**, 174-185 (doi: 10.1016/j.precamres.2015.06.010).

Paper II:

Kampmann, T.C., Gumsley, A.P., de Kock, M.O., Söderlund, U., 2015: U–Pb geochronology and paleomagnetism of the Westerberg Sill Suite, Kaapvaal Craton – Support for a coherent Kaapvaal–Pilbara Block (Vaalbara) into the Paleoproterozoic? *Precambrian Research* **269**, 58-72 (doi: 10.1016/j.precamres.2015.08.011).

Paper III:

Gumsley, A., Rådman, J., Söderlund, U., Klausen, M., 2016: U–Pb baddeleyite geochronology and geochemistry of the White Mfolozi Dyke Swarm: unravelling the complexities of 2.70–2.66 Ga dyke swarms across the eastern Kaapvaal Craton, South Africa. *GFF* **138**, 115-132 (doi: 10.1080/11035897.2015.1122665).

Paper IV:

Alebouyeh Semami, F., de Kock, M., Söderlund, U., Gumsley, A., da Silva, R., Beukes, N., Armstrong, R., 2016: New U–Pb geochronologic and palaeomagnetic constraints on the late Palaeoproterozoic Hartley magmatic event: evidence for a potential large igneous province in the Kaapvaal Craton during Kalahari assembly, South Africa. *GFF* **138**, 164-168 (doi: 10.1080/11035897.2015.1124917).

Paper V:

Gumsley, A.P., Chamberlain, K.R., Bleeker, W., Söderlund, U., de Kock, M.O., Larsson, E.R., Bekker, A., 2017: Timing and tempo of the Great Oxidation Event. *Proceedings of the National Academy of Sciences of the United States of America* **114**, 1811-1816 (doi: 10.1073/pnas.1608824114).

Paper VI:

Evans, D.A.D., Smirnov, A.V., Gumsley, A.P., 2017, Paleomagnetism and U–Pb geochronology of the Black Range dykes, Pilbara Craton, Western Australia: a Neoarchean crossing of the polar circle. *Australian Journal of Earth Sciences* **64**, 225-237 (doi: 10.1080/08120099.2017.128998

1. Introduction

On the 6th of January 1912, Alfred Wegener presented his hypothesis on the movement of the continents through geological time, and proposed that they were once connected in a hypothetical supercontinent which later became known as Gondwana (e.g., Wegener, 1929). Despite drawing evidence from the geological and fossil records, as well as the apparent fit of continents such as Africa and South America, Alfred Wegener garnered very little scientific support for his ideas. He lacked a mechanism to support his 'continental drift hypothesis'. It was not until the 1960's that scientific community began to take the continental drift hypothesis seriously with the advent of paleomagnetic studies. Paleomagnetic studies could predict the placement of the continents on Earth as a particular time for a particular event, and it soon became evident that India, for example, was not always in its present location. Additionally, in the 1960's, the theory of plate tectonics was born out of the continental drift hypothesis. The mapping of the sea floor using a variety of geophysical methods revealed the existence of oceanic ridges and trenches which could be linked to seafloor spreading and subduction zones. These features presented direct evidence for the collision and separation of the continents presented in the Wilson Cycle (Wilson, 1963). The Wilson Cycle was the mechanism necessary to compliment Alfred Wegener's continental drift hypothesis. This was further supported in the 1990's with the launch of the global positioning system of satellites, which have been able to directly record the movement of the continents directly down to millimeter scales.

With the ability to be able to reconstruct Earth's youngest supercontinent, it soon became evident with developments in geochronology and paleomagnetism that absolute and relative temporal and spatial constraints could be placed on the continents throughout geological time. It also became known through these studies that the process of supercontinent formation and dispersal was actually a cycle, and that (possibly) many supercontinents existed before Pangea. This supercontinent record, however, becomes increasingly fragmentary back in deep time, as oceanic (and to a much lesser extent, continental) crust is either created or destroyed continuously. Destruction includes both subduction and erosion, and many pieces of crust are also altered and overprinted through deformation and metamorphism during orogenesis. The likeliness of orogenesis occurring on ancient crust increases with time.

On the present day Earth, there are approximately thirty-five relatively well-preserved ancient pieces of Archean crust preserved globally, called cratons (Figure 1; e.g., Bleeker, 2003). These cratons form the nucleus of the present-day continents, and are a 'window' back into the environments of the early Earth. In addition, there is a less defined number of poorly preserved slivers of Archean crust. Clues to supercontinents before the extensively studied Pangea, although continuously refined (e.g., Domeier et al., 2012), become increasingly speculative and conceptual, especially with a fragmentary record which has often been altered. This is also due to the lack of matches of near-complete sedimentary and volcanic strata with a known fossil record. This also includes the lack of a puzzle piece-like fit between the continents, and the loss of preserved oceanic crust. However, the amalgamation and separation of the continents through time became the first natural beacons in spatial paleogeography. This paleogeographic process is aided using temporal frameworks guided by geochronology to match deeply eroded mountain belts (orogenic belts) together, for example, the SAMBA (South AMerica and BAltica) model of Johansson (2009). A global compilation of U–Pb ages of zircon from these orogenic belts, felsic plutons and batholiths, as well as provenance studies display a number of peaks reflecting periods of crustal preservation and/or production. Peaks in preservation and/or production age spectra are thought to correlate with periods of supercontinent assembly, whereas troughs reflect continental dispersal (e.g., Condie, 1998; Condie and Aster, 2010; Hawkesworth et al., 2009; 2010). Although the exact configuration of these Precambrian supercontinents (or supercratons) still remains conjectural (e.g., Reddy and Evans, 2009), there is growing evidence for the existence of at least two supercontinents before Pangea. Precambrian supercontinents include the Neoproterozoic Rodinia (e.g., Li et al., 2008), and the Paleoproterozoic Nuna/Columbia (e.g., Hoffman, 1997; Rogers and Santosh, 2002), and the less accepted Paleopangea of Piper (2010). These supercontinents are clearly reflected in the zircon production/preservation record (e.g., Hawkesworth et al., 2010). Additionally, zircon age spectra clearly point toward either a Neoarchean supercraton, or supercontinent (Condie, 1998; Condie and Aster, 2010; Hawkesworth et al., 2009; 2010). Bleeker (2003) sought to address this by proposing the existence of either a single supercontinent, termed Kenorland by Williams et al. (1991), or clans of cratons or supercratons. The original Kenorland concept comprises the Archean provinces of North America (e.g., Williams et al., 1991), although Aspler and Chiarenzelli (1998) proposed the inclusion of Siberia and Baltica into the Kenorland configuration. Aspler and Chiarenzelli (1998) also proposed the existence of a second Neoarchean supercontinent: Zimvaalbara, which includes the Zimbabwe, Kaapvaal, Pilbara and São Francisco cratons, and possibly other cratonic blocks of present-day India. The single large Archean supercontinent proposed by Bleeker (2003) was thought to have included all these crustal blocks as an end-member solution. However, Bleeker (2003) also proposed a second end-member solu-

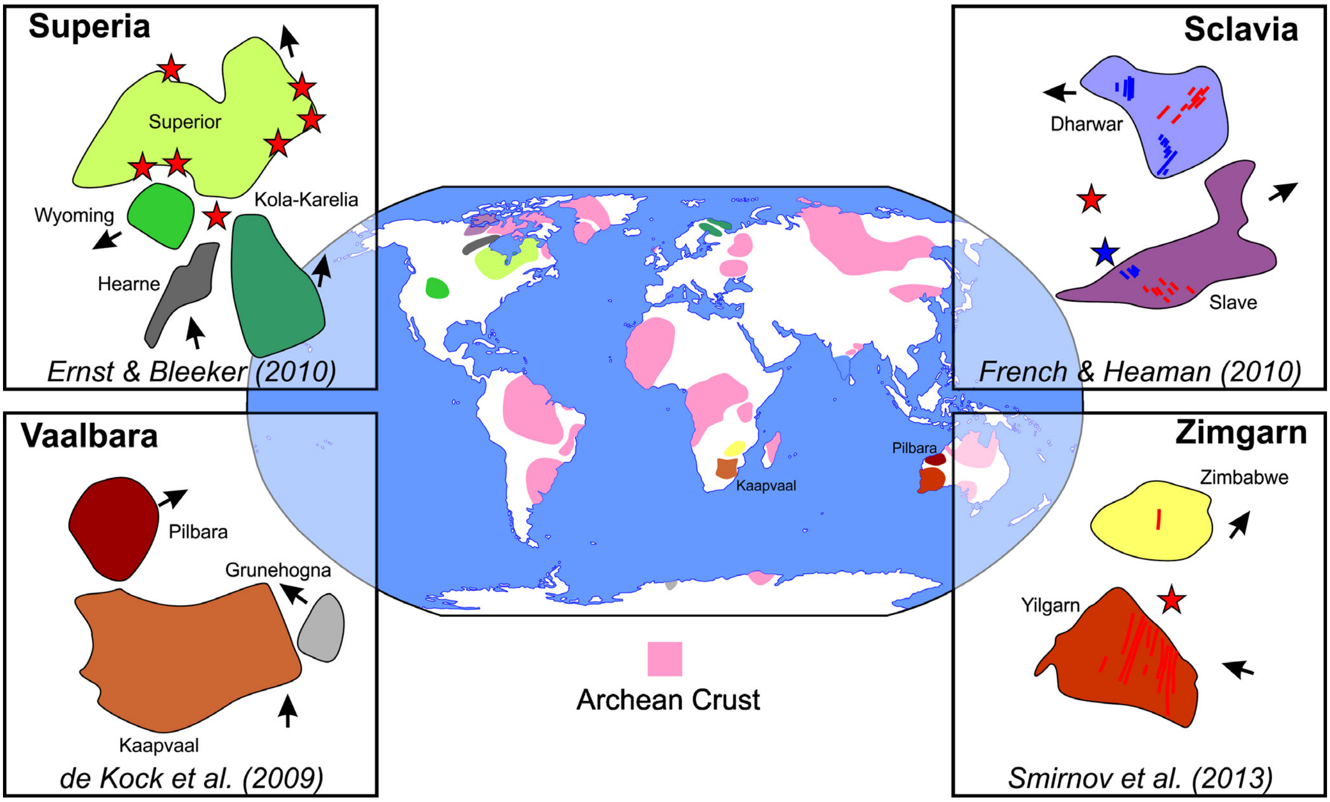

Figure: 1. Distribution of preserved Archean crust globally, with the various supercratonic configurations proposed at left and right. These supercraton configurations include Superia after Ernst and Bleeker (2010), Vaalbara after de Kock et al. (2009), Sclavia after French and Heaman (2010) and Zimgarn after Smirnov et al. (2013). The current outline of the cratons that make up these supercratons are shown. This includes the proposed cratonic configurations along with the present-day truth north directions in each craton with defining magmatism from coeval dyke swarms and sill provinces also shown.

tion that may have included clans of cratons, namely Superia, Sclavia and Vaalbara (Figure 1). The term Vaalbara was first proposed by Cheney (1996), building on the early work by Trendall (1968) and Button (1979), and the existence of Vaalbara forms the focus of this thesis. Sclavia and Superia, and more recently, Zimgarn, however, have been the subject of a number of much more recent studies (e.g., Bleeker, 2003; Bleeker and Ernst, 2006; Nilsson et al., 2010; French and Heaman, 2010; Smirnov et al., 2013).

2. LIPs as temporal and spatial markers

Many cratons show rifted or faulted margins, which infers that they are were fragments of larger ancestral landmasses. On many of these cratonic margins, large igneous provinces (LIPs) are preserved. LIPs are commonly linked to a mantle plume which may trigger supercontinental break-up into fragments (e.g., Courtillot et al., 1999; Storey, 1995). LIPs are anonymously high volume volcanic eruptions (with flood basalts that may extend several thousand kilometers) that are short-lived (usually less than ten million years) (Coffin and Eldholm, 1994; Ernst, 2014). Flood basalts associated with LIPs are temporal markers in the stratigraphic record, but are typically weathered and eroded away in Precambrian supracrustal rock successions. However, the deep-seated plumbing system of LIPs is typically well-preserved in the underlying basement terrane. This feeder plumbing system is composed of large-scale mafic dyke swarms and sill provinces, as well as layered intrusions. These intrusions can now be dated with precision and accuracy using isotope dilution-thermal ionization mass spectrometry (ID-TIMS) on the geochronometer baddeleyite (Heaman and LeCheminant, 1993; Krogh et al., 1987). The geochronometer zircon is rarer in mafic rocks. These mafic dyke swarms, sill provinces and layered intrusions are commonly preserved on conjugate margins of cratons that have been rifted apart. Numerous Phanerozoic LIPs have been documented, including continental flood basalts, dykes and sills of the ca. 130 Ma Paraná-Etendeka provinces preserved across present-day South America and Africa in Brazil and Namibia, for example. The formation of these LIPs has been linked to various causal mechanisms in both the lithosphere and asthenosphere, extending all the way down through the mantle to the core-mantle boundary. Mantle plumes are commonly evoked, with hot spot volcanism being the site at the Earth's surface for thermal upwelling from deep within the mantle (Morgan, 1971). However, there is much debate on both the existence and mechanics of mantle plumes (e.g., Foulger and Natland, 2003; McHone, 2000).

Well-exposed and preserved Archean cratons and cratonic fragments typically display numerous episodes of mafic dyke and sill intrusions associated with LIPs, and therefore a well-defined rock record of mafic magmatism (and LIPs) is recorded. Bleeker and Ernst (2006) introduced the concept of a magmatic 'barcode' record of mafic magmatism through time for specific cratonic blocks which can be easily visualized (Figure 2). Each mafic magmatic event from a mafic dyke swarm, sill province, layered intrusion or indeed a continental flood basalt province is defined by a temporal line in the barcode. Biases in this record can include both sampling bias as well as poor age constraints on the LIP event. However, with the recent advances in both separations of baddeleyite (e.g., Söderlund and Johansson, 2002) and dating of these mafic events (e.g., Chamberlain et al., 2010; Heaman and LeCheminant, 1993; Ibanez-Mejia et al., 2014; Wohlgemuth-Ueberwasser et al., 2015), the magmatic barcode record continues to be refined and developed for each craton. An assessment of a common history between various cratons and terranes is provided by the ability to match up barcode lines of more than one mafic magmatic event (or LIP), to assess whether they were contiguous crustal fragments or nearest neighbours over the time interval of the barcode (Figure 2). Together with geological and geochronological similarities, mafic dyke swarm geometries, geochemistry and importantly, paleomagnetic studies, paleogeographic reconstructions back in time can now be evaluated robustly using this multi-proxy approach. Paleomagnetic studies on these mafic rocks provide records of remnant magnetization recorded by magnetic minerals such as magnetite. These ferromagnetic minerals preserve inclination and declination directions of the magnetic moment preserved in the rocks relative to Earth's magnetic field at a particular time and place. These inclinations and declinations can in turn be converted into paleopoles with paleo-latitudes and paleo-longitudes back in time for a crustal block at a specific time.

3. Tools of the trade: U-Pb geochronology

Several minerals allow us to determine the age of an igneous or metamorphic rock, and these include zirconium-bearing minerals that take up uranium in their crystal lattice, but only allow for trace amounts of initial lead. These minerals include zirconium silicate or zircon ($ZrSiO_4$) and zirconium oxide or baddeleyite (ZrO_2), among others, and they are important accessory minerals that can now be routinely separated from coarse-grained igneous rocks. This allows us to employ U-Pb geochronology to both accurately and precisely date an igneous rock using mass spectrometry. U-Pb geochronology utilizes the radioactive decay series of ^{238}U to ^{206}Pb and ^{235}U to ^{207}Pb. The rate of radioactive decay from parent to daughter isotopes over time is constant. This constant, known as half-life, was determined by Jaffey et al. (1971) for ^{238}U and ^{235}U, and is different for both uranium isotopic systems. Therefore, the ratios of $^{206}Pb/^{238}U$, $^{207}Pb/^{235}U$ as well as $^{207}Pb/^{206}Pb$ are unique at a set time, enabling an age to be determined by mass spectrometry, which measure the intensities and relative concentrations of ^{238}U, ^{235}U, ^{207}Pb and ^{206}Pb. The Pb/U isotopic ratios can be plotted in concordia diagram with $^{206}Pb/^{238}U$ versus $^{207}Pb/^{235}U$ (Figure 3). If an analysis of a sample is determined along a concordia curve (and is deemed concordant) of either $^{206}Pb/^{238}U$ against $^{207}Pb/^{235}U$ (Wetherill, 1956) as shown in Figure 3,

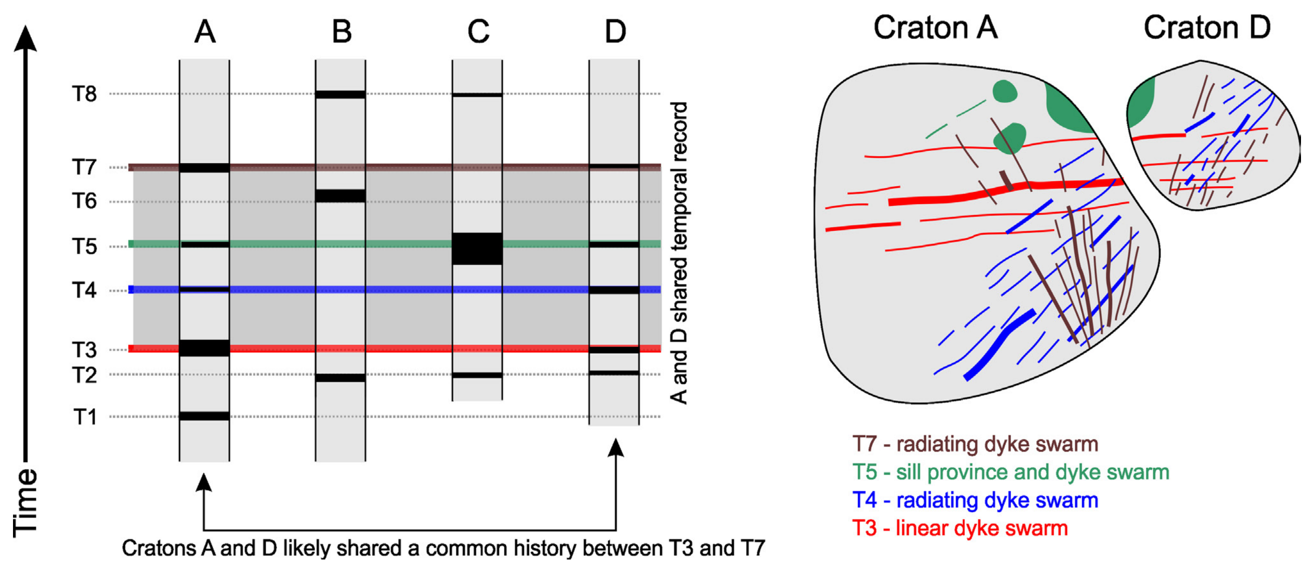

Figure: 2. A hypothetical magmatic 'barcode' (left), illustrating ages of magmatic events in cratons A to D after Nilsson (2016). Cratons A and D show multiple individual matches at T3, T4, T5 and T7. This suggests that these cratons shared a common history in an ancestral landmass between T3 and T7. A hypothetical paleogeographic reconstruction of cratons A and D (right) is show using the geometry of coeval dyke swarms and sill provinces.

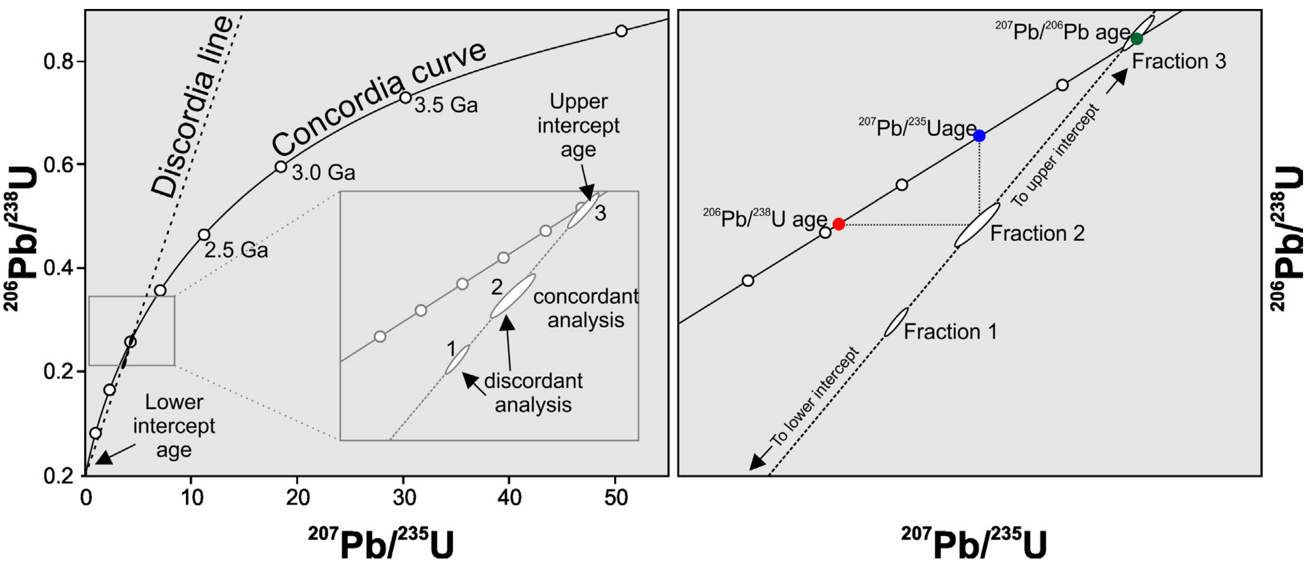

Figure: 3. Wetherill concordia diagram. Left: the concordia curve is an exponential curve composed of ^{207}Pb/^{235}U and ^{206}Pb/^{238}U ages from the present time to 4.6 Ga. This diagram allows graphical visualization of discordance. In this example, fraction 3 is the only concordant analyses whereas fractions 1 and 2 are variably discordant. A best-fit regression (discordia) line through all three analyses define two intercepts. The upper intercept is where the discordia intersects the concordia curve is usually taken as the age of the sample. The lower intercept reflects the age discordance developed, for instance by Pb-loss or isotopic mixing. In this case, the lower intercept age is 0 Ma. The ^{207}Pb/^{206}Pb age is defined by the intersection between the concordia curve and a discordia line for the individual fraction. In the case of normal discordance, a ^{207}Pb/^{206}Pb age represents a minimum age of the sample. For the concordant fraction 3, ^{207}Pb/^{235}U, ^{206}Pb/^{238}U and ^{207}Pb/^{206}Pb ages are statistically identical (i.e. concordant).

or with ^{206}Pb/^{238}U against ^{207}Pb/^{206}Pb (Tera and Wasserburg, 1972), it implies that the two decay systems in the sample have not been disturbed through loss or gain of either uranium or lead. However, deviation above or below the concordia curve in the concordia diagram reflects disagreement in the two isotopic systems, and is termed discordant, also shown on Figure 3. In very young samples, this can reflect the presence of short-lived intermediate daughter isotopes in the decay chain before equilibrium is reached. In zircon, this discordance is often attributed to Pb loss through metamorphism. In baddeleyite, metamorphism produces a zircon rim on the baddeleyite core, resulting in a mixture of primary baddeleyite and secondary zircon which produces this discordance (Heaman and LeCheminant, 1993). Discordance above the concordia curve however is not well understood, and is sometimes attributed to analytical artifacts or incomplete homogenization between sample and tracer solution,

Baddeleyite is used to date coarse-grained silica-undersaturated rocks (e.g., gabbro), which are key components of the feeder system of mafic dykes and sills present in LIPs (e.g., Heaman and LeCheminant, 1993). Baddeleyite is more sensitive to metamorphism than zircon, and readily transforms to secondary polycrystalline zircon in response to changes in temperature, pressure and fluid activity (Heaman and LeCheminant, 1993; Söderlund et al., 2013). Secondary and xenocrystic baddeleyite is rare, and therefore the interpretation of Pb/U baddeleyite dates of mafic rocks is straight forward, providing the igneous crystallization ages of rocks. Age determinations for baddeleyite typically employ either ID-TIMS (isotope dilution-thermal ionisation mass spectrometry), LA-ICP MS (laser ablation-inductively coupled plasma mass spectrometry) or SIMS (secondary ion mass spectrometry) on separated grains, with certain advantages and disadvantages inherent in each analytical technique (e.g., Schaltegger et al., 2015). The ID-TIMS analytical technique typically yields ages with a precision better than 0.1% at 95% confidence intervals (2 sigma). However, the technique is time consuming, and as whole grains are analyzed even the slightest amount of isotopic disturbance, for instance in Pb-loss along margins, will be recorded (i.e, yielding a discordant analysis). The SIMS and LA-ICP MS spot dating techniques offer the ability to restrict analysis to the inner (and usually undisturbed) domain of a baddeleyite grain. Both these techniques can yield ages at sensitivities of approximately 1% precision (2 sigma), with SIMS being more time consuming than LA-ICP MS. Spot sizes can be made down to 5 µm on a SIMS, with the ability to use the aperture to filter out erroneous mass counts and focus the ion beam on the centre of the grain. LA-ICP MS has the advantage of speed, although spot sizes can only realistically be made down to 10 µm. There are many complications inherent to both these spot dating techniques (e.g., down-hole fractionation, matrix affects, mass interference, common Pb, crystal orientation effects, etc.) that require various types of corrections. Therefore, the age of a sample is usually taken from the measured ^{207}Pb/^{206}Pb ratio.

4. Tools of the trade: Paleomagnetism

Most rocks, and in particular mafic igneous rocks are magnetic and can preserve a record of Earth's magnetic field through time, termed remnant magnetization. These minerals lock-in a direction and intensity of the magnetic moment at which they formed. This magnetic moment can be used to understand either the past behaviour of the Earth's magnetic field, or provide spatial constraints on the location of an igneous or metamorphic rock at its time of formation. Paleomagnetic studies have been made possible due to ferromagnetic minerals such as magnetite. However, the size and presence of single or multi-domains of the magnetic mineral is also important when evaluating magnetism. When magnetic minerals cool after crystallization, they preserve the direction of Earth's magnetic field through the Curie temperature of a specific mineral. This occurs at approximately 580°C in the case of single domain and chemically pure magnetite. The minerals do not physically rotate into the Earth's magnetic field, which occurs at crystallization temperatures, but record the orientation of the field at the Curie temperature. Remnant rock magnetism allows us to establish paleomagnetic poles for different continents (or cratons), at different times. This is done by using magnetism to establish both inclination and declination vectors of the magnetism, which allows us to determine a paleo-latitude and paleo-longitude or virtual geographic pole (VGP). A statistically relevant series of VGPs allow us to average out paleosecular variation of the magnetic north and south poles, and present a specific paleopole at a specific time.

Using different paleomagnetic poles through time for a fixed piece of Earth's crust (i.e., a craton or continent), allows us to present the motion of the crust relative to a fixed point, either to the southern or northern hemisphere geographic poles. This creates a path which the craton has moved along through time, and is known as an apparent polar wander path (APWP) after Creer et al. (1954). It is important to keep these 'paths' relative to a fixed point, which is labelled a 'Euler pole'. This process is relatively straight forward for the last 200 million years, with a good record of oceanic crust preserved since the breakup of Pangea. However, further back in time, many complications arise in the analysis of such rocks. Paleomagnetic poles require quality criteria that assesses their reliability, as defined by van der Voo (1990). Sampling requires the determination of magnetic components present at a number of sites (usually above twenty to balance out paleosecular variation of the magnetic field). Sampling at each site must be statistically reproducible (usually a minimum of at least five specimens per site), with each specimen oriented using both a sun and magnetic compass to correct for human error and sample error imposed by magnetism of the rocks. Geological field tests require either a baked contact, fold or conglomerate/breccia test, in addition to recording a magnetic reversal (Buchan, 2013; van der Voo, 1990) to test the primary nature of the principal magnetic component. The analysis itself also requires that the magnetic component vectors determined in the remnant magnetic field display a mean angle of deviation less than 10°, and for the age of magnetization to equate to the age of crystallization (usually determined in conjunction with the field tests). This also usually requires that there is no paleomagnetic similarity to younger magmatic or metamorphic events in the vicinity which may have overprinted the primary direction obtained. Satisfying all these requirements allows a paleomagnetic pole to become a key paleomagnetic pole as defined by Buchan (2013). Paleomagnetic poles not meeting sufficient quality criteria should be termed virtual geomagnetic poles (VGPs).

Rock analyses are made on a magnetometer, which enables the measurement of magnetic moments in both x, y and z directions. Rocks are successively demagnetized using alternating field, thermal and chemical demagnetization techniques in a near-zero magnetic field, until the Curie temperature is reached. Using the principal component analysis of Kirschvink (1980), Zijderveld diagrams (Zijderveld, 1967) can be used to determine a number of magnetic components which may be preserved in a rock, and can equate to either primary or secondary manetizations. The final component measured is located usually at high temperatures, trending toward the origin in the Zijderveld diagram, preserving the primary magnetic component, and thus the remnant paleomagnetic direction.

5. Vaalbara

5.1. Introduction

The recognition of Vaalbara as either a supercontinent or a supercraton began with the recognition of similar stratigraphic units between the Kaapvaal Craton in southern Africa and the Pilbara Craton in Western Australia during the Neoarchean to Paleoproterozoic (Figure 4). The Kaapvaal and Pilbara cratons are the only two cratons to preserve relatively pristine 3.6 Ga to 2.7 Ga crust represented by similar granitoid(gneiss)-greenstone terranes, and are thought to be among the first to stabilize as micro-continents. It was Trendall (1968) who first identified the geological similarities based on the presence of large-scale Neoarchean-Paleoproterozoic iron formations in each craton. This was expanded by Button (1979) to

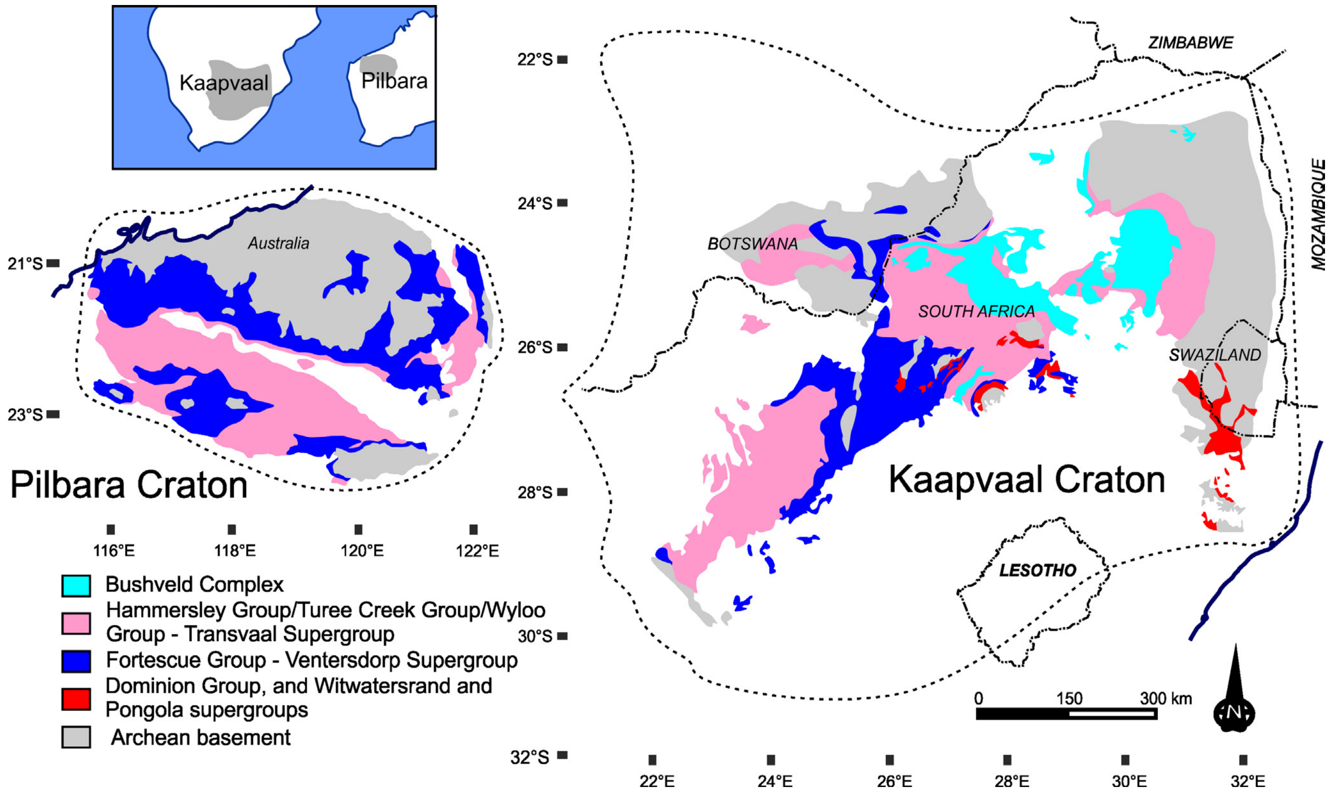

Figure: 4. The geology of the Pilbara Craton (left) and the Kaapvaal Craton (right), against an outline of the respective craton margins. Denoted rock units include the underlying Archean basement in each craton, as well as the overlying Mesoarchean to Paleoproterozoic supracrustal successions. This includes the Neoarchean Fortescue and Ventersdorp basins on the Pilbara and Kaapvaal cratons, respectively, followed by the Hammersley (and Tureek Creek and Wyloo) and Transvaal basins. *Inset*: the localities of the Kaapvaal Craton within southern Africa and the Pilbara Craton within Western Australia.

include the larger Mesoarchean-Paleoproterozoic unconformity-bounded successions. Vaalbara was proposed to be part of a single long-lived supercontinent (e.g., Piper, 1974), of which Rogers (1996) called 'Ur'. Using sequence stratigraphy, however, Cheney (1996) proposed that the Kaapvaal and Pilbara cratons were connected using the unconformity-bounded 2.7 Ga to 2.1 Ga supracrustal successions in each cratonic block, and formalized the term 'Vaalbara'. Other similarities exist between the cratons in the 3.5 Ga to 1.8 Ga terranes, basins and mineral deposits (e.g., Anhaeusser et al., 1969; Beukes, 1984; Button, 1979; 1973b; Cheney, 1996; Martin et al., 1998; Nelson et al., 1992; Zegers et al., 1998), although some of these have been attributed to global processes (e.g., Bekker and Kaufman, 2007; Nelson et al., 1999; 1992), especially in older continental configurations such as Ur which place the Kaapvaal and Pilbara cratons far apart (e.g., Rogers, 1996). Button (1979), however, described the Mesoarchean to Paleoproterozoic basins as being separate but broadly coeval. Since these early contributions, abundant new data have become available that can both support and discredit the concept of Vaalbara. In general, this new data necessitates the revision of some of the Cheney (1996) sequence stratigraphic correlations and the paleogeographic reconstruction of the relative positions of the Kaapvaal and Pilbara cratons through time. A definition of Vaalbara or any supercraton/supercontinent pairing in the Precambrian thus should require the following elements:

1. Knowledge of the timing of formation and stabilization of the cratonic cores.

2. Studies on the post-stabilization history of the cratons, including the stratigraphy of the supracrustal successions, and provenance studies, etc.

3. Timing of rifting, orogenesis, as well as the emplacement of large igneous provinces and their association intrusions.

4. Paleogeographic reconstructions, using a synthesis of the above techniques coupled with paleomagnetism.

In meeting these components, a more in-depth understanding of the paleogeography can be made, and whether it fits to just a single craton, or a supercraton/continent/supercontinent as a whole. It is important to address all these pieces of crust separately. These fragments of crust may be thought of as puzzle-pieces, which are needed in order to assemble the puzzle, even if it is well known that some of the puzzle-pieces may be missing.

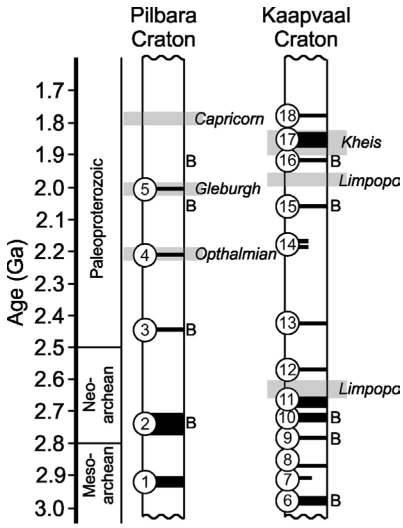

Figure: 5. Magmatic barcode for the Pilbara and Kaapvaal cratons, with each individual magmatic event denoted. These include the following LIPs: 1, Munni Munni, 2, Fortescue, 3, Woongarra, 4, Moodogara, 5, Panhandle, 6, Nsuze, 7, Crown, 8, Hlagothi, 9, Derdepoort, 10, Ventersdorp, 11, Rykoppies-White Mfolozi, 12, Mvunyana, 13, Ongeluk, 14, Hekpoort, 15, Bushveld, 16, Hartley, 17, Black Hills and 18, Soutpansberg. 'B' denotes bimodal and grey denotes orogenesis

5.2. The Paleo- to Mesoarchean

The connection between the Pilbara and Kaapvaal cratons begins with a comparison between the geology and geochronology of both cratons, and the parallel development of the Neoarchean-Paleoproterozoic stratigraphy that is the core of the Vaalbara hypothesis. Cheney (1996) defined a number of sequence stratigraphic Neoarchean to Paleoproterozoic units for the Kaapvaal and Pilbara cratons, which have been developed by Beukes and Gutzmer (2008), among others. However, it was Zegers et al. (1998) and Nelson et al. (1999) who extended the arguments of Cheney (1996) back into the Paleo- and Mesoarchean. Using the data available, there appears to be have been cycles of magmatic activity in the Archean basement granitoid(gneiss)-greenstone terrane of the Kaapvaal Craton at 3580-3430 Ma, 3250-3220 Ma, 3120-3090 Ma, 2990-2970 Ma, 2870 Ma, with additional well-dated episodes at 2780-2770 Ma and 2730-2720 Ma (e.g., Nelson et al., 1999). On the Pilbara Craton basement terrane, magmatic events have been identified at 3470-3400 Ma, 3330-3290 Ma, 3270-3230 Ma, 3140-3090 Ma, 3030-2990 Ma, as well as at 2950-2910 Ma and 2760 Ma (e.g., Nelson et al., 1999). It becomes apparent that these magmatic cycles before the stabilization of the crust in both cratons show little temporal similarity between each other. This lack of similarity becomes especially apparent within the short-lived events, which includes the 2990-2970 Ma, 2870 Ma and 2780-2770 Ma magmatic events, which can be linked to the Pongola Supergroup and early Ventersdorp Supergroup on the Kaapvaal Craton, and the 2760 Ma magmatic event in the Fortescue Group on the Pilbara Craton (Nelson et al., 1999).

Events after 3090 Ma formed on more stabilized crust in the Kaapvaal Craton, and it is from where the updated magmatic barcode presented in this study begins (Figure 5). Zegers et al. (1998) drew comparison between the ca. 2860 Ma Usushwana Complex (Kaapvaal Craton) and the ca. 2860 Ma Millindinna Complex (Pilbara Craton) using both ages and paleomagnetism, noting the geological similarity both temporally and spatially. The Usushwana Complex however was subsequently dated in this thesis work to be between 2990 Ma and 2978 Ma (Event 6 in Figure 5; Gumsley et al., 2015), which invalidates any connection between the two layered complexes, and indeed the cratons themselves at that time. It was noted that the bulk of the Piet Retief Suite of the Usushwana Complex was composed of 2990-2978 Ma gabbros (Gumsley et al., 2015), with the lesser group of Hlelo Suite granophyres dated to 2871 ± 30 Ma (Hegner et al., 1984). As the crust stabilized on the Kaapvaal Craton after 3090 Ma, the Mesoarchean Dominion Group, Witwatersrand Supergroup and Pongola Supergroup supracrustal successions began to form, into which the Usushwana Complex was emplaced, along with the 290 Ma to 2966 Ma Badplaas mafic dyke swarm from 2980 Ma (Olsson et al., 2010; Gumsley et al., 2015). On the Pilbara Craton, craton stabilization commenced after 2910 Ma, almost 200 million years later than on the Kaapvaal Craton. This cratonic stabilization renders comparisons between the Lalla Rookh and Whim Creek basins on the Pilbara Craton with the Witwatersrand and Pongola basins arguable, although all appear to show similar ages, and all appear to be upward coarsening. Gumsley et al. (2013) drew possible comparison between the 2866 ± 2 Ma Hlagothi Complex (Event 8 in Figure 5) and associated intrusions, with that of the Zebra Hills dyke swarm on the Pilbara Craton. The Zebra Hills dyke swarm intrudes into the 3015-2925 Ma Ma Munni Munni Complex (Event 1 in Figure 5; Barnes and Hoatson, 1994), and is overlain by the ≤2765 Ma Hardey Formation sandstone (Hoatson and Sun, 2002). However, recent unpublished U-Pb age constraints (Gumsley, unpublished data) place the Zebra Hills dyke swarm as intruding at ca. 2.91 Ga into the Pilbara Craton, invalidating any further comparison (Event 1 in Figure 5).

5.3. The early Neoarchean

The Neoarchean Ventersdorp Supergroup and broadly coeval units form the most extensive predominantly volcanic supracrustal successions on the Kaapvaal Craton. The Ventersdorp Supergroup has been compared with Neoarchean Fortescue Group on the Pilbara Craton, which is also predominantly volcanic. Neoarchean volcanism commences on the Kaapvaal Craton with the eruption of the 2782 ± 5 Ma Derdepoort Belt basalts in the central Kaapvaal Craton in South Africa (Wingate, 1998), with its feeders (e.g., the Modipe Complex) dated to 2784 ± 1 Ma (Denyszyn et al., 2013) (Event 9 in Figure 5). The Derdepoort Belt volcanic pile is bimodal, with the rhyolites dated to 2781 ± 5 Ma (Wingate, 1998), and can is coeval with that of the nearby Kanye and Lobatse volcanic rocks in Botswana, as well as the granites of the ca. 2783 Ma Gaborone Complex (Grobler and Walraven, 1993; Moore et al., 1993). The Derdepoort Belt basalts were correlated with the Klipriviersberg Group flood basalts at the base of the Ventersdorp Supergroup further to the south (e.g., Grobler and Walraven, 1993, and references therein), which conformably overlies the Witwatersrand Supergroup in the central Kaapvaal Craton (e.g., van der Westhuizen et al., 1991). However, this correlation was challenged by age determinations on the Klipriviersberg Group flood basalts that were dated to 2714 ± 8 Ma (Armstrong et al., 1991), although this age was questioned by Wingate (1998) and de Kock et al. (2012). Further doubts have been raised by U-Pb ages on baddeleyite from mafic sills dated to ca. 2.78 Ga immediately beneath the Klipriviersberg Group in Witwatersrand Supergroup strata (Stamsjnijder, unpublished data).

On the Pilbara Craton, supracrustal volcanism commenced with the eruption of 2775-2663 Ma Mount Roe Formation flood basalts and the Black Range mafic dyke swarm unconformably on to the basement granitoid(gneiss)-greenstone terrane at the base of Fortescue Group (Event 2 in Figure 5; Arndt et al., 1991; Evans et al., 2017; Wingate, 1999). This magmatism may almost temporally correlate with the Derdepoort Belt, despite an approximate 10 million years difference in age. The Makwassie Formation in the Platberg Group, which unconformably overlies the Klipriviersberg Group in the Ventersdorp Supergroup basin has been dated to 2709 ± 4 Ma (Event 10 in Figure 5; Armstrong et al., 1991). The Makwassie Formation is a quartz porphyry underlain by the sedimentary rocks of the Kameeldoorns Formation, and which is overlain by the volcanic Rietgat Formation (e.g.,van der Westhuizen et al., 1991). The Hartwater Group, one of the Platberg Group equivalent basins on the western Kaapvaal Craton, however, have been dated to 2733-2724 Ma (de Kock et al., 2012; Poujol et al., 2005), which directly challenges the ca. 2714 Ma Klipriviersberg Group basalt age (Armstrong et al., 1991). Instead it has been proposed that the Klipriviersberg Group flood basalts are ca. 2.78 Ga (de Kock et al., 2012; Wingate, 1998).

Unconformably overlying the Mount Roe Formation floode basalts is the Hardey Formation on the Pilbara Craton, which is composed of sandstones and smaller volcanic units (i.e., the Spinaway and Bamboo quartz porphyries) within the larger basin that have been dated to 2768-2750 Ma (Event 2 in Figure 5; Arndt et al., 1991; Blake et al., 2004; Hall, 2005; Pidgeon, 1984). These ages appear to make the Hardey Formation older than the Platberg Group, but younger than the Derdepoort-Kanye-Lobatse-Gabarone magmatic event on the Kaapvaal Craton. The 2750-2745 Ma Sylvania mafic dyke swarm (Wingate, 1999) is temporally linked to volcanism within the Hardey Formation. The conformably overlying Kylena Formation basalts on the Pilbara Craton have not been dated, but the conformably overlying Maddina Formation basalts have been dated between 2718-2713 Ma (Blake et al., 2004). Several quartz porphyries located between the Kylena and Maddina basalts have been dated to 2724-2721 Ma, and are termed the Tubiana Formation according to Blake et al. (2004). These quartz porphyries may be related to volcanism within the Platberg Group, although no exact age match is yet to be made. The Platberg Group is unconformably overlain by the Bothaville Formation sandstones and Allanridge Formation flood basalts in the central and western Kaapvaal Craton (e.g., van der Westhuizen et al., 1991). The Bothaville and Allanridge formations have not been dated, but are bracketed between ca. 2709 Ma Makwassie Formation age (Armstrong et al., 1991) and 2664 ± 1 Ma (Barton et al., 1995), the age of the sedimentary and volcanic Buffelsfontein Group beneath the Transvaal Supergroup (Eriksson et al., 2006). This volcanic event is broadly coeval with mafic dykes across the eastern and southeastern Kaapvaal Craton which were emplaced between 2.70 Ga and 2.65 Ga (Event 11 in Figure 5; Olsson et al., 2010; 2011; Gumsley et al., 2016).

5.4. The late Neoarchean and Paleoproterozoic

Structurally above the Ventersdorp Supergroup successions on the Kaapvaal Craton, follows the sandstones and conglomerates of the 2643 ± 3 Ma Vryburg Formation (Walraven et al., cited in Nelson et al., 1999) in the western Griqualand West sub-basin of the Transvaal Supergroup (e.g., Eriksson et al., 2006). Further to the east on the centre and eastern side of the Kaapvaal Craton, the Black Reef Formation was deposited as the equivalent of the Vryburg Formation in the Transvaal sub-basin of the Transvaal Supergroup. In both the Griqualand West and Transvaal sub-basins, conglomerates, and then sandstones gradually give way to shallow marine carbonates of the Ghaap and Chuniespoort groups in both sub-basins, respectively (e.g., Eriksson et al., 2006). Tuffs have been dated from within these carbonates, and identify that the carbonates were deposited approximately between approximately 2588 Ma (Altermann and Nelson, 1998) to 2521 Ma (Sumner and Bowring, 1996) in the Ghaap Group, and from 2588 Ma (Martin et al., 1998) in the

Chuniespoort Group and onwards. On the Pilbara Craton, Jeerinah Formation sandstones, at the base of the Hammersley Group, are dated to 2684 ± 6 Ma (Trendall et al., 2004). These sandstones are overlain conformably by Wittenoom Formation carbonates which are dated to approximately between 2629 Ma to 2565 Ma (Trendall et al., 2004). They are the lithological equivalent of the lower Transvaal Supergroup, although the Jeerinah Formation is slightly older. On both the Kaapvaal and Pilbara cratons, iron formations conformably overlie the carbonates, and represent the further drowning of both the cratons. Iron formations in the Griqualand West sub-basin consist of the Kuruman and Griquatown formations, and are dated to approximately 2460 ± 5 Ma (Pickard, 2003), whereas iron formations in the Transvaal sub-basin are dated to approximately 2480 ± 6 Ma Penge Formation (Trendall et al., cited in Nelson et al., 1999). The Brockman and Weeli Wooli iron formations of the Hammersley Group, Pilbara Craton, are dated to approximately 2481 ± 4 Ma and 2461 ± 5 Ma (Trendall et al., 2004), and correlate well with the Kuruman and Griquatown formations of the Kaapvaal Craton.

The new deviation in the stratigraphic correlation between the Kaapvaal and Pilbara cratons in the Transvaal and Hammersley basins occurs with the bimodal basalts and rhyolites of the 2449-2445 Ma Woongarra Formation of the Pilbara Craton (Event 3 in Figure 5; Blake et al., 2004), which has no temporal equivalent on the Kaapvaal Craton. Mafic sills and dykes, however, occur in the iron formations of both cratons, which were thought to be feeders to the Woongarra Formation. These volcanic and plutonic rocks were dated to 2449 ± 3 Ma on the Pilbara Craton (Blake et al., 2004), and to 2441 ± 6 Ma and 2426 ± 1 Ma on the Kaapvaal Craton (Kampmann et al., 2015) in the Westerberg Sill Province, and were originally thought to be coeval. Iron formations then begin to be replaced by sandstone and shale in the Griqualand West sub-basin in the Koegas Group, above the Griquatown Formation. Meanwhile, in the Transvaal sub-basin, shale and carbonate sedimentation in the Tongwane Formation began (e.g., Eriksson et al., 2006). The same transition is observed in the Bolgeeda Formation of the Pilbara Craton. Above the Koegas Group, a sea-level fall associated with a global glaciation (e.g., Evans et al., 1997; Polteau et al., 2006) led to the removal of stratigraphy above the Koegas Group in the Griqualand West sub-basin. Further deposition is preserved only 200 million years later in the Makganyene Formation glacio-marine diamictites. This is followed by the conformable 2222 ± 13 Ma Ongeluk Formation flood basalts (Cornell et al., 1996), which were also deposited sub-aqueously. Deposition in the Transvaal Supergroup, however, was preserved above the unconformity at the top of the Tongwane Formation in the Duitschland Formation of the Transvaal sub-basin. Deposition continued with the Rooihoogte Formation. On the Pilbara Craton, an unconformity is also developed on top of the Hammersley Group, with deposition of glacial diamictites of the Turee Creek Group called the Meteorite Bore. Dating in the study by Gumsley et al. (2017) demonstrated that the Ongeluk Formation flood basalts erupted at 2426 ± 3 Ma (Event 13 in Figure 5), 200 million years earlier than previously thought by Cornell et al. (1996), and also revised the 2441 ± 6 Ma age by Kampmann et al. (2015) to 2428 ± 4 Ma. This meant that sub-volcanic mafic sills (the Westerberg Sill Province) and dykes in the underlying iron formations on the Kaapvaal Craton were linked to the Ongeluk LIP, and not the Wooongarra mafic dykes and sills which are approximately 20 million years older. This new age constraint also breaks the correlation between Meteorite Bore Member and Duitschland Formation diamictites, and makes the Meteorite Bore Member and Makganyene Formation diamictites potentially coeval, in a deviation from the traditionally accepted stratigraphic correlation (e.g., Beukes and Gutzmer, 2008; Cheney, 1996).

Deposition, however, continued up from the Ongeluk Formation basalts into the alternating iron- and manganese formations of the Hotazel Formation, before deposition of the Mooidraai Formation carbonates at 2392 ± 23 Ma (Bau et al., 1999; Fairey et al., 2013) in the Griqualand West sub-basin. Although the isolated Hotazel and Mooidraai formations are not observed beneath the Duitschland Formation, the Mooidraai Formation may correlate with carbonates in either the Kazput or Kungarra formations of the Turee Creek Group on the Pilbara Craton. Above the Mooidraai Formation, a large unconformity exists before further deposition is preserved approximately 300 million years later in the Olifantshoek Supergroup on the western Kaapvaal Craton. Above the Rooihoogte Formation in the eastern Kaapvaal Craton, however, the shales and sandstones of the conformably overlying Timeball Hill Formation are preserved, and have been dated to 2316-2256 Ma (Hannah et al., 2004; Rasmussen et al., 2013; Schröder et al., 2016). This is followed by the Boshoek Formation, which then gives way to the flood basalts of the subaerial Hekpoort Formation (e.g., Eriksson et al., 2006), which are ≤2250-2240 Ma (Event 14 in Figure 5; Schröder et al., 2016). The Hekpoort Formation volcanic rocks were long thought to be correlated with the Ongeluk Formation volcanic rocks (e.g., Cornell et al., 1996), however this is now shown to be incorrect. Instead, Hekpoort Formation may be related to 2209-2207 Ma mafic sills in the Pilbara Craton (Event 4 in Figure 5; Müller et al., 2005), which in turn may be related to the Cheela Springs Formation basalts of the lower Wyloo Group.

The upper parts of the Transvaal Supergroup in the main Transvaal sub-basin may be correlated with parts of the lower Olifantshoek Supergroup further west, and to the Turee Creek (and Wyloo) Group on the Pilbara Craton.

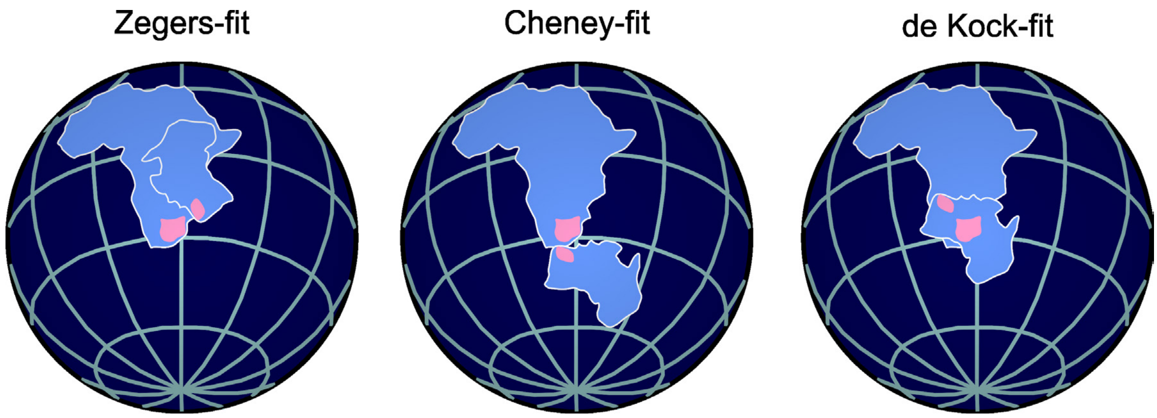

Figure: 6. Paleomagnetic reconstructions of the Kaapvaal and Pilbara cratons relative to the present-day Kaapvaal Craton position. Paleogeographic configurations proposed include that from left to right of Zegers et al. (1998), Cheney (1996) and de Kock et al. (2009). The de Kock-fit is the only reconstruction that could fit the two-pole comparison before the work of Denyszyn et al. (2013) and Evans et al. (2017) invalidated it..

No vestiges of the 2056-2055 Ma Bushveld Complex (Event 15 in Figure 5; Zeh et al., 2015) and its related volcanic rocks on the Kaapvaal Craton are found on the Pilbara Craton. The same can be seen for the ca. 2.02 Ma Vredefort Impact and Limpopo and the Kheis orogenies on the Kaapvaal Craton, and for the Opthalmian, Glenburgh and Capricorn orogenies on the Pilbara Craton. In addition, the newly identified 1923 ± 6 Ma Tsineng mafic dyke swarm on the western Kaapvaal Craton has not been identified on the Pilbara Craton (Event 16 in Figure 5; Alebouyeh Semami et al., 2016), along with the emplacement of the large-scale dyke swarms and sill provinces dated to 1880-1830 Ma on the Kaapvaal Craton (Event 18 in Figure 5; Olsson et al., 2016; Hanson et al., 2004). This appears to indicate definite divergence of the cratons before these events.

5.5. Paleomagnetism and configuration of Vaalbara

Originally, the Pilbara Craton was positioned juxtaposed next to the southwestern margin of the Kaapvaal Craton in what is now known as the 'Cheney-fit' (Figure 6; Cheney, 1996). The Zimbabwe and Yilgarn cratons were originally included in this configuration with respect to the Kaapvaal and Pilbara cratons in the definition of Vaalbara by Cheney (1996). The Grunehogna Craton of eastern Antarctica can also be included in this configuration (Jones et al., 2003). However, paleomagnetically, a comparison between the Kaapvaal Craton and Pilbara Craton at 2.78-2.77 Ga failed in the study by Wingate (1998) using the Derdepoort and Mount Roe paleopoles. However, an updated paleomagnetic comparison by Strik et al. (2003) made a direct fit more feasible, based on paleo-latitude constraints, which mostly increased the error margins of the allowable fit. This was subsequently discredited in Denyszyn et al. (2013) when paleomagnetic constraints from the coeval Modipe Complex gabbros were added to the Derdepoort paleopole. The configuration of Zegers et al. (1998) was allowable based on ca. 2.87 Ga paleomagnetic comparisons between the Usushwana Complex (Layer et al., 1988) on the Kaapvaal Craton, and the Millindinna Complex (Schmidt and Embleton, 1985) on the Pilbara Craton, and with the alignment of supposed structural trends (e.g., lineaments and shear zones) in the cratonic blocks that divide the terranes. This fit, known as 'Zegers-fit', placed the Pilbara Craton toward the east of the Kaapvaal Craton (Figure 6). The east-northeast-trending lineaments of the older eastern terrane on the Kaapvaal Craton are truncated by younger north-trending lineaments of the western terrane at approximately ca. 2.7 Ga (de Wit et al., 1992; Eglington and Armstrong, 2004; Schmitz et al., 2004). The Pilbara Craton is shown to be divided by north-northeast to northeast trends dated to between 2.96 Ga and 2.93 Ga from west to east (Zegers et al., 1998), with the oldest rocks also preserved in the eastern terranes (Krapez and Barley, 1987). The progression from early thrusting to later strike-slip deformation and broadly coeval ages suggested a common history according to Zegers et al. (1998). However, with the updated age constraints provided by Gumsley et al. (2015), the comparison between the Usushwana Complex and Millindinna Complex is now shown to be invalid. The Usushwana Complex, as already described, is shown to be a composite intrusion dated between 2990 Ma and 2978 Ma for the Piet Retief Suite gabbros, as well as younger intrusions dated to between 2874 Ma and 2866 Ma, which makes these rocks coeval with the Hlagothi Complex (Gumsley et al., 2015; 2013).

Several authors (Denyszyn et al., 2013; Strik et al., 2003; Wingate, 1998; Zegers et al., 1998) used a method of single-age pole comparison. Single-age paleopole comparison, however, does not provide longitudinal constraints, and thus it may mean that the cratons being compared were far apart along their respective lines of latitude. Cratons may also have been positioned in the opposite hemisphere due to the geomagnetic polar ambiguity. The paleomagnetic comparison performed by de Kock et al. (2009) between the Kaapvaal and Pilbara cratons utilizing the Derdepoort-Mount Roe and Allanridge-Kylena flood basalts of the Neoarchean Ventersdorp Supergroup and Fortescue Group, however, allows for a better estimate of the distances between paleopoles from the two cratons. This is done through a better constrained time interval using two near-coeval pairs of paleopoles from the two cratons, and provides better longitudinal constraints. This configuration is known as the 'de Kock- fit' (Figure 6; de Kock et al., 2009), and utilizes modern demagnetization techniques, and presents field tests which are paleomagnetically plausible as suggested by van der Voo (1990). This paleomagnetic comparison can be updated to include the paleomagnetic constraints on the coeval Modipe Complex by Denyszyn et al. (2013) and the Black Range dykes by Evans et al. (2017). However, the smaller uncertainties surrounding the Derdepoort paleopole using the coeval Modipe Complex paleomagnetic data show no overlap with the Black Range mafic dykes on the Pilbara Craton. The Black Range dykes of the Pilbara Craton, with which the Derdepoort-Modipe pole of the Kaapvaal Craton are compared, has been complemented by further age and paleomagnetic constraints by Evans et al. (2017). The study by Evans et al. (2017) builds on the work by Wingate (1999) and Embleton (1978), and invalidates any similarity paleomagnetically between the magmatic events. In addition, although the Allanridge Formation is paleomagnetically well-studied, age constraints between 2708 Ma and 2664 Ma should negate any comparison with the ca. 2717 Ma flood basalts in the upper Fortescue Group due to the large age span. The 2.70-2.66 Ga Rykoppies mafic dyke swarm on the Kaapvaal Craton has also been paleomagnetically studied by Lubnina et al. (2010). Without firmer age constraints though, this paleopole lacks the clarity to resolve the paleomagnetic direction and remains a VGP.

In the Hammersley and Transvaal basins, no firm paleomagnetic constraints exist from the Allanrige Formation at the top of the Ventersdorp Supergroup until the ca. 2426 Ma Ongeluk Formation flood basalts. This key paleomagnetic pole on the Ongeluk LIP places the Kaapvaal Craton at equatorial paleo-latitudes at this time (Evans et al., 1997; Gumsley et al., 2017; Kampmann et al., 2015; Lubnina et al., 2010). Further paleomagnetic constraints of mafic rocks in the Transvaal Supergroup basin have recently been made by Humbert et al. (2017), who studied the Hekpoort Formation. The Hekpoort Formation paleopole shows paleomagnetic differences with the Ongeluk Formation with which it was previously correlated (Humbert et al., 2017). This paleomagnetic difference further validates the distinction between these two volcanic units, although the Hekpoort Formation paleopole remains a VGP. In the Pilbara Craton, no documented paleomagnetic studies have been performed on rocks younger than the Fortescue Group until the studies on the Capricorn orogenesis at approximately 1.80 Ga.

6. Discussion

Although there appears to be little geochronological and paleomagnetic similarities between the Kaapvaal Craton and the Pilbara Craton outside of the late Neoarchean to early Paleoproterozoic stratigraphy of both cratons, there is growing evidence for the existence of a much large continent or supercontinent in this time frame. This land mass, which was originally termed Kenorland by Williams et al. (1991), has been geologically and paleomagnetically evaluated by Personen et al. (2003) and Bleeker (2003). However, the original hypothesis infers that the Churchill Province of the Canadian Shield with the Rae Craton being part of Kenorland appears invalid according to Pehrsson et al. (2013). Bleeker (2003) noted the distinct geological differences between cratons, leading to the proposal of two distinct clans of cratons. As defined by Bleeker (2003), the Superior Craton represents one of the larger and better preserved fragments of the supercraton 'Superia', which is fundamentally different from the 'Sclavia' supercraton which includes the Slave Craton. The Superia Craton underwent progressive 'rift-and-drift' throughout the Paleoproterozoic, leading to deposition of the Huronian Supergroup, a supracrustal succession which can be compared with the upper Transvaal Supergroup and Hamersley Group basins (e.g., Gumsley et al., 2017). Along with the Kola-Karelia Craton in Finland and Russia, all these cratons appear to preserve early Paleoproterozoic strata (e.g., Hoffman, 2013), with evidence of several episodes of glaciation along with multiple large igneous provinces (e.g., Gumsley et al., 2017). Superia, however, began to break apart in the later Paleoproterozoic, forming the many cratonic fragments that have since dispersed. Previous work has also demonstrated the similarity between Wyoming (Kilian et al., 2016), Hearne (Ernst and Bleeker, 2010) and a number of other cratons proposed to form Superia along with the Superior Craton. Salminen et al. (2014) appeared though to invalidate the Kola-Karelia Craton connection with Superia at ca. 2339 Ma using paleomagnetic studies. Several studies now appear to highlight a geological similarity between the Kaapvaal Craton and the Pilbara Craton with that of Superia (Bleeker et al., 2016), which is aided by the near-equatorial paleo-latitudes of the ca. 2426 Ma Kaapvaal Craton (Evans et al., 1997), with that of the Superior Craton at ca. 2460 Ma (Bates and Halls, 1990; Bleeker et al., 2015). All these cratons form the core of a newly proposed supercraton, which we term 'Supervaalbara'. This supercraton incorporates Superia and Vaalbara, which share a similar granitoid(granitic gneiss)-greenstone terrane of the eastern Kaapvaal Craton, together with the core of the Wyoming Craton and the Minnesota River Valley terrane of the Superior Craton (Bleeker et al., 2016) and possibly the Kola-Karelia Craton. All these terranes share a fundamentally similar 3.7-3.2 Ga magmatic history, and are a high-μ domains of Eo- to Mesoarchean crust that document a peak in magmatism and metamorphism at 2.60 Ga during the growth of the Supervaalbara landmass.

Numerous other geological similarities exist between the cratons in the Supervaalbara landmass, and include the 2713-2703 Ma Stillwater Complex (Premo et al., 1990) on the Wyoming Craton, which can be compared with dykes within the Rykoppies mafic dyke swarm in the Kaapvaal Craton (Olsson et al., 2011, 2010). This dyke swarm is related to volcanism within the upper Ventersdorp Supergroup (Armstrong et al., 1991). The massive amount of volcanism, preserved in LIPs across the Supervaalbara Craton in the 2510-2440 Ma time interval may be related to deposition of banded iron formation preserved in the Kaapvaal, Pilbara and Samartia cratons in the 2440-2420 Ma time interval (e.g., Konhauser et al., 2017). This is due to Supervaalbara straddling the equator at this time, and undergoing weathering and erosion of the LIPs (e.g., Bleeker et al., 2016; Gumsley et al., 2017). Layers of tuffs within both the iron formations of the Kaapvaal Craton and that of the Pilbara Craton provide evidence of Matachewan LIP magmatism from the lower Huronian Supergroup on the Superior Craton fueling this volcanism (Bleeker et al., 2015), while banded iron formation was deposited synchronously (e.g., Trendall et al., 1990). Later, the basalts in the ≤2250-2240 Ma Hekpoort Formation (Schröder et al., 2016) of the upper Transvaal Supergroup may represent the extrusive equivalent of 2210-2220 Ma Nipissing-Karjalitic sill province (Corfu and Andrews, 1986), and ca. 2208 Ma sills documented within the Pilbara Craton. These mafic sills may also be the equivalent of the Cheela Springs flood basalts (Müller et al., 2005). The biggest enigma concerns the 2056-2055 Ma Bushveld Complex. No coeval satellite mafic dykes or sills reported from Bushveld Complex have been on any other craton, although some potentially coeval mineralizing systems of similar ages are reported in the Kola-Karelia Craton.

The reconstruction of Supervaalbara is almost fully compatible with existing paleomagnetic constraints. Establishing an apparent polar wander path between the Kaapvaal Craton and the Superior Craton, there is good continuity between key paleomagnetic poles established at 2460-2450 Ma from the Superior Craton and at 2426 Ma from the Kaapvaal Craton. However, the paleomagnetic poles for igneous rocks of the Hekpoort Formation and Nipissing LIP magmatic events do not agree, although the Hekpoort Formation paleopole only represents a VGP, and needs further resolution. The ca. 2170 Ma Biscotasing LIP had no equivalent on the Kaapvaal Craton, until the work of Larsson (2015), which established the magmatic event also occurs on the Kaapvaal Craton, and may actually define Hekpoort Formation volcanism. Paleopoles on the Superior Craton between 2126 Ma and 2060 Ma shows broad similarities to the Bushveld Complex paleopole on the Kaapvaal Craton. Also, similarities exist between paleopoles existing between the upper Waterberg Group on the Kaapvaal Craton and the Circum-Superior LIP on the Superior Craton at 1870 Ma. Equivalents of the Hartley Formation and its associated LIP on the Superior Craton remain to be found, however. In addition, the recent work of Kumar et al. (2017) shows the broad geochronological and paleomagnetic similarity between the Kaapvaal Craton with that of Singhbhum Craton in India at 2.81-2.77 Ga. This demonstrates that the Singhbhum Craton was also likely part of Supervaalbara at this time. Another potential part of Supervaalbara is the Sarmatia Block (Savko et al., 2017), which shares many geological similarities, and does not make the Kaapvaal Craton to Pilbara Craton connection necessarily unique, but part of a much larger geological framework.

7. Outlook and reflection

Within the advances since the 1990's of geochronological methods and techniques, the ability to establish accurate and precise crystallization ages of mafic rocks is steadily improving. Innovative new in-situ techniques to date smaller and smaller crystals of baddeleyite and zircon are also now being employed. With the addition of multi-proxy approaches, including detrital zircon provenance studies as well as other geological and paleomagnetic constraints, the puzzle-pieces of Earth's cratons are increasingly being refined in terms of their paleogeography, even into the Neoarchean and Paleoproterozoic. This time period reflects the now known reasonable limit for most reliable paleogeographic reconstructions. However, with these new analytical developments, an increasing complexity is also being realized in our geological and paleogeographic understanding. As one door closes, another two (or three) open, so to speak.

The existence of LIPs, for example, as traditionally defined by Coffin and Eldholm (1993) is now routinely challenged through increasing amounts of accurate high precision geochronological data. Some dyke swarms and sill provinces thought to be associated with short-lived LIPs are now known thought to be more long-lived magmatic events. An obvious example is the Matachewan mafic dyke swarm on the Superior Craton. The Matachewan dyke swarm is sufficiently large enough to be a LIP, but is now known to have intruded over a 50-million-year time interval from 2500 Ma to 2450 Ma. It likely includes bi-modal volcanic rocks located at the base of the Huronian Supergroup (Bleeker et al., 2015). Short-lived LIPs still exist, with for instance the Bushveld, Umkondo and Karoo LIPs all standing up to the geochronological test of time on the Kaapvaal Craton. However, only better age constraints, matched with geochemical and numerical modelling can help us better understand all such mafic magmatic events, and what makes a dyke or sill event either long- or short-lived, and whether it is a reflection of underlying mantle dynamics. Also, dyke swarms of a single geographical orientation (trend) have, for example, been demonstrated to be composite in age (e.g, Jourdan et al., 2006), with up to three generations of dykes present in a single swarm. The overall trend of a dyke swarm is still crucial to know, however, as structural features such as lineaments in the basement may control the local trend of a single dyke, without invalidating the general trend. This can be observed through use of satellite images, for example. Studying such composite dyke swarms is challenging but necessary in order to further the science. By combining geochemistry and paleomagnetism with increasing amounts of geochronological data can help to address these complexities, and also addresses the petrogenesis of LIPs themselves. This remains another controversial point, especially whether LIPs are generated by mantle plumes or not, but can be further addressed in more research on LIPs. Mantle plumes form another debate, and although they may be long-lived, they are also transient and generate hot spot tracks. This usually cannot be observed in the geological record, but it can be assumed that a plume only records short-lived magmatic pulses in one locality before migrating due to the movement of the overriding tectonic plates.

Increasingly, geochemical and paleomagnetic studies in mafic dyke swarms and sill provinces without age constraints can yield complex and meaningless results as the data set might contain a mixture of unrelated magmatic events or periods. This complication occurs because of either contamination from the host rock (e.g., Gumsley et al., 2016) or more likely by combining geochemical studies unknowingly of dykes or sills of different ages. Paleomagnetically, overprinting of the primary magnetic component of a dyke generation by dykes of a younger generation within the same swarm can also lead to confusing or complex sets of results (e.g., Lubnina et al., 2010). A good strategy moving forward would be to sample a representative number of mafic dykes and sills for quick reconnaissance age dating. With knowledge of the different generations of dyke swarms and sill provinces present, complete high-precision age dating can be made on selected mafic dykes and sills of each generation. This can then finally be followed up with complimentary geochemical or paleomagnetic studies on the wider swarm, depending on how composite it is in nature.

Mafic dykes and sills can also be linked with volcanic successions preserved within the stratigraphy, and can assist in providing direct high-precision ages to that succession if they can be definitively linked, and not just relative age relationships. Such a study was presented by Gumsley et al. (2017), with a combination of ID-TIMS dating on the volcanic feeders and in-situ SIMS analysis on the volcanic succession itself for the Ongeluk Formation of the Kaapvaal Craton. This was further complimented with paleomagnetic studies, which further demonstrated the linkage. Such age dating can be important with sequence stratigraphy, with very far-reaching implications. In addition, mafic dykes and sills as essential components of LIPs, which can be linked to environmentsl catastrophies ranging from mass extinctions to global glaciations and the rise of both atmospheric oxygenation and tmulti-cellular life. All appear to be built into the Supercontinent Cycle, and will become better and better understood with time with further new geochronological constraints to validate its relationship with true polar wander.

As for the existence of Vaalbara, although it is not immediately obvious as to whether it existed, it now appears more likely that a large continent was present during the Neoarchean to Paleoproterozoic, which we term herein, Supervaalbara. This large continent appears fundamentally different from the 'Rae' continent of Pehrsson et al. (2013), and appears, at least in part, to support the existence of the 'clans of cratons' proposed by Bleeker (2003). With the aid of new databases, including PALEOMAGIA (Veikkolainen et al., 2014), and the variety of geospatial databases, conclusions are beginning to be made aided by high-precision ages and paleomagnetic constraints, which have been realized in projects like the Supercontinent Project (www.supercontinent.org) and IGCP 648. These projects aim to test new limits of supercontinents, their paleogeography, and the links both with mantle dynamics, as well as with the evolving Earth system. However, such databases are only as strong as the data within them, and strict quality criteria are now needed both for geochronological and paleomagnetic data, which is not as commonly implemented as it should. Reliability criteria is needed for geochronological data in a similar way that has already been defined for paleomagnetic data (e.g., van der Voo, 1990; Buchan, 2013).

With the realization of these goals, it should be possible to retrieve at least a partial picture of Earth's first supercontinent, or clan of cratons. With this, a better understanding of the world that exists today will begin to emerge, and the processes that led to its formation.

8. Summary of papers

The following papers form the basis of this dissertation. They are arranged in chronological succession, and each paper is accompanied by a summary of central results and conclusions.

8. 1. Paper I

Gumsley, A., Olsson, J., Söderlund, U., de Kock, M., Hofmann, A., Klausen, M., 2015, Precise U-Pb baddeleyite age dating of the Usushwana Complex, southern Africa–Implications for the Mesoarchaean magmatic and sedimentological evolution of the Pongola Supergroup, Kaapvaal Craton. *Precambrian Research* **267**, 174-185.

This paper presents new geochronological data from the Usushwana Complex. It is established than the Usushwana Complex is almost 130 million years older than previously thought, and is actually composed of two separate mafic magmatic events related to either the Pongola Supergroup magmatic event from 2990-2960 million years ago, and the Hlagothi Complex at 2870 million years ago. The new ages have implications for the Pongola Supergroup on the Kaaapvaal Craton, with magmatism appearing to be dispersed in two main pulses in the Nsuze Group (Pongola Supergroup).

8.2. Paper II

Kampmann, T.C., Gumsley, A.P., de Kock, M.O., Söderlund, U., 2015, U–Pb geochronology and paleomagnetism of the Westerberg Sill Suite, Kaapvaal Craton–Support for a coherent Kaapvaal–Pilbara Block (Vaalbara) into the Paleoproterozoic? *Precambrian Research* **269**, 58-72.

In this paper, the first identification of 2441-2426 Ma magmatic rocks on the western Kaapvaal Craton is presented from the Westerberg Sill Province in the Transvaal Supergroup. These rocks were studied paleomagnetically and geochronologically, and it is speculated whether the Westerberg Sill Province is related to the Ongeluk Formation owing to similar paleomagnetic characteristics. Also, similarities to the Woongaara large igneous province on the Pilbara Craton are discussed, with more questions than answers.

8.3. Paper III

Gumsley, A., Rådman, J., Söderlund, U., Klausen, M., 2016, U–Pb baddeleyite geochronology and geochemistry of the White Mfolozi Dyke Swarm: unravelling the complexities of 2.70–2.66 Ga dyke swarms across the eastern Kaapvaal Craton, South Africa. *GFF* **13**, 115-132

This paper presents geochronology and geochemical constraints on a newly recognized dyke swarm on the south-easternmost Kaapvaal Craton, the White Mfolozi mafic dyke swarm. This new swarm appears to intrude into the craton in the waning stages of another radial dyke swarm located further to the north on the eastern margin of the Kaapvaal Craton which intruded 2.70-2.66 billion years ago. However, the geochemistry of this dyke swarm differs significantly from the radial dyke swarm located further north. It has more primitive chemical signatures, unlike those further north, which is more enriched, with enrichment quite likely due to contamination from the basement host rock.

8.4. Paper IV

Alebouyeh Semami, F., de Kock, M., Söderlund, U., Gumsley, A., da Silva, R., Beukes, N., Armstrong, R., 2016, New U–Pb geochronologic and palaeomagnetic constraints on the late Palaeoproterozoic Hartley magmatic event: evidence for a potential large igneous province in the Kaapvaal Craton during Kalahari assembly, South Africa. *GFF* **138**, 164-168.

This paper presents a new mafic dyke swarm on the western Kaapvaal Craton, termed the Tsineng dyke swarm, which intruded 1.92 billion years ago. This dyke swarm is coeval with the Hartley Formation volcanic rocks and establishes a possible new large igneous province, aided by detrital zircon provenance studies, which are also presented in this paper. Refined geochronologicand paleomagnetic constraints presented in paper for the Hartley Formation refine the late Paleoproterozoic apparent polar wander path of the Kaapvaal Craton, with implications for red bed successions across the craton at this time.

8.5. Paper V

Gumsley, AP., Chamberlain, K.R., Bleeker, W., Söderlund, U., de Kock, M.O., Larsson, E.R., Bekker, A., 2017, Timing and tempo of the Great Oxidation Event. *Proceedings of the National Academy of Sciences of the United States of America* **114**, 1811-1816

This paper provides geochronological and paleomagnetic constraints on the newly identified Ongeluk large igneous province. This includes both ID-TIMS and SIMS U-Pb mass spectrometry on baddeleyite, both on separated material and in-situ on thin sections. The new results make the Ongeluk Formation nearly two hundred million years older than previously thought at 2.43 billion years ago, and demands a stratigraphic revision of the Transvaal Supergroup on the Kaapvaal Craton. It also established that the Great Oxidation Event and Earth's first global glaciation occurred at approximately 2.43 billion years ago, and was part of an oscillatory cycle of oxygenation over the Paleoproterozoic in junction with glaciation which is very similar to similar events in the Neoproterozoic.

8.6. Paper VI

Evans, D.A.D., Smirnov, A.V., Gumsley, A.P., 2017, Paleomagnetism and U–Pb geochronology of the Black Range dykes, Pilbara Craton, Western Australia: a Neoarchean crossing of the polar circle. *Australian Journal of Earth Sciences* **64**(2), 225-237

This paper presents new geochronology and paleomagnetic constraints on the Black Range mafic dyke swarm in the Pilbara Craton. The new temporal and spatial constraints show that the Black Range dykes both intrude and cross-cut the Mount Roe flood basalts, demanding new revisions to either the stratigraphy or geological mapping of the lower Fortescue Group. The new paleopole established for the Black Range dykes establishes a new apparent polar wander path for the Pilbara Craton as it transitions from the equator and across the pole regions in the Neoarchean.

9. Acknowledgements

A doctoral thesis is the accumulation of a large amount of data, and in the case of Sweden, is the accumulation of papers in several sub-projects which aim to resolve the much bigger hypothesis which needs to be tested. Such projects are not possible without the help and assistance a doctoral candidate receives over his or her past four years.

To start with, I wish to thank Ulf Söderlund, my principal supervisor. I cannot stress how much help I have received from you. You have been the best possible supervisor, both in providing assistance and encouragement, as well as giving me a lot of freedom to pursue my own ideas and collaborations, and for that I am very grateful. You also always kept up the pressure of on me in the most constructive of ways. Ulf, you will always be a good mentor and friend to me, and I will miss those Friday beers at Gloria's or Valvet, or you reminding me how DAMNNN GOOD you are. I know, I know, it's true…

I also wish to thank Michiel de Kock, my co-supervisor and friend in South Africa. You has been increasingly busy with both family and administration over the last four years, but you were always available for my calls, and to share ideas about geology with, and to provide some up-to-date thoughts on what is happening in our world of the Kaapvaal Craton. You inspired me throughout my master's and doctoral work, and I hope for many more years of successful collaboration, both with yourself and Ulf. Thank you! I also have to thank David Evans from Yale University who has really assisted me with everything related to the Pilbara Craton, as Michiel did for the Kaapvaal. He helped me in both the field and the laboratory, and welcomed me into his own home during my stay at Yale, for which I was really grateful. In many ways, you felt like a co-supervisor to me, even if it was only unofficially, and I really appreciate all the brilliant ideas you have.

I have also had the priveledge to co-operate with some of the leading scientists in the large igneous province community and beyond, including among others, Martin Klausen, Axel Hoffman, Wouter Bleeker, Kevin Chamberlain, Richard Ernst, Aleksey Smirnov, Herwe Wabo and Andrey Bekker. You have all assisted me a lot in my various projects and I really couldn't have asked for a nicer community to work with!

From the Department of Geology in Lund, I have to send my thanks to all the staff from the bedrock and quarternary divisions for all the support and friendship over the years. The brilliant Anders, to crazy Carl, Lotta, Tomas, Leif, Mats, Johan, Per, Sylvain, Vivi, Svetlana and Mikael. The same goes to all the Ph.D students who passed through: Johan, Mimmi, Vicky, Lorraine, Andreas, Sanna, Elisabeth, Karolina and Kristina. A special mention of course has to go to my office mates, who are some of the craziest people who I know, but who I love completely: Johan, Anders, and Maria. I could not have asked for better office mates, who tolerate all the insults I throw at them daily basis, and who reply with just a smile and a middle finger. All the people on the floors above me, past and present, you are all great too, although I don't understand what half of you do up there?! :-) You are all good company, and that is all that matters! You know who you are, and I have many enjoyed evenings at the department, at sittnings, and Friday beers with you. Special thank yous to Florian, Guiliaume, Edyta and Petra for all the good times.

I also wish to thank students and staff at UCLA, Yale, UJ and UWA for all the support and assistance they provided, as well as the staff at the Department of Geosciences at the Swedish Museum of Natural History. My work up at the museum would not have been possible without you. Thank you! I must not forget the master's students I co-supervised along the way: Farnaz, Johan, Emilie, and Joaen, who become good friends, and aided in my work. Lastly, many thanks to all the financial, administrative and technical staff at the Department of Geology at Lund University, who were always willing to help, and without who life in the Department would have been much harder.

My thesis work has also would not have been possible without financial support. I am indebted to both the Swedish Research Council through a grant to Ulf Söderlund, and the Royal Physiographic Society in Lund provided me with grants and travel grants which made this work possible. I am also grateful to both the Bokelunds Foundation which administers travel grants to the Faculty of Science in Lund, as well as the Nordic Council and European Union who provided funds for various conferences, courses and summer schools I was lucky enough to have been financed for in my time as a student at Lund University.

10. References

Alebouyeh Semami, F., de Kock, M., Söderlund, U., Gumsley, A., da Silva, R., Beukes, N., Armstrong, R., 2016: New U–Pb geochronologic and palaeomagnetic constraints on the late Palaeoproterozoic Hartley magmatic event: evidence for a potential large igneous province in the Kaapvaal Craton during Kalahari assembly, South Africa. *GFF* **138**, 164–182.

Altermann, W., Nelson, D.R., 1998: Sedimentation rates, basin analysis and regional correlations of three Neoarchaean and Palaeoproterozoic sub-basins of the Kaapvaal craton as inferred from precise U-Pb zircon ages from volcaniclastic sediments. *Sedimentary Geology* **120**, 225–256.

Anhaeusser, C.R., Mason, R., Viljoen, M.J., Viljoen, R.P., 1969: A Reappraisal of Some Aspects of Precambrian Shield Geology. *Geological Society of America Bulletin* **80**, 2175–2200.

Armstrong, R.A., Compston, W., Retief, E.A., Williams, I.S., Welke, H.J., 1991. Zircon ion microprobe studies bearing on the age and evolution of the Witwatersrand triad. *Precambrian Research* 53, 243–266.

Arndt, N.T., Nelson, D.R., Compston, W., Trendall, A.F., Thorne, A.M., 1991: The age of the Fortescue Group, Hamersley Basin, Western Australia, from ion microprobe zircon U-Pb results. *Australian Journal of Earth Sciences* **38**, 261–281.

Aspler, L.B., Chiarenzelli, J.R., 1998. Two Neoarchean supercontinents? Evidence from the Paleoproterozoic. *Sedimentary Geology* **120**, 75–104.

Barnes, S.J., Hoatson, D.M., 1994: The Munni Munni Complex, Western Australia: Stratigraphy, Structure and Petrogenesis. *Journal of Petrology* **35**, 715–751.

Barton, J.M., Blignaut, E., Salnikova, E.B., Kotov, A.B., 1995: The stratigraphical position of the Buffelsfontein group based on field relationships and chemical and geochronological data. *South African Journal of Geology* **98**, 386–392.

Bates, M.P., Halls, H.C., 1990: Regional variation in paleomagnetic polarity of the Matachewan dyke swarm related to the Kapuskasing Structural Zone, Ontario. *Canadian Journal of Earth Sciences* **27**, 200–211.

Bau, M., Romer, R.L., Lüders, V., Beukes, N.J., 1999: Pb, O, and C isotopes in silicified Mooidraai dolomite (Transvaal Supergroup, South Africa): implications for the composition of Paleoproterozoic seawater and "dating" the increase of oxygen in the Precambrian atmosphere. *Earth and Planetary Science Letters* **174**, 43–57.

Bekker, A., Kaufman, A.J., 2007: Oxidative forcing of global climate change: A biogeochemical record across the oldest Paleoproterozoic ice age in North America. *Earth and Planetary Science Letters* **258**, 486–499.

Beukes, N.J., 1984: Sedimentology of the Kuruman and Griquatown iron-formations, Transvaal Supergroup, Griqualand West, South Africa. *Precambrian Research* **24**, 47–84.

Beukes, N.J., Gutzmer, J., 2008: Origin and Paleoenvironmental Significance of Major Iron Formations at the Archean-Paleoproterozoic Boundary. *In:* S. Hagemann, C. Rosière, J. Gutzmer,, N.J. Beukes (eds.), *Band Iron Formation-Related High-Grade Ore*, 5–47. Society of Economic Geologists, Littleton.

Blake, T.S., Buick, R., Brown, S.J.A., Barley, M.E., 2004: Geochronology of a Late Archaean flood basalt province in the Pilbara Craton, Australia: constraints on basin evolution, volcanic and sedimentary accumulation, and continental drift rates. *Precambrian Research* **133**, 143–173.

Bleeker, W., 2003: The late Archean record: a puzzle in ca. 35 pieces. *Lithos* **71**, 99–134.

Bleeker, W., Chamberlain, K., Kamo, S., Kilian, T., Buchan, K., 2016: Kaapvaal, Superior and Wyoming: nearest neighbours in supercraton Superia. *In: 35th International Geological Congress*, Cape Town.

Bleeker, W., Ernst, R., 2006: Short-lived mantle generated magmatic events and their dyke swarms: the key unlocking Earth's paleogeographic record back to 2.6 Ga. *In:* E. Hanski, S. Mertanen, T. Rämö, J. Vuollo (eds.), *Dyke Swarms - Time Markers of Crustal Evolution*, 3-26. Taylor & Francis, London.

Bleeker, W., Kamo, S.L., Ames, D.E., Davis, D., 2015: New field observations and U-Pb ages in the Sudbury area: toward a detailed cross-section through the deformed Sudbury Structure. *Geological Survey of Canada*, **Open File 7856**, 151–166.

Buchan, K.L., 2013: Key paleomagnetic poles and their use in Proterozoic continent and supercontinent reconstructions: A review. *Precambrian Research* **238**, 93–110.

Button, A., 1979: Transvaal and Hamersley Basins - review of basin development and mineral deposits. *Mineral Science Engineering* **76**, 229–247.

Chamberlain, K.R., Schmitt, A.K., Swapp, S.M., Harrison, T.M., Swoboda-Colberg, N., Bleeker, W., Peterson, T.D., Jefferson, C.W., Khudoley, A.K., 2010: In situ U-Pb SIMS (IN-SIMS) micro-baddeleyite dating of mafic rocks: Method with examples. *Precambrian Research* **183**, 379–387.

Cheney, E.S., 1996: Sequence stratigraphy and plate tectonic significance of the Transvaal succession of southern Africa and its equivalent in Western Australia. *Precambrian Research* **79**, 3–24.

Coffin, M.F., Eldholm, O., 1994: Large igneous provinces: Crustal structure, dimensions, and external consequences. *Reviews of Geophysics* **32**, 1–36.

Condie, K.C., 1998: Episodic continental growth and supercontinents: a mantle avalanche connection? *Earth and Planetary Science Letters* **163**, 97–108.

Condie, K.C., Aster, A.C., 2010: Episodic zircon age spectra of orogenic granitoids: The supercontinent connection and continental growth. *Precambrian Research* **180**, 227–236.

Corfu, F., Andrews, A.J., 1986: A U–Pb age for mineralized Nipissing diabase, Gowganda, Ontario. *Canadian Journal of Earth Science* **23**, 107–109.

Cornell, D.H., Schütte, S.S., Eglington, B.L., 1996: The Ongeluk basaltic andesite formation in Griqualand West, South Africa: submarine alteration in a 2222 Ma Proterozoic sea. *Precambrian Research* **79**, 101–123.

Courtillot, V., Jaupart, C., Manighetti, I., Tapponier, P., Besse, J., 1999: On causal links between flood basalts and continental breakup. *Earth and Planetary Science Letters* **166**, 177–195.

Creer, K.M., Irving, E., Runcorn, S.K., 1954: The Direction of the Geomagnetic Field in Remote Epochs in Great Britain. *Journal of Geomagnetism and Geoelectricity* **6**, 163–168.

de Kock, M.O., Beukes, N.J., Armstrong, R.A., 2012: New SHRIMP U–Pb zircon ages from the Hartswater Group, South Africa: Implications for correlations of the Neoarchean Ventersdorp Supergroup on the Kaapvaal craton and with the Fortescue Group on the Pilbara craton. *Precambrian Research* **204–205**, 66–74.

de Kock, M.O., Evans, D.A.D., Beukes, N.J., 2009: Validating the existence of Vaalbara in the Neoarchean. *Precambrian Research* **174**, 145–154.

de Wit, M.J., Roering, C., Hart, R.J., Armstrong, R.A., de Ronde, C.E.J., Green, R.W.E., Tredoux, M., Peberdy, E., Hart, R.A., 1992: Formation of an Archaean continent. *Nature* **357**, 553–562.

Denyszyn, S.W., Feinberg, J.M., Renne, P.R., Scott, G.R., 2013: Revisiting the age and paleomagnetism of the Modipe Gabbro of South Africa. *Precambrian Research* **238**, 176–185.

Domeier, M., van der Voo, R., Torsvik, T.H., 2012. Paleomagnetism and Pangea: The road to reconciliation. *Tectonophysics* **514–517**, 14–43.

Eglington, B.M., Armstrong, R.A., 2004: The Kaapvaal Craton and adjacent orogens, southern Africa: a geochronological database and overview of the geological development of the craton. *South African Journal of Geology* **107**, 13–32.

Embleton, B.J.J., 1978: The palaeomagnetism of 2400 m.y. old rocks from the Australian Pilbara craton and its relation to Archaean-Proterozoic tectonics. *Precambrian Research* **6**, 275–291.

Eriksson, P.G., Altermann, W., Hartzer, F.J., 2006: The Transvaal Supergroupand and its precursors. *In:* M.J. Johnson, C.R. Anhaeusser, R.J. Thomas (eds.), *The Geology of South Africa*, 237-260, Geological Society of South Africa/Council for Geoscience, Johannesburg/Pretoria.

Ernst, R., Bleeker, W., 2010: Large igneous provinces (LIPs), giant dyke swarms, and mantle plumes: significance for breakup events within Canada and adjacent regions from 2.5 Ga to the Present. *Canadian Journal of Earth Sciences* **47**, 695–739.

Ernst, R.E., 2014: *Large Igneous Provinces*. Cambridge University Press, Cambridge.

Evans, D.A., Beukes, N.J., Kirschvink, J.L., 1997: Low-latitude glaciation in the Palaeoproterozoic era. *Nature* **386,** 262–266.

Evans, D.A.D., Smirnov, A.V., Gumsley, A.P., 2017: Paleomagnetism and U–Pb geochronology of the Black Range dykes, Pilbara Craton, Western Australia: a Neoarchean crossing of the polar circle. A*ustralian Journal of Earth Sciences* **64**, 225–237.

Fairey, B., Tsikos, H., Corfu, F., Polteau, S., 2013: U-Pb systematics in carbonates of the Postmasburg Group, Transvaal Supergroup, South Africa: Primary versus metasomatic controls. *Precambrian Research* **231**, 194–205.

Foulger, G.R., Natland, J.H., 2003: Is "Hotspot" Volcanism a Consequence of Plate Tectonics? *Science* **300**, 921–922.

French, J.E., Heaman, L.M., 2010: Precise U–Pb dating of Paleoproterozoic mafic dyke swarms of the Dharwar craton, India: Implications for the existence of the Neoarchean supercraton Sclavia. *Precambrian Research* **183**, 416–441.

Grobler, D.F., Walraven, F., 1993: Geochronology of Gaborone Granite Complex extensions in the area north of Mafikeng, South Africa. *Chemical Geology* **105**, 319–337.

Gumsley, A., Olsson, J., Söderlund, U., de Kock, M., Hofmann, A., Klausen, M., 2015: Precise U-Pb baddeleyite age dating of the Usushwana Complex, southern Africa - Implications for the Mesoarchaean magmatic and sedimentological evolution of the Pongola Supergroup, Kaapvaal Craton. *Precambrian Research* **267**, 174–185.

Gumsley, A.P., Chamberlain, K.R., Bleeker, W., Söderlund, U., de Kock, M.O., Larsson, E.R., Bekker, A., 2017: Timing and tempo of the Great Oxidation Event. *Proceedings of the National Academy of Sciences of the United States of America* **114**, 1811–1816.

Gumsley, A.P., de Kock, M.O., Rajesh, H.M., Knoper, M.W., Söderlund, U., Ernst, R.E., 2013: The Hlagothi Complex: The identification of fragments from a Mesoarchaean large igneous province on the Kaapvaal Craton. *Lithos* **174**, 333–348.

Gumsley, A.P., Rådman, J., Söderlund, U., Klausen, M.B., 2016: U–Pb baddeleyite geochronology and geochemistry of the White Mfolozi Dyke Swarm: unravelling the complexities of 2.70–2.66 Ga dyke swarms across the eastern Kaapvaal Craton, South Africa. *GFF* **138**, 115–132.

Hall, C.E., 2005: SHRIMP U – Pb depositional age for the lower Hardey Formation: evidence for diachronous deposition of the lower Fortescue Group in the southern Pilbara region, Western Australia. *Australian Journal of Earth Sciences* **52**, 403–410.

Hannah, J.L., Bekker, A., Stein, H.J., Markey, R.J., Holland, H.D., 2004: Primitive Os and 2316 Ma age for marine shale: implications for Paleoproterozoic glacial events and the rise of atmospheric oxygen. *Earth and Planetary Science Letters* **225**, 43–52.

Hanson, R.E., Gose, W.A., Crowley, J.L., Ramezani, J., Bowring, S.A., Bullen, D.S., Hall, R.P., Pancake, J.A., Mukwakwami, J., 2004: Paleoproterozoic intraplate magmatism and basin development on the Kaapvaal Craton: Age, paleomagnetism and geochemistry of ~1.93 to ~1.87 Ga post-Waterberg dolerites. *South African Journal of Geology* **107**, 233–254.

Hawkesworth, C., Cawood, P., Kemp, T., Storey, C., Dhuime, B., 2009: Geochemistry: a matter of preservation. *Science* **323**, 49–50.

Hawkesworth, C.J., Dhuime, B., Pietranik, A.B., Cawood, P.A., Kemp, A.I.S., Storey, C.D., 2010: The generation and evolution of the continental crust. *Journal of the Geological Society*. **167**, 229–248.

Heaman, L.M., LeCheminant, A.N., 1993: Paragenesis and U-Pb systematics of baddeleyite (ZrO_2). *Chemical Geology* **110**, 95–126.

Hegner, E., Kröner, A., Hofmann, A.W., 1984: Age and isotope geochemistry of the Archaean Pongola and Usushwana suites in Swaziland, southern Africa: a case for crustal contamination of mantle-derived magma. *Earth and Planetary Science Letters* **70**, 267–279.

Hoatson, D.M., Sun, S.-S., 2002: Restricted access Archean Layered Mafic-Ultramafic Intrusions in the West Pilbara Craton, Western Australia: A Synthesis of Some of the Oldest Orthomagmatic Mineralizing Systems in the World. *Economic Geology* **97**, 847–872.

Hoffman, P.F., 2013: The Great Oxidation and a Siderian snowball Earth: MIF-S based correlation of Paleoproterozoic glacial epochs. *Chemical Geology 362*, 143–156.

Hoffman, P.F., 1997: Tectonic genealogy of North America. *In:* B.A. Van der Pluijm, S. Marshak (eds.), *An Introduction to Structural Geology and Tectonics,* 459–464, McGraw-Hill, New York.

Humbert, F., Sonnette, L., de Kock, M.O., Robion, P., Horng, C.S., Cousture, A., Wabo, H., 2017: Palaeomagnetism of the early Palaeoproterozoic, volcanic Hekpoort Formation (Transvaal Supergroup) of the Kaapvaal craton, South Africa. *Geophysical Journal International* **209**, 842–865.

Ibanez-Mejia, M., Gehrels, G.E., Ruiz, J., Verwoort, J.D., Eddy, M.P., Li, C., 2014: Small-volume baddeleyite (ZrO_2) U–Pb geochronology and Lu–Hf isotope geochemistry by LA-ICP-MS. Techniques and applications. *Chemical Geology* **384**, 149–167.

Jaffey, A.H., Flynn, K.F., Glendenin, L.E., Bentley, W.C., Essling, A.M., 1971: Precision measurement of half-lives and specific activities of U235 and U238. *Physical Review C* 4, 1889–1906.

Johansson, Å., 2009: Baltica, Amazonia and the SAMBA connection—1000 million years of neighbourhood during the Proterozoic? *Precambrian Research* **175**, 221–234.

Jones, D.L., Bates, M.P., Li, Z.X., Corner, B., Hodgkinson, G., 2003: Palaeomagnetic results from the ca. 1130 Ma Borgmassivet intrusions in the Ahlmannryggen region of Dronning Maud Land, Antarctica, and tectonic implications. *Tectonophysics* **375**, 247–260.

Jourdan, F., Feraud, G., Bertrand, H., Watkey, M.K., Kampunzu, A.B., Le Gall, B., 2006: Basement control on dyke distribution in Large Igneois Provinces: Case study of the Karoo triple junction. *Earth and Planetary Science Letters* **241**, 307–322.

Kampmann, T.C., Gumsley, A.P., de Kock, M.O., Söderlund, U., 2015: U-Pb geochronology and paleomagnetism of the Westerberg Sill Suite, Kaapvaal Craton - Support for a coherent Kaapvaal-Pilbara Block (Vaalbara) into the Paleoproterozoic? *Precambrian Research* **269**, 58–72.

Kilian, T.M., Bleeker, W., Chamberlain, K., Evans, D.A.D., Cousens, B., 2016: Palaeomagnetism, geochronology and geochemistry of the Palaeoproterozoic Rabbit Creek and Powder River dyke swarms : implications for Wyoming in supercraton Superia. *Geological Society, London, Special Publications* **424**, 15–45.

Kirschvink, J.L., 1980: The least-squares line and plane and the analysis of paleomagnetic data. *Geophysical Journal International* **62**, 699–718.

Konhauser, K.O., Planavsky, N.J., Hardisty, D.S., Robbins, L.J., Warchola, T.J., Haugaard, R., Lalonde, S.V., Partin, C.A., Oonk, P.B.H., Tsikos, H., Lyons, T.W., Bekker, A., Johnson, C.M., 2017: Iron formations: A global record of Neoarchaean to Palaeoproterozoic environmental history. *Earth-Science Reviews* **172**, 140–177.

Krapez, B., Barley, M.E., 1987: Archaean strike-slip faulting and related ensialic basins: evidence from the Pilbara Block, Australia. *Geological Magazine* **124**, 555–567.

Krogh, T.E., Corfu, F., Davis, D.W., Dunning, G.R., Heaman, L.M., Kamo, S.L., Machado, N., Greenough, J.D., Nakamura, E., 1987: Precise U–Pb isotopic ages of diabase dykes and mafic to ultramafic rocks using trace amounts of baddeleyite and zircon. *Geological Association of Canada, Special Publications* **34**, 147–152.

Kumar, A., Parashuramulu, V., Shankar, R., Besse, J., 2017: Evidence for a Neoarchean LIP in the Singhbhum craton, eastern India: Implications to Vaalbara supercontinent. *Precambrian Research* 292.

Larsson, E.R., 2015: *U-Pb baddeleyite dating of intrusions in the south-eastermost Kaapvaal Craton (South Africa): revealing multiple events of dyke emplacement*. Master thesis (unpublished), Lund University.

Layer, P.W., Kröner, A., McWilliams, M., Burghele, A., 1988: Paleomagnetism and age of the Archean Usushwana Complex, southern Africa. *Journal of Geophysical Research, Solid Earth* **93**, 449–457.

Li, Z.X., Bogdanova, S.V., Collins, A.S., Davidson, A., De Waele, B., Ernst, R.E., Fitzsimons, I.C.W., Fuck, R.A., Gladkochub, D.P., Jacobs, J., Karlstrom, K.E., Lu, S., Natapov, L.M., Pease, V., Pisarevsky, S.A., Thrane, K., Vernikovsky, V., 2008: Assembly, configuration, and break-up history of Rodinia: A synthesis. *Precambrian Research* **160**, 179–210.

Lubnina, N., Ernst, R.E., Klausen, M., Söderlund, U., 2010: Paleomagnetic study of NeoArchean-Paleoproterozoic dykes in the Kaapvaal Craton. *Precambrian Research* **183**, 523–552.

Martin, D.M., Clendenin, C.W., Krapez, B., McNaughton, N.J., 1998: Tectonic and geochronological constraints on late Archaean and Palaeoproterozoic stratigraphic correlation within and between the Kaapvaal and Pilbara cratons. *Geological Society, London, Special Publications* **155**, 311–322.

McHone, J.G., 2000: Non-plume magmatism and rifting during the opening of the central Atlantic Ocean. *Tectonophysics* **316**, 287–296.

Moore, M., Davis, D.W., Robb, L.J., Jackson, M.C., Grobler, D.F., 1993: Archean rapakivi granite-anorthosite-rhyolite complex in the Witwatersrand basin hinterland, southern Africa. *Geology* **21**, 1031–1034.

Morgan, W.J., 1971: Convection plumes in the lower mantle. *Nature* **230**, 42–43.

Müller, S.G., Krapež, B., Barley, M.E., Fletcher, I.R., 2005: Giant iron-ore deposits of the Hamersley province related to the breakup of Paleoproterozoic Australia: New insights from in situ SHRIMP dating of baddeleyite from mafic intrusions. *Geology* **33**, 577–580.

Nelson, D.R., Trendall, A.F., Altermann, W., 1999: Chronological correlations between the Pilbara and Kaapvaal cratons. *Precambrian Research* **97**, 165–189.

Nelson, D.R., Trendall, A.F., de Laeter, J.R., Grobler, N.J., Fletcher, I.R., 1992: A comparative study of the geochemical and isotopic systematics of late archaean flood basalts from the Pilbara and Kaapvaal cratons. *Precambrian Research* **54**, 231–256.

Nilsson, M.K.M., 2016: *New constraints on paleoreconstructions through geochronology of mafic dyke swarms in North Atlantic Craton*. PhD thesis (unpublished), Lund University.

Nilsson, M.K.M., Söderlund, U., Ernst, R.E., Hamilton, M.A., Scherstén, A., Armitage, P.E.B., 2010: Precise U–Pb baddeleyite ages of mafic dykes and intrusions in southern West Greenland and implications for a possible reconstruction with the Superior craton. *Precambrian Research* **183**, 399–415.

Olsson, J.R., Klausen, M.B., Hamilton, M.A., März, N., Söderlund, U., Roberts, R.J., 2016: Baddeleyite U–Pb ages and gechemistry of the 1875–1835 Ma Black Hills Dyke Swarm across north-eastern South Africa: part of a trans-Kalahari Craton back-arc setting? *GFF* **138**, 183-202.

Olsson, J.R., Söderlund, U., Hamilton, M.A., Klausen, M.B., Helffrich, G.R., 2011: A late Archaean radiating dyke swarm as possible clue to the origin of the Bushveld Complex. *Nature Geoscience* 4, 865–869.

Olsson, J.R., Söderlund, U., Klausen, M.B., Ernst, R.E., 2010: U–Pb baddeleyite ages linking major Archean dyke swarms to volcanic-rift forming events in the Kaapvaal craton (South Africa), and a precise age for the Bushveld Complex. *Precambrian Research* **183**, 490–500.

Pehrsson, S.J., Berman, R.G., Eglington, B., Rainbird, R., 2013: Two Neoarchean supercontinents revisited: The case for a Rae family of cratons. *Precambrian Research* **232**, 27–43.

Personen, L.J., Elming, S.-Å., Mertanen, S., Pisarevsky, S.A., D'Agrella-Filho, M.S., Meert, J.G., Schmidt, P.W., Abrahamsen, N., Bylund, G., 2003: Palaeomagnetic configuration of continents during the Proterozoic. *Tectonophysics* **375**, 289–324.

Pickard, A.L., 2003: SHRIMP U-Pb zircon ages for the Palaeoproterozoic Kuruman Iron Formation, northern Cape Province, South Africa: Evidence for simultaneous BIF deposition on Kaapvaal and Pilbara cratons. *Precambrian Research* **125**, 275–315.

Pidgeon, R.T., 1984: Geochronological constraints on early volcanic evolution of the Pilbara Block, Western Australia. *Australian Journal of Earth Science* **31**, 237–242.

Piper, J.D.A., 2010: Protopangaea: Palaeomagnetic definition of Earth's oldest (mid-Archaean-Palaeoproterozoic) supercontinent. *Journal of Geodynamics* **50**, 154–165.

Piper, J.D.A., 1974: Proterozoic crustal distribution, mobile belts and apparent polar movements. *Nature* **251**, 381–384.

Polteau, S., Moore, J.M., Tsikos, H., 2006: The geology and geochemistry of the Palaeoproterozoic Makganyene diamictite. *Precambrian Research* **148**, 257–274.

Poujol, M., Kiefer, R., Robb, L.J., Anhaeusser, C.R., Armstrong, R.A., 2005: New U-Pb data on zircons from the Amalia greenstone belt Southern Africa: insights into the Neoarchaean evolution of the Kaapvaal Craton. *South African Journal of Geology* **108**, 317–332.

Premo, W.R., Helz, R.T., Zientek, M.L., Langston, R.B., 1990: U-Pb and Sm-Nd ages for the Stillwater Complex and its associated sills and dikes, Beartooth Mountains, Montana: Identification of a parent magma? *Geology* **18**, 1065-1068.

Rasmussen, B., Bekker, A., Fletcher, I.R., 2013: Correlation of Paleoproterozoic glaciations based on U-Pb zircon ages for tuff beds in the Transvaal and Huronian Supergroups. *Earth and Planetary Science Letters* **382**, 173–180.

Reddy, S.M., Evans, D.A.D., 2009: Palaeoproterozoic supercontinents and global evolution: correlations from core to atmosphere. *Geological Society, London, Special Publications* **323,** 1–26.

Rogers, J.J.W., 1996: A History of Continents in the past Three Billion Years. *Journal of Geology* **104**, 91–107.

Rogers, J.J.W., Santosh, M., 2002: Configuration of Columbia, a Mesoproterozoic Supercontinent. *Gondwana Research* **5**, 5–22.

Salminen, J., Halls, H.C., Mertanen, S., Pesonen, L.J., Vuollo, J., Söderlund, U., 2014: Paleomagnetic and geochronological studies on Paleoproterozoic diabase dykes of Karelia, East Finland-Key for testing the Superia supercraton. *Precambrian Research* **244**, 87–99.

Savko, K.A., Samsonov, A.V., Kholin, V.M., Bazikov, N.S., 2017: The Sarmatia megablock as a fragment of the Vaalbara supercontinent: Correlation of geological events at the Archean−Paleoproterozoic transition. *Stratigraphy and Geological Correlation* **25**, 123–145.

Schaltegger, U., Schmitt, A.K., Horstwood, M.S., 2015: U–Th–Pb zircon geochronology by ID-TIMS, SIMS, and laser ablation ICP-MS: Recipes, interpretations, and opportunities. *Chemical Geology* **402**, 89–110.

Schmidt, P.W., Embleton, B.J.J., 1985: Prefolding and overprint magnetic signatures in Precambrian (2.9–2.7 Ga) Igneous rocks from the Pilbara Craton and Hamersley Basin, NW Australia. J*ournal of Geophysical Research, Solid Earth* **90**, 2967–2984.

Schmitz, M.D., Bowring, S.A., de Wit, M.J., Gartz, V., 2004: Subduction and terrane collision stabilize the western Kaapvaal craton tectosphere 2.9 billion years ago. *Earth and Planetary Science Letters* **222**, 363–376.

Schröder, S., Beukes, N.J., Armstrong, R.A., 2016: Detrital zircon constraints on the tectonostratigraphy of the Paleoproterozoic Pretoria Group, South Africa. *Precambrian Research* **278**, 362–393.

Smirnov, A.V., Evans, D.A.D., Ernst, R.E., Söderlund, U., Li, Z.-X., 2013: Trading partners: Tectonic ancestry of southern Africa and western Australia, in Archean supercratons Vaalbara and Zimgarn. *Precambrian Research* **224,** 11-22.

Söderlund, U., Ibanez-Mejia, M., El Bahat, A., Ernst, R.E., Ikenne, M., Soulaimani, A., Youbi, N., Cousens, B., El Janati, M., Hafid, A., 2013: Reply to Comment on "U–Pb baddeleyite ages and geochemistry of dolerite dykes in the Bas-Drâa inlier of the Anti-Atlas of Morocco: Newly identified 1380 Ma event in the West African Craton" by André Michard and Dominique Gasquet. *Lithos* **174**, 101–108.

Söderlund, U., Johansson, L., 2002: A simple way to extract baddeleyite (ZrO_2). *Geochemistry, Geophysics, Geosystems* **3**, 1–7.

Storey, B.C., 1995: The role of mantle plumes in continental breakup: Case histories from Gondwanaland. *Nature* **377**, 301–308.

Strik, G., Blake, T.S., Zegers, T.E., White, S.H., Langereis, C.G., 2003. Palaeomagnetism of flood basalts in the Pilbara Craton, Western Australia: Late Archaean continental drift and the oldest known reversal of the geomagnetic field. J*ournal of Geophysical Research, Solid Earth* **108**, 1–21.

Sumner, D.Y., Bowring, S.A., 1996: U-Pb geochronologic constraints on deposition of the Campbellrand Subgroup, Transvaal Supergroup, South Africa. *Precambrian Research* **79**, 25–35.

Tera, F., Wasserburg, G.J., 1972: U-Th-Pb systematics in three Apollo 14 basalts and the problem of initial Pb in lunar rocks. E*arth and Planetary Science Letters* **14**, 281–304.

Trendall, A.F., 1968: Three Great Basins of Precambrian Banded Iron Formation Deposition: A Systematic Comparison. G*eological Society of America Bulletin* **79**, 1527–1544.

Trendall, A.F., Compston, W., Nelson, D.R., de Laeter, J.R., Bennett, V.C., 2004: SHRIMP zircon ages constraining the depositional chronology of the Hamersley Group, Western Australia. *Australian Journal of Earth Sciences* **51**, 621–644.

Trendall, A.F., Nelson, D.R., Thorne, A.M., Compston, W., Williams, I.S., Armstrong, R.A., 1990: Precise zircon U-Pb chronological comparison of the volcano-sedimentary sequences of the Kaapvaal and Pilbara Cratons between about 3.1 and 2.4 Ga. *In:* J.E. Glover, S.E. Ho (eds.), *Third International Archaean Symposium*, 81-83, University of Western Australia, Perth.

van der Voo, R., 1990: The reliability of paleomagnetic data. *Tectonophysics* **184**, 1–9.

van der Westhuizen, W.A., de Bruijn, H., Meintjes, P.G., 1991: The Ventersdorp supergroup: an overview. *Journal of African Earth Sciences (and the Middle East)* **13**, 83–105.

van Kranendonk, M.J., Smithies, R.H., Hickman, A.H., Champion, D.C., 2007: Review: secular tectonic evolution of Archean continental crust: interplay between horizontal and vertical processes in the formation of the Pilbara Craton, Australia. *Terra Nova* **19**, 1–38.

Veikkolainen, T., Personen, L.J., Evans, D.A.D., 2014: PALEOMAGIA: A PHP/MYSQL database of the Precambrian paleomagnetic data. *Studia Geophysica et Geodaetica* **58**, 425–441.

Wegener, A., 1929: *Die Entstehung der Kontinente und Ozeane*. Friedrich Vieweg & Sohn, Braunschweig.

Wetherill, G.W., 1956: Discordant Uranium-Lead ages, I. *Transactions, American Geophysical Union* **37**, 320–326.

Williams, H., Hoffman, P.F., Lewry, J.F., Monger, J.W.H., Rivers, T., 1991: Anatomy of North America: thematic geologic portrayals of the continent. *Tectonophysics* **187**, 117–134.

Wilson, J.T., 1963: A possible origin of the Hawaiian islands. *Canadian Journal of Physics* **41**, 863–870.

Wingate, M.T.D., 1999: Ion microprobe baddeleyite and zircon ages for Late Archaean mafic dykes of the Pilbara Craton, Western Australia. *Australian Journal of Earth Sciences* **46**, 493–500.

Wingate, M.T.D., 1998: A palaeomagnetic test of the Kaapvaal-Pilbara (Vaalbara) connection at 2.78 Ga. South African J. Geol. 101, 257–274.

Wingate, M.T.D., Compston, W., 2000: Crystal orientation effects during ion microprobe U–Pb analysis of baddeleyite. *Chemical Geology* **168**, 75–97.

Wohlgemuth-Ueberwasser, C.C., Söderlund, U., Pease, V., Nilsson, M.K.M., 2015: Quadrupole LA-ICP-MS U/Pb geochronology of baddeleyite single crystals. *Journal of Analytical Atomic Spectrometry* **30**, 1191–1196.

Zegers, T.E., de Wit, M.J., Dann, J., White, S.H., 1998: Vaalbara, Earth's oldest assembled continent? A combined structural, geochronological, and palaeomagnetic test. *Terra Nova* **10**, 250–259.

Zeh, A., Ovtcharova, M., Wilson, A.H., Schaltegger, U., 2015: The Bushveld Complex was emplaced and cooled in less than one million years - results of zirconology, and geotectonic implications. *Earth and Planetary Science Letters* **418**, 103–114.

Zijderveld, J.D.A., 1967: A.C. demagnetization of rocks: analysis of results. *In*: D.W. Collinson, K.M. Creer, S.K. Runcorn (eds.), *Methods in Palaeomagnetism*, 254-286, Elsevier, Amsterdam.

Svensk sammanfattning

Det är allmänt känt att kontinenter under Jordens historia har separerat och kolliderat i ett cykliskt förlopp vilket har lett till existensen av större landmassor, superkontinenter eller superkratoner under vissa tidsperioder. En av de tidigaste föreslagna superkratonerna är Vaalbara, som sedan 1960-talet har ansetts bestå av Kaapvaalkratonen i södra Afrika och Pilbarakratonen i västra Australien. I denna avhandling har jag testat validiteten av Vaalbara med radiometriska och paleomagnetiska studier av magmatiska, mantelderiverade bergarter. Många tidigare studier har visat på geologiska likheter i arkeisk till proterozoisk berggrund, som Kaapvaal och Pilbara domineras av. Dessa inkluderar både vulkaniska och sedimentära bergarter, såsom återfinns i Fortescue- and Hammersleybassängerna i Pilbara och motsvarande bergarter Ventersdorp- och Transvaalbassängerna i Kaapvaal. Några exakta överenstämmelser av åldrar för basiska bergarter har hittills inte kunnat påvisas. I detta doktorandprojekt har jag med nya åldersbestämningar försökt identifiera möjliga matchningar genom undersökningar av regionala diabasgångsvärmar, och även utfört paleomagnetiska studier på vissa av de bergarter som åldersbestämts. Den generella slutsatsen är att de nya resultaten utgör ringa stöd för att Kaapvaal- och Pilbarakratonerna var i direkt kontakt med varandra under tidsperioden från 2,99 till 1,92 miljarder år sedan. I stället föreslår jag att dessa kratoner under denna tidsperiod ingick en betydligt större kontinent, vilken dessutom inkluderade block från dagens Nordamerika (USA och Kanada), Finland, Ryssland, Ukraina och Indien. Denna slutssats styrks av att samtliga dessa krustala block delar många geologiska, geokronologiska och paleomagnetiska likheter under denna tidsperiod. Detta stödjer hypotesen om att två landmassor existerade från arkeikum till första delen av paleoproterozoikum, där Kaapvaal och Pilbara utgjorde delar av en av dessa, vilken jag valt att kalla “Supervaalbara”.

PAPER I

Precambrian Research 267 (2015) 174–185

Contents lists available at ScienceDirect

Precambrian Research

journal homepage: www.elsevier.com/locate/precamres

Precise U-Pb baddeleyite age dating of the Usushwana Complex, southern Africa – Implications for the Mesoarchaean magmatic and sedimentological evolution of the Pongola Supergroup, Kaapvaal Craton

Ashley Gumsley[a,*], Johan Olsson[a], Ulf Söderlund[a,b], Michiel de Kock[c], Axel Hofmann[c], Martin Klausen[d]

[a] Department of Geology, Lund University, Sölvegatan 12, Lund, 223 62, Sweden
[b] Department of Geosciences, Swedish Museum of Natural History, P.O. Box 50, 104 05, Stockholm, Sweden
[c] Department of Geology, University of Johannesburg, P.O. Box 524, Auckland Park, 2006, South Africa
[d] Department of Earth Sciences, Stellenbosch University, Private Bag X1, Matieland 7602, South Africa

ARTICLE INFO

Article history:
Received 24 November 2014
Received in revised form 17 June 2015
Accepted 23 June 2015
Available online 2 July 2015

Keywords:
Usushwana Complex
Pongola Supergroup
Dolerite dykes
Dolerite sills
U-Pb baddeleyite
ID-TIMS

ABSTRACT

The Usushwana Complex of the south-eastern Kaapvaal Craton (South Africa and Swaziland), intrudes the ca. 3.6–3.1 Ga basement of the craton, as well as the Mesoarchaean volcanic and sedimentary cover succession of the Pongola Supergroup. New high-precision U-Pb dating of gabbros belonging to the Piet Retief Suite of the Usushwana Complex yield ages of 2989 ± 1 Ma, 2990 ± 2 Ma and 2978 ± 2 Ma. The Piet Retief Suite represents part of an intricate magmatic feeder to a major volcanic event which gave rise to the oldest known continental flood basalts on Earth, the Nsuze volcanic rocks. Broadly coeval SE-trending dolerite dykes of the Barberton-Badplaas Dyke Swarm in the larger region of the south-eastern Kaapvaal Craton formed along the same structural trend as the Usushwana Complex. One such dyke is dated herein to 2980 ± 1 Ma. Using the high-precision U-Pb geochronological data, the Nsuze volcanic rocks can now be resolved into at least two magmatic episodes which can be correlated with parts of the Pongola Supergroup. The first episode at ca. 2.99–2.98 Ga is broadly coeval with the Pypklipberg (Nhlebela) volcanic rocks, whereas the second at ca. 2.97–2.96 Ga was near synchronous to the Agatha volcanic rocks. A dolerite sill intruding into the Mozaan Group of the Pongola Supergroup, thought to be part of the Usushwana Complex, was dated to 2869 ± 5 Ma, and is instead coeval with the Hlagothi Complex further to the south, and provides a new minimum age for deposition of the Mozaan Group.

1. Introduction

The reconstruction of tectonic, sedimentological and magmatic events that shaped the Kaapvaal Craton in the Meso- to Neoarchaean is increasingly being aided by high-precision U-Pb geochronology of zirconium minerals (e.g., Gumsley et al., 2013; Mukasa et al., 2013; Olsson et al., 2010, 2011). U-Pb baddeleyite age dating of mafic dykes and sills help in establishing magmatic 'barcodes' and assist with continental reconstructions (e.g., Ernst et al., 2010, 2013; Bleeker & Ernst, 2006 and references therein). Additionally, emplacement ages of dolerite dykes and sills constrain the ages of supracrustal successions using cross-cutting relationships.

The Usushwana Complex in the south-eastern Kaapvaal Craton (South Africa and Swaziland), is a 'layered' intrusion of Archaean age (Anhaeusser, 2006). It is composed of the lower mafic Piet Retief Suite of gabbros, and the upper felsic Hlelo Suite granophyres. The Usushwana Complex is reported to intrude into the sedimentary and volcanic rocks of the Pongola Basin, as well as basement rocks of the craton. However, uncertainty surrounds the precise emplacement age of the Usushwana Complex. Geochronological and field relationships provided a 'best-estimate' age of ca. 2860 Ma (Anhaeusser, 2006; Hunter and Reid, 1987; Hammerbeck, 1982). We present new U-Pb baddeleyite ID-TIMS ages for the Usushwana Complex and related dolerite dykes and sills to further our understanding of the magmatic and sedimentological evolution of the Pongola Supergroup. A revised stratigraphy for the south-eastern

* Corresponding author at: Department of Geology, Lund University, Sölvegatan 12, Lund 223 62, Sweden. Tel.: +46 0762108563.
E-mail address: ashley.gumsley@geol.lu.se (A. Gumsley).

http://dx.doi.org/10.1016/j.precamres.2015.06.010

Kaapvaal Craton interprets the two suites of the Usushwana Complex, as well as SE-trending dolerite dykes and dolerite sills, as magmatic feeders during separate episodes of Nsuze Group volcanism, as well as possibly to volcanism within the Amsterdam Formation or upper Mozaan Group.

2. Geology

The Pongola Supergroup and the Usushwana Complex play an important part in the Mesoarchaean geological history of the Kaapvaal Craton in south-eastern South Africa and Swaziland. Summaries of the regional and local geology of the area are presented below, derived from the in-depth work of Hammerbeck (1982), Hunter (1970) and Winter (1965), and shown in Fig. 1, with a summary of previously published ages given in Fig. 2 (with the data in the supplementary material). The reader is referred to Fig. 3 for an idealised summary of the lithological units in cross-section within the Piet Retief-Amsterdam area.

2.1. Basement Granitoid-Greenstone Terrain

The eastern and south-eastern Kaapvaal Craton in South Africa and Swaziland records a geological history starting ca. 3.6 Ga in the Ancient Gneiss Complex (AGC), as summarised in Robb et al. (2006). The AGC forms the nucleus onto which several granitoid sub-domains accreted, along with a number of greenstone belts as it continued to grow northward and westward from the Eo- to the Mesoarchaean (e.g., Eriksson et al., 2009; Eglington & Armstrong, 2004; Poujol et al., 2003; de Wit et al., 1992). These rocks form the basement onto which the supracrustal units of the Pongola Supergroup and Amsterdam Formation were deposited (Hunter, 1973).

2.2. Pongola Supergroup

The Pongola Supergroup is composed of the lower volcano-sedimentary Nsuze Group, and the upper predominantly sedimentary Mozaan Group (Wilson et al., 2013; Gold, 2006). The Mozaan Group has been correlated lithostratigraphically with the Witwatersrand Supergroup on the central Kaapvaal Craton (Beukes and Cairncross, 1991). The Nsuze Group has also been tentatively correlated with the Dominion Group underlying the Witwatersrand Supergroup (Cole, 1994). Upper age constraints for the formation of the Pongola Basin are given by a 3105 ± 3 Ma age of the Mpuluzi Batholith, forming an eroded peneplane on to which the Pongola Supergroup was deposited (Kamo and Davis, 1994). A lower age limit is provided by a 2837 ± 5 Ma quartz porphyry sill that is intrusive into, but was also folded together with the Mozaan Group (Gutzmer et al., 1999). The post-Pongola granitic Mhlosheni Pluton in Swaziland has been dated at 2838 ± 10 Ma by Mukasa et al. (2013), and is therefore coeval with the quartz porphyry sill. The 2824 ± 6 Ma Mooihoek Pluton is in close proximity to the 2837 ± 5 Ma quartz porphyry sill (Maphalala and Kröner, 1993). As the Mooihoek Pluton is undeformed, Gutzmer et al. (1999) suggested that these two ages bracket the period of folding in the Mozaan Group.

2.2.1. The Nsuze Group

U-Pb zircon ages from the Nsuze volcanics range from 2985 ± 1 Ma, 2977 ± 5 Ma to 2967 ± 9 Ma (Mukasa et al., 2013; Nhleko, 2003; Hegner et al., 1994). Burger and Coertze (1973) reported U-Pb zircon ages for the Nsuze volcanics of 3083 ± 150 Ma and 3090 ± 90 Ma, although no sample description, locality or analytical data for these dates are available.

The base of the Nsuze Group is made up of sandstone and volcanic rocks of the Mantonga and Wagendrift formations (Warmbad Subgroup), overlain by the mafic to felsic volcanic rocks of the Bivane Subgroup (Wilson et al., 2013; Gold, 2006). Wilson et al. (2013) and Cole (1994) distinguished between the lower more mafic Pypklipberg (Nhlebela) volcanic rocks and the upper mafic to felsic Agatha volcanic rocks within the greater volcanic package of the Bivane Subgroup. Other studies grouped these volcanic rocks together, despite the presence of the intervening sedimentary Nkemba (White Mfolozi) Formation between these two volcanic packages (Wilson et al., 2013; Gold, 2006; Cole, 1994). In addition to the broader Pypklipberg and Agatha volcanic rocks, Nhleko (2003) further subdivided the Agatha volcanic rocks along a shale unit called the Ntambo Member, resulting in three possible volcanic cyclic units within the Nsuze Group in Swaziland. An additional unit was also noted in the Nkandla and Nongoma areas of northern KwaZulu-Natal: the Ekombe volcanic rocks (Nhleko, 2003; Groenewald, 1984), which may reflect partly overlapping volcanic rocks within a rift zone.

2.2.2. The Mozaan Group

According to Gold (2006) and references therein, the Mozaan Group unconformably overlies the Nsuze Group, and is made up of shale and sandstone. Locally developed banded iron formation (BIF), as well as volcanic rocks are preserved towards the top of the succession (Tobolsk and Gabela basalts and basaltic andesites). In the Piet Retief-Amsterdam area, the Mozaan Group is composed of Skurwerant Formation sandstones and minor shales at the base, followed by shales, iron formations and minor sandstones of the Redcliff Formation (Hammerbeck, 1982). These formations are termed the Sinqeni and Ntombe formations in the larger Pongola Supergroup. A ferruginous shale in this region has been dated at 2860 ± 26 Ma by Walraven and Pape (1994).

2.3. The Thole Complex

The Thole Complex consists of folded layered sills of harzburgite at the base, grading upwards into pyroxenite and, in some instances, into gabbro or norite at the top (Hammerbeck, 1982). According to Hammerbeck (1982), the Thole Complex was emplaced as concordant sills at several levels in the Mozaan Group and the basement. Thole Complex sills are regarded to have preceded magmatism in both the Amsterdam Formation and the Usushwana Complex.

2.4. The Amsterdam Formation

Initially, the whole Amsterdam Formation was considered to be made up of granophyre, but two distinctly different members, the Gobosha and Vaalkop, were distinguished by Hammerbeck (1982). The Gobosha Member unconformably overlies the Pongola Supergroup and consists mainly of dacite and minor rhyolite and associated tuff. In Swaziland, Hunter (1970) identified granophyre which he grouped with the Usushwana Complex. The descriptions and field relationships of these granophyres in Swaziland are characteristic of the Gobosha Member, and could be the same rock unit according to Hammerbeck (1982). The Vaalkop Member however is essentially a rhyolite (Hammerbeck, 1982), but has previously been described as a granophyre, like the Gobosha Member (Hunter, 1970; Winter, 1965; Humprey and Krige, 1931). Humprey and Krige (1931), as well as Hunter (1970) related the granophyre to a composite gabbro-granophyre magma of the Usushwana Complex.

2.5. The Usushwana Complex

The Usushwana Complex is a large linear intrusion which crops out in the form of an inverted “h” (Fig. 1). The Usushwana Complex was emplaced along north-west trending structures in the

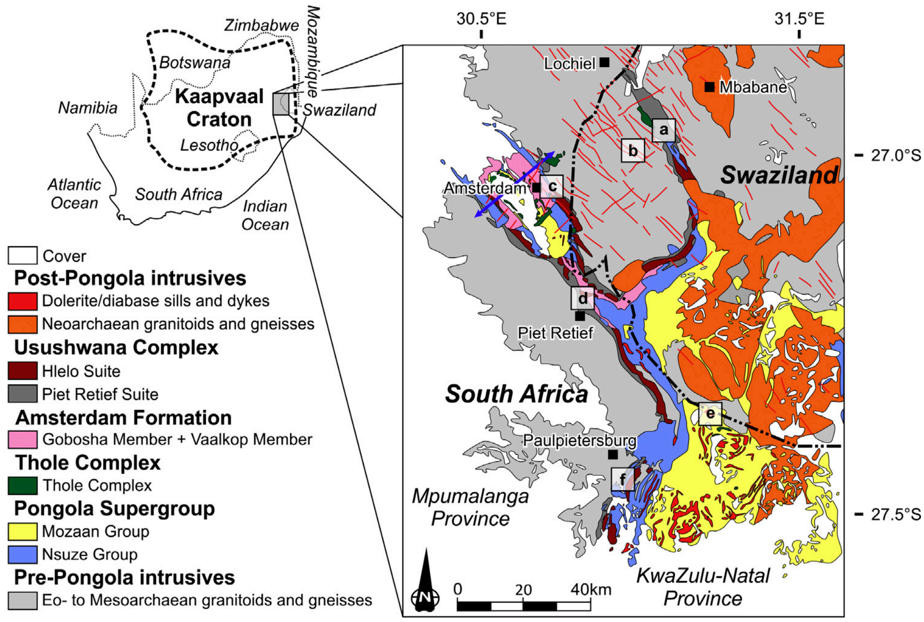

Fig. 1. Geological map of a portion of the south-eastern Kaapvaal Craton illustrating the various geological units relevant to this study. A blue line of the idealised geological cross-section presented in Fig. 3 and is shown near Amsterdam. Inset boxes refer to sample localities shown in greater detail in Fig. 4. This map is modified from the 1:250 000 Mbabane (2630), Vryheid (2730) and Swaziland geological maps (Geological Survey of South Africa, 1988; 1984; Geological Survey and Mines Department of Swaziland, 1988).

basement. It is subdivided into mafic and felsic suites (Anhaeusser, 2006 and references therein). The mafic suite, or Piet Retief Gabbro Suite, consists predominantly of a variety of gabbros, with minor occurrences of pyroxenite. Geochemically, however, these pyroxenites do not follow the same fractionation trend as the gabbros, and therefore may represent a different pulse of magmatism (Hammerbeck, 1982). A gabbroic phase is also intrusive into the Thole Complex. Granodiorite and micro-granite constitute the 'granophyre' of the felsic Hlelo Suite, but considerable textural, mineralogical and chemical differences between the two end-members exist (Hammerbeck, 1982). The Hlelo Suite is associated with the Piet Retief Suite, but it has an intermittent mode of occurrence. The granophyre and gabbro of the two suites may not be part of the same layered complex, however, because the Usushwana Complex lacks characteristic modal and/or cryptic layering (Hammerbeck, 1982). Hammerbeck (1982) also noted that the granophyres of the Hlelo Suite do not differ greatly from the Vaalkop Member, indicating that these rocks may be closely related to each other, and may be the product of assimilation of the country rocks.

The gabbros are preferentially emplaced along the interface between basement granitoids and the Pongola Supergroup. They also intrude along zones of weakness into the Pongola Supergroup, namely in the Mantonga sandstone and Bivane volcanic rocks. Xenoliths of granitoids, volcanic rocks, and quartzite can be seen in the gabbro. Gabbro is intrusive into granophyre, but dykes of aplite also intrude into the gabbroic rocks, resulting in an unclear temporal relationship between the two, although back-veining is possible. Different varieties of gabbro also exist (ferro-gabbro, quartz gabbro and hypersthene gabbro), as noted by Hammerbeck (1982), and may constitute different pulses or episodes. van Vuuren (1965) considered two large bodies of mafic rocks which are intrusive into the Redcliff and Skurwerant formations of the Mozaan Group to be diabase sills, whereas Hammerbeck (1982) assigned them to the Usushwana Complex.

Several attempts to date the Usushwana Complex have been made using different geochronological techniques (Fig. 2). A Rb-Sr isochron for granophyres, and a combined mineral and whole-rock Sm-Nd isochron for a pyroxenite yielded consistent ages of 2874 ± 30 Ma and 2871 ± 30 Ma, respectively (Davies & Allsopp, 1970; Hegner et al., 1984). The pyroxenite sampled was almost certainly Thole Complex however, as it was sampled in the Thole Complex type area near Amsterdam, and intrudes into the Mozaan Group. Hegner et al. (1984) also obtained a Sm-Nd isochron age of 3124 ± 123 Ma based on whole-rock analyses of nine different gabbro samples of the Usushwana Complex. This surprisingly old age was considered at the time to be invalid due to the inferred intrusive relationship of the Usushwana Complex into the Pongola Supergroup. The Sm-Nd system was regarded to have been affected by either crustal contamination or open-system behaviour. Layer et al. (1988) presented $^{40}Ar/^{39}Ar$ ages of 2386 ± 58 Ma and 2377 ± 58 Ma for pyroxene separates and 2094 ± 54 Ma for hornblende separates, but found that these samples had been subjected to severe argon loss, which they explained by isotopic re-setting during the intrusion of the ca. 2.06 Ga Bushveld Complex. The most recently published 2671 ± 18 Ma age for the Usushwana Complex was derived from a Pb-Pb isochron on a magnetite layer in the Piet Retief Gabbro Suite (Walraven and Pape, 1994). However, this result is contradicted by the fact that the Usushwana Complex is intruded by the Ngwempisi and Sicunusa plutons, which have both been dated at ca. 2720 Ma using Pb-Pb zircon evaporation and U-Pb on zircon (Mukasa et al., 2013; Maphalala and Kröner, 1993). Hence, according to previous isotopic investigations, field and structural evidence (Fig. 3), the gabbros of the Usushwana Complex should not be older than ca. 2860 Ma or younger than ca. 2720 Ma (Hunter and Reid, 1987). Recently, Gumsley et al. (2013) obtained a U-Pb baddeleyite age of 2874 ± 2 Ma on a SE-trending dolerite dyke and 2866 ± 2 Ma on the Hlagothi Complex in the south-easternmost portion of the Kaapvaal Craton. These ages are broadly coeval with granophyres and pyroxenites within the Usushwana Complex.

2.6. Post-Pongola Event(s)

In the south-eastern Kaapvaal Craton, SE-trending dolerite dykes were dated by Olsson et al. (2010), providing U-Pb

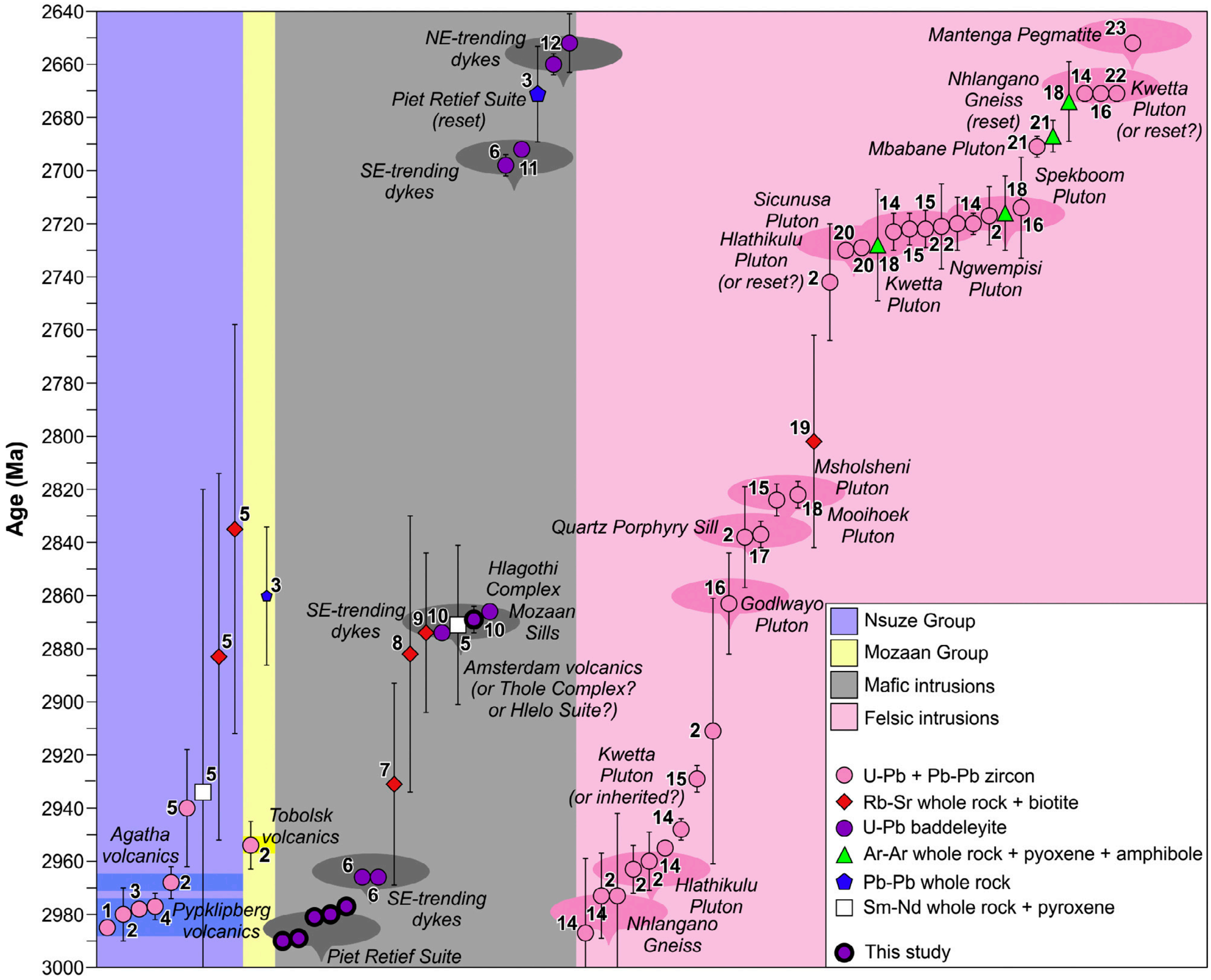

Fig. 2. Summary of previously published ages on the syn- and post-Pongola Supergroup magmatic events on the south-eastern Kaapvaal Craton from 3000 Ma to 2640 Ma, found as either volcanic units within the Nsuze or Mozaan groups, as mafic or felsic plutons intruding into the basement granitoid-greenstone terrain or the Pongola Supergroup, or as gneisses. Ages are given with 2σ error bars, and the isotopic system used, and whether it was a whole rock or a mineral technique. Geochronological data points are given in the figure, with the following references: 1, Hegner et al. (1994); 2, Mukasa et al. (2013); 3, Walraven and Pape (1994); 4, Nhleko (2003); 5, Hegner et al. (1984); 6, Olsson et al. (2010); 7, Davies et al. (1970); 8, Layer et al. (1988); 9, Gumsley et al. (2013); 10, Olsson et al. (2011); 11, Olsson (2012); 12, Gumsley (2013); 13, Hoffman et al. (2015); 14, Maphalala and Kröner (1993); 15, Reimold et al. (1994); 16, Gutzmer et al. (1999); 17, Eglington and Armstrong (2004); 18, Barton et al. (1983); 19, Schoene and Bowring (2010); 20, Layer et al. (1989); Meyer et al. (1993); Maphalala and Trumbull (1998). Additional data can be found in the supplementary material. Coloured ellipses denote possible age ranges of a magmatic event from the published geochronological data found in the supplementary material.

baddeleyite ages of ca. 2966 and ca. 2665 Ma. Other SE-trending and NE-trending dykes have been preliminarily dated to ca. 2682 Ma and ca. 2652 Ma, respectively (Gumsley, 2013; Olsson, 2012).

A number of granitic plutons crop out in close association with the Pongola Supergroup and are known as post-Pongola granites. The Hlatikulu granite was dated at 2729 ± 1 Ma by Schoene and Bowring (2010). The Kwetta granite has yielded

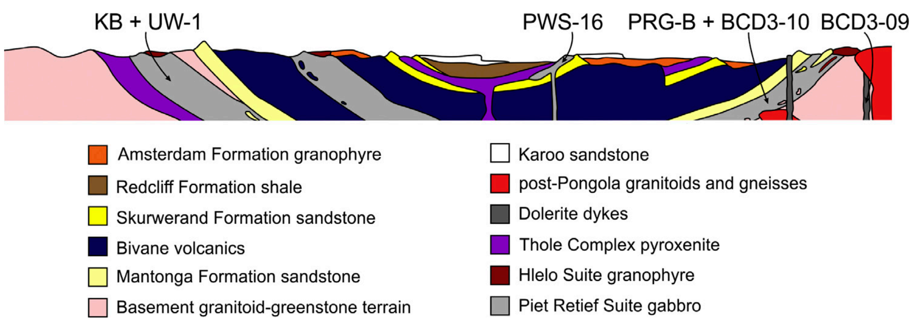

Fig. 3. An idealised geological cross-section through the Piet Retief-Amsterdam area illustrating the various geological units and there field relationships, combined with geological units and field relationships found in other areas of the south-eastern Kaapvaal Craton (adapted from Hammerbeck, 1982). Sampling localities within the stratigraphy are also shown.

several contradictory dates from 2671 ± 3 Ma to 2722 ± 6 Ma (Reimold et al., 1993; Maphalala and Kröner, 1993). The Mswati Suite granitoids have been dated at 2717 ± 11 Ma, 2824 ± 6 Ma and 2822 ± 5 Ma (Mukasa et al., 2013; Maphalala and Kröner, 1993). High-grade ortho- and paragneisses locally occur in southern Swaziland (Hunter and Wilson, 1988). The Nhlangano and Mahamba gneisses, at their type localities have been shown to be ca. 2.99 Ga and 2.95 Ga, and are high-grade metamorphic equivalents of Nsuze Group volcanic, sedimentary and plutonic rock packages according to Hofmann et al. (2015).

3. Geochronology

3.1. Sampling

Gabbroic samples from a variety of localities within the Piet Retief Suite of the Usushwana Complex, a dolerite sill intruding the Mozaan Group thought to be of Usushwana Complex equivalent age, as well as a SE-trending dolerite dyke in the vicinity of the complex were collected from six sites (Figs. 1 and 4). Sample BCD3-10 (Fig. 4a), is the only sample gathered from the eastern arm of the Usushwana Complex in Swaziland, where it intrudes directly into basement granitoids. The eastern arm of the Usushwana Complex is assumed from limited geophysical surveys to have intruded as a dyke (Hammerbeck, 1982; Winter, 1965). Sample BCD3-09 was taken from a SE-trending dolerite dyke in Swaziland near BCD3-10 (Fig. 4b). It is intrusive into Mesoarchean Tsawela Gneiss between the eastern and western arms of the Usushwana Complex. The dyke has geochemical affinities to the ca. 2966 Ma Barberton-Badplaas Dyke Swarm (Klausen et al., 2010; Olsson et al., 2010). The western arm of the Usushwana Complex is represented by sample PRG-B (Fig. 4c), taken from where the western arm splits in the vicinity of Amsterdam, forming a sill on each side of a raft of Pongola Supergroup and Amsterdam Formation rocks. PRG-B was sampled from the easternmost flank of this syncline, where the Usushwana Complex is thought to have intruded as

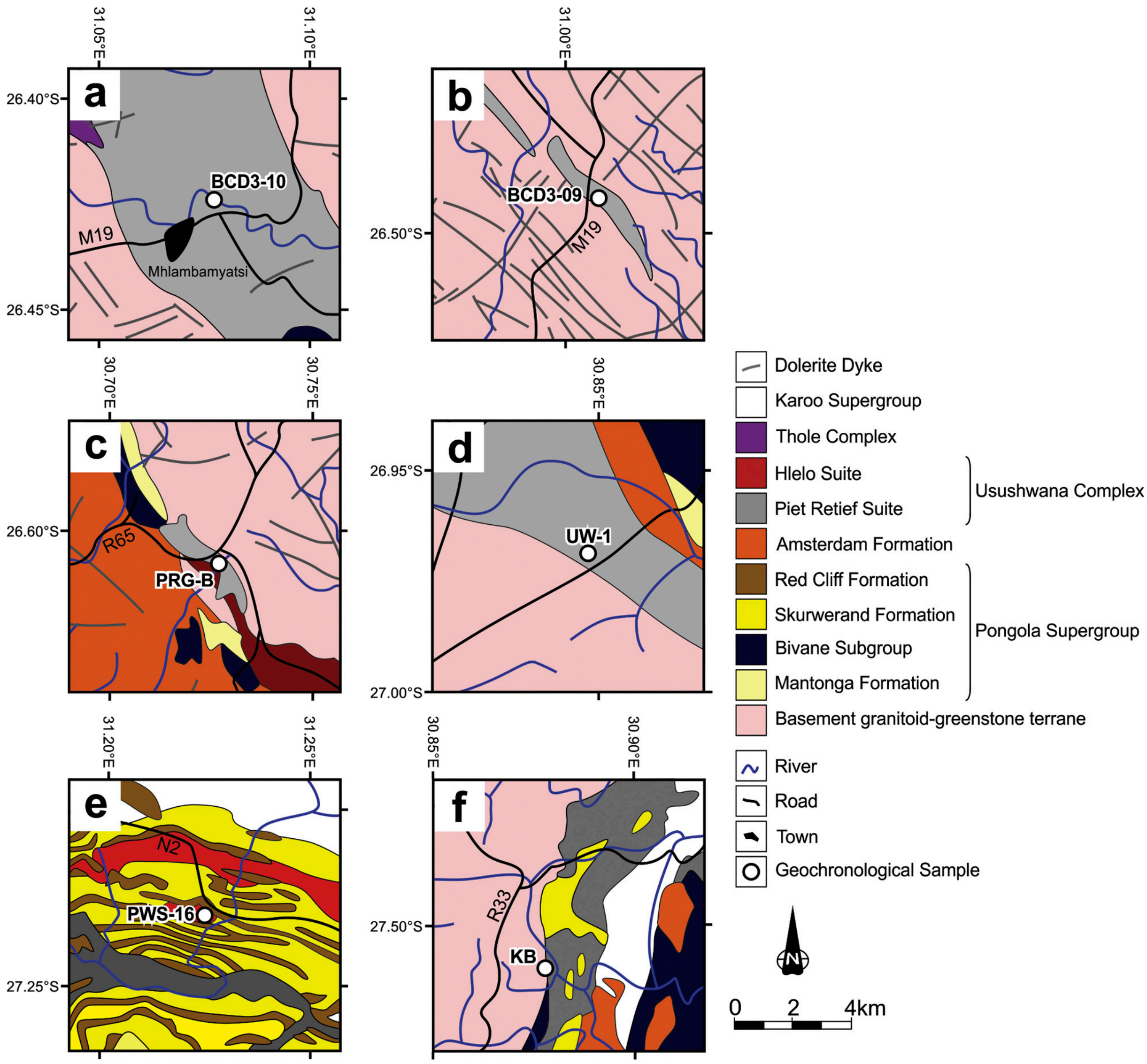

Fig. 4. Sample localities and geological associations. Locality a: **BCD3-10** – 26.455210° S, 31.054320° E. Locality b: **BCD3-09** – 26.490440° S, 31.000730° E. Locality c: **PRG-B** – 26.610767° S, 30.722400° E. Locality d: **UW-1** – 26.955917° S, 30.814806° E. Locality e: **PWS-16** – 27.241940° S, 31.224200° E. Locality f: **KB** - 27.516890° S, 30.887470° E. Maps modified from the 1:250 000 Mbabane (2630), Vryheid (2730) and Swaziland geological maps (Geological Survey of South Africa, 1988; 1984; Geological Survey and Mines Department of Swaziland, 1988).

Table 1
U-Pb isotopic data.

Sample	Fraction	n[a]	Th/U [b]	Pb*/Pbc [c]	$^{206}Pb/^{204}Pb$	$^{207}Pb/^{235}U$	± 2σ % error	$^{206}Pb/^{238}U$	± 2σ % error	Correlation coefficient	$^{207}Pb/^{235}U$	$^{206}Pb/^{238}U$	$^{207}Pb/^{206}Pb$	± 2σ abs. error	Discordance
					measured[d]	[corrected][e]					[Age, Ma]				
BCD3-10	A	2	0.019	45.8	2429	17.87	0.3532	0.5864	0.3410	0.9646	2982.7	2974.8	2987.9	1.5	0.9
	B	5	0.038	125.4	6751	17.09	0.4108	0.5607	0.4044	0.9839	2939.8	2869.7	2988.1	1.2	5.0
	C	1	0.013	62.9	3399	17.62	0.4107	0.5780	0.4067	0.9890	2969.3	2940.6	2988.8	1.0	2.2
	D	4	0.016	32.4	1767	17.96	0.2431	0.5887	0.2373	0.9606	2987.5	2984.2	2989.7	1.1	0.7
BCD3-09	A	3	0.024	44.2	2390	17.91	0.2295	0.5907	0.2230	0.9628	2985.1	2992.1	2980.4	1.0	-0.4
	B	6	0.024	23.7	1266	15.18	0.2914	0.5022	0.2854	0.9710	2826.7	2623.2	2975.2	1.1	11.8
	C	4	0.072	8.2	442	17.39	0.5044	0.5740	0.4763	0.9420	2956.8	2924.3	2979.0	2.7	1.8
	D	1	0.099	4.8	270	17.08	1.8690	0.5646	1.8515	0.9873	2939.5	2885.5	2976.6	4.8	3.1
PRG-B	A	4	0.031	106.3	6107	16.16	0.2204	0.5346	0.2098	0.9452	2886.4	2760.8	2975.3	1.2	7.7
	B	3	0.032	109.7	6330	17.19	0.2830	0.5681	0.2775	0.9768	2945.7	2899.9	2977.2	1.0	3.1
	C	3	0.018	37.1	2160	16.90	0.4369	0.5582	0.4224	0.9541	2929.2	2859.2	2977.7	2.1	4.5
UW-1	A	7	0.016	101.2	5392	14.85	0.2425	0.4913	0.2335	0.9618	2805.6	2576.3	2974.9	1.1	13.4
	B	6	0.040	15.0	777	16.54	0.4928	0.5443	0.4674	0.9527	2908.5	2801.6	2983.3	2.4	6.1
	C	5	0.012	64.9	3686	16.91	0.2485	0.5558	0.2406	0.9580	2929.6	2849.3	2985.2	1.1	4.5
	D	1	0.713	40.9	2032	15.13	0.3718	0.5006	0.3662	0.9683	2823.7	2616.4	2975.3	1.5	12.1
PWS-16	A	1	0.125	41.9	2480	15.75	0.5105	0.5557	0.4570	0.8853	2861.7	2848.7	2870.8	3.9	1.3
	B	2	n.m.[f]	10.5	639	15.71	0.7431	0.5537	0.7320	0.9699	2859.1	2840.6	2872.1	2.9	1.7
	C	3	n.m.[f]	23.0	1443	15.51	0.6071	0.5485	0.5999	0.9704	2846.9	2819.0	2866.8	2.4	2.2
	D	2	0.471	8.9	555	15.42	1.7906	0.5460	1.7794	0.9741	2841.5	2808.6	2865.0	6.6	2.5
KB	A	5	0.088	77.5	4212	15.68	0.3454	0.5270	0.3206	0.9261	2857.6	2729.0	2949.7	2.1	8.0
	B	1	n.m.[f]	37.6	2138	17.06	0.3811	0.5622	0.3779	0.9815	2938.1	2875.6	2981.1	1.2	4.1
	C	4	0.028	89.6	4992	14.99	0.2514	0.5006	0.2473	0.9795	2814.7	2616.2	2960.2	0.8	12.1

[a] n = number of baddeleyite crystals.
[b] Th/U model ratio inferred from $^{208}Pb/^{206}Pb$ ratio and age of sample.
[c] Pb* = radiogenic lead; Pbc = total common lead (initial + blank lead).
[d] measured ratio, corrected for fractionation and spike.
[e] isotopic ratios corrected for fractionation (0.1% per amu for Pb), spike calibration, blank (1 pg Pb and <1 pg U) and residual initial common Pb. Initial common Pb corrected with isotopic compositions from the model of Stacey and Kramers (1975) for the age of the sample.
[f] Not measured.

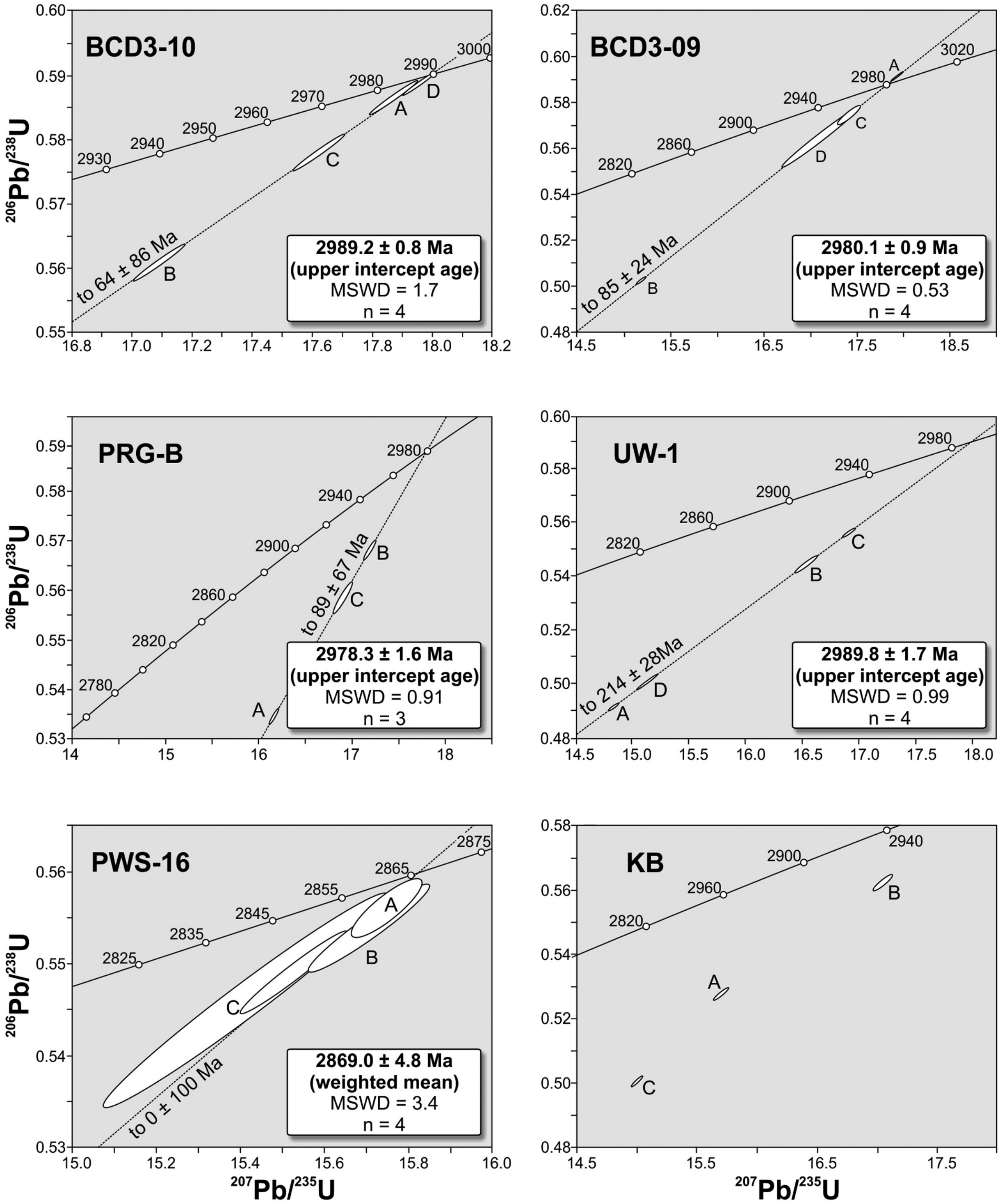

Fig. 5. Concordia diagrams of the 6 studied samples, with $^{206}Pb/^{238}U$ versus $^{207}Pb/^{235}U$ isotopic ratios of the analysed baddeleyite fractions. All data point error ellipses and age calculations are shown at the 95% (2σ) confidence level, and ^{238}U and ^{235}U decay constant uncertainties are ignored. MSWD equals Mean Square of Weighted Deviates, and n refers to the total number of fractions analysed. Error ellipses symbols (A, B, C and D) refer to the fractions analysed and shown in Table 1.

a sub-horizontal sheet before folding. It was taken from an area where the complex intrudes into Mantonga Formation sandstone and Pypklipberg (Nhlebela) volcanic rocks. Sample UW-1 was collected near the town of Piet Retief in Mpumalanga, South Africa, close to the contact with granitoid basement (Fig. 4d). It was obtained from the westernmost flank of the same syncline on which sample PRG-B was taken. Sample PWS-16 was taken from a dolerite sill south-west of Swaziland within the Nkoneni Subgroup of the Mozaan Group (Fig. 4e), thought to be synchronous with the Usushwana Complex (Hammerbeck, 1982). Finally, sample KB was taken on the Koudbad Farm near the Natal Spa (Paulpietersburg) in northern KwaZulu-Natal, at the southernmost extension of the

Table 2
Summary of U-Pb geochronology.

Lithology	Sample	Age (Ma)	MSWD	Method
Piet Retief Suite	BCD3-10	2989.2 ± 0.8	1.70	Upper Intercept Age, Free Regression
	PRG-B	2978.3 ± 1.6	0.91	Upper Intercept Age, Free Regression
	UW-1	2989.8 ± 1.7	0.99	Upper Intercept Age, Free Regression
	KB	2981.1 ± 1.2	n.a	207/206Pb age, oldest fraction
Mafic Dyke	BCD3-09	2980.1 ± 0.9	0.53	Upper Intercept Age, Free Regression
Mafic Sill	PWS-16	2869.0 ± 4.8	3.4	Weighted Mean

Usushwana Complex (Fig. 4f). The sampling site is near where the gabbro has an intrusive contact into both the Nsuze Group volcanic rocks and basement granitoids.

3.2. Analysis

Baddeleyite (ZrO_2) is a well-established mineral used in U-Pb isotope dating of silica-undersaturated rocks (Heaman and LeCheminant, 1993; Krogh et al., 1987). It can now be readily extracted using the water-based separation technique of Söderlund and Johansson (2002), and dated by isotope dilution or even dated in situ by spot techniques (e.g., Ibanez-Mejia et al., 2014; Schmitt et al., 2010). We applied the Isotope Dilution-Thermal Ionisation Mass Spectrometry (ID-TIMS) method for the dating of the samples in this study. Mineral separation was completed at the Department of Geology, Lund University, following the extraction technique of Söderlund and Johansson (2002). Mass spectrometry analysis was done at the Department of Geosciences in the Swedish Museum of Natural History in Stockholm. After handpicking, the best-quality baddeleyite grains from the samples were selected and transferred to Teflon© dissolution capsules using ethanol and handmade micropipettes. The grains were subsequently rinsed repeatedly in 7 N HNO_3 and ultraclean water to remove ethanol and dilute the Pb blank. A HF-HNO_3 mixture (10:1) were added to the dissolution capsules together with one drop of a ^{205}Pb-$^{233-236}U$ tracer solution before they were put into steel jackets and placed in the oven at 205 °C for 3 days until fully dissolved. After dissolution, the samples were dried down on a hot plate at 100 °C and re-dissolved in 6 M HCl, with the addition of a small portion of 0.25 N H_3PO_4. The samples were left on a hot plate to dry down again at 100 °C, leaving a small droplet. The sample droplets were dissolved in 2 μl of silica gel (Gerstenberg and Haase, 1997), and were then loaded on out-gassed single rhenium (Re) filaments using an automatic pipette. The U and Pb isotope intensities were measured on a Finnigan Triton thermal ionisation multi-collector mass spectrometer equipped with Faraday Cups and a Secondary Electron Multiplier (SEM). Intensities of ^{204}Pb, ^{205}Pb, ^{206}Pb and ^{207}Pb were analysed at filament temperatures of 1220–1300 °C, while the measurement of ^{233}U, ^{236}U and ^{238}U was done subsequently at filament temperatures exceeding 1350 °C. The U and Pb data reduction was done using an in-house excel Isoplot macro spreadsheet (written by Per-Olof Persson, Department of Geosciences, Swedish Museum of Natural History) based upon the algorithms of Ludwig (1991), where the initial Pb compositions were taken from Stacey and Kramers (1975). The decay constants for ^{235}U, ^{238}U and ^{232}Th are from Jaffey et al. (1971). Procedural Pb blank levels at the Department of Geosciences in the Swedish Museum of Natural History are typically at 1.0 pg for Pb and 0.1 pg for U. The isotopic composition of the laboratory blank (errors at 2σ) is: $^{206}Pb/^{204}Pb$ = 18.5 (2), $^{207}Pb/^{204}Pb$ = 15.6 (0.2) and $^{208}Pb/^{204}Pb$ = 38.5 (0). The U-Pb data are presented in Table 1 and the calculated isotopic ages are shown in concordia diagrams in Fig. 5 with the preferred ages. Summaries of the age data are presented in Table 2.

3.3. Results

Baddeleyite extraction of BCD3-10 yielded 100 dark brown, blade-like crystals between 50 and 100 μm in their longest dimension. Regression of four variably discordant (0.7–5.0%) fractions, comprising 1 to 5 baddeleyite crystals each, yields an upper intercept date of 2989.2 ± 0.8 Ma with a Mean Square of Weighted Deviates (MSWD) of 1.7, and a free lower intercept date of 64 ± 86 Ma.

Sample BCD3-09 yielded ca. 200 dark brown baddeleyite crystals of 50–100 μm in their longest dimension. Regression through one slightly reverse (−0.4%), and three normally (1.8–11.8%) discordant analyses, with 1 to 6 crystals in each fraction, yielded an upper intercept of 2980.1 ± 0.9 Ma, with a free lower intercept date of 85 ± 24 Ma (MSWD = 0.53).

Sample PRG-B yielded ca. 30 clear, dark-brown baddeleyite grains ca. 50 μm in size and mostly of good quality. Regression through three fractions of 3 to 4 grains resulted in an upper intercept date of 2978.3 ± 1.6 Ma with an MSWD = 0.91, with a lower intercept of 89 ± 67 Ma (3.1–7.7% discordance).

Mineral separation of UW-1 resulted in ca. 50 dark brown baddeleyite grains or fragments thereof. The grains are up to 100 μm in length, and most of them have frosty surfaces of suspected polycrystalline zircon. Grains without visible light rims were selected for geochronology. Regression through four variably discordant (4.5–13.4%) ellipses, representing 1 to 7 crystals each, resulted in upper and lower intercept dates of 2989.8 ± 1.7 Ma and 214 ± 28 Ma (MSWD = 0.99), respectively.

Mineral separation of PWS-16 resulted in approximately 100 clear, dark-brown baddeleyite grains of good quality. Except for some larger grains, most of them were in the range of 40 to 50 μm. One single-grain fraction, and an additional three fractions of 2–3 grains each, were used in a regression resulting in an upper intercept date of 2869.0 ± 4.8 Ma, with the percentage of discordance varying from 1.3 to 2.5. A locked lower intercept at 0 ± 100 Ma (MSWD = 3.4) was used. A calculated weighted $^{207}Pb/^{206}Pb$ mean date is 2869 ± 4.8 Ma (MSWD = 3.4).

Sample KB yielded only 20 mottled baddeleyite crystals, mostly less than 50 μm in their longest dimension. Three fractions of 1 to 5 grains in each generated a poorly defined upper intercept date, with variable discordance from 4.1 to 12.1%, and non-linear $^{207}Pb/^{206}Pb$ ages. The $^{207}Pb/^{206}Pb$ date from the oldest fraction of 2981.1 ± 1.2 Ma gives the minimum date of the sample.

4. Discussion

4.1. The Usushwana Complex and its relationship with Nsuze volcanism

The most recent U-Pb ion probe zircon ages of the Nsuze volcanics span a range from 2980 ± 10 Ma to 2968 ± 6 Ma across the various stratigraphic intervals within the Hartland Basin of the Nsuze Group (Mukasa et al., 2013). Hegner et al. (1994) also reported a single zircon U-Pb age of 2985 ± 1 Ma, and Nhleko (2003) an age of 2977 ± 3 Ma also using ion probe on zircon. The new U-Pb ID-TIMS upper intercept baddeleyite dates of BCD3-10 and UW-1 at 2989 ± 1 Ma and 2990 ± 2 Ma, respectively, from the Piet Retief Suite of the Usushwana Complex would attest to the crystallisation ages of this suite being broadly coeval with the oldest dated Nsuze volcanic units. However, it has been observed

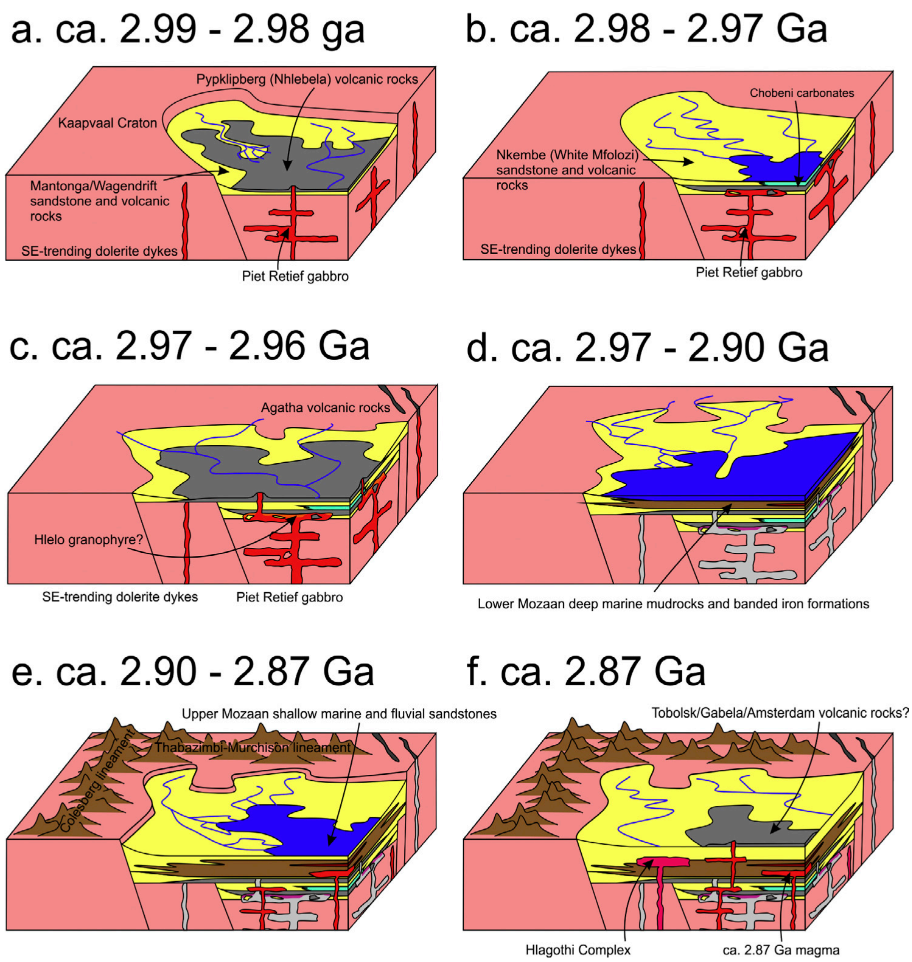

Fig. 6. Tectonic model for the south-eastern Kaapvaal Craton during the Mesoarchaean for the pre-, syn- and post-Pongola events.

that the Piet Retief gabbro near sample locality PRG-B intrudes into the basal Mantonga sandstone and lower Pypklipberg (Nhlebela) volcanic rocks in the Nsuze Group on the western arm of the complex. Sample PRG-B yields a crystallisation age of 2978 ± 2 Ma that renders the sandstones and volcanic rocks older than 2978 Ma at this locality, but not necessarily as old as 2989–2990 Ma. This suggests a complex set of magmatic feeders which included the Usushwana Complex, which was made up of different magma pulses at different times over at least 10 million years, and which experienced different cooling histories, as well as supplying magma for the volcanic successions within the Nsuze Group.

Sample KB was collected from the most southern arm of the Usushwana Complex. This arm is much less studied, and much further south from where Mukasa et al. (2013) obtained ages on the Nsuze volcanic rocks. Although the baddeleyite in the KB sample was partially altered to polycrystalline zircon, it yielded a minimum $^{207}Pb/^{206}Pb$ crystallisation age of 2981 ± 1 Ma for this part of the Usushwana Complex, that is broadly coeval with the Nsuze Group volcanic rocks already discussed above. However, in this region, rocks of the Usushwana Complex have also intruded rocks of the Nsuze Group.

The SE-trending dolerite dykes in the Barberton-Badplaas area further north of the study area have been dated by Olsson et al. (2010) to 2966 ± 1 Ma and 2967 ± 1 Ma, respectively. The Usushwana Complex follows the same trend towards the south-east as these dykes, appearing to exploit the same basement structures. The development of the Pongola Supergroup and Usushwana Complex may possibly be attributed to a zone of weakness between contrasting crustal blocks, as was already noted by Mukasa et al. (2013) when assessing the region's pre-Pongola Supergroup basement. A SE-trending dolerite dyke between the two SE-trending arms of the Usushwana Complex (BCD3-09) is here dated at 2980 ± 1 Ma, within error of two of the dated Usushwana Complex gabbro samples. These ages confirm a geochronological and structural connection between the SE-trending dolerite dykes and the gabbros of the Usushwana Complex, both being broadly coeval to the Nsuze volcanic rocks. The magmatic event would have formed during two episodes, however, at ca. 2.99–2.98 Ga and ca. 2.97–2.96 Ga, which may correlate with the two broad volcanic stratigraphic packages in the Nsuze Group: the stratigraphically lower Pypklipberg (Nhlebela) Formation and the upper Agatha Formation. This is supported by broadly coeval ages between the Piet Retief Suite gabbros (Usushwana Complex), the SE-trending dolerite dykes and the volcanic rocks in the area of the Nsuze Group. The Usushwana Complex gabbros, however, are only associated with the earlier 2.99–2.98 Ga episode of magmatism at present, with SE-trending dolerite dykes across the Barberton-Badplaas area generated during the subsequent 2.97–2.96 Ga episode.

4.2. The Hlagothi Event – a second magmatic event within the Usushwana Complex

New age data of 2.99–2.98 Ga for the Usushwana Complex contradicts the interpretations based on field observations and geochronology presented by Anhaeusser (2006), Walraven and Pape (1994), Layer et al. (1988), Hunter and Reid (1987), Hegner et al. (1984, 1994) and Hammerbeck (1982). These studies used gabbroic sills in the Mozaan Group as evidence for a post-Pongola magmatic event at ca. 2860 Ma, which they attributed to the Usushwana Complex. This study renders the earlier interpretations invalid. The gabbroic sill dated at 2869 ± 5 Ma (PWS-16), which is interpreted as a crystallisation age, is over 100 million years younger than the magmatic events that generated the Piet Retief Suite of the Usushwana Complex, SE-trending dolerite dykes and the Nsuze volcanic rocks, and provides conclusive evidence for two separate magmatic events. This new 2869 Ma age shows that the gabbroic sill is coeval with the Hlagothi Complex, an intrusion much further to the south, which has been dated at 2866 ± 2 Ma (Gumsley *et al.*, 2013). The Hlagothi Complex also intrudes into sandstones of the Pongola Supergroup, indicating this ca. 2870 Ma magmatic event affected a large portion of the south-eastern Kaapvaal Craton. Similar ages have also been reported from the Amsterdam Formation, which was mistakenly referred to as the Hlelo Suite of the Usushwana Complex according to Hammerbeck (1982), with Davies *et al.* (1970) having reported an age of 2874 ± 30 Ma for a granophyre. A pyroxenite of the Thole Complex intruding into the Mozaan Group was also dated to 2871 ± 30 Ma by Hegner et al. (1984) and assigned to the Usushwana Complex. Most ages are at around ca. 2860 Ma (Anhaeusser, 2006 and references therein), and therefore at least parts of the Hlelo Suite most likely cannot be related to the Piet Retief Gabbro Suite.

4.3. The relationship between the Hlelo Suite, Amsterdam Formation, Thole Complex and Hlagothi Complex

The felsic rocks of the Hlelo Suite and the Amsterdam Formation bear similarities. The Hlelo Suite is composed of granodiorites and micro-granites, and the Amsterdam Formation consists, dacites, rhyolites and tuff. It has been shown that the original use of the term granophyre for all these lithologies was too broad and generic, highlighting the difficulty in differentiating between these suites and formations in the field and literature (Hammerbeck, 1982). This becomes particularly apparent in the age data, as many of the granophyres and pyroxenites in the Piet Retief-Amsterdam area appear to be related in age to the Hlagothi Complex, which is unrelated to the Piet Retief Suite of the Usushwana Complex as shown in this study.

Because exposures in the area where the Usushwana Complex, Pongola Supergroup and Amsterdam Formation are in contact are poor, this makes any differentiation of the units uncertain. It has also been observed that there are different generations of gabbro within the Piet Retief Suite, with Hammerbeck (1982) noting at least three. Hammerbeck (1982) also observed gabbro intruding into the Hlelo Suite, and the Hlelo Suite intruding into gabbro, an apparent contradiction. These uncertainties attest to different magmatic events, at discrete times or to a process of back-veining. A further example is the ca. 2.87;Ga ages from pyroxenites thought to be associated with the Usushwana Complex by Hegner et al. (1984). Outside of the SE-trending arm of the Usushwana Complex in Swaziland, only small isolated occurrences of ultramafic rocks are found associated with the Piet Retief Suite. Rocks of this composition are generally assigned to the Thole Complex, a mafic-ultramafic intrusion which intrudes into Mozaan strata, which was dated to 2871 ± 30 Ma by Hegner et al. (1984). The pyroxenites in Swaziland assigned to the Usushwana Complex are more likely part of the Thole Complex, as are the ultramafic sills occurring sporadically in Mozaan strata. This association may be coeval with the Hlagothi Complex, a layered mafic intrusion dated to 2866 ± 2 Ma (Gumsley et al., 2013).

In conclusion, the Piet Retief Suite of the Usushwana Complex should be seen as a magmatic feeder to the ca. 2.99–2.96 Ga Nsuze Group volcanism in multiple pulses and episodes accounting for its occasional layering, and which was intruded by more magma during a subsequent ca. 2.87 Ga event, which include the Hlagothi Complex, and possibly the Thole Complex, as well as felsic magmas of the Amsterdam Formation and the genetically-related parts of the Hlelo Suite. Other parts of the Hlelo Suite may have been derived during assimilation of the overlying Nsuze Group, as the magmatic feeders of the Piet Retief Suite grew and invaded into the overlying sandstones and volcanic rocks.

4.4. Tectonic Model

Fig. 6 illustrates a tentative tectonic model of the greater Pongola Basin, with the recognition of the 2990–2966 Ma Usushwana Complex, SE-trending dolerite dykes and the Nsuze volcanic rocks, as well as the 2874–2866 Ma Hlagothi Complex and related intrusions as two independent magmatic events. The Usushwana Complex, although broadly coeval with the volcanic rocks of the Nsuze Group, does in places intrude and transgress the lower sandstones and volcanic rocks of the group. This is indicative of the Usushwana Complex representing a series of magmatic feeders that were actively feeding the Nsuze Group volcanism (in the Pypklipberg/Nhlebela and Agatha volcanic successions). At least two magmatic episodes are recorded over a period of 25 million years, accompanied by the emplacement of a number of contemporaneous 2980 to 2966 Ma SE-trending dolerite dykes. We suggest that the Usushwana Complex was emplaced from 2990 to 2978 Ma (Fig. 6a and b), growing with time, invading and assimilating the older Nsuze Group Pypklipberg (Nhlebela) volcanic rocks above it, with some of the early granophyres of the Hlelo Suite forming through assimilation of the country rock at the Piet Retief Suite-Pongola Supergroup interface. A hiatus in magmatism would have led to the deposition of the Nkembe (White Mfolozi) Formation, before the establishment of more feeder dykes and sills between 2967 and 2966 Ma (Fig. 6b and c). The Agatha volcanic rocks were produced during this later event, and once again with the possible assimilation of the host rock and the production of granophyres. After ca. 2966 Ma, extension, mechanical subsidence and volcanism ended, and thermal subsidence led to deposition of the Mozaan Group. Initially, sedimentary rocks of the Mozaan Group were deposited in an epicontinental sea (Fig. 6d). As magmatism was reactivated during the onset of the Hlagothi event after 2900 Ma, the Pongola Basin was uplifted and sediments of a more fluvial nature were deposited (Fig. 6e). At ca. 2870 Ma, this renewed magmatism within the south-eastern Kaapvaal Craton led to the emplacement of dolerite sills in the Mozaan Group, as well as the Hlagothi Complex itself (Fig. 6f). This event may also include the emplacement of the Thole Complex, although this link remains to be confirmed (Groenewald, 2006). In addition, the Amsterdam Formation (and parts of the Hlelo Suite) may have been the volcanic equivalent of the Thole Complex, if sedimentation of the Mozaan Group had already ceased by this time. Alternatively, volcanic units within the upper Mozaan Group, such as the Tobolsk and Gabela volcanic rocks may be considered as the volcanic equivalent of the Thole and Hlagothi complexes, and related dolerite sills. This interpretation requires that the age of the Tobolsk volcanic rocks of 2954 ± 5 Ma by Mukasa et al. (2013) is too old because of zircon inheritance, and because this age is in fact within error of the age of Agatha volcanism.

One of the arguments raised in this study is a need for better geochronological control of the detailed stratigraphic analyses carried out by Wilson et al. (2013) and Cole (1994). These authors described in detail aspects of the volcanic rock units of the Nsuze Group in its various sub-basins. The volcanic rocks within these sub-basins vary significantly in thickness and distribution, and in none of the localities there is a complete exposed stratigraphic profile. Facies changes are related to local conditions, and based on the observation of modern systems, it is possible that the complexities in the lava flows may differ substantially, especially over a 25 Myr time frame in which they were deposited. Significant differences could record a shift of magmatic centres and changes in topography. This is especially important for the Pongola Supergroup, because recent geochronology for the Nsuze Group is constrained only by ages within the Hartland Basin, whereas corresponding studies from other areas are lacking. Volcanic sequences in the Bivane Subgroup from the Nsuze Group from different sub-basins cannot easily be assigned to either the Pypklipberg (Nhlebela) or Agatha volcanic rocks, and there is up to a 25 Myr difference in time between deposition. This is especially true in the absence of what is now recognised as the complete volcano-sedimentary package.

5. Summary

The Usushwana Complex is composed of the gabbroic Piet Retief Suite, and the Hlelo Suite granodiorites and micro-granites. The Piet Retief Suite intruded into Eo- to Mesoarchaean granitoid-greenstone basement of the south-eastern Kaapvaal Craton and overlying Mesoarchaean Pongola Supergroup. U-Pb baddeleyite ID-TIMS ages obtained in this study show that parts of the Usushwana Complex are up to 130 Myr older than previously thought, with ages of 2989 ± 1 Ma, 2990 ± 2 Ma and 2978 ± 2 Ma from samples of the Piet Retief Suite. These ages are consistent with the gabbroic parts of Usushwana Complex being broadly coeval with Nsuze Group volcanism of the Pongola Supergroup, along with parts of the granophyric Hlelo Suite derived through crustal assimilation and contamination. This connection is confirmed by the presence of a SE-trending dolerite dyke dated in this study using the same techniques to 2980 ± 1 Ma. It follows the same trend as the two broad arms of the Usushwana Complex, as well as the two previously dated ca. 2967–2966 Ma old SE-trending dolerite dykes of the Barberton-Badplaas Dyke Swarm further to the north (Olsson et al., 2010). The SE-trending lineaments represent zones of weakness that were intermittently under extension during a 25 million year time interval, and thereby acted as pathways for magma that gave rise to Nsuze volcanic rocks of the Pypklipberg (2.99–2.98 Ga) and Agatha volcanic episodes (2.97–2.96 Ga), as well as the subvolcanic SE-trending dykes and Piet Retief Suite of the Usushwana Complex.

A dolerite sill in the Mozaan Group strata, previously thought to be of Usushwana Complex age, was dated using U-Pb on baddeleyite to 2869 ± 5 Ma. This age is in agreement with previous age determinations of the Usushwana Complex, indicating two independent phases of intrusive magmatic activity, with the latter being coeval to the intrusion of the 2866 ± 2 Ma Hlagothi Complex (Gumsley et al., 2013). This magmatic event may include the Thole Complex, as well as parts of the Hlelo Suite and Amsterdam Formation. In addition, this new age provides a new maximum and minimum age for the deposition of the Pongola Supergroup, from 2.99 to 2.87 Ga.

Acknowledgements

The authors wish to thank the editor and two anonymous reviewers for helping to improve this manuscript. This study has benefited from the Swedish Research Council, through research grants to Ulf Söderlund, from which field work, followed by sample processing at the Department of Geology at Lund University and analysis at the Department of Geosciences at the Museum of Natural History in Stockholm has been possible. Special thanks to Per-Olof Persson, Hans Schöberg and Kjell Billström, as well as the rest of the staff at the Department of Geoscienceat the Swedish Museum of Natural History in Stockholm for help during ID-TIMS analysis. Axel Hofmann acknowledges support from the National Research Foundation of South Africa. Ashley Gumsley also acknowledges support from the Royal Physiographic Society in Lund for a travel grant.

Appendix A. Supplementary data

Supplementary data associated with this article can be found, in the online version, at http://dx.doi.org/10.1016/j.precamres.2015.06.010

References

Anhaeusser, C.R., 2006. Ultramafic and mafic intrusions of the Kaapvaal Craton. In: Johnson, M.R., Anhaeusser, C.R., Thomas, R.J. (Eds.), The Geology of South Africa. Geological Society of South Africa/Council of Geoscience, Johannesburg/Pretoria, pp. 95–134.

Barton Jr., J.M., Hunter, D.R., Jackson, M.P.A., Wilson, A.C., 1983. Geochronologic and Sr-isotopic studies of certain units in the Barberton granite-greenstone terrane, Swaziland. Trans. Geol. Soc. S. Afr. 86, 71–80.

Beukes, N.J., Cairncross, B.C., 1991. A lithostratigraphic-sedimentological reference profile of the late Archaean Mozaan Group. Pongola Supergroup: application to sequence stratigraphy and correlation to the Witwatersrand Supergroup. S. Afr. J. Geol. 94, 44–59.

Bleeker, W., Ernst, R.E., 2006. Short-lived mantle generated magmatic events and their dyke swarms: The key unlocking Earth's paleogeographic record back to 2. 6 Ga. In: Hanski, E., Mertanen, S., Rämö, T., Vuollo, J. (Eds.), Dyke Swarms – Time Markers of Crustal Evolution. Taylor & Francis, London, pp. 3–26.

Burger, A.J., Coertze, F.J., 1973. Radiometric age measurements on rocks from southern Africa to the end of 1971. Geological Survey of South Africa Bulletin 58, Pretoria, 46 p.

Cole, E.G., 1994. Lithostratigraphy and depositional environment of the Archaean Nsuze Group, Pongola Supergroup. Unpublished M.Sc thesis, Rand Afrikaans University, Johannesburg. 166 pages.

Davies, R.D., Allsopp, H.L., Erlank, A.J., Manton, W.I., 1970. Sr-isotopic studies on various layered mafic intrusions in southern Africa. In: Visser, D.J.L., von Gruenewaldt, G. (Eds.), Symposium on the Bushveld Complex and other Layered Intrusions. Geological Society of South Africa Special Publication 1, Johannesburg, pp. 576–593.

de Wit, M.J., de Ronde, C.E.J., Tredoux, M., Roering, C., Hart, R.J., Armstrong, R.A., Green, R.W.E., Peberdy, E., Hart, R.A., 1992. Formation of an Archaean continent. Nature 357, 553–562.

Eglington, B.M., Armstrong, R.A., 2004. The Kaapvaal Craton and adjacent orogens, southern Africa: a geochronological database and overview of the geological development of the craton. S. Afr. J. Geol. 107, 13–32.

Eriksson, P.G., Banerjee, S., Nelson, D.R., Rigby, M.J., Catuneanu, O., Sarkar, S., Roberts, R.J., Ruban, D., Mtimkulu, M.N., Raju, P.V.S., 2009. A Kaapvaal craton debate: nucleus of an early small supercontinent or affected by an enhanced accretion event? Gondwana Res. 15, 354–372.

Ernst, R.E., Bleeker, W., Söderlund, U., Kerr, A.C., 2013. Large Igneous Provinces and supercontinents: toward completing the plate tectonic revolution. Lithos 174, 1–14.

Ernst, R.E., Srivastava, R., Bleeker, W., Hamilton, M., 2010. Precambrian Large Igneous Provinces (LIPs) and their dyke swarms: new insights from high-precision geochronology integrated with paleomagnetism and geochemistry. Precambrian Res. 183, vii–xi.

Gerstenberg, H., Haase, G., 1997. A highly effective emitter substance for mass spectrometric Pb isotope ratios determinations. Chem. Geol. 136, 309–312.

Gold, D.J.C., 2006. The Pongola Supergroup. In: Johnson, M.R., Anhaeusser, C.R., Thomas, R.J. (Eds.), The Geology of South Africa. Geological Society of South Africa/Council of Geoscience, Johannesburg/Pretoria, pp. 135–154.

Groenewald, P.B., Unpublished M.Sc thesis, 1984. The lithostratigraphy and petrogenesis of the Nsuze Group, northwest of Nkandla. Natal. University of Natal, Pietermaritzburg, 240 p.

Groenewald, P.B., 2006. Hlagothi Complex. In: Johnson, M.R. (Ed.), Catalogue of South African Lithostratigraphic Units. South African Committee for Statigraphy, Pretoria, pp. 3–4.

Gumsley, A.P., Unpublished M.Sc thesis, 2013. Towards a magmatic 'barcode' for the south-easternmost terrane of the Kaapvaal Craton, South Africa. University of Johannesburg, Johannesburg, 227 p.

Gumsley, A.P., de Kock, M.O., Rajesh, H.M., Knoper, M.W., Söderlund, U., Ernst, R.E., 2013. The Hlagothi Complex: The identification of fragments from a Mesoarchaean large igneous province on the Kaapvaal Craton. Lithos 174, 333–348.

Gutzmer, J., Nhleko, N., Beukes, N.J., Pickard, A., Barley, M.E., 1999. Geochemistry and ion microprobe (SHRIMP) age of a quartz porphyry sill in the Mozaan Group of the Pongola Supergroup: implications for the Pongola and Witwatersrand Supergroups. S. Afr. J. Geol. 102, 139–146.

Hammerbeck, E.C.I., 1982. The geology of the Usushwana Complex and associated formations - south-eastern Transvaal. Pretoria: Geological Survey of South Africa Memoir 70, 119 p.
Heaman, L.M., LeCheminant, A.N., 1993. Paragenesis and U-Pb Systematics of Baddeleyite (ZrO2). Chem. Geol. 110, 95–126.
Hegner, E., Kröner, A., Hofmann, A.W., 1984. Age and Isotope Geochemistry of the Archean Pongola and Usushwana Suites in Swaziland, Southern Africa - a case for Crustal Contamination of Mantle-Derived Magma. Earth Planet. Sci. Lett. 70, 267–279.
Hegner, E., Kröner, A., Hunt, P., 1994. A precise U-Pb zircon age for the Archaean Pongola Supergroup volcanics in Swaziland. J. Afr. Earth Sci. 18, 339–341.
Hofmann, A., Kröner, A., Xie, H., Hegner, E., Belyanin, G., Kramers, J., Bolhar, R., Slabunov, A., Reinhardt, J., Horváth, P., 2015. The Nhlangano gneiss dome in south-west Swaziland – A record of crustal destabilization of the eastern Kaapvaal craton in the Neoarchaean. Precambrian Res. 258, 109–132.
Humprey, W.A., Krige, L.J., 1931. The geology of the country south of Piet Retief: an explanation of sheet no. 68 (Piet Retief). Geological Survey of South Africa, Pretoria, 72 p.
Hunter, D.R., 1970. The geology of the Usushwana Complex in Swaziland. In: Visser, D.J.L., von Gruenewaldt, G. (Eds.), Symposium on the Bushveld Complex and other Layered Intrusions. Geological Society of South Africa Special Publication 1, Johannesburg, pp. 645–660.
Hunter, D.R., 1973. The granitic rocks of the Precambrian in Swaziland. In: Lister, L.A. (Ed.), Symposium on Granites, Gneisses and Related Rocks. Geological Society of South Africa Special Publication 3, Johannesburg, pp. 131–147.
Hunter, D.R., Reid, D.L., 1987. Mafic Dyke Swarms in Southern Africa. In: Halls, H.C., Fahrig, W.F. (Eds.), Mafic Dyke Swarms. Geological Association of Canada Special Paper 34. St. John's, pp. 445–456.
Ibanez-Mejia, M., Gehrels, G.E., Ruiz, J., Vervoort, J.D., Eddy, M.P., Li, C., 2014. Small-volume baddeleyite (ZrO_2) U–Pb geochronology and Lu–Hf isotope geochemistry by LA-ICP-MS. Techniques and applications. Chem. Geol. 384, 149–167.
Jaffey, A.H., Flynn, K.F., Glendenin, L.E., Bently, W.C., Essling, A.M., 1971. Precision Measurement of Half-Lives and Specific Activities of U^{235} and U^{238}. Phys. Rev. C 4, 1889–1906.
Kamo, S.L., Davis, D.W., 1994. Reassessment of Archean Crustal Development in the Barberton Mountain Land, South-Africa, Based on U-Pb Dating. Tectonics 13, 167–192.
Klausen, M.B., Soderlund, U., Olsson, J.R., Ernst, R.E., Armoogam, M., Mkhize, S.W., Petzer, G., 2010. Petrological discrimination among Precambrian dyke swarms: Eastern Kaapvaal craton (South Africa). Precambrian Res. 183, 501–522.
Krogh, T.E., Corfu, F., Davis, D.W., Dunning, G.R., Heaman, L.M., Kamo, S.L., Machado, N., Greenough, J.D., Nakamura, E., 1987. Precise U-Pb isotopic ages of diabase dykes and mafic to ultramafic rocks using trace amounts of baddeleyite and zircon. In: Halls, H.C., Fahrig, W.F. (Eds.), Mafic Dyke Swarms. Geological Association of Canada Special Paper 34. St. John's, pp. 147–152.
Layer, P.W., Kroner, A., Mcwilliams, M., Burghele, A., 1988. Paleomagnetism and Age of the Archean Usushwana Complex, Southern-Africa. J. Geophys. Res.-Solid Earth Planets 93, 449–457.
Layer, P.W., Kröner, A., McWilliams, M., York, D., 1989. Elements of the Archean thermal history and apparent polar wander of the eastern Kaapvaal Craton, Swaziland, from single grain dating and paleomagnetism. Earth Planet. Sci. Lett. 93, 23–24.
Ludwig, K.R., 1991. Isoplot - a plotting and regression program for radiogenic isotopic data, USGS Open-File Report., pp. 91–445.
Maphalala, R., Kröner, A., 1993. Pb-Pb single zircon ages for the younger Archaean granitoids of Swaziland. In: Maphalala, R., Mubuza, M. (Eds.), 16th Colloquium of African Geology extended abstracts. Mbabane, Swaziland. , pp. 201–206.
Maphalala, R., Trumbull, R.B., 1998. A geochemical and Rb-Sr isotopic study of Archaean pegmatite dykes in the tin belt of Swaziland. S. Afr. J. Geol. 101, 53–65.
Meyer, F.M., Reimold, W.U., Walraven, F., 1993. The evolution of the Archaean granitic crust in the south-eastern Kaapvaal Craton, South Africa. Terra 5, 319.
Mukasa, S.B., Wilson, A.H., Young, K.R., 2013. Geochronological constraints on the magmatic and tectonic development of the Pongola Supergroup (Central Region), South Africa. Precambrian Res. 224, 268–286.
Nhleko, N., Unpublished Ph.D thesis, 2003. The Pongola Supergroup in Swaziland. Rand Afrikaans University, Johannesburg, 132 p.
Olsson, J.R., Unpublished Ph.D thesis, 2012. U-Pb baddeleyite geochronology of Precambrian mafic dyke swarms and complexes in southern Africa. Lund University, Lund, 125 p.
Olsson, J.R., Söderlund, U., Klausen, M.B., Ernst, R.E., 2010. U-Pb baddeleyite ages linking major Archean dyke swarms to volcanic-rift forming events in the Kaapvaal craton (South Africa), and a precise age for the Bushveld Complex. Precambrian Res. 183, 490–500.
Olsson, J.R., Söderlund, U., Hamilton, M.A., Klausen, M.B., Helffrich, G.R., 2011. A late Archaean radiating dyke swarm as possible clue to the origin of the Bushveld Complex. Nature Geosci. 4, 865–869.
Poujol, M., Robb, L.J., Anhaeusser, C.R., Gericke, B., 2003. A review of the geochronological constraints on the evolution of the Kaapvaal Craton, South Africa. Precambrian Res. 127, 181–213.
Reimold, W.U., Meyer, F.M., Walraven, F., Matthews, P.E., 1993. Geochemistry and chronology of pre- and post-Pongola granitoids from northeastern Natal. In: Maphalala, R., Mubuza, M. (Eds.), 16th Colloquium of African Geology extended abstracts. Mbabane, Swaziland, pp. 294–296.
Robb, L.J., Brandl, G., Anhaeusser, C.R., Poujol, M., 2006. Archaean Granitoid Intrusions. In: Johnson, M.R., Anhaeusser, C.R., Thomas, R.J. (Eds.), The Geology of South Africa. Geological Society of South Africa/Council of Geoscience, Johannesburg/Pretoria, pp. 57–94.
Schmitt, A.K., Chamberlain, K.R., Swapp, S.M., Harrison, T.M., 2010. In situ U-Pb dating of micro-baddeleyite by secondary ion mass spectrometry. Chem. Geol. 269, 386–395.
Schoene, B., Bowring, S.A., 2010. Rates and mechanisms of Mesoarchean magmatic arc construction, eastern Kaapvaal craton, Swaziland. Geol. Soc. Am. Bull. 122, 408–429.
Söderlund, U., Johansson, L., 2002. A simple way to extract baddeleyite (ZrO_2). Geochem. Geophys. Geosyst. 3, http://dx.doi.org/10.1029/2001GC000212
Stacey, J.S., Kramers, J.D., 1975. Approximation of terrestrial lead isotope evolution by a two-stage model. Earth Planet. Sci. Lett. 26, 207–221.
van Vuuren, C.J., Unpublished M.Sc thesis, 1965. Die geologie van 'n gebied suid van Amsterdam, Oos-Transvaal. University of the Orange Free State, Bloemfontein.
Walraven, F., Pape, J., 1994. Pb-Pb whole-rock ages for the Pongola Supergroup and the Usushwana Complex, South Africa. J. Afr. Earth Sci. 18, 297–308.
Wilson, A.H., Groenewald, B., Palmer, C., 2013. Volcanic and Volcaniclastic Rocks of the Mesoarchaean Pongola Supergroup in South Africa and Swaziland: Distribution, Physical Characteristics, Stratigraphy and Correlations. S. Afr. J. Geol. 116, 119–168.
Winter, P.E., 1965. The Usushwana Igneous Complex. Geological Survey of Swaziland, Mbabane, 29 p.

PAPER II

Precambrian Research 269 (2015) 58–72

Contents lists available at ScienceDirect

Precambrian Research

journal homepage: www.elsevier.com/locate/precamres

U–Pb geochronology and paleomagnetism of the Westerberg Sill Suite, Kaapvaal Craton – Support for a coherent Kaapvaal–Pilbara Block (Vaalbara) into the Paleoproterozoic?

Tobias C. Kampmann[a,*], Ashley P. Gumsley[a], Michiel O. de Kock[b], Ulf Söderlund[a,c]

[a] Department of Geology, Lund University, Sölvegatan 12, Lund 223 62, Sweden
[b] Department of Geology, University of Johannesburg, P.O. Box 524, Auckland Park 2006, South Africa
[c] Department of Geosciences, Swedish Museum of Natural History, P.O. Box 50, 104 05 Stockholm, Sweden

ARTICLE INFO

Article history:
Received 17 December 2014
Received in revised form 13 July 2015
Accepted 3 August 2015
Available online 12 August 2015

Keywords:
Apparent polar wander path
Baddeleyite U–Pb geochronology
Kaapvaal
Paleomagnetism
Paleoreconstruction
Vaalbara

ABSTRACT

Precise geochronology, combined with paleomagnetism on mafic intrusions, provides first-order information for paleoreconstruction of crustal blocks, revealing the history of supercontinental formation and break-up. These techniques are used here to further constrain the apparent polar wander path of the Kaapvaal Craton across the Neoarchean–Paleoproterozoic boundary. U–Pb baddeleyite ages of 2441 ± 6 Ma and 2426 ± 1 Ma for a suite of mafic sills located on the western Kaapvaal Craton in South Africa (herein named the Westerberg Sill Suite), manifests a new event of magmatism within the Kaapvaal Craton of southern Africa. These ages fall within a ca. 450 Myr temporal gap in the paleomagnetic record between 2.66 and 2.22 Ga on the craton. Our older Westerberg Suite age is broadly coeval with the Woongarra magmatic event on the Pilbara Craton in Western Australia. In addition, the Westerberg Suite on the Kaapvaal Craton intrudes a remarkably similar Archean-Proterozoic sedimentary succession to that on the Pilbara Craton, supporting a stratigraphic correlation between Kaapvaal and Pilbara (i.e., Vaalbara). The broadly coeval Westerberg–Woongarra igneous event may represent a Large Igneous Province. The paleomagnetic results are more ambiguous, with several different possibilities existing. A Virtual Geomagnetic Pole obtained from four sites on the Westerberg sills is 18.9°N, 285.0°E, A_{95} = 14.1°, K = 43.4 (Sample based VGP, n = 34: 16.8°N, 2879.9°E, dp = 4.4°, dm = 7.7°). If primary (i.e., 2441–2426 Ma), it would provide a further magmatic event within a large temporal gap in the Kaapvaal Craton's Paleoproterozoic apparent polar wander path. It would suggest a relatively stationary Kaapvaal Craton between 2.44 Ga and 2.22 Ga, and ca. 35° of latitudinal drift of the craton between ca. 2.66 Ga and 2.44 Ga. This is not observed for the Pilbara Craton, suggesting breakup of Vaalbara before ca. 2.44 Ga. However, it is likely that the Woongarra paleopole represents a magnetic overprint acquired during the Ophtalmian or Capricorn Orogeny, invalidating a paleomagnetic comparison with the Westerberg Sill Suite. Alternatively, our Westerberg Virtual Geographic Pole manifests a 2.22 Ga magnetic overprint related to Ongeluk volcanism. The similarity between Ongeluk and Westerberg paleopoles however may also infer magmatic connections if both are primary directions, despite the apparent 200 million year age this difference.

1. Introduction

A fundamental question concerning the arrangement of late Archean continental blocks is whether they were amalgamated into a single supercontinent, Kenorland, or if they were dispersed into several smaller supercratons such as Superia, Sclavia and Vaalbara (e.g., Bleeker, 2003). Paucity of the paleomagnetic record for most Archean continental crust, and a lack of reliable geochronology on units with paleomagnetic constraints are the main problems preventing resolution of this question. Precise emplacement ages from igneous units of different ages, together with paleogeographic studies can be used to construct magmatic barcodes and apparent polar wander paths (APWPs) of these Archean crustal blocks. Similar magmatic barcode and APWPs indicate if the cratons were a part of a common crustal framework, whereas divergent magmatic barcodes and APWPs indicate the

* Corresponding author. Present address: Department of Civil, Environmental and Natural Resources Engineering, Luleå University of Technology, 97187 Luleå, Sweden. Tel.: +46 0920492891.
E-mail address: tobias.kampmann@ltu.se (T.C. Kampmann).

http://dx.doi.org/10.1016/j.precamres.2015.08.011
0301-9268/

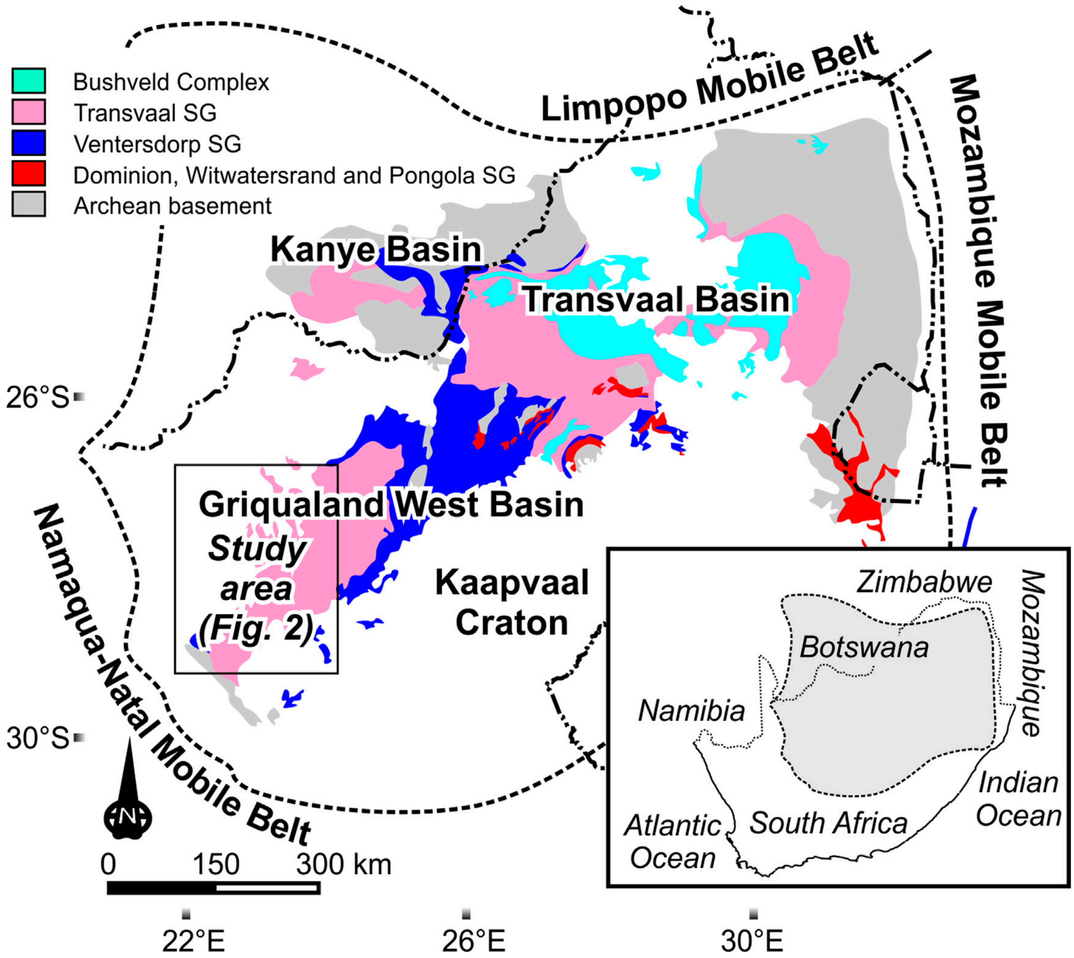

Fig. 1. Geological map of the Kaapvaal Craton, showing the major >2.0 Ga units (simplified after Keyser, 1997). The spatial subdivision of the Transvaal Supergroup successions into the Transvaal, Griqualand West and Kanye (in Botswana) basins is shown. The schematic division into three tectonic blocks is based on Eglington and Armstrong (2004). Abbreviation SG = Supergroup.

cratons were presumably dispersed during this time interval (e.g. Bleeker and Ernst, 2006).

The Kaapvaal Craton of southern Africa has long attracted the attention of research, and it is one of the best-studied Archean cratons. This is partly due to the extraordinary preservation of >2.0 Ga supracrustal successions, such as the Witwatersrand and Transvaal supergroups, as well as the Bushveld Complex, with the associated deposits of gold, iron, diamonds, manganese, platinum, chromium and vanadium (Fig. 1). The most studied connection regarding the Kaapvaal Craton during the Archean and Paleoproterozoic is with the Pilbara Craton of Western Australia. The Neoarchean-Paleoproterozoic continuity of these two cratons (i.e., Vaalbara) was first proposed by Cheney et al. (1988). The exact configuration of the two cratons at this time has since been tested (Smirnov et al., 2013; De Kock et al., 2009a; Strik et al., 2003; Wingate, 1998; Zegers et al., 1998). Vaalbara is currently paleomagnetically well constrained between ca. 2.78 Ga and 2.66 Ga during Ventersdorp volcanism on the Kaapvaal Craton (e.g., De Kock et al., 2009a). After this volcanism, a remarkable stratigraphic match between the Ghaap Group (Transvaal Supergroup) on the Kaapvaal Craton and the Hamersley Group, Pilbara Craton, suggests a cohesive Vaalbara into the Paleoproterozoic (e.g., Beukes and Gutzmer, 2008). However, the next youngest well-constrained paleopoles from either craton, are from rocks in which correlation is much more problematic. For the Kaapvaal Craton, the next youngest paleopole is dated at ca. 2.22 Ga, or ca. 2.43 Ga (Evans et al., 1997), due to contradicting age determinations discussed below; whereas for the Pilbara Craton they are between 1.75 and 1.95 Ga (Schmidt and Clark, 1994; Li et al., 1993). A primary paleomagnetic record for the lower part of the Ghaap Group and the Hamersley Group has so far proved elusive (De Kock et al., 2009b; Schmidt and Clark, 1994; Li et al., 1993).

This study reports U–Pb geochronology and paleomagnetism for the newly identified Westerberg Sill Suite, which forms semi-continuous outcrops in the Griqualand West sub-basin of the Transvaal Supergroup on the western margin of the Kaapvaal Craton. These mafic intrusions occur in the upper parts of the 2465 ± 6 Ma Kuruman Iron Formation, in the Ghaap Group (Pickard, 2003). If the Westerberg Sill Suite is coeval with the 2449 ± 3 Ma dolerites that intrude the Weeli Wolli Iron Formation near the top of the Hamersley Group on the Pilbara Craton (Barley et al., 1997), the geochronological magmatic “barcode” match and similar stratigraphies could support the existence of Vaalbara as a continuous cratonic block well into the Paleoproterozoic Era. This may also refine relative positions of these cratons using paleomagnetic studies at this time.

2. Geological setting

2.1. Regional geology

The Kaapvaal Craton in southern Africa is composed of ca. 3.6–2.7 Ga granitoid-greenstone basement overlain by ca. 3.1–1.7 Ga supracrustal cover successions. The Neoarchean Ventersdorp Supergroup (which provides paleomagnetic constraints used to support Vaalbara), and the Paleoproterozoic Transvaal Supergroup (that matches the Pilbara Craton temporally and stratigraphically), are two such cover successions that developed across the ca. 3.6 and 2.7 Ga crustal basement (Fig. 1).

Following the extensive volcanism and sedimentation that resulted in the deposition of the Ventersdorp Supergroup, deposition of clastic and carbonate sedimentary rocks (with subordinate volcanic rock units) of the Transvaal Supergroup began. The Transvaal Supergroup is today preserved in three 'basins' or erosional remnants. These remnants consist of the Transvaal Basin on the central and eastern parts of the Kaapvaal Craton, and the Griqualand West Basin on the western Kaapvaal Craton (both occurring in South Africa), while the isolated and largely Kalahari sand-covered occurrences in Botswana are referred to as the Kanye Basin (Fig. 1). The spatially separated remnants share a similar geological evolution and stratigraphy. Geological units have therefore been defined representing similar lithologies that can span over more than one basin. An estimate for the onset of sedimentation is provided by volcanic rocks in the Vryburg Formation in the Griqualand West Basin, which is dated to 2642 ± 3 Ma (Walraven and Martini, 1995). This is temporally similar to the 2664 ± 6 Ma age reported for the Wolkberg Group further to the east (Barton et al., 1995), which is considered to be a protobasinal fill of sedimentary and volcanic rocks before the onset of sedimentation in the main Transvaal Basin. The Wolkberg Group is overlain by the Black Reef Formation in both the Transvaal and Kanye basins. The Vryburg Formation is an equivalent of the Black Reef Formation, and forms the base of the Transvaal Supergroup in the Griqualand West Basin. The carbonate to banded iron formation (BIF) platform successions (Chuniespoort, Ghaap and Taupone groups in the Transvaal, Griqualand West and Kanye basins, respectively), and the overlying mixed clastic and chemical sedimentary rocks (Pretoria, Postmasburg and Segwagwa groups), are widespread and present in all three basins (Eriksson et al., 2006). The Ghaap Group of the Griqualand West Basin hosts the Westerberg Sill Suite, which is the focus of this study (Fig. 2).

The Ghaap Group (Schröder et al., 2006), is a ca. 1.5 km thick carbonate and BIF succession, with a four-fold subdivision (i.e., the Schmidtsdrif, Campbellrand, Asbestos Hills, and Koegas subgroups). The Koegas Subgroup has alternatively been placed into the Ghaap and Postmasburg groups (Eriksson et al., 2006). The Schmidtsdrif Subgroup, which can include the 2642 ± 3 Ma Vryburg Formation (Walraven and Martini, 1995), is a mixed clastic-carbonate ramp succession that is conformably overlain by the Campbellrand Subgroup. The Malmani Subgroup in the main Transvaal Basin represents laterally equivalent strata of carbonate rocks (Beukes, 1987). This carbonate strata consists of a thin basinal deep water succession near the south-west margin of the craton in the Griqualand West Basin, and a relatively thick continental shelf succession deposited in shallower water on the craton in both the Griqualand West and Transvaal basins. Chert and BIF of the Asbestos Hills Subgroup conformably overlie the Campbellrand Subgroup, representing drowning of the platform at about 2.5 Ga (Pickard, 2003; Sumner and Bowring, 1996). The ca. 950 m thick Asbestos Hills Subgroup comprises of the 2464 ± 6 Ma Kuruman Iron Formation and the conformably overlying Griquatown/Daniëlskuil Iron Formation (Beukes and Gutzmer, 2008; Pickard, 2003; Eriksson et al., 2006). Dolerites intrude the finely laminated micritic iron formation of the Westerberg Member in the upper stratigraphic levels of the Kuruman Iron Formation (e.g., the Westerberg Sill near Prieska; Fig. 2). Discontinuous intrusive dolerite sills have been mapped along strike from north-east of Prieska all the way to Kuruman with decreasing occurences. Iron formations and clastic rocks of the Koegas Subgroup conformably overlies the Griqualand/Daniëlskuil iron formations, and represent the stratigraphic top of the Ghaap Group. These iron formation successions are progressively cut down into toward the north-east by a regional glacial unconformity overlain by the Makganyene Formation diamictites. Extrusion of the Ongeluk Formation volcanic rocks followed conformably over the Makganyene Formation at 2222 ± 13 Ma, according to a Pb–Pb whole-rock isochron age by Cornell et al. (1996). The reliability of this age, however, is under debate because of the altered nature of the volcanic rocks, and subsequent whole-rock Pb–Pb and U–Pb isochron age determinations of 2394 ± 26 Ma and 2392 ± 26 Ma, respectively on the overlying Mooidraai Formation dolomite in the upper Postmasburg Group (Bau et al., 1999; Fairey et al., 2013). This presents an alternative, significantly older, minimum age for the Ongeluk and Makganyene formations, with implications discussed by Hoffman (2013) and Kirschvink et al. (2000). In addition, a stratigraphic correlation of rocks of the Postmasburg Group with rocks of the Pretoria Group in the Transvaal Basin remains contested (e.g., Moore et al., 2001, 2012). Deposition of the Transvaal Supergroup sedimentary rocks ended abruptly with the emplacement of the Bushveld Complex (Fig. 1) at ca. 2.05 Ga.

At ca. 1.20 Ga, the Namaqua-Natal Mobile Belt started to form by successive accretion of terranes to the western margin of the Kaapvaal Craton. Accretion and collision of these terranes with the Kaapvaal Craton continued until approximately 1.02 Ga according to Eglington and Armstrong (2004), resulting in orogenesis and regional metamorphism along the western and southern margins of the craton (Fig. 1).

2.2. Local geology

The Westerberg Sill near Prieska on the western margin of the Kaapvaal Craton (Prieska study area, Fig. 2b), intruded in close proximity to the region that was thoroughly reworked and metamorphosed between ca. 1.20 and 1.02 Ga during the Namaqua-Natal Orogeny (Figs. 1 and 2; Eglington, 2006). Extensive folding of the Transvaal Supergroup stratigraphy on this western margin of the craton, including the Kuruman Iron Formation and the Westerberg Sill, however, is related to deformation during an older (pre-1.9 Ga) tectonic event. This folding is expressed in the Prieska study area as a large synclinal structure with a north–south axis and smaller parasitic folds (Altermann and Hälbich, 1990). Toward the north and east of Prieska (Kuruman study area, Fig. 2a), dolerite bodies that are less deformed and metamorphosed intrude into the cratonic hinterland. These intrusions, now linked in this study to the Westerberg Sill near Prieska, define a more extensive sill suite (Fig. 2), with a regional tilt of bedding <10° to the west.

The intermittent intrusive dolerite bodies have varying overall thicknesses of 50–200 m, and are composed of fine- to medium-grained gray-green dolerite. Sericitisation of plagioclase is common, indicating a secondary event of alteration which increases with proximity to the craton margin in the south and west. Magnetite occurs throughout the groundmass as small, euhedral crystals ca. 0.1–0.3 mm in diameter. The outer surfaces of the crystals are slightly altered. Almost all primary pyroxenes have undergone varying amounts of uralitisation, although relict pyroxene rafts are occasionally preserved. The BIF that hosts the dolerite shows clear evidence of contact metamorphism up to ca. 0.5 m away from the intrusive contacts. The preservation of the original

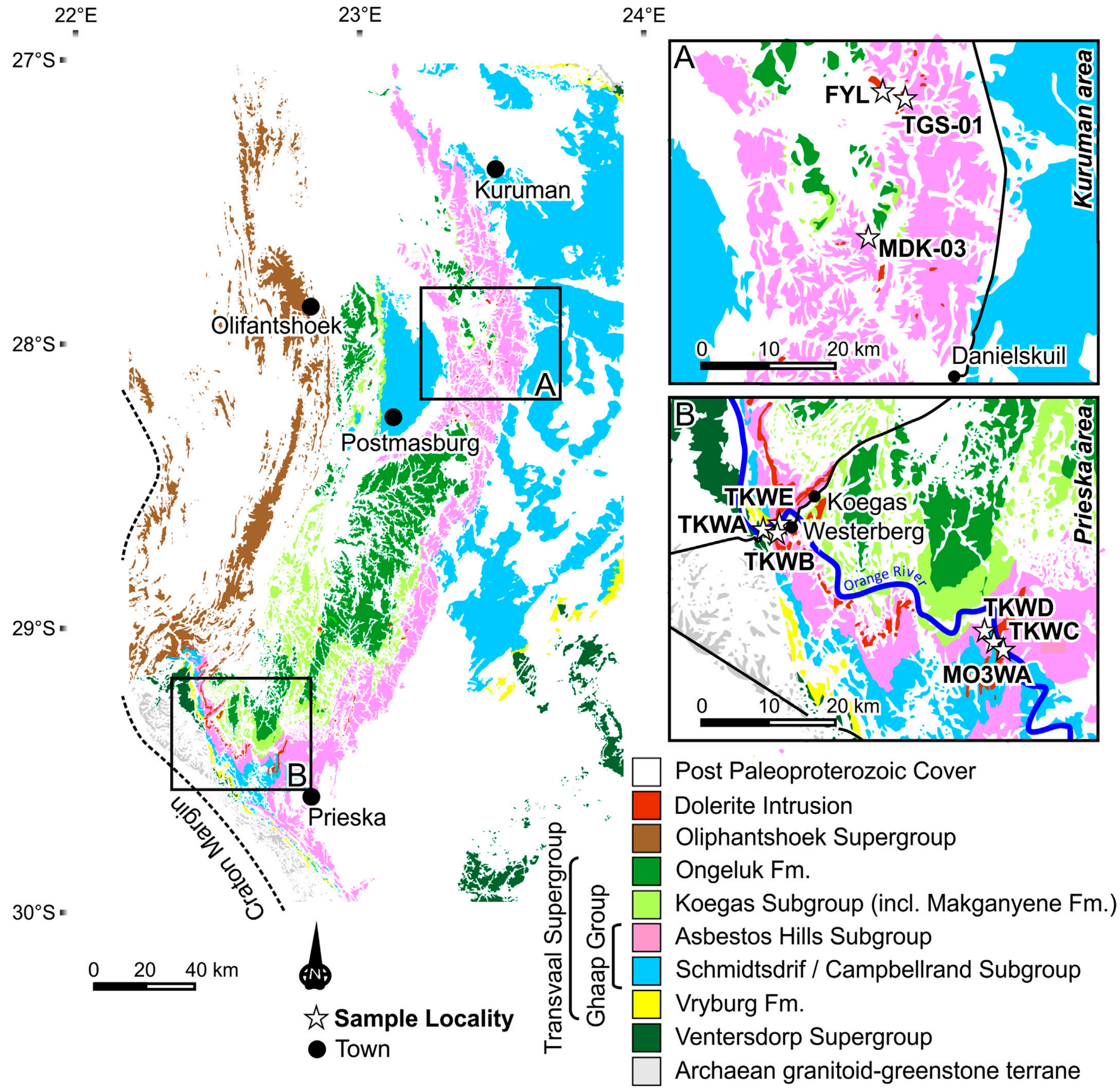

Fig. 2. Simplified geological map of the study area modified from 1:250 000 maps produced by the Council for Geoscience, South Africa. Inset maps show sample localities A (Kuruman study area) and B (Prieska study area) in the north-east and south-west respectively.

sedimentary layering in the BIF indicates that the intrusion of the sills occurred after the sediments were lithified.

Although there have been several studies on the geology of the study area (Fig. 2), none have focused on the dolerite intrusions. Dreyer (1982) interpreted the Westerberg dolerite intrusions as sills, whereas Altermann and Hälbich (1990) described the intrusions as dyke-like bodies intruding at a low angle to the bedding of the host sedimentary rock. A correct classification of the Westerberg intrusions in relation to the host lithology is crucial, since it controls the structural correction used during paleomagnetic studies. As no foliation in the dolerite themselves has been observed, the contact zone to the surrounding BIFs was examined at several outcrops in the Prieska study area. No signs of angular discordance were observed in the field. Columnar jointing of the dolerite perpendicular to bedding of the iron formation in the country rock further confirms that the intrusions should be classified as sills rather than dykes.

3. Methodology

3.1. Baddeleyite ID-TIMS U–Pb geochronology

The center of the Westerberg dolerite (sample M03WA, collected on the Naauwte Farm in the Prieska study area; Fig. 2b), was sampled for U–Pb geochronology, along with sample TGS-01 further to the north in the Kuruman study area (Fig. 2a). Sample processing and dissolution were done at Lund University, Sweden. The highest quality baddeleyite grains were identified under the

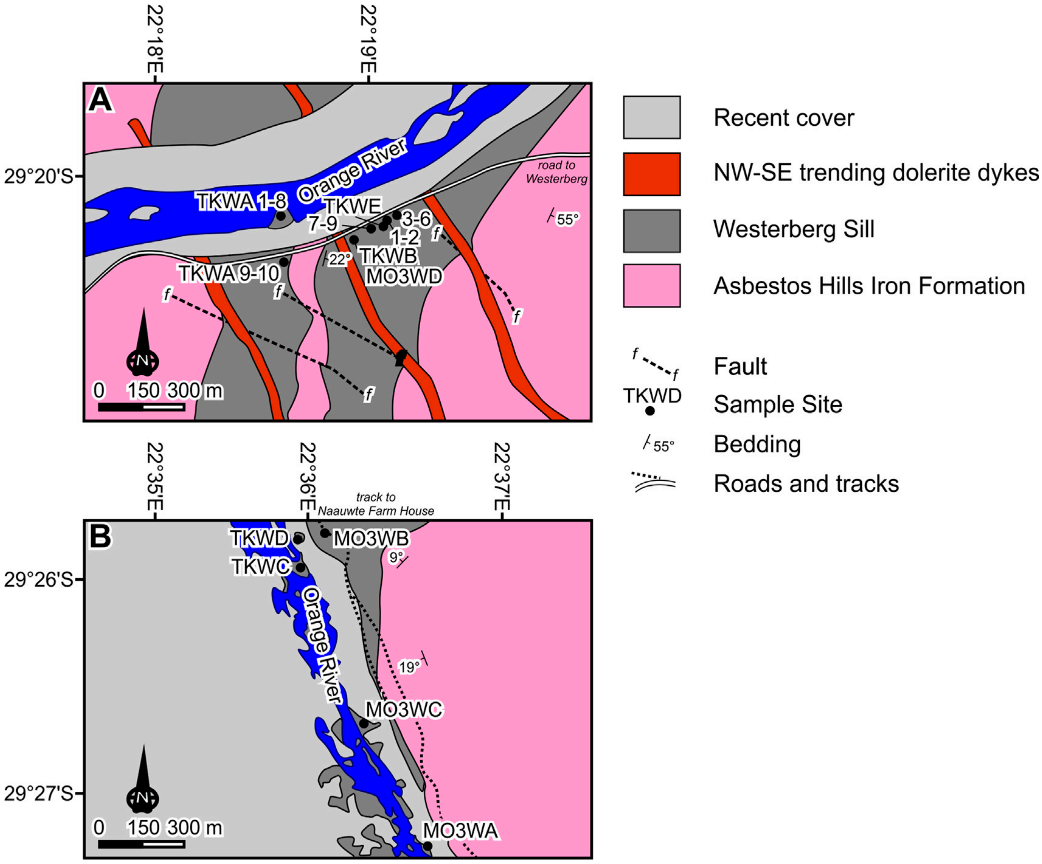

Fig. 3. Field localities along the Orange River illustrating various structural relationships between the intrusion and the country rocks. Sedimentary bedding data from the Westerberg area (Dreyer, 1982), was used to calculate the fold axis of the regional syncline with an azimuth of 19.1° and a plunge of 19.4°. Maps are simplified after Dreyer (1982).

optical microscope and divided into five fractions from each sample, comprising 1–5 grains each. Further details on the water-based separation technique used in this study are given in Söderlund and Johansson (2002).

Mass spectrometry analysis was done using a Finnigan Triton Thermal Ionization Mass Spectrometer in the Department of Geosciences at the Swedish Museum of National History in Stockholm. Regressions were carried out using Isoplot (Ludwig, 1991), with U decay constants taken from Jaffey et al. (1971). The initial common Pb correction was done using the isotopic compositions from the global common Pb evolution model by Stacey and Kramers (1975). Further details on the methodology are given in Olsson et al. (2010).

3.2. Paleomagnetic studies

Samples were drilled and collected from two localities (three sites) in the Westerberg Sill itself along the banks of the Orange River in the Prieska study area (Figs. 2 and 3), and from two sites further to the north-east in the Kuruman study area (Fig. 2). One of the localities in the Prieska study area is located in the vicinity of the abandoned asbestos mining village of Westerberg, where two parallel sills intrude the Kuruman Iron Formation (Fig. 3a). Samples were collected from the thick interior of a sill outcropping in the Orange River, and from its finer-grained upper contact (TKWA). Additional samples were collected from a second sill that intrudes stratigraphically higher in the succession and outcrops along the R383 provincial road above the river (TKWB/TKWE/M03WD). Samples from this locality constitute two sites on the western limb of a north-east plunging syncline (Fig. 2). The remaining sample specimens from the Prieska study area were from outcrops situated east of Westerberg on the Naauwte Farm, and are representative of a single thick sill (Fig. 3b). These constitute one site on the eastern limb of the same syncline. As shown (Fig. 3), samples were also collected from near the fine-grained basal contact of the sill (TKWD), from its coarser central portion (TKWC/M03WC/M03WA), as well as from its finer-grained upper contact with the iron formation (M03WB). Sampling along these two limbs allows for evaluation of the paleomagnetic fold test. From the Kuruman study area (Fig. 2a), samples were collected from medium-grained dolerite bodies forming scattered outcrops on the Simbambala Game Farm (FYL), and from the Kranzkop Farm (MDK03).

Core samples were collected using a portable petrol-powered drill and oriented using both a magnetic and a sun compass. Attitudes of the intrusions were derived from bedding of the host BIF, and determinations of paleo-vertical from columnar cooling joints in the sill were plotted on a stereographic projection. All measurements of magnetic remanence were made by using the superconducting rock magnetometer at the University of Johannesburg (a vertical 2G Enterprises DC-4K magnetometer), and at Yale University (a vertical 2G Enterprises DC SQUID magnetometer), both equipped with similar automatic sample changers (Kirschvink et al., 2008). Selected specimens were submerged in liquid nitrogen before further demagnetization was undertaken. All specimens were exposed to stepwise demagnetization including an alternating-field (AF) pre-treatment from 2 to 10 mT, followed by thermal demagnetization using an ASC Model TD48 shielded oven in 12 steps from 100 °C to 550 °C in decreasing temperature intervals. Specimens from sites FYL and TGS-03 were demagnetized

T.C. Kampmann et al. / Precambrian Research 269 (2015) 58–72 63

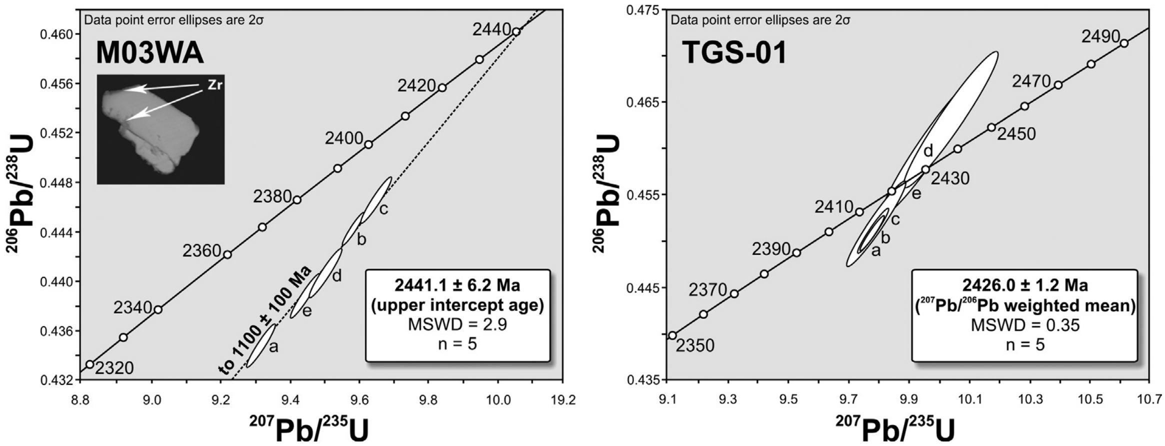

Fig. 4. Concordia diagrams of samples M03WA and TGS-01. The inset is a SEM-BSE image of a polished cross-section through a representative baddeleyite grain revealing thin zircon alteration along parts of the rim. White arrows point out zircon domains (Zr), which show up as brighter domains than the baddeleyite phase in BSE imaging.

via stepwise AF demagnetization from 2 to 100 mT. The process was abandoned when sample intensity dropped below instrument noise level (below ca. 1 pAm^2), or when samples started to show erratic behavior.

Magnetic components were quantified via the least-squares component analysis of Kirschvink (1980), and using the software Paleomag 3.1b2 (Jones, 2002). Linear fits were included in subsequent analyses if they had a Mean Angle Deviation (MAD) ≤ 10°. Additional digital handling was conducted with the PmagPy software of Tauxe (2010). Paleomagnetic pole calculations are based on the assumption of a geocentric axial-dipole field, and a stable Earth radius throughout geological time that equals the present day radius. Visualization of pole positions and paleogeographic reconstructions was achieved with GPlates (Williams et al., 2012).

4. Results

4.1. U–Pb geochronology

Extracted baddeleyite grains from M03WA were ca. 30–50 μm in length, elongated and brown in color. The grains have ‘frosty’ surfaces when viewed under the optical microscope, indicative of partial replacement of baddeleyite by zircon as a result of late- or post-magmatic reaction of baddeleyite with a silica-rich melt or fluid (e.g. Heaman and LeCheminant, 1993; Söderlund et al., 2013). Back scattered electron microscopy reveals the presence of zircon in ca. 0.5 μm thick semi-continuous rims and also in fractures (Fig. 4). Baddeleyite grains extracted from sample TGS-01 are >50 μm in length, dark brown and crystalline, without any signs secondary zircon. Data is presented in Table 1 with Concordia diagrams shown in Fig. 4.

For M03WA, the ^{207}Pb/^{206}Pb dates of five fractions range from 2405.8 ± 1.8 to 2420.2 ± 1.9 Ma and plot 2–4% discordant (Fig. 4). The ^{207}Pb/^{206}Pb date of the “oldest” fraction (2420.2 Ma) is taken as the minimum age of this sample. Free regression including all fractions yields an upper intercept age of 2434 ± 16 Ma and a lower intercept age of 920 ± 450 Ma (MSWD = 2.6). For various reasons discussed below, a forced lower intercept of 1100 ± 100 Ma is preferred in the regression, which results in a slightly older age of 2441 ± 6 Ma (MSWD = 2.9).

The ^{207}Pb/^{206}Pb dates for five fractions of TGS-01 range from 2424.1 ± 4.9 to 2426.5 ± 1.7 Ma, and all fractions plot less than 1% discordant. Using a free regression yields a lower intercept of −230 Ma. We prefer to use the weighted mean of ^{207}Pb/^{206}Pb dates, which is 2626.0 ± 1.2 Ma (MSWD = 0.35), as the best age estimate of this intrusion (Fig. 4).

4.2. Paleomagnetism

4.2.1. Demagnetization result(s)

A summary of the demagnetization results is provided here. All components are given in geographic (not tilt-corrected) coordinates. During demagnetization there was a clear distinction in the behavior of coarse-grained dolerite from the central parts of the thick sills (Fig. 5a and c), and that of samples from the finer grained contact zones or medium-grained thinner sills and intrusive bodies (Fig. 5b, d and e). Identified components are summarized in Table 2.

In the Prieska study area, coarse-grained samples from the lower sill at Westerberg (samples TKWA 1–8) are poor magnetic recorders and rapidly demagnetize to lose all significant magnetization by a demagnetization step as low as 350 °C. However, in some cases magnetization persists up to 545 °C. Besides a very low-coercivity random component of magnetization removed from these samples in the first couple of AF demagnetization steps, they are dominated by randomly oriented single linear components of magnetization that demagnetize toward the origin (Fig. 5a). The eight samples from this site are thus not given any further attention. Demagnetization of samples from near the upper contact of the lower sill, as well as from the stratigraphically upper sill at Westerberg proved to be more successful. Here once again a low-coercivity component of magnetization was removed from most samples (Fig. 5b). While being quite scattered, these low-coercivity components form a poorly constrained south-westerly cluster of data. After removal of this component, samples demagnetize along linear trajectories toward the origin, and are labeled “HIG” according to their higher stability. These trajectories generally define a moderate negatively inclined, north–northwesterly magnetization in geographic coordinates (Fig. 6b). This component is comparable to characteristic components seen in two samples from the lower sill (Decl. = 281.8°, Incl. = −55.1° seen in Fig. 6b). Characteristic components from samples TKWB 1 to 7 define significantly steeper and more scattered set of directions (average inclination = −76.0°; Fig. 6a), and there exists a distinct, but untested possibility that the nearby north-west trending dyke magnetically affected these samples (Fig. 3a). It is also possible that these samples have experienced greater alteration due to modern weathering compared to other samples, and that they may represent a present field-like magnetization. These components are labeled “PF” despite their persistence at high temperature demagnetization steps. Exclusion

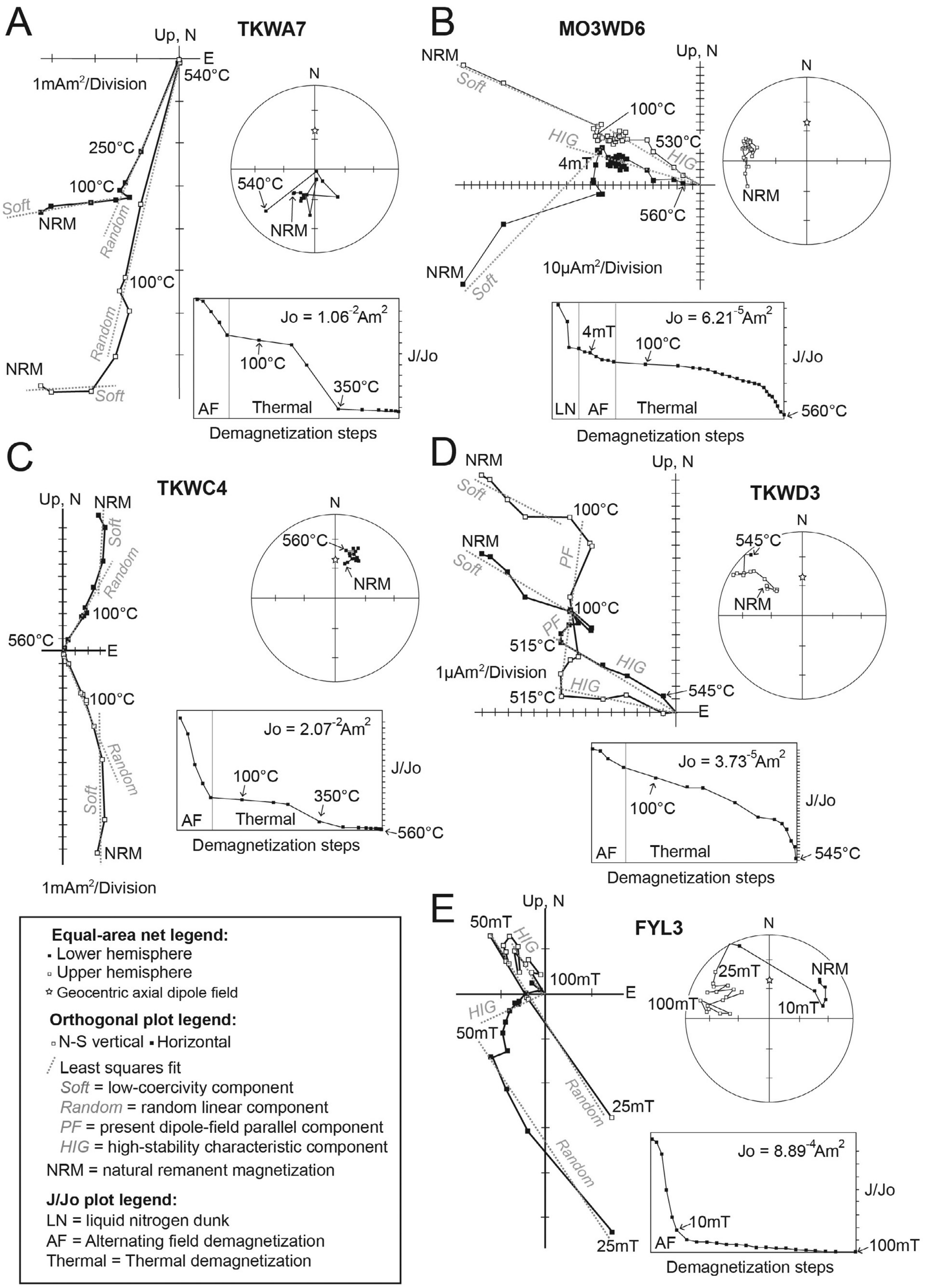

Fig. 5. Representative demagnetization behavior of selected coarse-grained and fine-grained samples from the investigated sites in the Kuruman (north-east) and the Prieska (south-west) study areas.

Table 1
U–Pb ID-TIMS isotopic data.

Analysis no. (number of grains)	U/Th	Pbc/Pbtot[a]	$^{206}Pb/^{204}Pb$ raw[b]	$^{207}Pb/^{235}U$	±2s % err	$^{206}Pb/^{238}U$	±2s % err	$^{207}Pb/^{235}U$	$^{206}Pb/^{238}U$	$^{207}Pb/^{206}Pb$	±2s % err	Concordance
				[corr][c]				[age, Ma]				
M03WA												
a (3 grains)	21.1	0.013	4623.5	9.3118	0.34	0.43470	0.32	2369.2	2326.9	2405.8	1.8	0.967
b (3 grains)	35.0	0.007	9006.7	9.5794	0.26	0.44414	0.25	2395.2	2369.2	2417.4	1.4	0.980
c (3 grains)	54.1	0.015	3969.7	9.6460	0.34	0.44650	0.32	2401.6	2379.7	2420.2	1.9	0.983
d (4 grains)	31.5	0.031	1898.7	9.5003	0.38	0.44061	0.36	2387.6	2353.4	2416.9	2.0	0.974
e (4 grains)	27.2	0.042	1320.1	9.4373	0.33	0.43858	0.29	2381.5	2344.3	2413.5	2.4	0.971
TGS-01												
a (5 grains)	22.3	0.048	1274.7	9.7785	0.39	0.45106	0.38	2414.1	2400.0	2426.1	2.2	0.989
b (5 grains)	11.9	0.027	2291.2	9.7747	0.31	0.45078	0.30	2413.8	2398.7	2426.5	1.7	0.989
c (1 grain)	−34.9	0.079	798.3	9.7839	0.80	0.45167	0.80	2414.6	2402.7	2424.7	3.9	0.991
d (2 grains)	−1.9	0.283	214.0	10.0422	1.25	0.46348	1.19	2438.7	2454.9	2425.1	8.0	1.012
e (2 grains)	−10.0	0.112	569.1	9.9282	1.05	0.45850	1.05	2428.1	2432.9	2424.1	4.9	1.004

[a] Pbc = common Pb; Pbtot = total Pb (radiogenic + blank + initial).
[b] measured ratio, corrected for fractionation and spike.
[c] isotopic ratios corrected for fractionation (0.1% per amu for Pb), spike contribution, blank (6 pg Pb and 0.06 pg U), and initial common Pb. Initial common Pb corrected with isotopic compositions from the model of Stacey and Kramers (1975) at the age of sample.

Table 2
– Summary of least-squares component analysis.

Component			In situ coordinates				Tilt-corrected coordinates			
Site	Region	*n*/*N*	Decl. in°	Incl. in°	A_{95} in°	*k*	Decl. in°	Incl. in°	α_{95} in°	*k*
PF										
TKWB	Westerberg upper sill	7/7	333.2	−76	20.2	8.4	263.2	−58.4	20.2	8.4
TKWD/MO3WB	Naauwte sill	15/15	14.2	−69	8.0	23.8	158.8	−87.4	8.0	23.7
INT										
MDK03	Kuruman	6/6	83.9	31.6	20.1	10.1	90.6	42.5	20.1	10.1
			VGP based on 6 in situ samples				2.8°N	275.5°E	dp = 12.7°	dm = 22.6°
			VGP based on 6 tilt-corrected samples				11.8°N	271.1°E	dp = 15.3°	dm = 24.8°
HIG										
MO3WD/TKWE (a)	Westerberg upper sill	14/17	296.6	−39.1	6.4	39.4	278.3	−35.1	6.6	37.2
TKWA	Westerberg lower sill	2/10	281.8	−55.1	34.6	27.1	308.6	−50.1	34.6	27.1
TKWD (b)	Naauwte sill	6/7	300.2	−12.4	6.2	116.2	294.5	−19	6.2	115.9
FYL	Kuruman	7/8	257.2	−53.4	23.2	6.6	258.5	−45.4	23.2	6.6
MDK03	Kuruman	5/6	282.2	−29.2	19.5	13	289.9	−36.7	19.5	13.1
Combined samples		*n* = 34	288.9	−37.4	7.8	11	279.2	−34.9	6.7	14.5
Combined as sites		*N* = 4	286.7	−34.5	26.6	12.9	281.7	−34.8	19.5	23.3
			VGP based on 34 tilt-corrected samples				16.8°N	279.9°E	dp = 4.4°	dm = 7.7°
			VGP based on 4 tilt-corrected sites (exclude site TKWA)				18.9°N	285.0°E	A_{95} 14.1°	*K* 43.4

Site coordinates: MO3WD, TKWA, TKWB & TKWE = 29.3°S 22.3°E; MO3WB, TKWC & TKWD = 29.4°S 22.6°E; MDK03 = 28.0 °S 23.4°E; FYL = 27.8°S 23.4°E.
Abbreviations: Decl. = declination, Incl. = inclination, α_{95} = radius of 95% confidence cone about the mean direction, *k* = precision parameter for direction, VGP = virtual geomagnetic pole, dp and dm = semi-axes of 95% confidence about the mean, A_{95} = radius of 95% confidence about the mean pole, *K* = precision parameter for pole. Sample based VGP was calculated for site coordinates at 28.5°S 23.0°E.

of these components (i.e., TKWB 1–7) from the HIG components identified in other samples yields a tight clustering mean for the upper sill in geographic coordinates (Decl. = 296.6°, −39.1°, k = 39.4, α_{95} = 6.4°, n = 14; Fig. 6b). Samples M03WD 7–9 are the exception to the behavior described above. These samples display single linear, north-westerly and upward directed magnetic components, not seen in any other of the samples, and were removed during demagnetization up to 570 °C. These anomalous, possibly lightning-induced magnetizations are excluded from further evaluation.

On the Naauwte Farm (Prieska study area), coarse-grained dolerite samples appeared to be poor recorders of the Earth's past magnetic field. Samples collected here were from the interior of the sill (M03WA/M03WC/TKWC; Fig. 3b). As was the case at Westerberg, these coarse-grained samples generally lost their magnetization quite rapidly (Fig. 5c). These samples can be characterized by randomly directed low-coercivity components, and randomly directed linear components that are not evaluated further (Fig. 5c). Again, finer-grained dolerite in proximity of the contact with the iron formation yielded better results. Samples M03WB 1–8 were collected from more weathered exposures from the track along the hillside above the Orange River, while samples TKWD 1–7 were collected from a fresh exposed outcrop within the river bed itself (Fig. 3b). Samples from both outcrops displayed randomly directed low-coercivity components during low-field AF demagnetization (Fig. 5d). The samples from the track exposure displayed northerly and upward directed linear components that demagnetized toward the origin. These PF components are near parallel to the present-day magnetic field of the Earth at the locality (Fig. 6a), and probably were acquired during recent

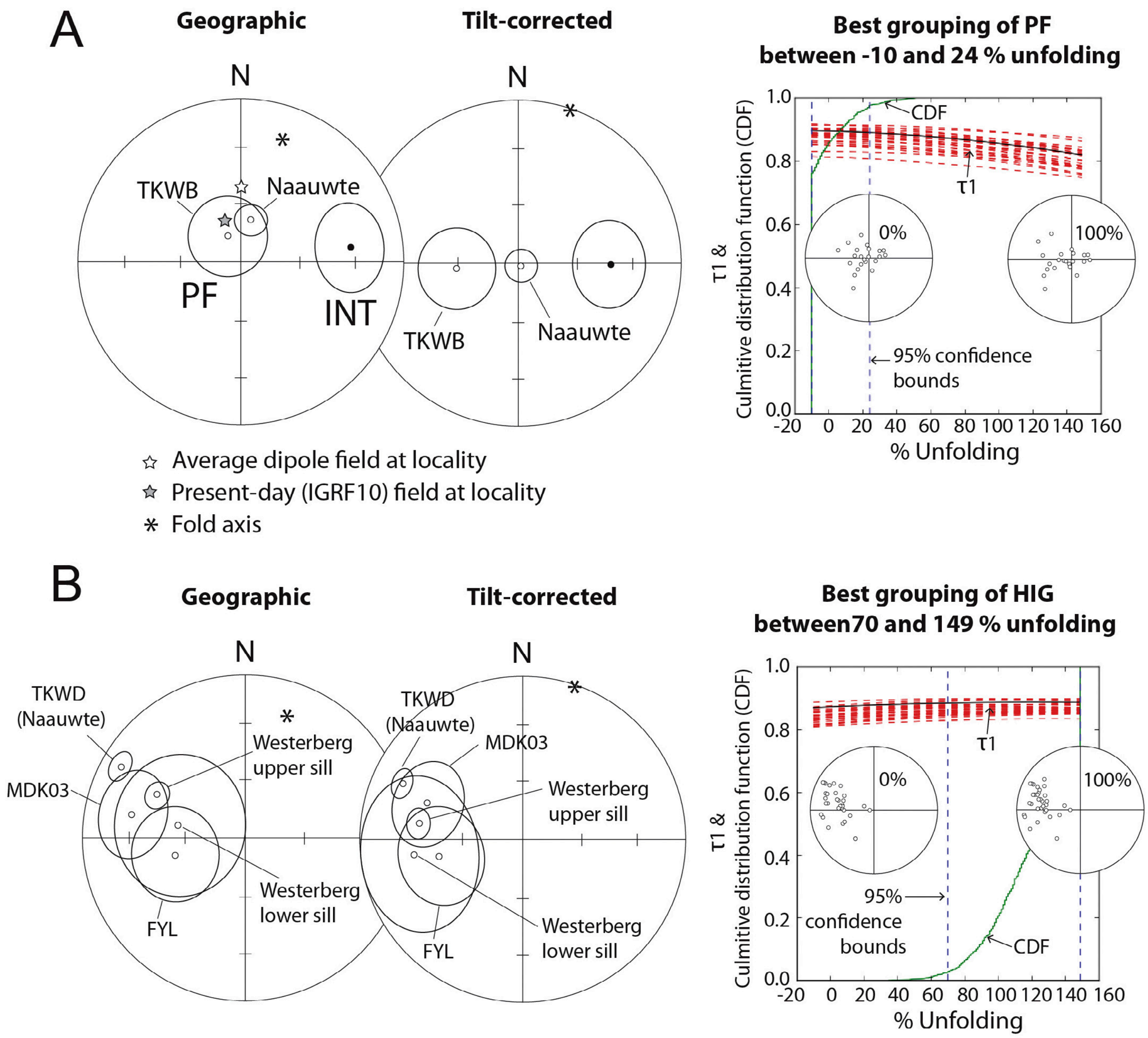

Fig. 6. Summary of means for identified magnetic components PLF and INT in A with corresponding bootstrap fold test of Tauxe et al. (1991) using PmagPy in Tauxe (2010), both in geographic and tilt-corrected coordinates. B shows HIG.

weathering. Samples TKWD 1–7 also display similar northerly present field-like (or PF) components within the 200 °C to 500 °C stepwise demagnetization range (Figs. 5d and 6a), but here a third magnetic component (HIG) is identified at demagnetization steps above 500 °C, as shallow easterly zero-seeking demagnetization trajectories in six of the seven samples (Fig. 5d). A mean was calculated for these six samples at a Decl. = 300.2°, Incl. = –12.4°, k = 116.2, α_{95} = 6.2°, n = 6 (Fig. 6b).

Samples from sites FYL and MDK03 in the Kuruman study area behaved similarly during demagnetization (Fig. 5e). Samples from both sites displayed randomly directed low-coercivity components that were removed during the first couple of demagnetization steps. Hereafter all samples displayed a magnetic component of medium- to low-coercively (7.5–30 mT). In samples from FYL, these components were randomly directed, but for samples from MDK03 these intermediate components form an easterly and downward directed cluster labeled "INT" (Decl. = 83.9°, Incl. = 31.6°, k = 10.07, α_{95} = 20.07°, n = 6; Fig. 6a). The INT component is near antipodal to the HIG component identified elsewhere, but it is clearly of lower coercivity. At demagnetization steps above 30 mT, and up to 85 mT (i.e., high-coercivity), samples from both sites revealed easterly and upward directed characteristic remanence directions. These directions are similar to that seen at the southern localities, and thus labeled HIG (Fig. 6b).

4.2.2. Structural correction, paleomagnetic fold test and pole calculation

A consistent characteristic remanence (i.e., component HIG) was identified from sites TKWA and TKWE/M03WD along the western limb of a gently north-east plunging syncline. Only two samples from site TKWA yielded the HIG component, while 21 samples recorded the HIG component at TKWE/M03WD. In addition, the HIG component was identified from two sites from the Kuruman study area. In order to restore bedding to paleo-horizontal, the regional fold axis (i.e., azimuth = 19.1° and plunge = 19.4°) in the Prieska study area first had to be restored to horizontal, and all identified components from the Westerberg and Naauwte areas had to be corrected accordingly. The plunge-corrected bedding data for samples from the Prieska study area (Westerberg and Naauwte), and the bedding data for samples from the Kuruman study area (FYL and MDK03) was then used to restore all components to horizontal (Fig. 6). Means of structurally corrected components were then calculated and are shown in Table 2.

The PF directions from the Prieska study area (Westerberg and Naauwte), become more disparate during the unfolding as set out above (Fig. 6). This suggests that the acquisition of this magnetization occurred after folding. Formal evaluation of the fold test of McFadden and Jones (1981) is not possible because the two groups do not share a common precision. We therefore make use of the bootstrap evaluation of the fold test from Tauxe et al. (1991) instead (Fig. 6a). This shows clearly that the PF component from the 22 samples was acquired after folding because 95% confidence limits on the degree of untilting required for maximizing concentrations of the data (i.e., maximum eigenvalue of $\tau 1$ of the orientation matrix), include 0% unfolding. The maximum concentrations of data are reached between −10% and 24% unfolding (Fig. 6a).

A slight visual improvement of grouping of HIG components is observed during unfolding (Fig. 6b). The HIG groups from the western limb (from the Westerberg upper sill), and the eastern limb (site TKWD at Naauwte Farm) in the Prieska study area do not share a common precision. We thus again use the bootstrap evaluation of the fold test following Tauxe et al. (1991) for all identified HIG components. The HIG component from 34 samples appears to have been locked in prior to folding because 95% confidence limits on the degree of untilting required for maximizing fits of the data (i.e., maximum eigenvalue of $\tau 1$ of the orientation matrix) occurs between 70% and 149% unfolding (Fig. 6b).

A VGP calculated for 34 tilt-corrected samples is situated at 16.8°N, 279.9°E (dp = 4.4°, dm = 7.7°). The tilt-corrected site-based (N = 4) is comparable at 18.9 °N, 285.0 °E, A_{95} = 14.1°, K = 43.4.

5. Discussion

5.1. Emplacement age of the Westerberg Sill

The upper intercept date of 2434 ± 16 Ma for sample M03WA using a free regression, yields a lower intercept date of 920 ± 450 Ma, the latter of which can be interpreted to reflect the time of disturbance of the U–Pb isotopic system in primary zirconium-bearing minerals. We assume that most of the discordance relates to the event causing partial transformation of baddeleyite to zircon (Fig. 4), at an approximate time given by the lower intercept. According to Colliston and Schoch (2013), the Namaqua-Natal Orogeny ended at ca.1030 Ma in a phase of comprehensive folding and shearing, and we assume that metamorphism at zeolite to greenschist facies in the area west of the town of Prieska relates to this metamorphic event (Cornell et al., 2006). Hence, we prefer to use a 1100 ± 100 Ma as a proxy for the lower intercept, since ca. 1100 Ma is normally referred to as the general time of metamorphism for the Namaqua-Natal Orogeny (e.g., Eglington, 2006). This approach results in an upper intercept age of 2441 ± 6 Ma, which is interpreted as the best estimate of the emplacement age of the Westerberg Sill in the Prieska study area. A multi-stage disturbance of the U–Pb isotopic system would theoretically bias both the upper and lower intercept dates in a discordant data set. The MSWD value of 2.9 indicates scatter beyond analytical uncertainty and we cannot rule out that a more recent Pb-loss event (younger than the Namaqua-Natal orogeny), may be superimposed.

The age results of M03WA and TGS-01 agree with previously obtained radiometric dates from the Kuruman BIF into which the Westerberg Sill intrudes. An unpublished single-grain zircon U–Pb age of 2480 ± 6 Ma for tuffaceous units at the base of the Kuruman BIF by Trendall et al. (1995) is thought to reflect the onset of BIF sedimentation according to Eriksson et al. (2006). U–Pb zircon ages of 2465 ± 6 Ma (Pickard, 2003), and an unpublished age of 2465 ± 7 Ma (cited in Martin et al., 1998) from the upper Kuruman Formation, are probably a good age estimate of the transition to a shallower depositional environment. This transitional depositional environment characterizes the deposition of the Griquatown Iron Formation (Beukes, 1984). Additionally, an unpublished age of 2432 ± 31 Ma is often cited for tuffaceous mudstone at the base of the Griquatown Iron Formation (Martin et al., 1998). Unpublished work cited in Kirschvink et al. (2000) for zircons from a tuffaceous bed near the top of the overlying Koegas Subgroup gave an age of 2415 ± 6 Ma. This suggests that the Westerberg Sill Suite may have been broadly coeval with the felsic magmatism during deposition of the Griquatown Iron Formation. However, field observations and thermal alteration of the surrounding country rock support the assertion that the Kuruman BIF was already lithified when the intrusion occurred. Consequently, the age range of 2441 ± 6 Ma to 2426 ± 1 Ma for the Westerberg Sill Suite reflects a minimum age for the Kuruman Iron Formation, in agreement with previously published age constraints.

5.2. Paleomagnetism – comparison with Paleoproterozoic paleopoles

The ca. 1.1 Ga Namaqua-Natal Orogeny was likely responsible for a significant disturbance of the U–Pb isotopic system in baddeleyite from the Westerberg Sill. None of our calculated poles however suggest that this event affected the magnetization of samples. Instead our paleopoles compare well with published paleomagnetic poles and VGPs, as well as known magnetic overprints from the Kaapvaal Craton during the Paleoproterozoic (Fig. 7). For this comparison we also included Neoarchean poles from the Kaapvaal Craton (all poles used in this comparison are listed in Table 3).

Our pre-fold high stability VGP (i.e., HIG) from the Westerberg Sill Suite plots well within an existing gap in the apparent polar wander path of the Kaapvaal Craton between ca. 2.66 Ga and the time of extrusion of the Ongeluk volcanics (Fig. 7). The HIG component VGP plots near the ca. 2.22 Ga Ongeluk Formation paleopole of Evans et al. (1997), and is indistinguishable from the intermediate component pole (i.e., INT) that was removed in some samples. This intermediate component is opposite in polarity to the HIG direction, and is clearly a younger magnetization. Besides being indistinguishable from the HIG pole, the INT pole is also very similar to the pole determined from the weathering profile that developed below the unconformity at the base of Gamagara-Mapedi Formation (Fig. 7). The age of the Gamagara-Mapedi Formation was recently revised to post-date the intrusion of the 2054 Ma Bushveld Complex based on a younger U–Pb age population of detrital zircon grains (Dreyer, 2014). It is interesting to note that such a young age was considered, but not preferred, by Evans et al. (2002).

This comparison of paleopoles allows for several possible interpretations. Although the magnetization of the Westerberg Sill Suite clearly pre-dates ca. 2.0 Ga deformation of the Postmasburg and Campbellrand groups, we have no further constraints on the timing of remanence acquisition. The magnetization could represent a ca. 2.22 Ga magnetic overprint associated with the extrusion of the Ongeluk volcanic rocks. However, this is unlikely given the lack of observations for a wider metamorphic and metasomatic influence of the Ongeluk Formation. A second, option would be that the HIG magnetization pre-dates deformation, and that it is a primary magnetization acquired at ca. 2.43 Ga during the

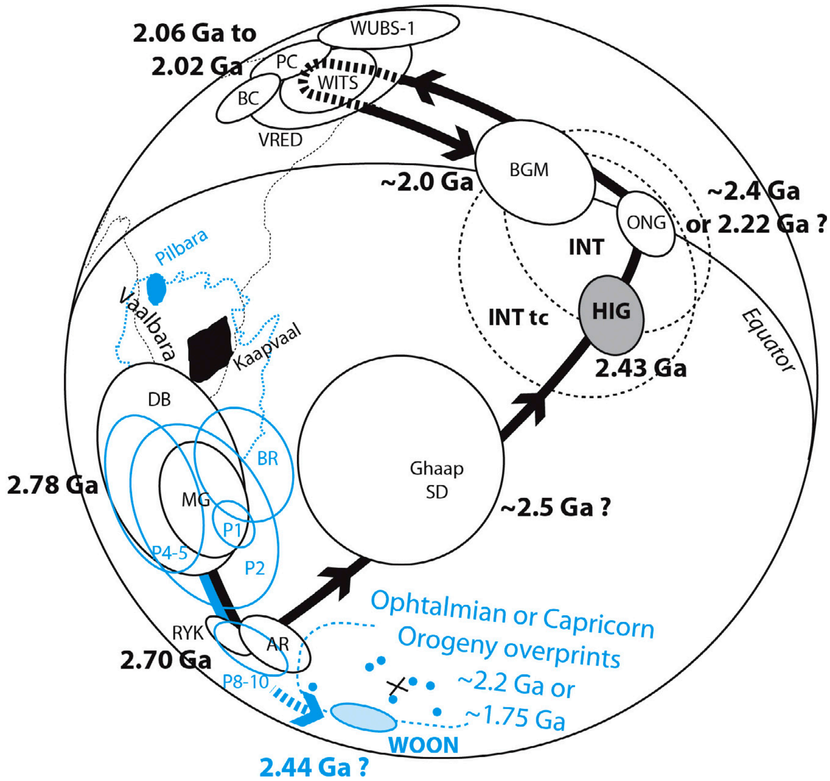

Fig. 7. Possible apparent polar wander path for the Kaapvaal Craton (black) and Pilbara Craton (blue) using known paleopoles for the Neoarchean-Paleoproterozoic (including component INT and HIG of this study). References for the Pilbara poles (blue): P1 = 2772 Ma Pilbara Flood basalt Package 1 (Strik et al., 2003), BR = 2772 ± 2 Ma Black Range dykes (Embleton (1978), P2 = 2767 Ma Pilbara Flood basalt Package 2 (Strik et al., 2003), P4-5 = 2739 Ma Pilbara Flood basalt Package 4–5 (Strik et al., 2003), P8-10 = 2717 ± 2 Ma Pilbara Flood basalt Package 8–10 (Strik et al., 2003), WOON = 2449 ± 3 Ma Woongarra Rhyolite (Evans, 2007; Evans, pers. comm., 2012). (For interpretation of reference to color in this figure legend, the reader is referred to the web version of this article.)

Table 3
Summary of VGPs and paleopoles for the Kaapvaal Craton in the Neoarchean to Paleoproterozoic.

Rock unit	Code	Age (Ma)	Age reference	Pole °N	Pole °E	A_{95} or *dp* (°)	*dm* (°)	Pole reference
Neoarchean poles								
Derdepoort Basalt	DB	2782 ± 5	Wingate (1998)	−39.6	4.7	17.5		Wingate (1998)
Modipe Gabbro	MG	2784 ± 1	Denyszyn et al. (2013)	−47.6	12.4	8.6	9.3	Denyszyn et al. (2013)
Allanridge Formation	AR	ca. 2700	De Kock et al. (2009a)	−69.8	345.6	5.8		De Kock et al. (2009a)
Rykoppies Dykes	RYK	2700–2660	Olsson et al. (2010)	−62.1	336	3.5	4.2	Lubnina et al. (2010)
Paleoproterozoic poles								
Sample-based HIG component (VGP), Westerberg Sill Suite	HIG	2441–2426	This study	16.8	279.9	4.4	7.7	This study
Tilt-corrected INT component, Westerberg Sill Suite	INT_{tc}		This study	11.8	271.1	15.3	24.8	This study
In situ INT component, Westerberg Sill Suite	INT_{is}		This study	2.8	275.5	12.7	22.6	This study
Ghaap SD component	Ghaap SD	2500–2300	De Kock et al. (2009b)	−48	65.6	14.7	17.3	De Kock et al. (2009b)
Ongeluk Lava	ONG	2222 ± 13[a]	Cornell et al. (1996)	−0.5	100.7	5.3		Evans et al. (1997)
Mamatwan Ore component 1	MAM-1	ca. 2200	Evans et al. (2001)	−8.2	111.1	5.6	11.1	Evans et al. (2001)
Gamagara/Mapedi Formation	BGM	ca. 2200	Evans et al. (2002)	2.2	81.9	7.2	11.5	Evans et al. (2002)
Ghaap W component	G W	ca. 2200	De Kock et al. (2009b)	−3.2	104.1	15		De Kock et al. (2009b)
Phalaborwa Complex	PB	2060 ± 4	Wu et al. (2011)	27.7	35.8	6.6		Letts et al. (2011)
B-1 Bushveld Sills	B1	2058 ± 6	Wabo et al. (2011)	13.1	44	14.3		Wabo et al. (in press)
Bushveld Complex	BC	2054.4 ± 1.3	Scoates and Friedman (2008)	19.2	30.8	5.8		Letts et al. (2009)
Waterberg unconformity bounded sequence 1	WUBS-1	2054 ± 4	Dorland et al. (2006)	36.5	51.3	10.9		De Kock et al. (2006)
Witwatersrand overprint	WITS	1945 ± 40	Layer et al. (1988)	19.1	45.6	7.8		Layer et al. (1988)
Ghaap ND component	G-ND	2000–1900	De Kock et al. (2009b)	26.5	22.8	7		De Kock et al. (2009b)
Vredefort	VRED	2023 ± 4	Kamo et al. (1996)	21.8	44.5	11.3	15.4	Carporzen et al. (2005)

A_{95} (in degrees) is the radius of the 95% confidence cone about a mean based on site poles, while *dp* and *dm* (in degrees) are semiaxis of the 95% confidence cone about a mean based on site direction.

[a] Reliability of age determination under debate (see text).

intrusion and subsequent cooling of the Westerberg Sill Suite. If correct, this suggests a relatively stationary Kaapvaal Craton for some 200 million years (i.e., between 2.43 Ga and 2.22 Ga). There is however a third option that we consider here, which suggests that the age of the Ongeluk Formation is not ca. 2.22 Ga as commonly accepted, but much closer in age to that of the Westerberg Sill Suite (i.e., ca. 2.43 Ga). An older age has been suggested for the Ongeluk volcanic rocks before (Moore et al., 2001, 2012; Bau et al., 1999), but requires a challenging revision of stratigraphic correlations between the various basins preserving the Transvaal Supergroup. If correct, the Westerberg Sill Suite may be a stratigraphically deeper, intrusive equivalent of the Ongeluk Formation volcanic rocks. This option remains speculative until conclusive geochronological data is presented for the Ongeluk Formation itself.

The INT magnetization or intermediate opposite polarity overprint was only observed from northerly sampling sites in the Kuruman study area, further away from the edge of the Kaapvaal Craton. Apart from being situated deeper into the interior of the craton, the sites are stratigaphically closer to the Ongeluk Formation due to the unconformity at the base of the Postmasburg Group. This unconformity cuts down into the Koegas Formation in the south-western extreme of the craton near Westerberg, but cuts out increasingly older stratigraphic units toward the north-east nearer Kuruman. The Postmasburg Group rests unconformably on top of the Griquatown Iron Formation. There is thus a possibility that the Ongeluk Formation could have overprinted the magnetization of the Westerberg Sill Suite in the Kuruman study area, where there is much less intervening rock units compared to the Prieska study area. Alternatively the INT magnetization may be related to the deep oxidative weathering experienced before the deposition of the Gamagara-Mapedi Formation at ca. 2.0 Ga. This second interpretation is currently favored based on the rather ambiguous results of the fold test for the INT component.

5.3. Implications for Vaalbara

5.3.1. Vaalbara so far

Based on analyses of sequence stratigraphy, lithostratigraphy and lithofacies, Cheney (1996, 1990) produced a reconstruction placing the Pilbara Craton at the southern margin of the Kaapvaal Craton. This reconstruction also included the Yilgarn and Zimbabwe cratons in the delimitation of Vaalbara. The relationships between these four cratons have recently been discussed in Smirnov et al. (2013). Similar time-stratigraphic development is present in both Kaapvaal and Pilbara cratons (Fig. 8). The volcanic rocks of the Ventersdorp Supergroup and the sedimentary rocks of the successive Transvaal Supergroup (Kaapvaal Craton), can be correlated with the volcanic rocks of the Fortescue Group and the sedimentary rocks of the Mount Bruce Supergroup (Pilbara Craton), respectively (Cheney, 1990). A comparison between similar poles of the Neoarchean Usushwana Complex on the Kaapvaal Craton, and the Millindina Complex (Pilbara Craton), in addition to correlation between Archean tectonic architecture of the respective cratons, led Zegers et al. (1998) to propose an alternative reconstruction with the Pilbara Craton on the eastern margin of the Kaapvaal Craton. Published paleomagnetic data disproved the traditional “Cheney-fit” scenario; De Kock et al. (2009a) revised paleomagnetic results for the 2.78–2.70 Ga interval, and also presented new data from the Ventersdorp Supergroup volcanic rocks. Based on this, a third reconstruction (herein referred to as the “de Kock-fit”), places the Pilbara Craton to the north-west of the Kaapvaal Craton. The alignment of platform sedimentary rocks, together with the overlapping paleopoles and parallel APWPs for the ca. 2.78–2.66 Ga time interval favor this model. In addition, new U–Pb baddeleyite ages of ca. 2990–2978 Ma for the Usushwana Complex (Gumsley et al. 2015) also contradicts the link tothe 2860 ± 20 Ma Millindina Complex, although it may be related to the Hlagothi Complex (Schmidt and Embleton, 1985; Gumsley et al., 2013).

The Vaalbara hypothesis is corroborated by geology, geochronology and paleomagnetism until ca. 2.66 Ga. The next possible pair of paleopoles of comparable age is at ca.1.9 Ga, but a general paleolatitudinal comparison of the Kaapvaal and Pilbara cratons at this time rules out the possibility of a connection due to a poleward drift of the Kaapvaal Craton, and the low-latitudinal position of the Pilbara Craton. The Pilbara Craton is at ca. 12° latitude for remagnetization seen during the Capricorn Orogeny, and Kaapvaal is at ca. 55° latitude for the post-Waterberg dolerites and Hartley-Tsineng volcanic rocks and dolerites (Alebouyeh Semami, 2014; Hanson et al., 2004). A possible break-up scenario at ca. 2.2 Ga is supported by the “barcode” age match between the 2222 ± 13 Ma Ongeluk volcanic rocks in the Kaapvaal Craton from Cornell et al. (1996) and 2208 ± 10 Ma volcanism in the Turee Creek Group of the Pilbara Craton (Müller et al., 2005). However, there is controversy concerning the ca. 2.22 Ga age of the Ongeluk volcanic rocks by Cornell et al. (1996). Two new indirect minimum age determinations at ca. 2394 Ma on the overlying Mooidraai Formation dolomites suggest this unit to be at least 200 Ma older (Fairey et al., 2013; Bau et al., 1999). Combined with the work of Moore et al. (2001, 2012), there is the possibility that the Westerberg Sill Suite may indeed reflect sub-volcanic intrusions linked to the Ongeluk volcanic event itself, which is supported by paleomagnetism presented in this study, unless this indeed reflects a magnetic overprint tied to the ca. 2.22 Ga Ongeluk volcanism.

5.3.2. A new barcode match at ca. 2.44 Ga?

The new age of 2441 ± 6 Ma age for the Westerberg Sill coincides within error with the zircon U-Pb SHRIMP age of 2449 ± 3 Ma for the Woongarra Rhyolite of the Pilbara Craton (Barley et al., 1997). This extrusive suite overlies the BIF successions of the Weeli Wolli Formation. Zircons from a tuffaceous sandstone layer in the Weeli Wolli Formation also yield the age of 2449 ± 3 Ma (Barley et al., 1997). Therefore, the Woongarra volcanism has been interpreted as representing a Large Igneous Province (LIP). There are also numerous doleritic and basaltic units intruding within the Weeli Wolli strata. These magmatic units likely reflect later magmatic episodes of the same LIP, which may date to 2426 ± 1 Ma, the same age as obtained for sample TGS-01 in this study.

The Woongarra Rhyolite at the top of the Weeli Wolli Formation is a felsic unit thought to have been emplaced in two magmatic pulses (Trendall et al., 1995). Although a directly equivalent unit is absent in the Griqualand West Basin of the Kaapvaal Craton, there are several coeval porphyroclastic stilpnomelane pelite beds in the upper part of the Kuruman Iron Formation which are thought to be derived from felsic volcanic activity (Beukes, 1984). Tuffaceous horizons can also be found within a sedimentary unit in the overlying Bolgeeda Iron Formation in the Pilbara Craton. Unpublished zircon U–Pb dating cited in Gutzmer and Beukes (1998) from one of these volcanic layers yielded an age of ca. 2440 Ma. We therefore suggest a major Westerberg–Woongarra LIP event may have taken place on the contiguous cratons of the Kaapvaal and Pilbara from approximately 2425–2445 Ma, despite the paleomagnetic discrepancy. The similarities between the geological histories during the ca. 2.8 to 2.2 Ga time interval are significant (e.g., Beukes and Gutzmer, 2008). Trendall (1968) and Button (1976) were the first to point out these resemblances between the sedimentary successions and basin configurations of the Transvaal Supergroup (Kaapvaal) and the Hamersley Group (Pilbara). Button (1976) concluded that the two largely coeval sedimentary successions represented spatially distinct basins, but probably shared similar depositional histories as part of a larger continental block.

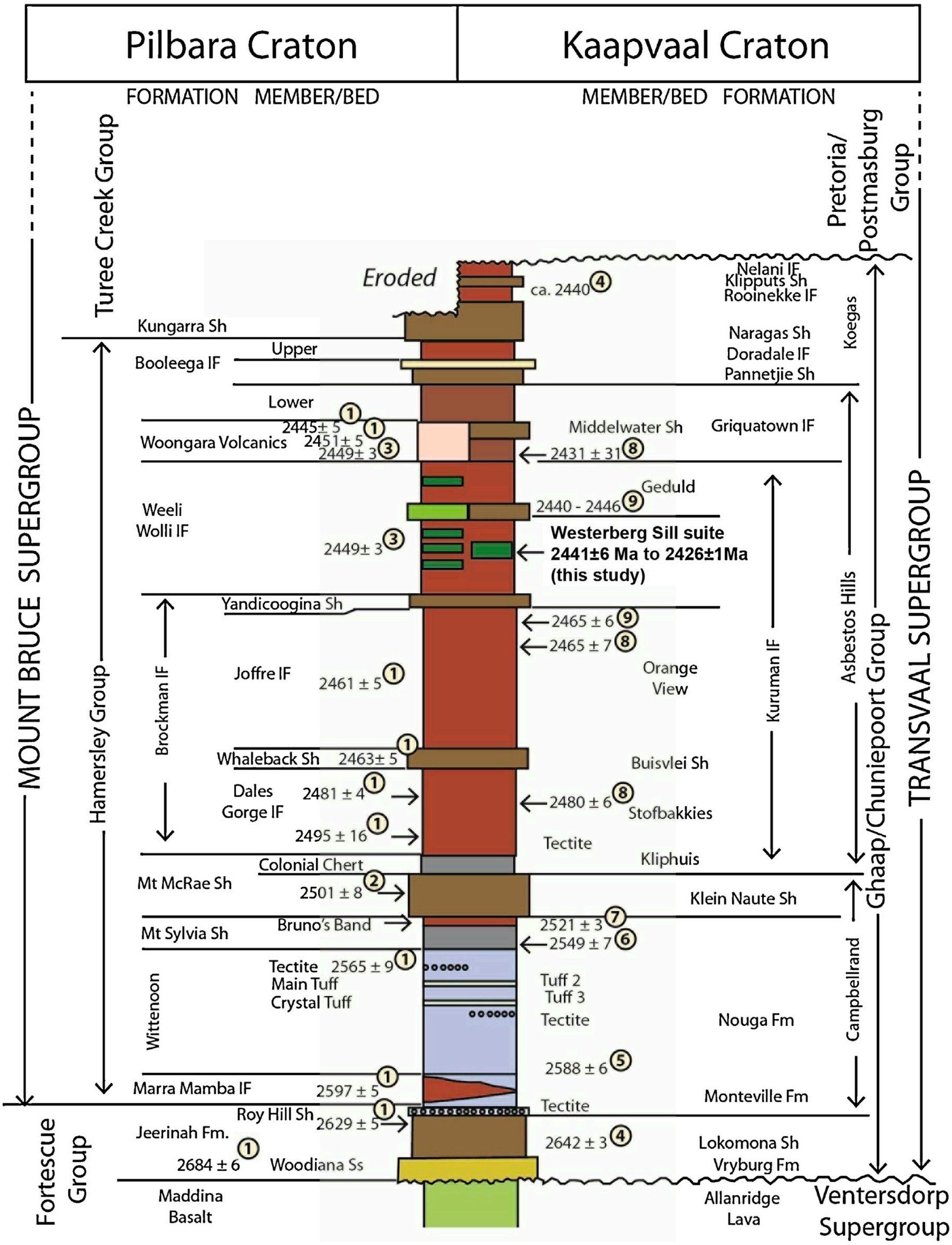

Fig. 8. Stratigraphic correlation diagram between late Neoarchean to Paleoproterozoic strata in the Transvaal and Hamersley basins (modified after Beukes and Gutzmer, 2008), including the stratigraphic positions and the newly obtained age data for the Westerberg Sill Suite. A shift from carbonate (light-blue) to BIF (red-brown) sedimentation at ca. 2500 Ma is shown. Age references are as follows: (1) = Trendall et al. (2004), (2) = Anbar et al. (2007), (3) = Barley et al. (1997), (4) = Gutzmer and Beukes (1998), (5) = Martin et al. (1998), (6) = Altermann and Nelson (1998), (7) = Sumner and Bowring (1996), (8) = Nelson et al. (1999), (9) = Pickard (2003). (For interpretation of reference to color in this figure legend, the reader is referred to the web version of this article.)

6. Conclusion

Baddeleyite U–Pb dating of the Westerberg Sill near the south-western margin of the Kaapvaal Craton and a dolerite sill suite further to the north-west in the cratonic hinterland yield crystallization ages of 2441 ± 6 Ma and 2426 ± 1 Ma, respectively. These two U–Pb ages date a new event of mafic magmatism on the craton, which may represent a new Large Igneous Province. These new ages define the herein named Westerberg Sill Suite which is similar in age to the 2449 ± 3 Ma Woongarra volcanic rocks of the Pilbara Craton, possibly indicating a common Westerberg–Woongarra LIP. However, if the Westerberg characteristic magnetization is primary, a comparison to coeval Pilbara Craton poles does not allow for a Vaalbara (Kaapvaal-Pilbara) reconstruction at 2.44–2.43 Ga, indicating crustal break-up before this time. It is important to bear in mind the primary nature of paleopoles on both cratons may be in doubt, as resetting by either the Ongeluk volcanism in the Kaapvaal Craton, or the Capricorn Orogeny in the Pilbara Craton may be apparent. In our preferred interpretation, despite the paleomagnetic discrepancy, the Kaapvaal and Pilbara cratons formed a single crustal block between 2449 and 2426 Ma. The magmatic barcode match, combined with similar depositional histories recorded in underlying carbonates and BIFs argue strongly for a shared history between these two cratonic blocks. This would extend the crustal association between these two blocks from 2.78 Ga, all the way through to 2.22 Ga.

Acknowledgements

This study has benefited from the Swedish Research Council, through research grants to Ulf Söderlund. Special thanks to Per-Olof Persson, Hans Schöberg and Kjell Billström, as well as the rest of the staff at the Department of Geosciences at the Swedish Museum of Natural History in Stockholm for technical support and help. The staff of the Department of Geology at the University of Johannesburg are acknowledged for the warm welcome and great hospitality during field work for this study. Leif Johansson is thanked for assisting with the SEM work. Johan Olsson supported this study with insightful comments and discussions. This is publication number 30 of the Industry-Academia-Government Consortium Project "Reconstruction of Supercontinents Back to 2.7 Ga Using the Large Igneous Province (LIP) Record, with Implications for Mineral Deposit Targeting, Hydrocarbon Resource Exploration, and Earth System Evolution".

References

Alebouyeh Semami, F., (M. Sc thesis) 2014. U–Pb geochronology of the Tsineng dyke swarm and paleomagnetism of the Hartley Basalt Formation, South Africa: evidence for two separate magmatic events at 1.93–1.92 and 1.88–1.84 Ga in the Kalahari craton. Lund University, Lund, Sweden.

Altermann, W., Hälbich, I.W., 1990. Thrusting, folding and stratigraphy of the Ghaap Group along the southwestern margin of the Kaapvaal Craton. South Afr. J. Geol. 93, 553–566.

Altermann, W., Nelson, D.R., 1998. Sedimentation rates, basin analysis and regional correlation of three Neoarchean and Paleoproterozoic subbasins of the Kaapvaal craton as implied by precise SHRIMP U-Pb zircon ages from volcanic sediments. J. Sediment. Geol. 120, 225–256.

Anbar, A.D., Duan, Y., Lyons, T.W., Arnold, G.L., Kendal, B., Creaser, R.A., Kaufman, A.J., Gordon, G.W., Scott, C., Gavin, J., Buick, R., 2007. A whiff of oxygen before the great oxidation event? Science 317, 1903–1906.

Barley, M.E., Pickard, A.L., Sylvester, P.J., 1997. Emplacement of a large igneous province as a possible cause of banded iron formation 2.45 billion years ago. Nature 385, 55–58.

Barton, J.M., Blignaut, E., Salnikova, E.B., Kotov, A.B., 1995. The stratigraphical position of the Buffelsfontein Group based on field relationships and chemical and geochronological data. South Afr. J. Geol. 98, 386–392.

Bau, M., Romer, R.L., Lüders, V., Beukes, N.J., 1999. Pb, O, and C isotopes in silicified Mooidraai dolomite (Transvaal Supergroup, South Africa): implications for the composition of Paleoproterozoic seawater and 'dating' the increase of oxygen in the Precambrian atmosphere. Earth Planet. Sci. Lett. 174, 43–57.

Beukes, N.J., 1984. Sedimentology of the Kuruman and Griquatown Iron-formations, Transvaal Supergroup, Griqualand West, South Africa. Precambrian Res. 24, 47–84.

Beukes, N.J., 1987. Facies relations, depositional environments and diagenesis in a major early Proterozoic stromatolitic carbonate platform to basinal sequence, Campbellrand Subgroup, Transvaal Supergroup, Southern Africa. Sediment. Geol. 54, 1–46.

Beukes, N.J., Gutzmer, J., 2008. Origin and paleoenvironmental significance of major iron formations at the Archean-Paleoproterozoic boundary. In: Hagemann, S., Rosiere, C., Gutzmer, J., Beukes, N.J. (Eds.), Banded Iron Formation-Related High-Grade Iron Ore. Society of Economic Geologists, Denver, pp. 5–47.

Bleeker, W., 2003. The late Archean record: a puzzle in ca 35 pieces. Lithos 71, 99–134.

Bleeker, W., Ernst, R.E., 2006. Short-lived mantle generated magmatic events and their dyke swarms: The key unlocking Earth's paleogeographic record back to 2.6 Ga. In: Hanski, E., Mertanen, S., Rämö, T., Vuollo, J. (Eds.), Dyke Swarms – Time Markers of Crustal Evolution. Taylor & Francis, London, pp. 3–26.

Button, A., 1976. Transvaal and Hamersley Basins – review of basin development and mineral deposits. Miner. Sci. Eng. 8, 262–290.

Carporzen, L., Gilder, S.A., Hart, R.J., 2005. Palaeomagnetism of the Vredefort meteorite crater and implications for craters on Mars. Nature 435, 198–201.

Cheney, E.S., 1990. Evolution of the "Southwestern" continental margin of Vaalbara. In: Geocongress'90. Geological Society of South Africa, Cape Town, pp. 88–91.

Cheney, E.S., 1996. Sequence stratigraphy and plate tectonic significance of the Transvaal succession of southern Africa and its equivalent in Western Australia. Precambrian Res. 79, 3–24.

Cheney, E.S., Roering, C., Stettler, E., 1988. Geocongress'88. Geological Society of South Africa, Durban, pp. 85–88.

Colliston, W.P., Schoch, A.E., 2013. Wrench-shearing during the Namaqua Orogenesis—Mesoproterozoic late stage deformation effects during Rodinia assembly. Precambrian Res. 233, 44–58.

Cornell, D.H., Schütte, S.S., Eglington, B.L., 1996. The Ongeluk basaltic andesite formation in Griqualand West, South Africa: submarine alteration in a 2222 Ma proterozoic sea. Precambrian Res. 79, 101–123.

Cornell, D.H., Thomas, R.J., Moen, H.F.G., 2006. The Namaqua-Natal Province. In: Johnson, M.R., Anhaeusser, C.R., Thomas, R.J. (Eds.), The Geology of South Africa. Geological Society of South Africa/Council of Geoscience, Johannesburg/Pretoria, pp. 325–379.

Denyszyn, S.W., Feinberg, J.M., Renne, P.R., Scott, G.R., 2013. Revisiting the age and paleomagnetism of the Modipe Gabbro of South Africa. Precambrian Res. 238, 176–185.

De Kock, M.O., Evans, D.A.D., Dorland, H.C., Beukes, N.J., Gutzmer, J., 2006. Paleomagnetism of the lower two unconformity-bounded sequences of the Waterberg Group, South Africa: Towards a better-defined apparent polar wander path for the Paleoproterozoic Kaapvaal Craton. South Afr. J. Geol. 109, 157–182.

De Kock, M.O., Evans, D.A.D., Beukes, N.J., 2009a. Validating the existence of Vaalbara in the Neoarchean. Precambrian Res. 174, 145–154.

De Kock, M.O., Evans, D.A.D., Kirschvink, J.L., Beukes, N.J., Rose, E., Hilburn, I., 2009b. Paleomagnetism of a Neoarchean-Paleoproterozoic carbonate ramp and carbonate platform succession (Transvaal Supergroup) from surface outcrop and drill core, Griqualand West region, South Africa. Precambrian Res. 169, 80–99.

Dorland, H.C., Beukes, N.J., Gutzmer, J., Evans, D.A.D., Armstrong, R.A., 2006. Precise SHRIMP U–Pb zircon age constraints on the lower Waterberg and Soutpansberg Groups South Africa. South Afr. J. Geol. 109, 139–156.

Dreyer, D., (M.Sc thesis) 2014. Geochronology and correlation of Paleoproterozoic red beds of the Elim Group in the Griqualand West Northern Cape Province. University of Johannesburg, Johannesburg, South Africa.

Dreyer, C.J.B., (PhD thesis) 1982. Amphibole Asbestos in South Africa. Rand Afrikaans University, Johannesburg, South Africa, pp. 301.

Eglington, B.M., 2006. Evolution of the Namaqua-Natal Belt, southern Africa – a geochronological and isotope geochemical review,. J. Afr. Earth Sci. 46, 93–111.

Eglington, B.M., Armstrong, R.A., 2004. The Kaapvaal Craton and adjacent orogens, southern Africa: a geochronological database and overview of the geological development of the craton. South Afr. J. Geol. 107, 13–32.

Embleton, B.J.J., 1978. The paleomagnetism of 2400 M.Y. old rocks from Australian Pilbara Craton and its relation to Archean-Proterozoic tectonics. Precambrian Res. 6, 275–291.

Eriksson, P.G., Altermann, W., Hartzer, F.J., 2006. The Transvaal Supergroup and its precursors. In: Johnson, M.R., Anhaeusser, C.R., Thomas, R.J. (Eds.), The Geology of South Africa. Geological Society of South Africa/Council of Geoscience, Johannesburg/Pretoria, pp. 237–260.

Evans, D.A.D., 2007. Key Paleomagnetic pole from the Woongarra/Weeli Wolli large igneous province, Pilbara Craton, Australia: A link between supercratons? Geol. Soc. Am. Abstr. Programs 39, 285.

Evans, D.A.D., Beukes, N.J., Kirschvink, J.L., 1997. Low-latitude glaciation in the Palaeoproterozoic era. Nature 386, 262–266.

Evans, D.A.D., Gutzmer, J., Beukes, N.J., Kirschvink, J.L., 2001. Paleomagnetic Constraints on Ages of Mineralization in the Kalahari Manganese Field, South Africa. Econ. Geol. 96, 621–631.

Evans, D.A.D., Beukes, N.J., Kirschvink, J.L., 2002. Paleomagnetism of a lateritic paleoweathering horizon and overlying Paleoproterozoic red beds from South Africa: implications for the Kaapvaal apparent polar wander path and a confirmation of atmospheric oxygen enrichment. J. Geophys. Res. 107, 2–22.

Fairey, B., Tsikosa, H., Corfu, F., Polteau, S., 2013. U–Pb systematics in carbonates of the Postmasburg Group, Transvaal Supergroup, South Africa: primary versus metasomatic controls. Precambrian Res. 231, 194–205.

Gumsley, A.P., Olsson, J.R., Söderlund, U., de Kock, M.O., Hofmann, A., Klausen, M., 2015. Precise U–Pb baddeleyite age dating of the Usushwana Complex, southern Africa – Implications for the Mesoarchaean magmatic and sedimentological evolution of the Pongola Supergroup, Kaapvaal Craton. Precambrian Res. 267, 174–185.

Gumsley, A.P., de Kock, M.O., Rajesh, H.M., Knoper, M.W., Söderlund, U., Ernst, R.E., 2013. The Hlagothi Complex: the identification of fragments from a Mesoarchaean large igneous province on the Kaapvaal Craton. Lithos 174, 333–348.

Gutzmer, J., Beukes, N.J., 1998. High-grade manganese ores in the Kalahari manganese field: characterization and dating of the ore forming events. Rand Afrikaans University Johannesburg, South Africa 221, Unpublished Report.

Hanson, R.E., Gose, W.A., Crowley, J.L., Ramezani, J., Bowring, S.A., 2004. Paleoproterozoic intraplate magmatism and basin development on the Kaapvaal Craton: Age, paleomagnetism and geochemistry of ~1.93 to ~1.87 Ga post-Waterberg dolerites. South Afr. J. Geol. 107, 233–254.

Heaman, L.M., LeCheminant, A.N., 1993. Paragenesis and U–Pb Systematics of Baddeleyite (ZrO_2). Chem. Geol. 110, 95–126.

Hoffman, P.F., 2013. The great oxidation and a Siderian snowball Earth: MIF-S based correlation of Paleoproterozoic glacial epochs. Chem. Geol., 143–156.

Jaffey, A.H., Flynn, K.F., Glendenin, L.E., Bently, W.C., Essling, A.M., 1971. Precision Measurement of Half-Lives and Specific Activities of U^{235} and U^{238}. Phys. Rev. C 4, 1889–1906.

Jones, C.H., 2002. User-driven integrated software lives: "Paleomag" Paleomagnetic analysis on the Macintosh. Comp. Geosci. 28, 1145–1151.

Kamo, S.L., Reimold, W.U., Krogh, T.E., Colliston, W.P., 1996. A 2.023 Ga age for the Vredefort impact event and a first report of shock metamorphosed zircons in pseudotachylitic breccias and Granophyre. Earth Planet. Sci. Lett. 144, 369–387.

Keyser, N., 1997. Geological map of the Republic of South Africa and the Kingdoms of Leshoto and Swaziland, 1:1,000,000. Council for Geoscience, Pretoria.

Kirschvink, J.L., 1980. The least-squares line and plane and the analysis of palaeomagnetic data. Geophys. J. Int. 62, 699–718.

Kirschvink, J.L., Gaidos, E.J., Bertani, L.E., Beukes, N.J., Gutzmer, J., Maepa, L.N., Steinberger, R.E., 2000. Paleoproterozoic snowball Earth: extreme climatic and geochemical global change and its biological consequences. Proc. Natl. Acad. Sci. U. S. A. 97, 1400–1405.

Kirschvink, J.L., Kopp, R.E., Raub, T.D., Baumgartner, C.T., Holt, J.W., 2008. Rapid, precise, and high-sensitivity acquisition of paleomagnetic and rock-magnetic data: development of a low-noise automatic sample changing system for superconducting rock magnetometers. Geochem. Geophys. Geosyst. 9, http://dx.doi.org/10.1029/2007GC001856.

Layer, P.W., Kröner, A., McWilliams, M., Clauer, N., 1988. Regional magnetic overprinting of Witwatersrand Supergroup Sediments, South Africa. J. Geophys. Res.–Sold Earth 93, 2191–2200.

Li, Z.X., McArthur-Powell, C., Bowman, P., 1993. Timing and genesis of Hamersley iron-ore deposits. Exploration Geophys. 24, 631–636.

Ludwig, K.R., 1991. Isoplot – a plotting and regression program for radiogenic isotopic data, Open File Report., pp. 445, USGS.

Martin, D.M.B., Clendenin, C.W., Krapez, B., McNaughton, N.J., 1998. Tectonic and geochronological constraints on Late Archaean and Palaeoproterozoic stratigraphic correlation within and between the Kaapvaal and Pilbara cratons. J. Geol. Soc. 155, 311–322.

McFadden, P.L., Jones, D.L., 1981. The fold test in palaeomagnetism. Geophys. J. Int. 67, 53–58.

Moore, J.M., Polteau, S., Armstrong, R.A., Corfu, F., Tsikosa, H., 2012. The age and correlation of the Postmasburg Group, southern Africa: Constraints from detrital zircon grains. J. Afr. Earth Sci. 64, 9–19.

Moore, J.M., Tsikos, H., Polteau, S., 2001. Deconstructing the Transvaal Supergroup, South Africa: implications for Palaeoproterozoic palaeoclimate models. J. Afr. Earth Sci. 33, 437–444.

Müller, S.G., Krapež, B., Barley, M.E., Fletcher, I.R., 2005. Giant iron-ore deposits of the Hamersley province related to the breakup of Paleoproterozoic Australia: new insights from in situ SHRIMP dating of baddeleyite from mafic intrusions. Geology 33, 577–580.

Nelson, D.R., Trendall, A.F., Altermann, W., 1999. Chronological correlations between the Pilbara and Kaapvaal Cratons. Precambrian Res. 97, 165–189.

Olsson, J.R., Soderlund, U., Klausen, M.B., Ernst, R.E., 2010. U–Pb baddeleyite ages linking major Archean dyke swarms to volcanic-rift forming events in the Kaapvaal craton (South Africa), and a precise age for the Bushveld Complex. Precambrian Res. 183, 490–500.

Lubnina, N., Ernst, R.E., Klausen, M.B., Söderlund, U., 2010. Paleomagnetic study of NeoArchean–Paleoproterozoic dykes in the Kaapvaal Craton. Precambrian Res. 183, 523–552.

Letts, S., Torsvik, T.H., Webb, S.J., Ashwal, L.D., 2009. Palaeomagnetism of the 2054 Ma Bushveld Complex (South Africa): implications for emplacement and cooling. Geophys. J. Int. 179, 850–872.

Letts, S., Torsvik, T.H., Webb, S.J., Ashwal, L.D., 2011. New Palaeoproterozoic palaeomagnetic data from the Kaapvaal Craton, South Africa. In: Hinsbergen, D.J.J., Buiter, S.J. H., Torsvik, T.H., Gaina, C., Webb, S.J. (Eds.), The Formation and Evolution of Africa: A Synopsis of 3. 8 Ga of Earth History. Geological Society of London, London, pp. 9–26.

Pickard, A.L., 2003. SHRIMP U–Pb zircon ages for the Palaeoproterozoic Kuruman Iron Formation, Northern Cape Province, South Africa: evidence for simultaneous BIF deposition on Kaapvaal and Pilbara Cratons. Precambrian Res. 125, 275–315.

Schmidt, P.W., Clark, D.A., 1994. Palaeomagnetism and magnetic anisotropy of Proterozoic banded-iron formations and iron ores of the Hamersley Basin, Western Australia. Precambrian Res. 69, 133–155.

Schmidt, P.W., Embleton, B.J.J., 1985. Prefolding and overprint magnetic signatures in Precambrian (~2.9–2.7 Ga) Igneous rocks from the Pilbara Craton and Hamersley Basin, NW Australia. J. Geophys. Res.-Solid Earth Planets 90, 2967–2984.

Schröder, S., Lacassie, J.P., Beukes, N.J., 2006. Stratigraphic and geochemical framework of the Agouron drill cores, Transvaal Supergroup (Neoarchean-Paleoproterozoic, South Africa). South Afr. J. Geol. 109, 23–54.

Scoates, J.S., Friedman, R.M., 2008. Precise age of the Plantinferous Merensky Reef, Bushveld Complex, South Africa, by the U–Pb Zircon chemical abrasion ID-TIMS technique. Econ. Geol. 103, 465–471.

Smirnov, A.V., Evans, D.A.D., Ernst, R., Soderlund, U., Li, Z.-X, 2013. Trading partners: tectonic ancestry of southern Africa and western Australia, in Archean supercratons Vaalbara and Zimgarn. Precambrian Res. 224, 11–22.

Söderlund, U., Ibanez-Mejia, M., El Bahat, A., Ernst, R.E., Ikenne, M., Soulaimani, A., Youbi, N., Cousens, B., El Janati, M., Hafid, A., 2013. Reply to Comment on "U–Pb baddeleyite ages and geochemistry of dolerite dykes in the Bas-Drâa inlier of the Anti-Atlas of Morocco: Newly identified 1380 Ma event in the West African Craton" by André Michard and Dominique Gasquet. Lithos 174, 101–108.

Söderlund, U., Johansson, L., 2002. A simple way to extract baddeleyite (ZrO_2). Geochem. Geophys. Geosyst. 3, 10029/2001GC000212.

Stacey, J.S., Kramers, J.D., 1975. Approximation of terrestrial lead isotope evolution by a two-stage model. Earth Planet. Sci. Lett. 26, 207–221.

Strik, G., Blake, T.S., Zegers, T.E., White, S.H., Langereis, C.G., 2003. Palaeomagnetism of flood basalts in the Pilbara Craton, Western Australia: Late Archaean continental drift and the oldest known reversal of the geomagnetic field. J. Geophys. Res.-Solid Earth Planets 108, 2551.

Sumner, D.Y., Bowring, S.A., 1996. U-Pb geochronologic constraints on deposition of the Campbellrand Subgroup, Transvaal Supergroup, South Africa. Precambrian Res. 79, 25–35.

Tauxe, L., 2010. Essentials of Paleomagnetism. University of California Press, Berkeley/Los Angeles/London, pp. 489.

Tauxe, L., Kylstra, N., Constable, C., 1991. Bootstrap statistics for paleomagnetic data. J. Geophys. Res.-Solid Earth Planets 96, 11723–11740.

Trendall, A.F., 1968. Three great basins of Precambrian iron formation deposition: a systematic comparison. Geol. Soc. Am. Bull. 79, 1527–1533.

Trendall, A.F., Compston, W., Nelson, D.R., De Laeter, J.R., Bennet, V.C., 2004. SHRIMP zircon ages constraining the depositional chronology of the Hamersley Group, Western Australia. Austr. J. Earth Sci. 51, 621–644.

Trendall, A.F., De Laeter, J.R., Nelson, D.R., 1995. Chronology of Gondwana BIFs: progress report from recent zircon U–Pb results. In: Third Australian Conference on Geochronology, pp. 1–3.

Wabo, H., de Kock, M., Rajesh, H.M., Beukes, N.J.,2011. Paleomagnetism and geochemistry of Bushveld-related intrusions, eastern Kaapvaal craton. In: AGU Fall Meeting, 2011. American Geophysical Union, San Francisco.

Walraven, F., Martini, J., 1995. Zircon Pb-evaporation age determinations of the Oak Tree Formation, Chuniespoort Group, Transvaal Sequence: implications for Transvaal-Griqualand West basin correlations. South Afr. J. Geol. 98, 58–67.

Williams, S.E., Müller, R.D., Landgrebe, T.C.W., Whittaker, J.M., GSA Today 22 2012. An open-source software environment for visualizing and refining plate tectonic reconstructions using high-resolution geological and geophysical data sets.

Wingate, M.T.D., 1998. A paleomagnetic test of the Kaapvaal-Pilbara (Vaalbara) connection at 2.78 Ga. South Afr. J. Geol. 101, 257–274.

Wu, F.-Y., Yang, Y.-H., Li, Q.-L., Mitchell, R.H., Dawson, J.B., Brandl, G., Yuhara, M., 2011. In situ determination of U–Pb ages and Sr–Nd–Hf isotopic constraints on the petrogenesis of the Phalaborwa carbonatite Complex, South Africa. Lithos 127, 309–322.

Zegers, T.E., de Wit, M.J., Dann, J., White, S.H., 1998. Vaalbara, Earth's oldest assembled continent? A combined structural, geochronological and palaeomagnetic test. Terra Nova 10, 250–259.

PAPER III

GFF, 2016
http://dx.doi.org/10.1080/11035897.2015.1122665

Article

U–Pb baddeleyite geochronology and geochemistry of the White Mfolozi Dyke Swarm: unravelling the complexities of 2.70–2.66 Ga dyke swarms across the eastern Kaapvaal Craton, South Africa

ASHLEY GUMSLEY[1], JOHAN RÅDMAN[2], ULF SÖDERLUND[1,2] and MARTIN KLAUSEN[3]

Gumsley, A., Rådman, J., Söderlund, U. & Klausen, M., U–Pb baddeleyite geochronology and geochemistry of the White Mfolozi Dyke Swarm: unravelling the complexities of 2.70-2.66 Ga dyke swarms across the eastern Kaapvaal Craton, South Africa. GFF, Vol. 00, pp. 1–18. © Geologiska Föreningen. doi: http://dx.doi.org/10.1080/11035897.2015.1122665

Abstract: On the south-easternmost Kaapvaal Craton, a NE-trending plagioclase-megacrystic dolerite dyke swarm, herein named the White Mfolozi Dyke Swarm (WMDS), has been identified. New U–Pb baddeleyite ages presented here indicate that the WMDS was emplaced within less than 10 million years, with our three most robust results yielding a weighted mean age of 2662 ± 2 Ma. The WMDS is coeval with the youngest dykes of a 2.70–2.66 Ga radiating dyke swarm already identified further north on the eastern side of the Kaapvaal Craton. This dyke swarm radiates out from the eastern lobe of the ca. 2.05 Ga Bushveld Complex. A clustering of ages from the WMDS and the 2.70–2.66 Ga radiating dyke swarm identify potential magmatic peaks at 2701–2692 Ma, 2686–2683 Ma and 2665–2659 Ma. Geochemical signatures of the dykes do not correlate with these age groups, but are rather unique to specific areas. The northern part of the eastern Kaapvaal Craton hosts relatively differentiated 2.70–2.66 Ga dolerite dykes that could have been derived from a moderately enriched mantle source, whereas the ca. 2.66 Ga WMDS from the southernmost area exhibit much more depleted signatures. In between these two margins, the central area hosts more andesitic 2.70–2.66 Ga dykes that may have assimilated substantial amounts of partly digested tonalite–trondhjemite–granodiorite crust from the basement. We investigate the evolution for the Kaapvaal Craton during a highly magmatic period that extends for over 60 million years from extensive Ventersdorp volcanism to the eruption of proto-basinal volcanic rocks at the base of the Transvaal Supergroup.

Keywords: geochemistry; Kaapvaal Craton; U–Pb baddeleyite geochronology; White Mfolozi Dyke Swarm

[1]Department of Geology, Lund University, Sölvegatan 12, Lund, 223 62, Sweden; ashley.gumsley@geol.lu.se
[2]Department of Geosciences, Swedish Museum of Natural History, P.O. Box 50 007, 104 05, Stockholm, Sweden
[3]Department of Earth Sciences, Stellenbosch University, Private Bag X1, Matieland, 7602, South Africa

Manuscript received 15 March 2015. Revised manuscript accepted 17 November 2015.

1. Introduction

Initial studies using U–Pb geochronology on baddeleyite grains extracted from mafic intrusions have revealed a record of at least five different dyke swarms and sill provinces across the Kaapvaal Craton, which are interpreted as feeders to major large igneous provinces (LIPs). Baddeleyite ages from these LIPs include: ca. 2.99–2.97 Ga (Olsson et al. 2010, Gumsley et al. 2015), ca. 2.78–2.66 Ga (Olsson et al. 2010, Denyszyn et al. 2013), ca. 1.93–1.87 Ga (Hanson et al. 2004b), ca. 1.11 Ga (Hanson et al. 2004a) and ca. 0.18 Ga (Svensen et al. 2012). These ages can be linked to the Pongola, Ventersdorp, Waterberg, Umkondo and Karoo magmatic events, respectively. The remnants of these magmatic events are well preserved within southern Africa's stratigraphic record. Only the ca. 2.06 Ga Bushveld Complex and its related volcanic rocks and marginal sills within the Transvaal Supergroup has yet to be linked to a significant feeder dyke swarm (Olsson et al. 2010, 2011). The apparent radiating pattern produced by the NW–SE-trending ca. 2.99–2.97 Ga Barberton-Badplaas Dyke Swarm (Olsson et al. 2010), the SW–NE-trending ca. 1.88–1.84 Ga Black Hills Dyke Swarm (Olsson et al. this volume) and the E–W-trending ca. 2.70–2.66 Ga dykes of the Rykoppies Swarm (Olsson et al. 2010), does not emanate from the eastern lobe of the Bushveld Complex. However, Olsson et al. (2011) later emphasised that overlapping ca. 2.70–2.66 Ga dolerite dyke swarms do radiate from the same locus, and thereby proposed a link between a Ventersdorp-aged plume event followed by the emplacement of the Bushveld Complex later due to lithospheric delamination. More detailed studies are now also beginning to elucidate other magmatic substages within some of

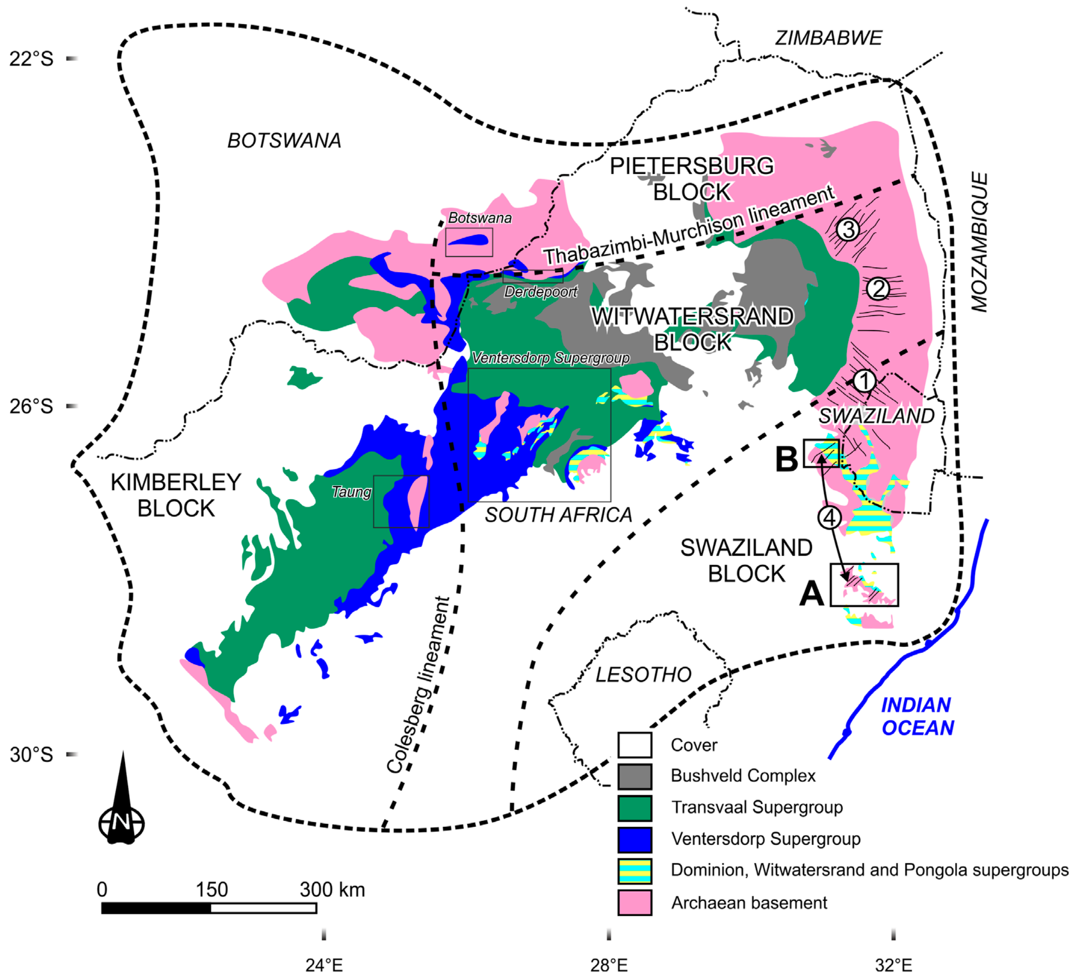

Fig. 1. Geological map of the Kaapvaal Craton, modified after Eglington & Armstrong (2004), highlighting the Archaean to Palaeoproterozoic lithological units of interest to this study. Numbers 1 to 4 denote: (1) dykes of the Barberton-Badplaas Swarm, (2) dykes of the Rykoppies Swarm, (3) dykes of the Black Hills Swarm and (4) dykes of the White Mfolozi Swarm. Rectangles A and B indicate areas of sampling of the WMDS for this study shown in Fig. 2. **A**. In northern KwaZulu-Natal. **B**. In south-eastern Mpumalanga. Other rectangles indicate outcrop areas of rock units, preserved in various half-grabens across the western part of the craton, that are correlated with the Venterdorp Supergroup. These areas are listed in Table 3, where more detail is provided.

the Kaapvaal Craton's major Precambrian LIP events, including: recognition of the ca. 2.87 Ga Hlagothi dykes and sills within the Pongola Supergroup (Gumsley et al. 2013), the 2.44–2.43 Ga Westerberg sills in the Transvaal Supergroup (Kampmann et al. 2015), as well as the 1.93–1.91 Ga Tsineng Dyke Swarm and volcanic rocks of the Hartley Formation in the Olifantshoek Supergroup (Semami et al. this volume) and lastly coeval dyke swarms radiating from different magmatic centres associated with the ca. 1.11 Ga Umkondo LIP (de Kock et al. 2014). These more detailed investigations represent a new generation of primarily geochronogical investigations that aim at better resolving how dyke swarms and sill provinces are emplaced within various tectonic settings on the Kaapvaal Craton. This builds on the initial investigations undertaken prior to this by Uken & Watkeys (1997), as well as by Hunter & Halls (1992).

In this paper, we report new U–Pb baddeleyite ages and geochemistry for seven dolerite dykes from a significant NE-trending dyke swarm bearing diagnostic plagioclase phenocrysts, which is located on the south-easternmost portion of the Kaapvaal Craton (Fig. 1). This dyke swarm, herein termed the 'White Mfolozi Dyke Swarm' (WMDS), was first investigated geochemically and palaeomagnetically by Klausen et al. (2010) and Lubnina et al. (2010), as well as Gumsley (2013). Apart from refining and expanding the magmatic barcode record for the Kaapvaal Craton, the tectonic and petrological relationship of the WMDS to the more northerly, yet broadly coeval ca. 2.70–2.66 Ga radiating dyke swarm is investigated and expanded upon.

2. Regional geology

The Kaapvaal Craton in southern Africa is one of approximately 35 pieces of Archaean crust that is preserved to this day (Bleeker 2003). The largest part of this Archaean basement granite–greenstone terrain is exposed along eastern part of the Kaapvaal Craton (pink in Fig. 1). South of this major basement exposure, in the northern KwaZulu-Natal Province of South Africa, the Archaean basement is exposed within isolated inliers, referred to as the south-easternmost window of Archaean basement

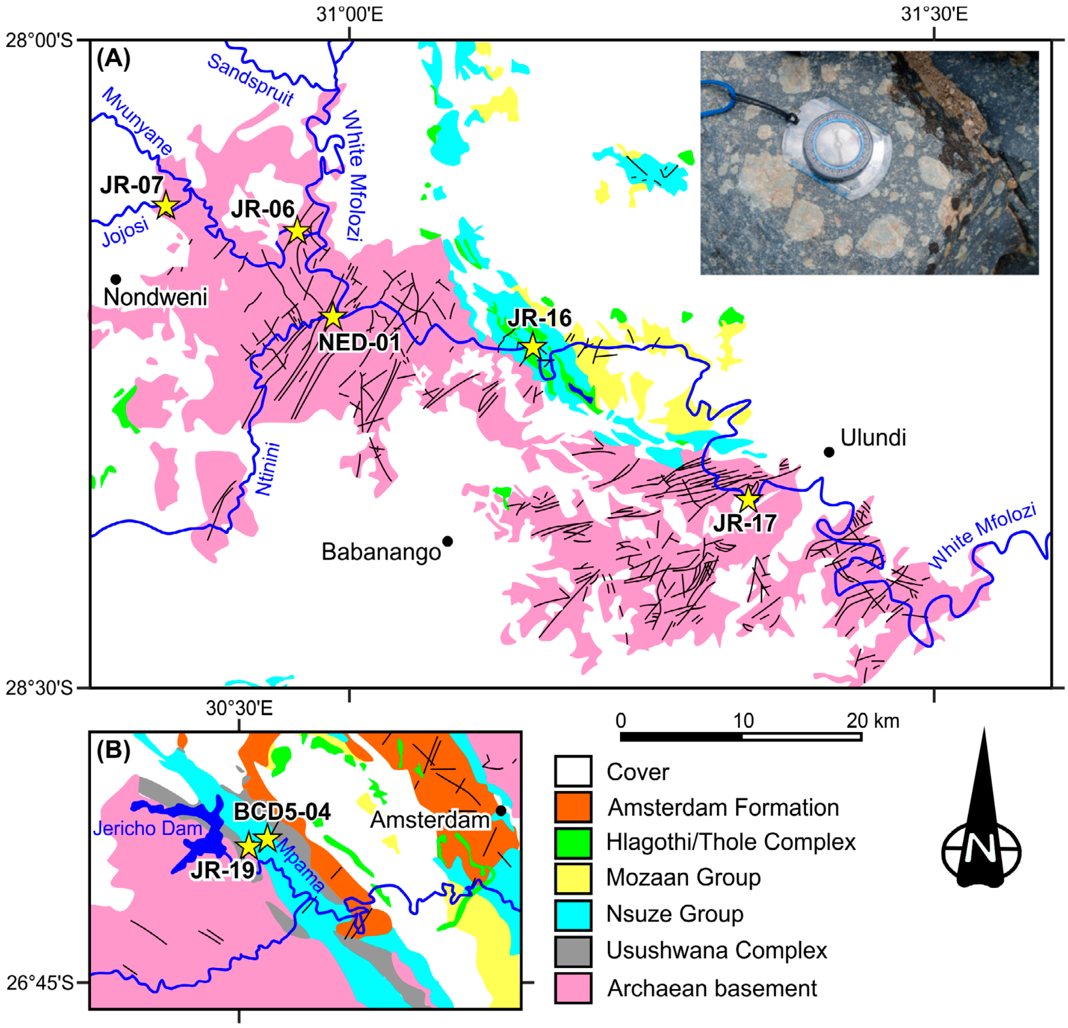

Fig. 2. Geological sampling areas and localities in northern KwaZulu-Natal. **A**. South-eastern Mpumalanga. **B**. Highlighted from Fig. 1, highlighting the Precambrian rock units and dyke trends within these Archaean-Palaeoproterozoic inliers, with sample localities denoted with a yellow star. The maps are modified after 1:250 000 geological maps from the Council for Geoscience for Mbabane and Dundee. Inset: field photograph of a diagnostic feldspar-megacrystic texture in a NE-trending WMDS dyke.

(Figs. 1 and 2). The south-easternmost part of the Archaean basement is mostly covered by sedimentary rocks of the Karoo Supergroup, and is truncated by Mesoproterozoic rocks of the Namaqua-Natal Orogen along the southern margin of the craton. On the eroded Eo to Mesoarchaean basement of the Kaapvaal Craton, a number of sedimentary and volcanic supracrustal successions have been deposited, including, from oldest to youngest, the Dominion, Pongola and Witwatersrand volcano-sedimentary sequences (alternating blue and yellow in Fig. 1).

The Neoarchaean Ventersdorp Supergroup overlying these Mesoarchaean successions (blue in Fig. 1), is a volcano-sedimentary succession deposited from 2714 to 2709 Ma (Armstrong et al. 1991, van der Westhuizen et al. 2006). These ages have been questioned by Wingate (1998) and de Kock et al. (2012), who argue that older U–Pb zircon and baddeleyite ages of 2782 ± 5 Ma and 2784 ± 1 Ma, respectively (Wingate 1998, Denyszyn et al. 2013), record the initiation of volcanism for the Ventersdorp Supergroup.

Unconformably overlying the Ventersdorp Supergroup is a series of discrete sedimentary and volcanic rocks that are proto-basinal to the Transvaal Supergroup (Eriksson et al. 2006). These volcanic units have been dated to 2664 ± 1 Ma using U–Pb on zircon (Barton et al. 1995). On top of the proto-basinal fills lies the entire Transvaal Supergroup (green in Fig. 1), a sequence of mainly sedimentary units that was deposited from 2600 to 2100 Ma (Eriksson et al. 2006). A 2222 ± 13 Ma age from the volcanic Ongeluk–Hekpoort Formation in the Transvaal Supergroup has been reported (Cornell et al. 1996), along with 2441 ± 6 Ma and 2426 ± 1 Ma ages for the Westerberg Sill Suite (Kampmann et al. 2015). The largest layered intrusion in the world, the economically important Bushveld Complex (grey in Fig. 1), intrudes through the Transvaal Supergroup (Cawthorn et al. 2006). The first U–Pb baddeleyite age for the mafic portion of the Bushveld Complex is 2058 ± 2 Ma (Olsson et al. 2010).

In the exposed eastern Kaapvaal Craton (Fig. 1), three distinct Precambrian dolerite dyke swarms appear to radiate out from the eastern lobe of the Bushveld Complex (Uken & Watkeys 1997, Olsson et al. 2011). The first precise U–Pb TIMS baddeleyite ages for some of these dykes (Olsson et al. 2010, 2011, Gumsley et al. 2015, Olsson et al. this volume) demonstrate that this radiating pattern is made up of the southern SE-trending Barberton-Badplaas Dyke Swarm of ca. 2.98–2.96 Ga and 2.70–2.66 Ga dykes, the central E-trending Rykoppies Dyke Swarm of ca. 2.70–2.66 Ga dykes, and the more pervasive northern NE-trending Black Hills Dyke Swarm of ca. 1.88–1.83 Ga ages, as well as 2.70–2.66 Ga dykes (Fig. 1). The south-easternmost Archaean basement is cut by some sills, as well as numerous mafic dykes of various trends (Figs. 1 and 2). Relatively older SE-trending dykes are presumed to be the southward extension of the Barberton-Badplaas Dyke Swarm (Klausen et al. 2010, Lubnina et al. 2010). The NE-trending dykes are easily distinguished from the other swarms by being remarkably feldspar-megacrystic, and they were noted to cut both SE-trending dolerite dykes, as well as the Pongola Supergroup, but not any E- to ENE-trending dykes or the sedimentary Karoo Supergroup cover with its ca. 0.18 Ga dolerite sills and dykes. One SE-trending dolerite dyke from this south-easternmost window has been dated prior to this study at ca. 2.87 Ga (Gumsley et al. 2013), which correlates with the coeval Hlagothi Complex. The NE-trending and characteristically feldspar-megacrystic dolerite dyke swarm in the south-easternmost basement window is the focus of this study, which was tentatively assigned a ca. 1.90 Ga age (Klausen et al. 2010, Lubnina et al. 2010), based on how all of the NE-trending dykes appeared to be geochemically and palaeomagnetically distinct from the Archaean dykes. Similar reconnaissance studies were also done further north on the eastern Kaapvaal Craton by Klausen et al. (2010) and Lubnina et al. (2010), with more extensive geochemical and palaeomagnetic investigations in the Barberton-Badplaas area by Maré & Fourie (2012), as well as Hunter & Halls (1992).The WMDS is primarily exposed and thereby sampled in and around the White Mfolozi River, from which its name, the 'WMDS', is derived (Fig. 2).

3. The WMDS

Dolerite samples of the WMDS were collected from the Archaean basement terrane of the Kaapvaal Craton in the northern KwaZulu-Natal and south-eastern Mpumalanga provinces of South Africa (Figs. 1 and 2). Suitable dolerite dykes and sample sites inside the Archaean inliers were identified through Google Earth, with the dykes usually best exposed either along outcrop pavements in dry river sections or along distinct boulder trains on ridges outside the rivers. The NE-trending dolerite dykes were observed to cross-cut SE-trending dolerite dykes in the region, but in turn are cross-cut by more E- to ENE-trending dolerite dykes, in agreement with previous observations (Klausen et al. 2010, Lubnina et al. 2010). All of the NE-trending dykes are variably plagioclase-phyric, with markedly pale pink-weathered phenocrysts (Fig. 2), typically set in a grey–green and medium-grained dolerite groundmass that becomes more fine-grained towards the dyke's aphanitic chilled margins. The plagioclase phenocrysts vary considerably in both size and distribution, with some individual phenocrysts up to 10 cm in length, and these are thus referred to as megacrysts (used for the remainder of this paper). Most euhedral megacrysts are typically rectangular, but some are more equidimensional (or even rounded). Despite being strongly altered, many megacrysts preserve a compositional zonation, suggesting that these grew freely within a differentiating magma. These megacrysts are typically concentrated into margin-parallel bands that are best explained by flow segregation. Exceptionally high megacryst concentrations (up to ~60%) are typically found at dyke offsets, and could therefore have accumulated within local eddy currents or flow constrictions.

4. Petrography

Polished thin sections were made from all dated dolerite dyke samples in this study. The NE-trending dolerite dykes sampled farther to the north in south-eastern Mpumalanga are less metamorphosed than those farther south and closer to the ca. 1.1 Ga Natal-Namaqua Belt in northern KwaZulu-Natal. The samples are devoid of olivine, or its diagnostic alteration products of iddingsite and serpentine. The mafic groundmass in all thin sections is partly chloritised, which is tentatively used as an indication of lower greenschist facies metamorphism. Actinolite and tremolite are the usually observed amphiboles, which are primarily thought to be a product of the uralitisation of clinopyroxene (although some orthopyroxene was also noted). Some pyroxenes remain as preserved cores within amphibole, particularly in samples collected in south-east Mpumalanga. Sericitisation and minor saussauritisation of plagioclase is common in all samples, with some NE-trending dykes in northern KwaZulu-Natal typically being more strongly sericitised. Accessory minerals include Fe–Ti oxides, and occasional interstitial quartz and biotite, consistent with the absence of olivine.

5. Geochronology

5.1. Analytical protocol

From a total of twenty collected samples, seven dolerite dyke samples yielded a sufficient amount of baddeleyite for geochronology (Fig. 2). At the Department of Geology in Lund University, the rock samples were crushed and milled. Water-based separation of baddeleyite was done using the method of Söderlund & Johansson (2002). For every sample, the best quality baddeleyite crystals were combined into fractions of 1 to 6 crystals each, and put in separate pre-cleaned Teflon capsules. The fractions were then washed thoroughly in steps with small quantities of ultrapure HNO_3 and H_2O, including one heating step of the solutions by placing the capsules on a hot plate for ~30 min (in 3 M HNO_3). A trace of a ^{205}Pb-$^{233–236}U$ spike solution was added to each capsule together with 10 drops of concentrated HF-HNO_3 (10:1). The capsules were then placed in oven for three days at 190 °C to dissolve the baddeleyite grains and homogenise U and Pb from the spike and sample. At the Department of Geoscience in the Museum of Natural History in Stockholm, the Teflon capsules were again put on a hot plate until the solution had evaporated. An addition of 10 drops of ultrapure 6 M HCl and 1 drop of 0.25 M H_3PO_4 were added to each capsule before being dried down once again on a hot plate. The sample fractions were then dissolved in 2-μl silica gel before being loaded on an outgassed Re filament. Further details are given in Olsson et al. (2010) and Nilsson et al. (2013).

U and Pb isotopic ratios were measured on a Finnigan Triton mass spectrometer. Pb isotopes were measured after heating to a temperature range of approximately 1200–1250 °C. The intensities of ^{204}Pb, ^{205}Pb, ^{206}Pb, ^{207}Pb and ^{208}Pb were measured in either static mode with Faraday Cups, or in peak-switching mode using a Secondary Electron Multiplier. The temperature was then increased to approximately 1270–1320 °C. At this temperature the U isotopes were emitted and measured. An "in-house" programme made by Per-Olof Persson (Natural History Museum, Stockholm), with calculations following Ludwig (1991), was used for data reduction.

5.2. *Results*

U–Pb isotopic data are presented in Table 1 and concordia diagrams are shown in Fig. 3. A summary of the results are reported individually and comments regarding analytical issues follow at the end of this chapter.

Fractions comprising three, four and five baddeleyite grains were analysed from NED-01 (Fig. 3(A)). The grains show frosty surfaces, indicating post-magmatic metamorphism and/or alteration. Analyses plot strongly discordant between 14 and 43%, supporting partial transformation of baddeleyite to polycrystalline zircon. Free regression yielded an upper intercept age of 2661 ± 11 Ma (MSWD = 0.05), which is similar to the mean age of ca. 2662 Ma for the WMDS, despite all three analyses being strongly discordant. The lower intercept age is 127 ± 70 Ma, suggesting a partial transformation of baddeleyite to zircon related to the Karoo magmatic event.

Four fractions of good-quality grains were analysed from JR-16 (Fig. 3(B)). They consisted of one to six relatively light brown grains in each fraction. One fraction plots concordant at a slightly younger age than the other analyses. The other three fractions give reproducible ^{207}Pb/^{206}Pb dates, of which two plot concordant. The weighted mean ^{207}Pb/^{206}Pb age of these fractions is 2654 ± 2 Ma (MSWD = 0.39), whereas the concordia date is 2648 ± 14 Ma (MSWD = 9.8). The weighted ^{207}Pb/^{206}Pb age of 2654 ± 2 Ma is considered as the best age estimate of JR-16.

Four baddeleyite fractions of brown, transparent grains of JR-17 were analysed (Fig. 3(C)). The grains were combined into fractions of three to five grains each. The fractions plot variably discordant (1.5–3.5%), and an anchored regression at 0 ± 100 Ma yields an upper intercept age of 2659 ± 7 Ma (MSWD = 1.5). A weighted mean value yields a precise age of 2659 ± 1 Ma (MSWD = 1.5). The fourth fraction plots slightly above the concordia curve at a lower ^{207}Pb/^{206}Pb date. The weighted ^{207}Pb/^{206}Pb result of 2659 ± 1 Ma of the remaining analyses is the preferred age of this sample.

The analysis of sample JR-19 comprised four fractions (Fig. 3(D)). One analysis was performed on a single large, clear grain, while the other fractions consisted of three to four smaller grains of moderate to good quality. Three fractions overlap within error, of which two plot concordant. Including fraction b in an unforced regression yields upper and lower intercept ages of 2657 ± 28 Ma and ca. 805 Ma, respectively, but the MSWD of 3.7 reveals scatter beyond analytical uncertainties. The weighted mean ^{207}Pb/^{206}Pb age, if excluding fraction b, is 2661 ± 4 Ma (MSWD = 1.2). This is the preferred age estimate for this dyke.

The grains from JR-06 are dark brown and of good quality, although many grains are fractured. The analyses plot less than 1% discordant, and are partly overlapping (Fig. 3(E)). The weighted mean ^{207}Pb/^{206}Pb age is 2659 ± 5 Ma (MSWD = 1.8), with a concordia age of 2658 ± 5 Ma (MSWD = 1.3).

Four fractions, composed of between three and five grains each were analysed from BCD5-04 (Fig. 3(F)). The baddeleyite grains selected for analysis are dark brown and clear. Some of these grains were long elongated crystals, and some are fragments. One fraction plots concordant whereas the other fractions are up to 2% discordant. Regression comprising all four analyses yields an age of 2662 ± 3 Ma. Using a forced lower intercept age of 0 ± 100 Ma gives an upper intercept that is identical to the weighted mean of ^{207}Pb/^{206}Pb age, i.e., 2662 ± 3 Ma (MSWD = 1.5).

Two fractions of JR-07 were analysed with three and four grains, respectively (Fig. 3(G)). The grains are dark brown without any trace of zircon rims. Both analyses plot concordant, allowing a concordia age to be calculated at 2665 ± 4 Ma (MSWD = 1.5), which is interpreted as the crystallisation age of this dyke.

One fraction each of samples JR-16, JR-17 and JR-19 have ^{207}Pb/^{206}Pb dates that appear significantly younger than the other analyses of the respective samples. Although two of them plot statistically concordant (JR-16 and JR-19), we have rejected these from the age calculations, as we consider them associated with analytical artefacts. If their relatively younger ^{207}Pb/^{206}Pb dates were indeed caused by a later metamorphic event it might have been justified to include those analyses in the regressions of JR-16 and JR-19 (although this would be problematic for JR-17, as the 'young' analysis plots above the concordia curve, Fig. 3(C)), and then their intrusion ages should be better reported as upper intercept dates. However, the bulk of the baddeleyite analyses forms tight clusters that plot concordant or only slightly discordant. The excellent reproducibility of ^{207}Pb/^{206}Pb dates of these samples, and the overall fresh quality of baddeleyite grains (e.g., lack of secondary zircon rims, with the exception of JR-17), suggest that small degree of discordance, if any, was relatively recent and not caused by partial transformation of baddeleyite to zircon during metamorphism/alteration. A relatively recent time of discordance is also indicated by the lower intercept of JR-17 (0 Ma within 2σ error). For these reasons we prefer to restrict the age calculation for JR-16, JR-17 and JR-19 to analyses that have reproducible ^{207}Pb/^{206}Pb dates. We hence assign the three "younger" analyses to record some analytical bias that we have no explanation for.

6. Geochemistry

6.1. *Analytical protocol*

All dated samples from Olsson et al. (2010, 2011), used for comparative studies, and JR-16, JR-19, NED-01 and BCD5-04 were prepared for analysis at Lund University, Sweden. Rock samples were sawed and crushed with a sledge hammer into small pieces. The pieces were hand-picked, in order to avoid phenocrysts of plagioclase feldspar, and pieces with saw smear marks or weathering. Dolerite pieces were then milled in a tungsten carbide mill tray to a very fine powder. The mill tray was thoroughly cleaned with water and washing liquid, and dried between every sample. Approximately 10 g of each sample was sent to ACME laboratories in Canada for XRF (X-ray fluorescence spectrometry) analysis of major elements and ICP-MS analysis for trace elements. Loss on ignition was also measured on every sample to

Table 1. U–Pb ID-TIMS data for baddeleyite analyses of seven dyke sample of the WMDS.

Analysis no. (number of grains)	U/Th	Pbc/Pbtot[a]	$^{206}Pb/^{204}Pb$	$^{207}Pb/^{235}U$	±2s% err	$^{206}Pb/^{238}U$	±2s % err	$^{207}Pb/^{235}U$	$^{206}Pb/^{238}U$	$^{207}Pb/^{206}Pb$	±2s	Concordance
			raw[b]		[corr][c]				[age, Ma]			
NED-01	28.210376° S, 30.982430° E											
a (4)	7.9	0.393	108.8	8.7049	2.20	0.35456	2.09	2307.6	1956.3	2634.9	12.6	0.742
b (3)	n.m.[d]	0.297	172.2	10.5693	1.52	0.42597	1.50	2486.0	2287.5	2652.5	7.5	0.862
c (5)	2.1	0.484	90.7	6.3776	4.36	0.26214	4.30	2029.2	1500.8	2619.7	21.3	0.573
JR-16	28.234830° S, 31.147900° E											
a (5)	7.2	0.037	1647.0	12.4720	0.62	0.50225	0.62	2640.6	2623.4	2653.8	2.5	0.989
b (1)	8.3	0.127	460.5	12.7011	1.59	0.51053	1.57	2657.7	2658.9	2656.9	7.3	1.001
c (2)	5.3	0.152	394.1	12.1810	2.14	0.49938	2.11	2618.4	2611.1	2624.1	10.3	0.995
d (6)	8.1	0.077	776.6	12.6311	1.09	0.50823	1.09	2652.5	2649.1	2655.2	4.4	0.998
JR-17	28.351620° S, 31.341771° E											
a (5)	13.1	0.066	793.4	12.4768	0.32	0.50097	0.28	2641.0	2618.0	2658.7	2.6	0.985
b (3)	9.8	0.018	3182.3	12.4936	0.34	0.50197	0.32	2642.2	2622.3	2657.6	2.1	0.987
c (5)	3.6	0.014	4208.2	12.6238	0.33	0.51066	0.31	2652.0	2659.5	2646.3	2.0	1.005
d (3)	8.3	0.018	3221.9	12.1955	0.82	0.48906	0.80	2619.6	2566.6	2660.8	2.9	0.965
JR-19	26.648985° S, 30.504398° E											
a (3)	6.1	0.248	185.4	12.7615	1.22	0.51309	1.05	2662.2	2669.8	2656.4	10.2	1.005
b (1)	8.4	0.124	481.5	12.3966	1.70	0.50288	1.70	2634.9	2626.1	2641.7	6.8	0.994
c (3)	5.4	0.148	417.1	12.8719	2.35	0.51760	2.35	2670.3	2689.0	2656.2	9.4	1.012
d (4)	3.1	0.044	1246.0	12.6607	0.64	0.50711	0.60	2654.7	2644.3	2662.7	4.3	0.993
JR-06	28.145580° S, 30.954920° E											
a (5)	6.2	0.151	362.0	12.5255	1.53	0.50413	1.49	2644.6	2631.5	2654.7	7.7	0.991
b (3)	5.9	0.102	584.8	12.7364	1.52	0.51051	1.51	2660.4	2658.8	2661.5	6.8	0.999
BCD5-04	26.646720° S, 30.521970° E											
a (2)	5.3	0.186	270.8	12.8879	1.23	0.51883	1.22	2671.5	2694.2	2664.3	5.3	1.015
b (3)	7.4	0.196	253.7	12.5149	1.11	0.50136	1.10	2643.8	2619.6	2662.4	5.0	0.984
c (3)	6.8	0.082	749.7	12.7736	1.29	0.51108	1.29	2663.1	2661.2	2664.5	6.8	0.999
d (5)	5.1	0.189	285.3	12.6248	1.86	0.50506	1.84	2652.1	2635.5	2664.7	8.6	0.989
JR-07	28.123850° S, 30.841676° E											
a (4)	7.4	0.061	992.3	12.8777	0.93	0.51504	0.92	2670.7	2678.1	2665.2	4.3	1.005
b (3)	n.m.[d]	0.281	198.8	12.7852	1.77	0.51244	1.76	2664.0	2667.0	2661.6	7.8	1.002

[a]Pbc = common Pb; Pbtot = total Pb (radiogenic + blank + initial).
[b]measured ratio, corrected for fractionation and spike.
[c]isotopic ratios corrected for fractionation (0.1% per amu for Pb), spike contribution, blank (1 pg Pb and 0.1 pg U), and initial common Pb. Initial common Pb corrected with isotopic compositions from the model of Stacey & Kramers (1975) at the age of the sample.
[d]not measured.

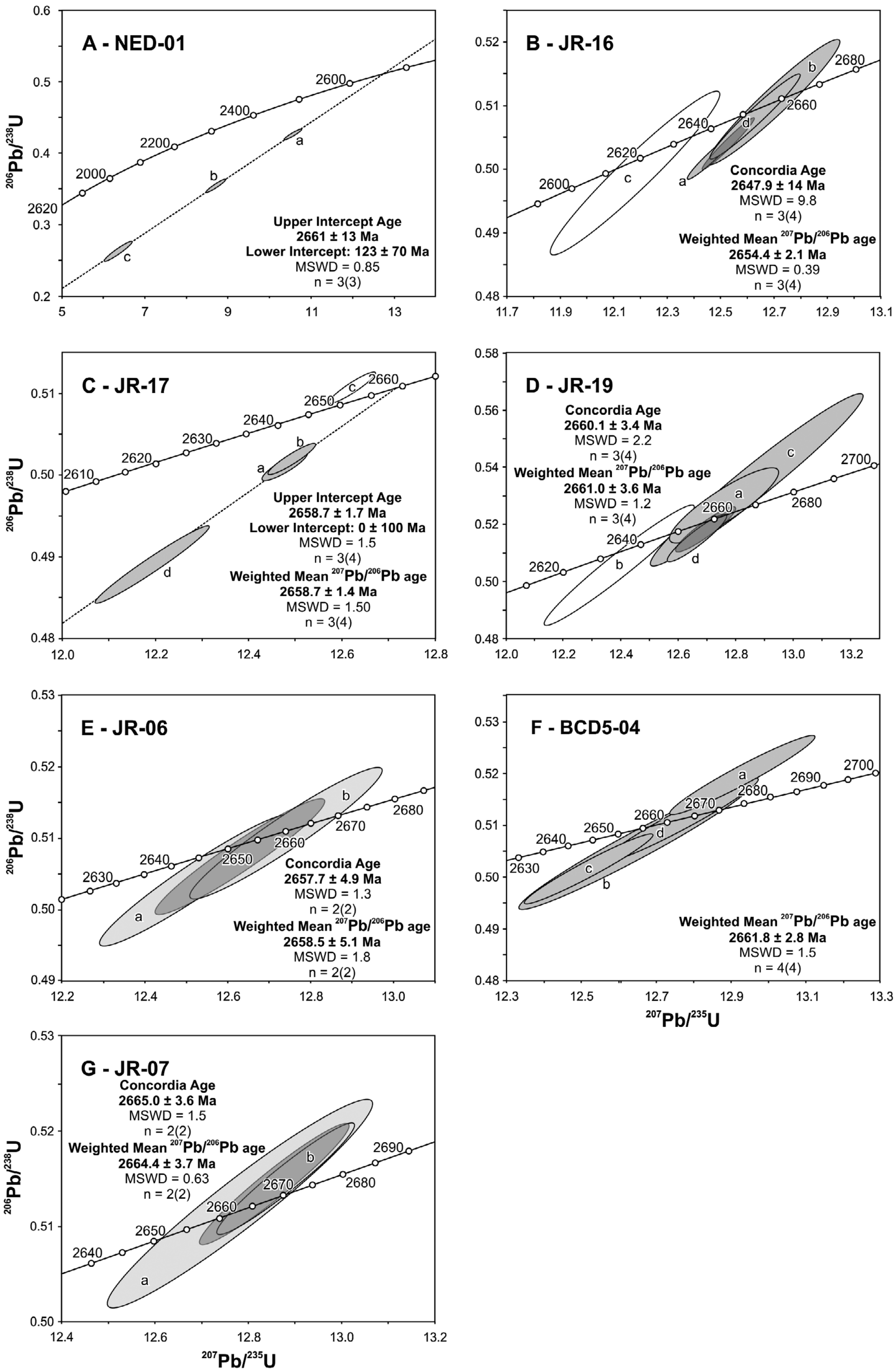

Fig. 3. Concordia diagrams for the seven dated NE-trending dolerite dykes from the WMDS. Error ellipses are reported at 2σ level. Shaded ellipses indicate fractions (e.g., a, b, etc.) used in age calculations, whereas unshaded ones were not. Darker shaded ellipses are error ellipses of concordia ages.

Table 2. Whole-rock major and trace element data for all dated 2.70–2.66 Ga dykes across the eastern Kaapvaal Craton.

Sample	JR-06	JR-07	JR-16	JR-17	JR-19	BCD5-04	NED-01	BCD5-17*	BCD5-18*	BCD5-19*	BCD5-22*	BCD5-23*	BCD1-09*	BCD5-27*
Major Elements (wt.%)														
SiO2	48.68	48.06	49.82	48.85	48.31	48.77	48.37	56.02	56.24	55.58	50.40	50.58	56.06	49.71
Al2O3	13.61	14.97	15.42	14.11	14.91	14.58	14.92	14.49	14.58	14.69	13.39	13.15	14.68	14.01
Fe2O3	14.74	12.93	11.46	13.41	13.28	12.73	13.11	9.21	9.19	9.56	16.59	16.63	9.09	15.20
MnO	0.22	0.20	0.18	0.20	0.19	0.19	0.19	0.12	0.13	0.13	0.21	0.20	0.13	0.19
MgO	5.93	6.46	7.06	6.63	6.67	7.23	6.95	4.81	4.67	4.82	4.71	4.28	4.84	5.25
CaO	9.77	10.69	10.01	10.42	9.42	10.43	9.52	8.26	7.27	8.05	8.93	8.22	7.82	9.22
Na2O	2.10	2.13	2.21	2.34	2.74	2.26	2.29	3.37	3.58	3.48	2.63	2.65	3.49	2.47
K2O	0.35	0.42	0.59	0.20	0.61	0.41	0.65	1.25	1.51	1.08	1.05	1.48	1.33	0.99
TiO2	1.49	1.16	1.00	1.26	1.31	1.14	1.27	0.75	0.82	0.79	1.91	2.32	0.79	1.65
P2O5	0.16	0.13	0.10	0.14	0.12	0.11	0.13	0.12	0.16	0.16	0.26	0.44	0.16	0.23
Cr2O3	0.02	0.03	0.03	0.03	0.03	0.04	0.04	0.01	0.02	0.02	0.01	0.01	0.03	0.02
L.O.I.	1.50	1.69	1.80	1.61	2.20	1.90	2.30	1.30	1.60	1.40	−0.40	−0.30	1.30	0.80
TOTAL	98.57	98.87	99.74	99.20	99.76	99.78	99.74	99.78	99.75	99.77	99.70	99.70	99.76	99.71
Trace Elements (ppm)														
Sc	40.64	35.53	36.00	39.81	33	35		22	21	23	39	34	21	35
V	312.98	258.30	234.00	284.83	246	231	303	165	170	160	324	276	155	293
Co	73.57	80.20	77.60	61.15	61.2	48.8		38.4	38.9	39.8	53.6	51.9	40.5	55.0
Ni	88.11	120.91	49.00	110.85	69.5	64.8		47.2	64.5	44.4	17.8	32.9	59.7	27.3
Cu	88.83	78.20	67.60	90.73	65.9	69.3		78.3	90.8	88.2	211.0	102.7	82.9	169.5
Zn	121.67	81.99	40.00	92.54	60	57		39	41	38	34	36	23	39
Rb	28.76	32.60	30.00	9.32	29.4	10.7	87.0	41.6	47.1	31.8	38.9	62.9	49.0	38.5
Sr	157.20	161.64	145.00	143.97	175.0	148.9	174.2	335.9	429.1	344.1	183.7	176.6	374.5	186.0
Y	29.64	22.75	19.20	24.59	23.6	22.6		15.6	19.0	17.3	40.3	51.5	20.6	35.0
Zr	89.93	68.68	57.60	73.52	77.3	71.1	78.1	110.7	133.2	123.7	197.8	285.9	131.9	167.0
Nb	3.91	3.05	2.20	3.25	2.9	2.9	3.5	4.0	4.2	3.8	10.6	16.6	4.2	8.8
Ba	66.37	46.89	99.00	36.89	106	80	119	371	500	360	238	343	375	202
La	5.86	4.34	3.70	4.76	6.6	5.6	5.2	17.5	20.5	19.4	21.3	32.7	20.0	18.2
Ce	15.15	11.35	9.50	12.26	14.6	13.4	13.1	35.0	40.1	38.2	48.0	74.3	39.8	40.8
Pr	2.26	1.75	1.48	1.89	2.13	2.06	2.02	4.25	4.86	4.76	6.21	9.17	4.68	5.28
Nd	11.99	8.81	7.60	9.39	10.9	10.1	9.8	16.1	21.4	19.7	27.7	39.1	18.1	23.5
Sm	3.58	2.79	2.03	2.75	2.70	2.80	2.93	3.06	3.81	3.68	5.89	7.83	3.84	5.13

Eu	1.29	1.05	0.90	1.10	1.08	1.10	1.13	1.04	1.29	1.14	1.75	2.15	1.23	1.57
Gd	4.48	3.48	2.90	3.78	3.90	3.66	3.66	3.40	3.94	3.53	6.53	8.43	4.00	5.71
Tb	0.74	0.61	0.52	0.63	0.66	0.65	0.67	0.55	0.57	0.59	1.17	1.48	0.62	1.02
Dy	5.31	4.26	3.47	4.45	3.80	4.05	4.22	2.90	3.33	3.35	6.95	8.65	3.20	5.94
Ho	1.13	0.86	0.81	0.95	0.86	0.96	0.96	0.57	0.71	0.68	1.46	1.83	0.63	1.26
Er	3.32	2.63	2.31	2.83	2.70	2.82	2.74	1.72	2.11	2.01	4.43	5.32	1.99	3.70
Tm	0.51	0.37	0.33	0.40	0.38	0.37	0.41	0.23	0.29	0.28	0.66	0.81	0.29	0.56
Yb	3.37	2.51	2.28	2.86	2.79	2.62	2.51	1.56	1.82	1.76	4.16	5.09	1.73	3.54
Lu	0.50	0.41	0.31	0.41	0.43	0.40	0.40	0.24	0.26	0.23	0.63	0.78	0.28	0.54
Hf	2.57	2.03	1.60	2.05	2.3	2.0	2.1	3.4	3.6	3.1	4.9	7.6	3.3	4.6
Ta	0.26	0.18	0.20	0.20	0.2	0.2	0.2	0.3	0.3	0.2	0.7	1.1	0.3	0.5
Pb	3.25	1.82	1.40	1.90	0.7	0.5	41.3	4.2	3.1	3.2	1.3	2.3	2.0	1.6
Th	0.45	0.30	0.20	0.32	0.6	0.5	0.3	2.5	2.4	2.5	2.9	4.2	2.0	2.6
U	0.12	0.09	0.10	0.10	0.1	0.1	0.1	0.7	0.5	0.5	0.8	1.2	0.5	0.6
Mo	0.90	0.63	0.20	0.72	0.2	0.2		0.5	0.4	0.4	0.8	1.2	0.5	0.7
Cs	1.09	1.79	2.40	0.67	1.4	1.2	1.1	1.0	0.7	0.5	1.4	3.0	2.0	2.2

*Dated in Olsson et al. (2010, 2011)

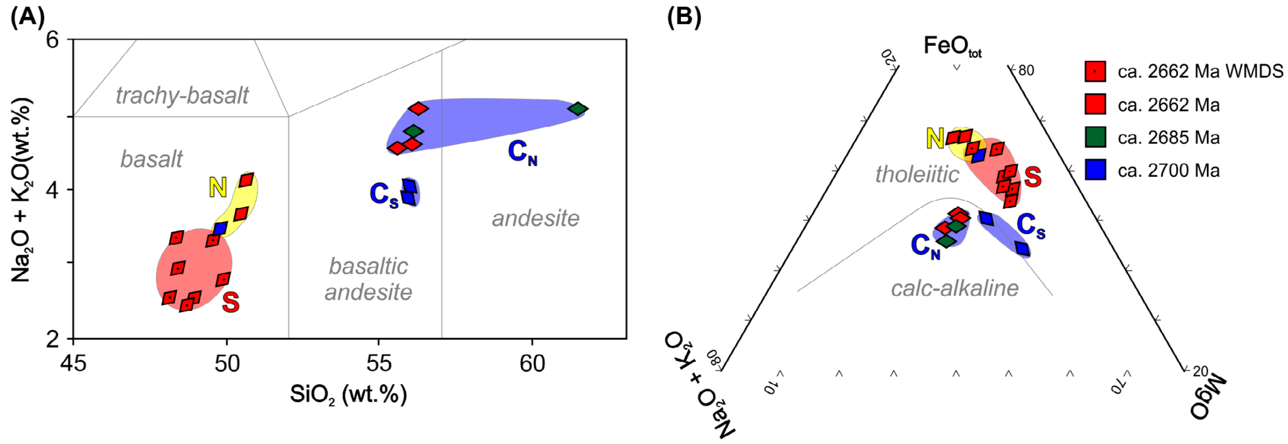

Fig. 4. **A**. TAS diagram by Le Bas et al. (1992), and **B**. An AFM diagram by Irvine & Baragar (1971) showing compositions for 17 dated ca. 2.70–2.66 Ga dykes that are either presented or reinvestigated geochemically in this study. Diamond symbols are orientated according to their general trends as either NE-, E- or SE-trending, as well as colour coded according to the relative age group they belong to, as indicated in the legend. Colour-coded background fields are used to indicate dykes that were sampled within one of three different areas of the eastern Kaapvaal Craton, as explained in the text. These are identified as: yellow ***N*** = northern, blue ***C_N/C_S*** = north/south central and red ***S*** = southern area, respectively of the eastern Kaapvaal Craton.

determine the volatile content. The XRF analysis was done for major and minor elements on glass beads, which was prepared from the whole-rock powder. The sample-to-flux ratio was 1:10, and the precision was better than ±1% of reported values. For the ICP-MS analysis, samples were dissolved in a 1.5-g lithium meta/tetraborate flux fusion. The resultant molten bead was digested in diluted nitric acid solution.

Three additional samples (JR-06, JR-07 and JR-17) were processed and analysed for both major and trace elements at the Central Analytical Facility at Stellenbosch University, South Africa. Any weathered, altered surfaces or veins were cut away by a rock saw, before cutting a representative sample size (typically 2–5 kg, depending on the groundmass grain size) into blocks that were cleaned before being put through a steel jaw crusher. The crushed material was then split down to a size that could be milled to powder in a tungsten–carbide swing mill. A weighed fraction of this powder was fused into La-free glass beads, which were analysed for major elements by XRF, using a Phillips PW1404w instrument with 2.4 kW Rh X-ray tube and controlled by a range of international NIST© standards. Trace elements were analysed from similar ultrapure fused beads using an Agilent 7500ce ICP-MS coupled with a Nd-YAG233 nm New Wave Laser Ablation system. It operated at a 12 Hz frequency, using a mixed He–Ar carrier gas. Each sample was analysed with three spots (30 s blank, followed by 60 s data collection each), and an average was calculated. Standards were run after every third sample.

6.2. *Results*

XRF major and ICP-MS trace element data are listed in Table 2. The geochemical presentation of data from the dated NE-trending dykes of the WMDS in this study also includes additional geochemical data on dated dykes from the coeval 2.70–2.66 Ga dyke swarms from further north in Olsson et al. (2010, 2011), which are not already published in Klausen et al. (2010).

The TAS (Total Alkali vs. Silica) classification diagram of Le Bas et al. (1992) in Fig. 4(A) shows that all the studied dykes are subalkaline. NE-trending dykes from both the northern and southern part of the exposed eastern margin of the Kaapvaal Craton are gabbroic (basaltic) whereas dykes with trends other than NE are more dioritic (basaltic to andesitic, respectively, Fig. 4(A)). This is consistent with results from Klausen et al. (2010), who also noted that NE-trending dykes tend to be more tholeiitic than dykes with other trends that tend to exhibit more calc-alkaline affinities in the Irvine & Baragar (1971) AFM diagram (Fig. 4(B)).

The new results show good consistency with the distinction recognised by Klausen et al. (2010) between NE-trending tholeiitic and E- to SE-trending calc-alkaline dykes, and this distinction is best illustrated using Sr/V, irrespective of degree of differentiation expressed by MgO (Fig. 5(A)). The results from a similar statistical correspondence analysis to that applied in Klausen et al. (2010) show how far apart Sr and V plot from each other in Fig. 5(B), highlighting these particular elements be combined in more discriminatory ratios. As explained in more detail in Appendix A, samples plotting closer to certain elements in these types of statistical diagrams also have relatively higher concentrations of these elements. Fig. 5(C–E) indicates that, statistically, NE-trending tholeiitic gabbroic dykes also are less light rare earth element (LREE)-enriched, and contain less large-ion lithophile elements (LILE), compared to the different trending calc-alkaline and more dioritic dykes. However, the three NE-trending gabbroic dykes from the northern area of the eastern Kaapvaal Craton also have higher concentrations of high field strength elements (HFSE), including in particular Nb–Ta, than NE-trending gabbroic dykes from the southern area (enriched in transitional metals, e.g., V). As a better multi-variable discriminator, Fig. 5(B) identifies compositionally distinct dykes from each of the three different craton areas, illustrated consistently throughout this paper using colour coding for dykes hosted within either a northern (yellow), central (blue) or southern (red) area of the eastern Kaapvaal Craton.

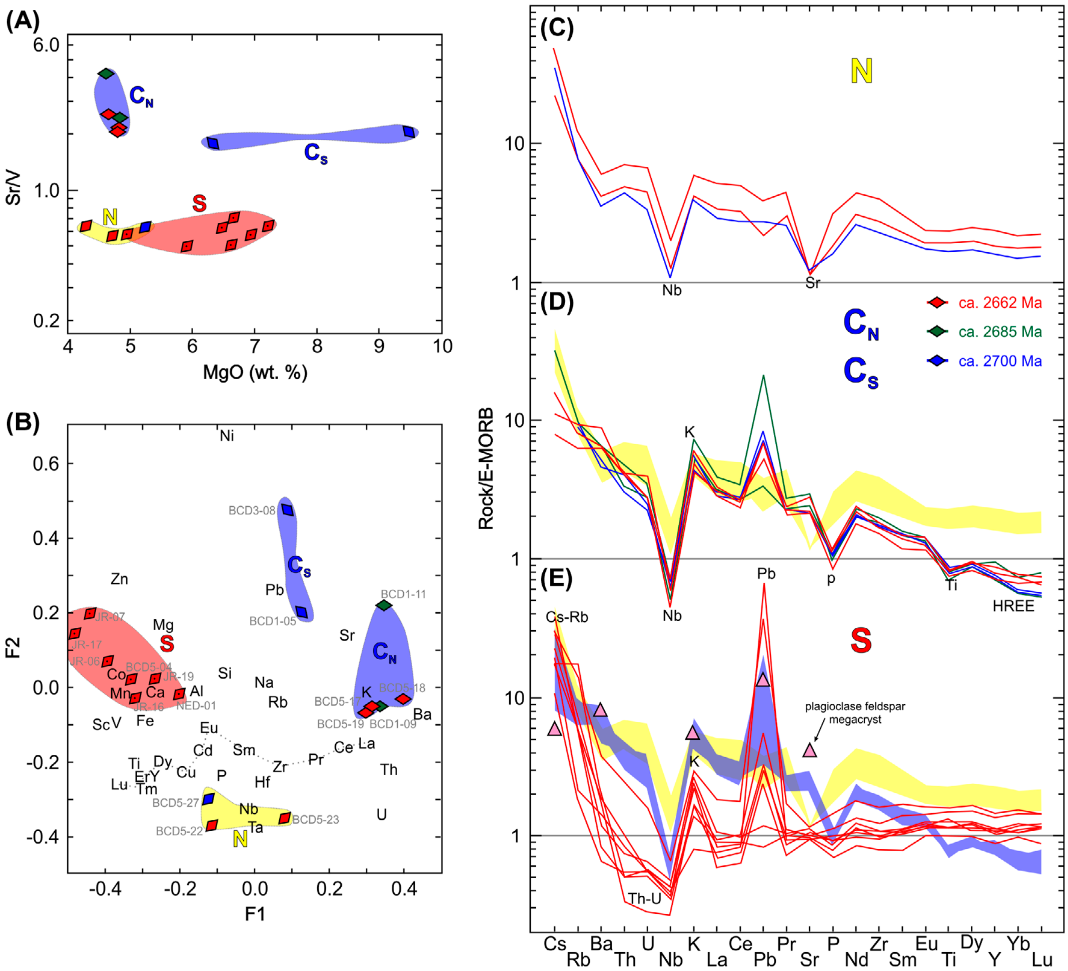

Fig. 5. **A**. Sr/V against MgO, **B**. Correspondent analysis results, which show 52% of all variations along F1 and 29% of all variations along F2 (see Appendix A for more details regarding this statistical method). **C–E**. E-MORB normalised incompatible element plots (Sun & McDonough 1989) for ca. 2.70–2.66 Ga dykes across the eastern Kaapvaal Craton, grouped according to the three areas identified in Fig. 4 and shown in Fig. 8. Colour-coded background fields in D–E show the range of previous patterns for comparison. An additional analysis of an extracted plagioclase megacryst is also added to **E**. Other symbols and colour coding are as in Fig. 4.

The three sample groups are also plotted in a more traditional E-MORB normalised multi-elemental diagram from Sun & McDonough (1989) in Fig. 5(C–E). With the exception of some distinct negative anomalies, most HFSE concentrations are similar to, or more enriched than E-MORB. As indicated by the correspondence analysis, Fig. 5(C–E) also shows how much more LREE-enriched (relative to HREE), E- and SE-trending dykes from the central area (Fig. 5(D)) are, compared to NE-trending dykes from both the northern (Fig. 5(C)) and southern (Fig. 5(E)) margins of the Kaapvaal Craton. NE-trending dykes from the northern area have more enriched (negative sloping) HFSE patterns compared to NE-trending dykes from the southern area, which have a more depleted (positive sloping) pattern with particularly low Th and U concentrations relative to E-MORB. In both cases, their overall HFSE patterns are less erratic than those from the intervening central area (e.g., negative P and Ti), and both have similar negative Nb anomalies and positive Cs and Rb. However, the NE-trending dykes from the northern area have distinctly negative Sr anomalies, whereas the NE-trending dykes from the southern area also are particularly more enriched in Cs, K and Pb, compared to HFSE.

Fig. 6(A) (after Pearce 2008) shows how much more LREE-enriched relative to chondrite the high-$(La/Sm)_N$ dykes from the east-central Kaapvaal Craton area are, compared to the NE-trending dykes from both ends of the eastern Kaapvaal Craton. These dykes from the central area also have higher $(Dy/Yb)_N$ and can therefore be viewed as more HREE-depleted. SE-trending dykes from the south-central area have even higher $(Dy/Yb)_N$ and are therefore even more HREE-depleted. In contrast to the E–W- and SE-trending dykes from the central area, all NE-trending dykes have lower $(La/Sm)_N$ and $(Dy/Yb)_N$ values in comparison. All of the NE-trending dykes possess relatively similar flat HREE patterns, characterising all NE-trending dykes from the southern craton area, exhibiting approximately chondritic LREE ratios, whereas our most northerly located NE-trending dykes are moderately LREE-enriched. Another Pearce (2008) diagram in Fig. 6(B) shows how well dyke compositions from the three major eastern Kaapvaal Craton areas differ from each other, with (1) E–W and SE-trending dykes of all

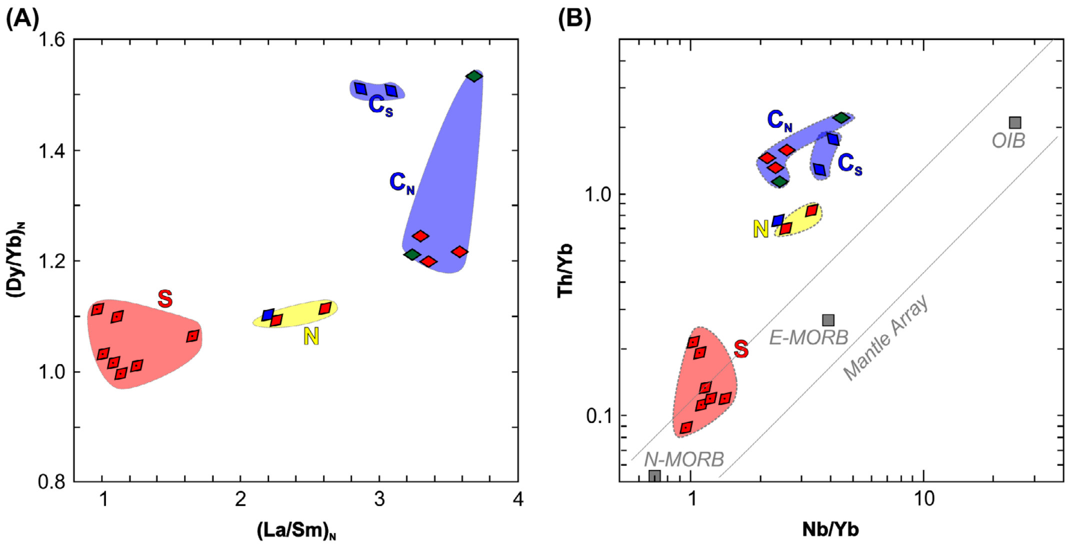

Fig. 6. **A**. Chondrite-normalised $(Dy/Yb)_N$ against $(La/Sm)_N$, and **B**. Th/Yb against Nb/Yb for ca. 2.70–2.66 Ga dykes across the eastern Kaapvaal Craton. The Mantle Array and modelled variable influence of a so-called subduction zone component in **B** is copied from Pearce (2008). Symbols and colour coding as in Fig. 4.

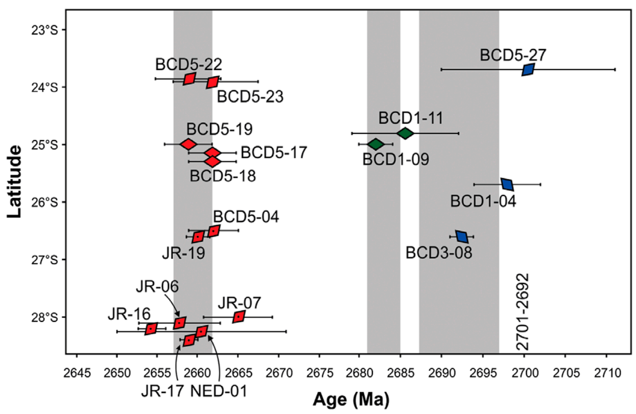

Fig. 7. Ages of the dated dolerite versus sample latitude and dyke trend to illustrate the mafic magmatic events on the eastern Kaapvaal Craton. Age data and spatial positions of samples are reported either in this study, or are taken from Olsson et al. (2010, 2011). Peaks in mafic magmatism (grey shading) denoted by weighted averages of the dated dykes at 2692 ± 5 Ma, 2683 ± 2 Ma and 2659 ± 2 Ma.

ages from the central craton area plotting at relatively high Th/Yb, well above the diagram's Mantle Array reference, (2) NE-trending dykes from the southern area clustering closer to the Mantle Array and (3) NE dykes from the northern craton area lying in between these two extremes.

7. Discussion

7.1. *Timing and distribution of the WMDS*

Very similar crystallisation ages were obtained for all dated dykes of the WMDS, consistent with a short duration of dyke emplacement. The three most robustly dated samples (JR-07, JR-19 and BCD5-04), have been chosen to represent a tentative mean age of the WMDS. A combined weighted mean of their emplacement ages has been calculated at 2662 ± 2 Ma (MSWD = 0.3), although the actual age range is from 2665 Ma to 2659 Ma. Fig. 7 summarises all U–Pb data presented in this study, and compares these data to age data published by Olsson et al. (2010, 2011). It shows that concordant data (JR-07, JR-19 and BCD5-04), yield slightly older ages (with weighted mean $^{207}Pb/^{206}Pb$ ages of 2662 ± 2 Ma), than most of the discordant data-sets (JR-06, JR-16, JR-17 and NED-01), which when combined yield a weighted mean age of 2659 ± 3 Ma. Considering emplacement ages constrained from weighted means of $^{207}Pb/^{206}Pb$ dates are minimum ages, one cannot rule out the possibility that the true ages of these sample could be a few million years older. If concordant data-sets represent the most robust emplacement ages, and the true ages of discordant sets are slightly older, then all dykes were emplaced within a shorter time interval than is given by the their mean ages. Therefore, the current U–Pb data does not preclude dykes of the WMDS being emplaced within a time interval of just a couple of million years, or even less.

As shown in Fig. 7, the three E–W-trending dykes (BCD5-17, BCD5-18 and BCD5-19) of Olsson et al. (2010, 2011) from the central area of the eastern Kaapvaal Craton are coeval to the WMDS. Moreover, two NE-trending dykes (BCD5-22 and BCD5-23) from the northern area, are also contemporaneous with the WMDS, indicating that this magmatic event might arguably have constituted a ~400-km wide swarm of coeval dykes with a combined weighted mean age of 2659 ± 2 Ma (Fig. 8).

7.2. *Magmatic episodes, coeval volcanic rocks and sub-swarm patterns*

Broadly coeval U–Pb baddeleyite ages of Neoarchaean dykes along the eastern portion of the Kaapvaal Craton have now been recognised inside the studied NE-trending WMDS, as

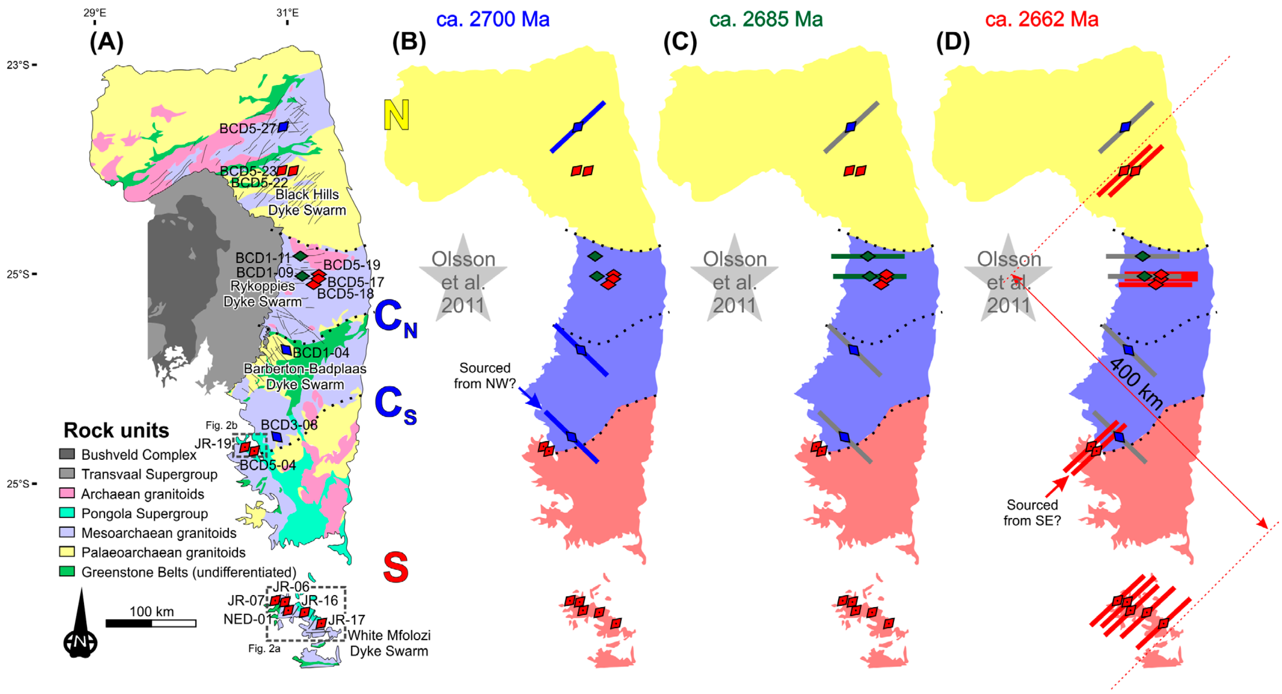

Fig. 8. Dyke sample localities and trends across the exposed eastern part of the Kaapvaal Craton. **A**. Sample localities indicated by orientated diamonds that are colour coded according to their age group, as determined in Fig. 7. **B–D**. Three outlines of the exposed eastern Kaapvaal Craton basement, subdivided into three colour-coded areas that roughly correspond to cratonic subdivisions. For each outline **B–D**, spatial and temporal distribution of the dated dykes is shown for each of the three age groups.

well as amongst all three branches of the Olsson et al. (2011) radiating dyke swarm. Collectively, these ages span a 40-Myr interval, but also cluster into three age groups that can reflect separate magmatic pulses at 2701–2692, 2686–2683 and 2674–2662 Ma (Figs. 7 and 8). This periodicity is visually illustrated by plotting ages with error bars against sample latitudes and dyke trends (Fig. 7). These dyking events may be correlated to volcanic units within the Kaapvaal Craton's stratigraphy (cover successions).

7.2.1. 2701–2692 Ma.

The oldest episode of magmatism recorded by our dated dyke episode (plotted as blue symbols in Fig. 7, and as blue dyke trends in Fig. 8) includes the absolute oldest NE-trending dyke (BCD5-27) in the northern Kaapvaal Craton area (yellow in Fig. 8), and two SE-trending dykes (BCD3-08 and BCD1-04), within the central Kaapvaal Craton area (blue in Fig. 8). A tentative minimum age of ca. 2673 Ma for BCD1-04 was earlier constrained from the least discordant baddeleyite fraction analysed by Olsson et al. (2010). The age of this dyke was subsequently refined to 2698 ± 4 Ma (Olsson et al. 2011), testifying that it belongs to the oldest magmatic episode.

NE-trending dykes cut across much of the Kaapvaal Craton, but those that are hosted within the Witwatersrand Supergroup have on the basis of field relationships and geochemical compositions (e.g., McCarthy et al. 1990, Meier et al. 2009) been correlated to the volcanic rocks of the Klipriviersberg Group (Ventersdorp Supergroup). The Klipriviersberg Group was deposited in a parallel series of NE-trending half-graben structures (Stanistreet & McCarthy 1991). This led Uken & Watkeys (1997) to tentatively attribute most NE-trending dykes as far north-east as the Limpopo Province in South Africa to the Ventersdorp Supergroup magmatism. From their correlation scheme, McCarthy et al. (1990) noted a change from NE-trending dykes feeding lower Ventersdorp Supergroup volcanic rocks to WNW–ESE-trending dykes feeding the volcanic rocks of the upper Ventersdorp Supergroup. It is possible for the oldest 2701 ± 11 Ma NE-trending dyke of the radiating swarm to have been emplaced during Klipriviersberg volcanic eruptions, if the Armstrong et al. (1991) age of 2714 ± 8 Ma for these volcanic rocks is deemed correct. It is impossible, however, to correlate this NE-trending dyke to the Klipriviersberg volcanic rocks if the Wingate (1998) and de Kock et al. (2012) ages of 2783 ± 5 Ma and 2735–2724 Ma for the Derdepoort and Hartswater volcanic rocks (in different half-grabens to the main Ventersdorp Basin, see Fig. 1 and Table 3), respectively, correlate with the Klipriviersberg and Platberg (overlying the Klipriviersberg Group) groups in the main Ventersdorp half-graben. If so, the oldest group of dykes dated can only be correlated to volcanic rocks in either the Rietgat or Allanridge formations in the upper Ventersdorp Supergroup. However, their orientations remain enigmatic unless they are part of an incompletely dated radiating swarm. As argued for other overlapping swarms (e.g., Jourdan et al. 2006), it is also possible that NE-trending dykes followed an old Klipriviersberg rift-trend.

Table 3. Stratigraphy with ages of the various half-grabens composed of Ventersdorp Supergroup and equivalent rocks (modified after de Kock et al. 2012).

Ventersdorp Supergroup	Taung	Derdepoort	Botswana
Pniel 'Sequence'			
Allanridge Fm.	*Allanridge Fm.*		
Amygdoidal andesitic lava	Amygdoidal andesitic lava		
Bothaville Fm.	*Bothaville Fm.*		
Quartzite, conglomerate and shale	Quartzite, conglomerate and shale		
Platberg Group	*Hartswater Group*		
Rietgat Fm.	*Phokwane Fm. (2724 Ma)*		
Porphyritic lava, quartzite, tuffs and limestone	Shale, andesitic lava and limestone		
Makwassie Fm. (2708 Ma)	Quartz porphyry		
Quartz porphyry	*Mohle Fm. (2734 Ma)*		
Kameeldoorns Fm.	Conglomerate, quartzite and tuff		
Breccia, conglomerate, quartzite and tuff			
Klipriviersberg Group (2714 Ma)		*Derdepoort (2769–2781 Ma)*	*Lobatse Group*
Basal conglomerate and quartzite		Basaltic to rhyolitic lava	*Nnyane Fm.*
Komatiitic lava and basaltic lava		Conglomerate, quartzite and shale	Tuff and quartz porphyry
			Kanye Fm. (2781 Ma)
			Rhyolitic lava

7.2.2. 2686–2683 Ma.

The U–Pb data of Olsson et al. (2010) for two E–W-trending dykes (BCD1-09 and BCD1-11) plot as green symbols in Fig. 7, as well as green trend lines in Fig. 8(C).

This intermediate-aged dyke record is likely related to volcanism which must at least have been younger than the Klipriviersberg Group. Olsson et al. (2010) proposed a possible correlation between the Rykoppies Dyke Swarm and the volcanic rocks of the undated Allanridge Formation (upper Ventersdorp Supergroup – see Table 3), which is supported by geochemical matching of the volcanic rocks and dykes (Klausen et al. 2010). These Rykoppies dykes could be the second in a succession of sub-swarms, simply controlled by an equally variable paleo-stress field over a period of 15 million years. It is also possible that these different trending dolerite dyke swarms represent branches within an incompletely dated radiating swarm.

7.2.3. 2665–2659 Ma.

The seven dated dykes from the WMDS, and coeval dykes from both the E–W-trending Rykoppies Dyke Swarm (BCD5-17 and BCD-18 from Olsson et al. 2010 and BCD5-19 from Olsson et al. 2011), as well as two NE-trending dykes across the eastern Kaapvaal Craton's northern area (BCD5-22 and BCD5-23), are plotted as red symbols in Fig. 7, and as red trend lines in Fig. 8(D). They represent the youngest and the spatially most extensive episode of dyke emplacement.

Lower intercepts for all dykes within the WMDS consistently record disturbances of the 1.88–1.83 Ga, 1.11 Ga and 0.18 Ga Soutpansberg, Umkondo and Karoo LIPs, which appear to have pervasively affected the eastern Kaapvaal Craton's southernmost area. The reported 2674 ± 11 Ma age of the NE-trending BCD5-23 dyke is constrained from a regression through only two fractions. We have chosen to use only the least discordant fraction (fraction 'a' in Olsson et al. 2011), with a $^{207}Pb/^{206}Pb$-age of 2662 ± 5 Ma, as a reliable minimum emplacement age for this sample. An unconstrained regression line through all ellipses in the WMDS intersects the concordia at 2662 ± 2 Ma. The youngest record of dyke injections across the exposed eastern Kaapvaal Craton, including the ca. 2662 Ma WMDS, is best correlated to volcanic rocks within the proto-basinal fill at the base of Transvaal Supergroup, which are dated at ca. 2664 Ma (U–Pb zircon, Barton et al. 1995). The two coeval E–W-trending dykes parallel earlier E–W lineaments in the precursors to the Transvaal Basin. Most dykes within this age period however appear to have made a return to the initial, older 'Klipriviersberg' rift-trend. Plagioclase-megacrystic NE-trending dykes appear to be concentrated farther to the south-east, however, and thereby appear to define a distinct sub-swarm. It is also possible for the two coeval E–W-trending dykes to locally have followed the pre-existing Rykoppies Dyke Swarm trend, and thereby be members of a more extensive, and predominantly NE-trending WMDS. The WMDS may then be up to 400-km wide, when including the two northerly located young NE-trending dykes (BCD5-22 and BCD5-23, Fig. 8(D)).

7.3. Petrogenesis and subsequent differentiation and assimilation

Different geochemical subgroups have been shown to correlate more with which part of the exposed Kaapvaal Craton the samples were collected from, as shown in Figs. 4–8, than the dyke's trend or relative age. This is consistent with either the initial petrogenesis and/or subsequent differentiation/assimilation giving rise to: (1) uniquely different coeval magmas being emplaced within different parts of the Kaapvaal Craton; and (2) compositionally similar magmas having been injected up to 40 Myr apart into the same part of the Kaapvaal Craton. From each perspective, this appears to argue for a remarkably local lithospheric control on geochemical signatures.

7.3.1. Northern part of eastern Kaapvaal Craton.

For the northern area of the eastern Kaapvaal Craton, three NE-trending dykes were emplaced both during the oldest and youngest magmatic period amongst all 2.70–2.66 Ga dykes (Fig. 8(B, D)), and yet all exhibit uniquely similar incompatible element patterns (Fig. 5(C)). These sub-parallel patterns have different elevations relating to different degrees of differentiation, which appear to have affected these northerly located magmas more than NE-trending dykes from the southern part of the craton (i.e., lower MgO and Mg# discussed in Section 7.3.3). This is supported by the increasingly more negative Sr anomalies in Fig. 5(C) which could reflect a more advanced differentiation stage including plagioclase fractionation. As evidenced by how close these data plot to Nb and Ta in Fig. 5(B), it is also clear that the incompatible element patterns of these three northerly located NE-trending dykes exhibit less negative Nb anomalies, compared to younger dykes, and correspondingly lower LILE/HFSE. Even if these characteristics are still indicative of some subduction zone component – which is unlikely to have been derived from any nearby active margin at that time – it is inherently difficult to decide whether this lithospheric component stems from either a subcontinental lithospheric mantle (SCLM) source and/or local assimilation of its overlying Archaean crust. From their more differentiated status (i.e., low MgO/Mg#), and relative positions within a mixing array between more tonalite–trondhjemite–granodiorite-assimilated dykes from the central craton area, and the 'primordial' part of the mantle array in Fig. 6(B), however, primary melts could have been derived from a moderately enriched (or ambient) mantle peridotite. From their relatively low $(Dy/Yb)_N$ in Fig. 6(A), this must have been a spinel-bearing mantle that could only have been asthenospheric if it had been able to rise above the <60-km stability depth for garnet below the thick Kaapvaal Craton lithosphere.

7.3.2. Central part of the eastern Kaapvaal Craton.

For the central area of the eastern Kaapvaal Craton, five E–W-trending and two SE-trending dykes are representatives of all three periods of dyking, yet exhibit even more closely matching incompatible element patterns (Fig. 5(D)), that are distinctly different from all other dykes in this study. Their distinctly lower HREE patterns could be attributed to a deeper garnet-bearing mantle source. However, the commonly observed inclusion of basement xenoliths and phenocrysts in most of these dykes (Klausen et al. 2010), as well as their more andesitic and calc-alkaline compositions (Fig. 4) and significant LILE/HFSE- and LREE-enrichments (Fig. 5(D)), attests to assimilation of a correspondingly large amounts of tonalite–trondhjemite–granodiorite material. It is beyond the scope of this paper on relatively few dyke samples to quantitatively model such assimilation, but the common field observation of partly digested crustal xenoliths and xenocrysts in these particular dykes (parts of which invariably were incorporated in the analysed material), and their andesitic composition attest to substantial proportions of assimilated crust). Even if it seems likely for all dykes from the central area to have been contaminated by tonalite–trondhjemite–granodiorite, it is still puzzling how such an unpredictable diversification process could have produced such similar patterns for dykes that were emplaced during all three episodes of the entire 2701–2662 Ma event. However, the relative position of samples along mixing curves (e.g., Fig. 6(B)), can be used to argue that primary magmas for the dykes injected into the central craton area were initially derived from a, moderately enriched or ambient, primordial mantle that was relatively similar to the source(s) from the other dyke groups.

7.3.3. Southern part of the eastern Kaapvaal Craton.

In the southern craton area (Figs. 1, 2 and 8), the seven dated NE-trending dykes from the WMDS, all exhibit uniquely similar incompatible element patterns (Fig. 5(E)), which are distinctly more HFSE-depleted than any of the other dykes in the other two craton areas. The lack of any significant LREE-enrichment and corresponding HREE-depletion argues against the kind of tonalite–trondhjemite–granodiorire-assimilation that appear to have affected dykes in the central craton area, which is also supported by a general absence of granitic xenoliths in the WMDS.

Nevertheless, some very marked positive LILE anomalies, accentuated against relatively low HFSE (Fig. 5(E)), require a selective addition of Cs, Rb, K and Pb. Rather than attributing these anomalies to some lithospheric overprint, similar to the crustal assimilation suggested for the central part of the craton (Section 7.3.2), more selective LILE enrichment could have been caused by pervasive metasomatism during regional greenschist metamorphism that appears to have affected the southern part of the southern area more than the north (Elworthy et al. 2000). As an example, the two NE-trending dykes located within the least metamorphosed northern part of the southern craton area (JR-19 and BCD5-04), do not exhibit any Pb anomalies, albeit still possessing high Cs, Rb and Ba (Fig. 5(E)). The fact that these anomalies persist even for those samples from which plagioclase megacrysts were carefully removed suggests that these are not the culprits. In addition, one plagioclase feldspar megacryst that was milled and analysed just like the bulk rock samples, exhibits many of the same selective enrichments in Cs, Rb, Ba, K, Pb, Sr and Eu against minute concentrations in all other incompatible elements shown in Fig. 5(E). If the LILE-enrichments in Fig. 5(E) can be attributed to secondary alteration, then the depleted patterns exhibited by the more robust HFSEs are consistent with primary magmas derived from an equally depleted spinel-bearing mantle source. This is consistent with the data overlap of the depleted end of the Mantle Array in Fig. 6(B), even if we cannot rule out that these selectively LILE-enriched magmas were either crustally contaminated or derived from a metasomatically enriched SCLM.

The depleted mantle source could have been asthenospheric if the WMDS was emplaced within a significant SW–NE-trending rift zone across the south-eastern margin of the present day Kaapvaal Craton. The depleted nature of the plagioclase-megacrystic WMDS contrasts with the other four coeval dykes emplaced across both the central and northern areas of the eastern Kaapvaal Craton (Fig. 8(D)), which could both host dykes derived from a more enriched SCLM. Magmas from the central area could have also become excessively contaminated by poorly digested tonalite–trondhjemite–granodiorite crust. Thus, there appears to be a clear geochemical distinction between Olsson et al.'s (2011) 'radiating' swarm to the north-eastern Kaapvaal Craton, and the newly discovered WMDS that cuts obliquely across its south-eastern extent which cannot have been derived from the same mantle source. Indeed the less than 30-km separation between depleted signature dykes BCD5-04 and JR-19 to enriched BCD3-08 highlights such discrete geochemical differences, despite being within the same cratonic area.

7.4. Tectono-magmatic model implications

The proposed radiating swarm of Olsson et al. (2011) is not supported by all its 2.70–2.66 Ga dykes having been derived from a heterogeneous, yet common mantle source. A spinel-bearing and moderately enriched mantle is not, however, what one would expect from a 'Ventersdorp' mantle plume, which Olsson et al. (2011) proposed impacted on the Kaapvaal Craton where the eastern lobe of the 2.06 Ga Bushveld Complex is currently located. Especially not when compared to the signatures of Phanerozoic ocean hot spots like Hawaii, where tholeiitic basalts are typically derived from a more enriched and deeper garnet-bearing mantle source. The 2.70–2.66 Ga dykes within the proposed radiating swarm also appear to be slightly younger than current ages of the Klipriviersberg's basal basaltic komatiites and most of the subsequent large volumes of overlying continental flood basalts, which Eriksson et al. (2002) attributed to a hot mantle plume source. Furthermore, it is questionable whether a mantle plume-induced radiating dyke swarm can remain active in the same place for as long as ~40 Myr (or possibly >120 Myr if the Derdepoort–Hartswater volcanic rocks and associated intrusions are included). This is at least close to (or more than) the maximum 50-Myr time limit for LIPs (Ernst 2014 and references therein), and arguably fed volcanism that episodically erupted to form not only the bulk of the Ventersdorp Supergroup, but also the Allanridge Formation and proto-basinal volcanic rocks. Instead we propose that the radiating swarm of Olsson et al. (2011) is an artefact of a succession of magmatic rifting events, following on from an initial Ventersdorp mantle plume.

Our new U–Pb ages identify the NE-trending WMDS, which clearly crosses the SE-trending branch of the radiating swarm (Fig. 8), and was also derived from a distinctly different, depleted mantle source. It is tempting to include more northerly located dykes from Olsson et al. (2011)'s 'radiating' swarm that are broadly coeval with the WMDS, and thereby both (1) reduce the age span of the proposed radiating swarm to perhaps a more realistic 15 Myr, and (2) argue for a more coherent, predominantly NE-trending WMDS, where a pair of E–W-trending dykes may locally have deflected along the pre-existing Rykoppies Dyke Swarm trend. However, a more extensive WMDS still requires that its coeval dykes were derived from two different mantle sources, i.e., a more enriched northerly and more depleted southerly mantle source.

8. Conclusions

New high-precision baddeleyite U–Pb ages for seven dykes sampled from the south-easternmost window into the Kaapvaal Craton identify the prominent NE-trending WMDS, with characteristic plagioclase megacrysts, to have been emplaced within a relatively narrow time span at approximately 2662 Ma. The WMDS cuts the south-eastern branch of the broadly coeval radiating dyke swarm across the central and northern parts of the eastern Kaapvaal Craton (Olsson et al. 2011). A closer scrutiny of this ca. 2.70–2.66 Ga radiating dyke swarm and the WMDS reveals three magmatic periods:

(1) The oldest 2701–2692 Ma feeder dykes, represented by one NE-trending and two SE-trending dykes, correlate, within analytical uncertainties, to the early lower Ventersdorp Supergroup volcanic rocks, which Uken & Watkeys (1997) argued to have been emplaced mainly in a SW–NE-trending regional rift, terminating with the emplacement of SE-trending feeders.

(2) The intermediate 2686–2683 Ma feeder dykes, only shown by two E–W-trending dykes across the eastern Kaapvaal Craton's central area, are on the basis of both geochronology (Olsson et al. 2010) and geochemical matching (Klausen et al. 2010) thought to be coeval with later volcanic rocks of the upper Ventersdorp Supergroup. These dykes form the original Rykoppies Dyke Swarm of Olsson et al. (2010).

(3) The youngest 2665–2659 Ma feeder dykes include nine NE-trending and three E–W-trending dykes, some of which were included into the radiating dyke swarm by Olsson et al. (2010, 2011) but on the basis of coeval ages and dyke trends can also be combined into a more regionally extensive, and overall NE-trending WMDS, spanning across much of the exposed eastern Kaapvaal Craton. The ages of these dykes correlate to so-called proto-basinal volcanic rocks (Eriksson et al. 2006), marking the significant transition from the Ventersdorp Supergroup to the Transvaal Supergroup, as was stated in Olsson et al. (2010).

Geochemical signatures on all 17 dated basaltic–andesitic dykes do not correlate with either dyke ages or trends, but are remarkably unique signatures for dykes of different ages and/or orientations that reside within one of the following three cratonic areas, across the exposed eastern part of the Kaapvaal Craton:

(1) The northern area, which has both the oldest and two of the youngest NE-trending basaltic dykes, is characterised by relatively enriched HFSE-signatures, with weak

negative Nb anomalies and less LILE enrichments, consistent with derivation from a correspondingly moderately enriched (or ambient primordial) and spinel-bearing mantle peridotite source.

(2) The central area hosts two dykes of intermediate age, three younger E–W-trending andesitic dykes, and two SE-trending dykes, all with remarkably similar incompatible element patterns. These patterns can be explained by a parental magma much like the ones described above for the northern area, after having assimilating typical tonalite–trondhjemite–granodiorite crust. This is supported by the common observation of xenoliths and xenocrysts in the field from these dykes.

(3) The southern area, which hosts NE-trending and characteristically feldspar-megacrystic dykes belonging to the studied WMDS, exhibit much more depleted HFSE patterns that are selectively enriched in the most mobile Cs, Rb, K and Pb elements. Some of these LILE-enrichments correlate with a southward increase in metasomatic greenschist facies overprint, and are therefore likely to be secondary. Their otherwise depleted magmas cannot be related to any of the more enriched dykes across either the central or northern craton areas, and were probably generated from a correspondingly more depleted spinel-bearing and asthenospheric mantle peridotite source.

Collectively, the data presented question the radiating 2.70–2.66 Ga dyke swarm of Olsson et al. (2011) across the Kaapvaal Craton. It is possible for a more prolonged and geochemically enriched radiating system to have been terminated by a peripheral, yet cross-cutting dyke swarm derived from a more depleted mantle source.

Acknowledgements—The authors wish to thank the reviews and comments from two anonymous reviewers and the guest editor Wouter Bleeker for helping to improve this article. The authors also wish to acknowledge the support from the Swedish Research Council for a research grant to Ulf Söderlund. Lund University is thanked for master's project assistance to Johan Rådman. The Department of Geology at the University of Johannesburg and Michiel de Kock are thanked for supplying logistic support during field work both in Mpumalanga and KwaZulu-Natal. Ashley Gumsley acknowledges support from the Royal Physiographic Society in Lund for a travel grant.

References

Armstrong, R.A., Compston, W., Retief, E.A., Williams, I.S. & Welke, H.J., 1991: Zircon ion microprobe studies bearing on the age and evolution of the Witwatersrand triad. *Precambrian Research 53*, 243–266.

Barton, J.M., Blignaut, E., Salnikova, E.B. & Kotov, A.B., 1995: The stratigraphical position of the Buffelsfontein Group based on field relationships and chemical and geochronological data. *South African Journal of Geology 98*, 386–392.

Benzécri, J.-P., 1973. *[Data Analysis Volume II the corresponding Analysis]*. Dunod, Paris.

Bleeker, W., 2003: The late Archean record: a puzzle in ca. 35 pieces. *Lithos 71*, 99–134.

Cawthorn, R.G., Eales, H.V., Walraven, F., Uken, R. & Watkeys, M.K., 2006: The Bushveld Complex. *In* M.R. Johnson, C.R. Anhaeusser & R. Thomas (eds.): *The Geology of South Africa*, 261–281. Geological Society of South Africa/Council for Geoscience, Johannesburg/Pretoria.

Cornell, D.H., Schütte, S.S. & Eglington, B.L., 1996: The Ongeluk basaltic andesite formation in Griqualand West, South Africa: submarine alteration in a 2222 Ma proterozoic sea. *Precambrian Research 79*, 101–123.

de Kock, M.O., Beukes, N.J. & Armstrong, R.A., 2012: New SHRIMP U–Pb zircon ages from the Hartswater Group, South Africa: implications for correlations of the Neoarchean Ventersdorp Supergroup on the Kaapvaal craton and with the Fortescue Group on the Pilbara craton. *Precambrian Research 204–205*, 66–74.

de Kock, M.O., Ernst, R., Söderlund, U., Jourdan, F., Hofmann, A., Le Gall, B., Bertrand, H., Chisonga, B.C., Beukes, N.J., Rajesh, H.M., Moseki, L.M. & Fuchs, R., 2014: Dykes of the 1.11Ga Umkondo LIP, Southern Africa: Clues to a complex plumbing system. *Precambrian Research 249*, 129–143.

Denyszyn, S.W., Feinberg, J.M., Renne, P.R. & Scott, G.R., 2013: Revisiting the age and paleomagnetism of the Modipe Gabbro of South Africa. *Precambrian Research 238*, 176–185.

Eglington, B.M. & Armstrong, R.A., 2004: The Kaapvaal Craton and adjacent orogens, southern Africa: a geochronological database and overview of the geological development of the craton. *South African Journal of Geology 107*, 13–32.

Elworthy, T., Eglington, B.M., Armstrong, R.A. & Moyes, A.B., 2000: Rb-Sr isotope constraints on the timing of late to post-Archaean tectonometamorphism affecting the southeastern Kaapvaal Craton. *Journal of African Earth Sciences 30*, 641–650.

Eriksson, P.G., Altermann, W. & Hartzer, F.J., 2006: The Transvaal Supergroup and its precursors. *In* M.R. Johnson, C.R. Anhaeusser & R. Thomas (eds.): *The Geology of South Africa*, 237–260. Johannesburg / Pretoria, Geological Society of South Africa / Council for Geoscience.

Eriksson, P.G., Condie, K.C., van der Westhuizen, W., van der Merwe, R., de Bruiyn, H., Nelson, D.R., Altermann, W., Catuneanu, O., Bumby, A.J., Lindsay, J. & Cunningham, M.J., 2002: Late Archaean superplume events: a Kaapvaal-Pilbara perspective. *Journal of Geodynamics 34*, 207–247.

Ernst, R., 2014: *Large Igneous Provinces*. Cambridge University Press, Cambridge. 666 pp.

Greenacre, M., 1983: *Theory and applications of correspondence analysis*. Academic Press, London. ISBN 0-12-299050-1.

Greenacre, M., 2007: *Correspondence analysis in practice*, 2nd ed. Chapman & Hall/CRC, London.

Gumsley, A.P., 2013: *Towards a magmatic 'barcode' for the southeasternmost terrane of the Kaapvaal Craton, South Africa*. Unpublished M. Sc thesis. University of Johannesburg, Johannesburg, South Africa. 217 pp.

Gumsley, A., Olsson, J., Söderlund, U., de Kock, M., Hofmann, A. & Klausen, M., 2015: Precise U–Pb baddeleyite age dating of the Usushwana Complex, southern Africa – implications for the Mesoarchaean magmatic and sedimentological evolution of the Pongola Supergroup, Kaapvaal Craton. *Precambrian Research 267*, 174–185.

Gumsley, A.P., de Kock, M.O., Rajesh, H.M., Knoper, M.W., Söderlund, U. & Ernst, R.E., 2013: The Hlagothi Complex: the identification of fragments from a Mesoarchaean large igneous province on the Kaapvaal Craton. *Lithos 174*, 333–348.

Hirschfeld, H.O., 1935: A connection between correlation and contingency. *Mathematical Proceedings of the Cambridge Philosophical Society 31*, 520–524.

Hanson, R.E., Crowley, J.L., Bowring, S.A., Ramezani, J., Gose, W.A., Dalziel, I.W.D., Pancake, J.A., Seidel, E.K., Blenkinsop, T.G. & Mukwakwami, J., 2004a: Coeval large-scale magmatism in the Kalahari and Laurentian Cratons during Rodinia assembly. *Science 304*, 1126–1129.

Hanson, R.E., Gose, W.A., Crowley, J.L., Ramezani, J., Bowring, S.A., Bullen, D.S., Hall, R.P., Pancake, J.A. & Mukwakwami, J., 2004b: Paleoproterozoic intraplate magmatism and basin development on the Kaapvaal Craton: Age, paleomagnetism and geochemistry of ~1.93 to ~1.87Ga post-Waterberg dolerites. *South African Journal of Geology 107*, 233–254.

Hunter, D.R. & Hall, H.C., 1992: A geochemical study of a Precambrian mafic dyke swarm, Eastern Transvaal, South Africa. *Journal of African Earth Sciences 15*, 153–168.

Irvine, T.N. & Baragar, W.R.A., 1971: A guide to the chemical classification of the common volcanic rocks. *Canadian Journal of Earth Sciences 8*, 523–548.

Janoušek, V., Farrow, C.M. & Erban, V., 2006: Interpretation of whole-rock geochemical data in igneous geochemistry: introducing geochemical data toolkit (GCDkit). *Journal of Petrology 47*, 1255–1259.

Jourdan, F., Féraud, G., Bertrand, H., Watkeys, M.K., Kampunzu, A.B. & Le Gall, B., 2006: Basement control on dyke distribution in large igneous provinces: case study of the Karoo triple junction. *Earth and Planetary Science Letters 241*, 307–322.

Kampmann, T.C., Gumsley, A.P., de Kock, M.O. & Söderlund, U., 2015: U–Pb geochronology and paleomagnetism of the Westerberg Sill Suite, Kaapvaal Craton – support for a coherent Kaapvaal-Pilbara Block (Vaalbara) into the Paleoproterozoic? *Precambrian Research 269*, 58–72.

Klausen, M.B., Söderlund, U., Olsson, J.R., Ernst, R.E., Armoogam, M., Mkhize, S.W. & Petzer, G., 2010: Petrological discrimination among Precambrian dyke swarms: Eastern Kaapvaal craton (South Africa). *Precambrian Research 183*, 501–522.

Le Bas, M.J., Le Maitre, R.W. & Woolley, A.R., 1992: The construction of the Total Alkali-Silica chemical classification of volcanic rocks. *Mineralogy and Petrology 46*, 1–22.

Lubnina, N., Ernst, R., Klausen, M. & Söderlund, U., 2010: Paleomagnetic study of NeoArchean–Paleoproterozoic dykes in the Kaapvaal Craton. *Precambrian Research 183*, 523–552.

Ludwig, K.R., 1991: *ISOPLOT; a plotting and regression program for radiogenic-isotopic data; version 2.53*. Open File Report, USGS, 445 pp.

Maré, L.P. & Fourie, C.J.S., 2012: New geochemical and palaeomagnetic results from Neoarchaean dyke swarms in the Barberton-Badplaas area, South Africa. *South African Journal of Geology 115*, 145–170.

McCarthy, T.S., Stanistreet, I.G., Cadle, A.B. & Durrheim, R.J., 1990: The geology of the Ventersdorp Supergroup (Bezuidenhout Valley) outlier to the east of Johannesburg and its relevance to the tectonics of a Witwatersrand Basin margin. *South African Journal of Geology 93*, 289–309.

Meier, D.L., Heinrich, C.A. & Watts, M.A., 2009: Mafic dikes displacing Witwatersrand gold reefs: evidence against metamorphic-hydrothermal ore formation. *Geology 37*, 607–610.

Nilsson, M.K.M., Klausen, M.B., Söderlund, U. & Ernst, R.E., 2013: Precise U–Pb ages and geochemistry of Palaeoproterozoic mafic dykes from southern West Greenland: linking the North Atlantic and the Dharwar cratons. *Lithos 174*, 255–270.

Olsson, J.R., Klausen, M.B., Hamilton, M.A., Marz, N., Söderlund, U. & Roberts, J.A., this volume: Baddeleyite U–Pb ages and geochemistry of the 1875–1835 Ma Black Hills Dyke Swarm across northeastern South Africa: part of a trans-Kalahari Craton back-arc setting? *GFF*. doi: 10.1080/11035897.2015.1103781

Olsson, J.R., Söderlund, U., Hamilton, M.A., Klausen, M.B. & Helffrich, G.R., 2011: A late Archaean radiating dyke swarm as possible clue to the origin of the Bushveld Complex. *Nature Geoscience 4*, 865–869.

Olsson, J.R., Söderlund, U., Klausen, M.B. & Ernst, R.E., 2010: U–Pb baddeleyite ages linking major Archean dyke swarms to volcanic-rift forming events in the Kaapvaal craton (South Africa), and a precise age for the Bushveld Complex. *Precambrian Research 183*, 490–500.

Pearce, J.A., 2008: Geochemical fingerprinting of oceanic basalts with applications to ophiolite classification and the search for Archean oceanic crust. *Lithos 100*, 14–48.

Semami, F., de Kock, M., Söderlund, U., Gumsley, A., da Silva, R., Beukes, N. & Armstrong, R., this volume: New U–Pb geochronology and paleomagnetic constraints on the late Paleoproterozoic Hartley magmatic event: evidence for a large igneous province in the Kaapvaal Craton during Kalahari assembly, South Africa. *GFF*. doi: 10.1080/11035897.2015.1124917

Söderlund, U. & Johansson, L., 2002: A simple way to extract baddeleyite (ZrO_2). *Geochemistry Geophysics Geosystems 3*. doi:10.1029/2001GC000212.

Stacey, J.S. & Kramers, J.D. 1975: Approximation of terrestrial lead isotope evolution by a two-stage model. *Earth and Planetary Science Letters 26*, 207–221.

Stanistreet, I.G. & McCarthy, T.S., 1991: Changing tectono-sedimentary scenarios relevant to the development of the Late Archaean Witwatersrand Basin. *Journal of African Earth Sciences 13*, 65–81.

Sun, S.-S. & McDonough, W.F., 1989: Chemical and isotopic systematics of oceanic basalts: implications for mantle composition and processes. *In* S.D. Saunders & M.J. Norry (eds.): *Magmatism in the Ocean Basins*, 313–345. London, Geological Society of London Special Publication 42.

Svensen, H., Corfu, F., Polteau, S., Hammer, Ø. & Planke, S., 2012: Rapid magma emplacement in the Karoo large igneous province. *Earth and Planetary Science Letters 325–326*, 1–9.

Uken, R. & Watkeys, M.K., 1997: An interpretation of mafic dyke swarms and their relationship with major mafic magmatic events on the Kaapvaal Craton and Limpopo Belt. *South African Journal of Geology 100*, 341–348.

van der Westhuizen, W.A., de Bruiyn, H. & Meintjes, P.G., 2006: The Ventersdorp Supergroup. *In* M.R. Johnson, C.R. Anhaeusser & R. Thomas (eds.): *The Geology of South Africa*, 187–208. Johannesburg/Pretoria, Geological Society of South Africa/Council for Geoscience.

Wingate, M.T.D., 1998: A paleomagnetic test of the Kaapvaal-Pilbara (Vaalbara) connection at 2.78 Ga. *South African Journal of Geology 101*, 257–274.

Appendix A: Correspondence analysis

Correspondence analysis is a descriptive multivariate statistical technique first proposed by Hirschfeld (1935) and later developed by Benzécri (1973). It is conceptually similar to principal component analysis, more often used (e.g., as a component in GCDkit, Janoušek et al. 2006) on geochemical data, but applies to categorical rather than continuous data. No data can be negative and should all be on the same scale for the correspondence analysis to be applicable, and the method treats rows and columns equivalently. The correspondence analysis first pre-processes such contingency tables by computing a set of weights for both its columns and rows. It then decomposes the chi-squared statistics associated with this pre-processed table into orthogonal components, which are finally reformulated as so-called Factor scores for both rows and columns (see Greenacre 1983, 2007, for more statistical details). Most of the statistical variation in a contingency table is represented by the first set of Factor scores and successively less in subsequent sets, and the rate by which the cumulative percentage of all statistical variation declines depends on how complexly variable a data-set is. Thus, in most igneous data-sets, a significant proportion of all statistical variation can typically be displayed by the first two to three sets of Factor scores.

Like principal component, correspondence analysis results provide a means of displaying or summarising a set of Factor scores in two-, or more, dimensional graphical form, which typically 'radiate' out from an 'averaged' origin. In such plots, Factor points that plot closer to each other (note that there are more dimensions not displayed in 2D) are more similar than points plotted farther apart and the relative distances between points is a statistical measure of their 'degree of similarity', or correspondence. As exemplified by Fig. 5(B), we see how compositionally similar samples, as well as elements that are known for their similar properties (e.g., Zr-Hf and Nb-Ta) plot closer to each other. One useful advantage of the correspondence analysis, compared to the principal component analysis, is that it can display both rows (e.g., samples) and columns (e.g., elements) in the same plot, and thereby allow the user to better link these to each other. As exemplified by Fig. 5(B), and noted in the related main text, one typically finds that a sample plotting closer to certain element also has a relatively higher concentration of that element, compared to samples plotting farther from it. That paragraph continues with providing more specific examples of such correspondences between certain sample and element groups, pertaining to the data-set presented in this paper.

PAPER IV

GFF, 2016
Vol. 138, No. 1, 164–182, http://dx.doi.org/10.1080/11035897.2015.1124917

Article

New U–Pb geochronologic and palaeomagnetic constraints on the late Palaeoproterozoic Hartley magmatic event: evidence for a potential large igneous province in the Kaapvaal Craton during Kalahari assembly, South Africa

FARNAZ ALEBOUYEH SEMAMI[1], MICHIEL DE KOCK[2], ULF SÖDERLUND[13], ASHLEY GUMSLEY[1], RICHARD DA SILVA[2], NICOLAS BEUKES[2] and RICHARD ARMSTRONG[24]

Semami Alebouyeh, F., de Kock, M., Söderlund, U., Gumsley, A., Da Silva, R., Beukes, N., & Armstrong, R., 2016: New U-Pb geochronologic and palaeomagnetic constraints on the late Palaeoproterozoic Hartley magmatic event: evidence for a potential large igneous province in the Kaapvaal Craton during Kalahari assembly, South Africa. *GFF*, Vol. 138, No. 1, pp.164–182. © Geologiska Föreningen. doi: http://dx.doi.org/10.1080/11035897.2015.1124917

Abstract: The volcanic Hartley Formation (part of the Olifantshoek Supergroup, which is dominated by red bed successions) in South Africa recorded depositional and tectonic conditions along the western Kaapvaal Craton during the late Palaeoproterozoic. It formed in association with red bed deposition elsewhere in the cratonic hinterland and along the craton's northern margin. However, the exact correlation of the Olifantshoek Supergroup with these other red-bed successions is hindered by poor geochronological constraints. Herein, we refine the age and palaeopole of the Hartley Formation, and provide geochronological constraints for large-scale 1.93–1.91 Ga bimodal magmatism on the Kaapvaal Craton (herein named the Hartley large igneous province). We present new age constraints for the mafic and felsic phases of this event at 1923 ± 6 Ma and 1920 ± 4 Ma, respectively, which includes the first reported age dating of the Tsineng Dyke Swarm that has been linked to Hartley volcanism. A mean 1.93–1.91 Ga palaeomagnetic pole for the Hartley large igneous province at 22.7°N, 328.6°E with A_{95} = 11.7° represents a significant improvement on a previously published virtual geomagnetic pole. This improved pole is used to refine the late Palaeoproterozoic apparent polar wander path of the Kaapvaal Craton. This can assist in correlation of red-bed successions in southern Africa.

Keywords: geochronology; large igneous province; dyke swarm; palaeomagnetism; apparent polar wander path; Orosirian period

[1]*Department of Geology, Lund University, Lund, Sweden*
[2]*Department of Geology, University of Johannesburg, Johannesburg, South Africa; mdekock@uj.ac.za*
[3]*Department of Geoscience, Swedish Museum of Natural History, Stockholm, Sweden*
[4]*Research School for Earth Sciences, The Australian National University, Canberra, Australia*
Manuscript received 17 March 2015. Revised manuscript accepted 20 November 2015.

1. Introduction

The identification and understanding of Mesoarchean to Proterozoic magmatic events on the Kaapvaal Craton, including short-lived large igneous provinces (LIPs), are becoming better understood using high-precision U–Pb geochronology on baddeleyite and zircon (e.g., Olsson et al. 2010, 2011; Gumsley et al. 2013, 2015a; Mukasa et al. 2013; de Kock et al. 2014; Kampmann et al. 2015). The late Palaeoproterozoic Hartley Formation represents a small volcanic component within the red bed-dominated Olifantshoek Supergroup (Cornell 1987; Moen 1999, 2006), which in southern Africa recorded conditions along the western Kaapvaal Craton margin (Fig. 1). Several magmatic rock units on the Kaapvaal Craton have previously been correlated to the Hartley Formation (Cornell et al. 1998; Hanson et al. 2004; Goldberg 2010), and hint at a wider spatial distribution of magmatism, but the association is as yet unconfirmed for most. The Olifantshoek Supergroup developed in broad association with red bed deposition elsewhere in the cratonic interior following the emplacement of the ca. 2.05 Ga Bushveld Complex and 2.04–2.02 Ga high-grade metamorphism during the assembly of the Kalahari Craton (Fig. 1). Thin-skin tectonic shortening of much of the Olifantshoek Supergroup occurred during the <1.93 Ga Kheis Orogeny (Cornell et al. 1998), and later tectonic reworking by the ca. 1.0 Ga Namaqua-Natal Orogeny (Eglington & Armstrong 2004). Structural complexity, younger cover and limited geochronology obstruct the exact correlation of the Olifantshoek Supergroup with other southern African red-bed suc-

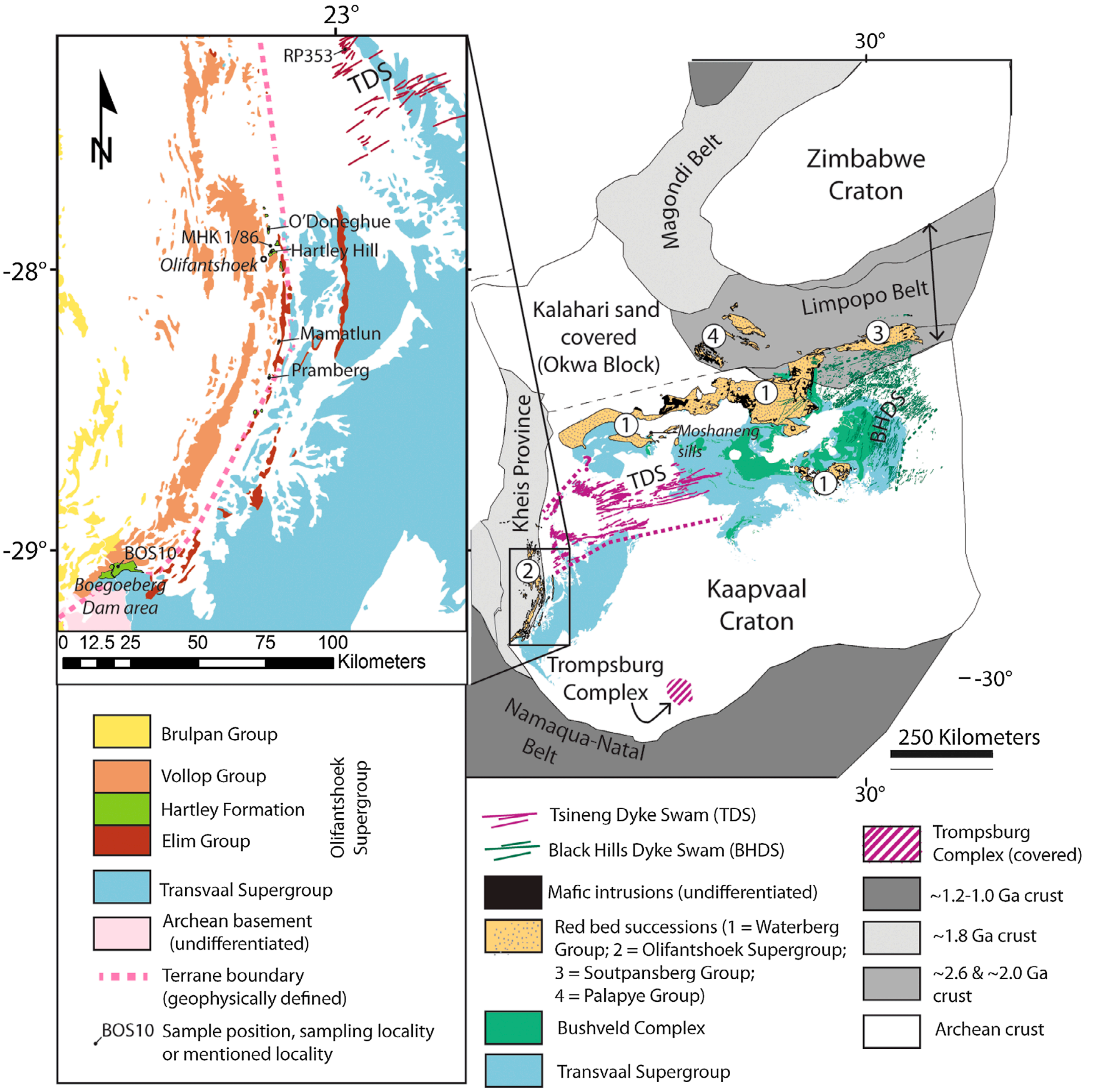

Fig. 1. An overview map of the Kaapvaal Craton and its surrounding environment which highlights the Olifantshoek-Waterberg-Soutpansberg-Palapye strata and the ~1.93–1.84 Ga dolerite dyke and sill intrusions. Inset shows a geological map of the western margin of the Kaapvaal Craton. Sample localities for palaeomagnetism and geochronology near the western margin of the craton are shown together with other localities mentioned in the text.

cessions. Previous attempts to date the Hartley Formation document imprecise Rb–Sr and Pb–Pb isochrons and errorchrons (Armstrong 1987; Cornell 1987). An exception is a $^{207}Pb/^{206}Pb$ age of 1928 ± 4 Ma for a quartz porphyry unit interbedded with the Hartley Formation basalts obtained by Cornell et al. (1998) via Pb–Pb evaporation. This provides the principal constraint on the Kheis Orogeny. Here we present a U–Pb SHRIMP zircon age of another porphyry occurrence that confirms the age for the Hartley Formation. U–Pb age constraints from two suggested Hartley Formation equivalents are reported to constrain the regional extent and establish LIP status of Hartley volcanism during the Kalahari Craton assembly. Coupled with a refinement of previous palaeomagnetic studies (Evans et al. 2002), our new ages further constrain the apparent polar wander (APW) path of the Kaapvaal and Kalahari Cratons during the Orisirian Period – a vital tool in the correlation of southern African red-bed successions.

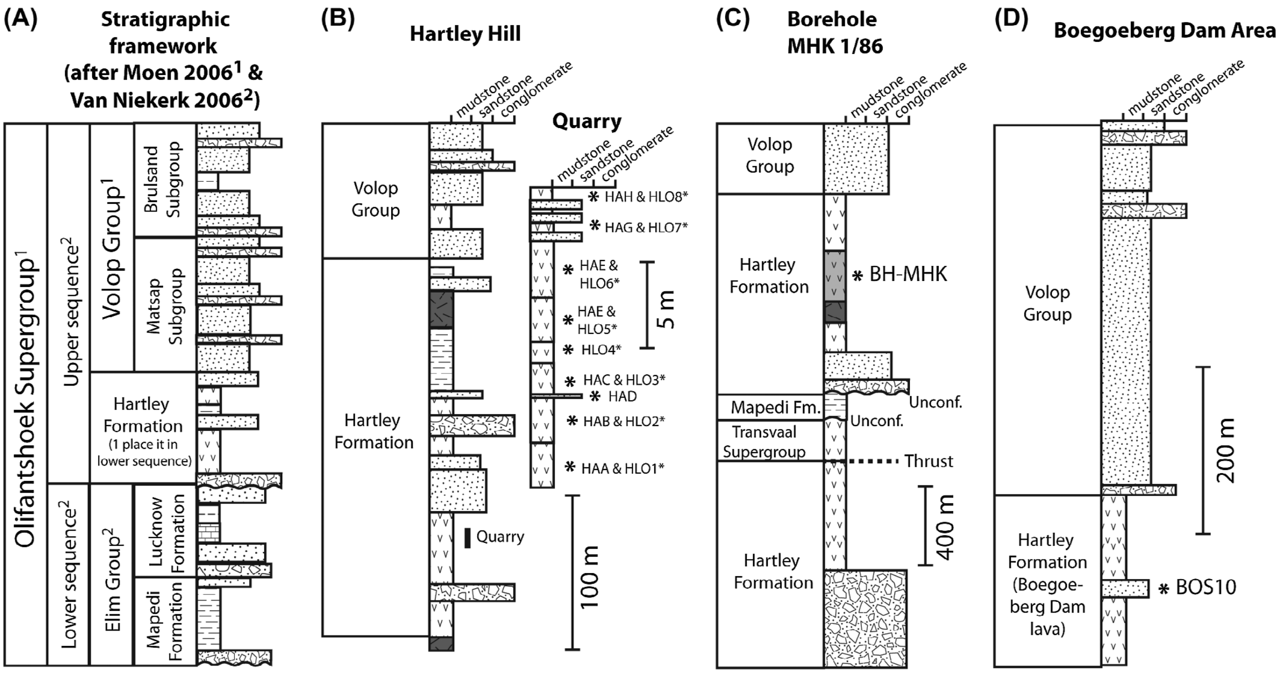

Fig. 2. Lithostratigraphy of the Olifantshoek Supergroup. **A**. Stratigraphic framework of the Olifantshoek Supergroup after Moen (2006) and Van Niekerk (2006) used in this study. **B.** Lithostratigraphy at Hartley Hill (modified after Cornell 1987). **C.** Lithostratigraphy of drill core MHK 1/86 from the farm Mooihoek, north of Olifantshoek, and **D**. Lithostratigraphy at Boegoeberg Dam. Position of U–Pb geochronology samples as well as palaeomagnetic sampling sites are indicated as stars. Asterix after sampling sites indicate sites of Evans et al. (2002).

2. Geological setting

2.1. *Regional geology*

The Kaapval Craton together with the Zimbabwe Craton, and several accreted terranes along their western margins (Eglington & Armstrong 2004), constitute the greater Kalahari Craton. To its north, the Kaapvaal Craton adjoins with the Zimbabwe Craton along the Limpopo Belt (Fig. 1), a 2.6–2.02 Ga polymetamorphic complex (Kramers & Mouri 2011). However, the exact timing of amalgamation of the Kalahari Craton remains controversial (Hanson et al. 2011). On its west, the Kaapvaal Craton is bounded by the Kheis Province (Fig. 1), a <1.93 Ga fold and thrust belt, which has largely been reworked during the ca. 1100 and 1050 Ma Namaqua-Natal Orogeny (Fig. 1), to the west and south of the craton (Eglington & Armstrong 2004; Cornell et al. 2006; Eglington 2006).

During the late Palaeoproterozoic extensive red-bed successions were deposited on the Kaapvaal Craton and its margins including the Limpopo Belt and Kheis Province. The Waterberg Group, Soutpansberg Group and Olifantshoek Supergroup of South Africa together with the Palapye Group (Botswana), and a number of smaller outliers, such as the Blouberg Formation, are erosional remnants of these late Palaeoproterozoic successions (e.g., De Kock et al. 2006; Dorland et al. 2006). It is now accepted that deposition of the Soutpansberg Group commenced some 200 million years after the initiation of deposition in the Waterberg Group and Blouberg Formation at 2.04 Ga (Dorland et al. 2006; Corcoran et al. 2013; Geng et al. 2014), while deposition continued possibly as late as 1604 Ma within the Palapye Group (Mapeo et al. 2004). Still elusive is the exact correlation of these successions with the Olifanshoek Supergroup.

2.2. *Olifanshoek Supergroup*

Structural complexities and poor geochronological control have resulted in several proposed lithostratigraphic frameworks for the Olifantshoek Supergroup. Here, we employ a combination of the recent frameworks of Moen (2006) and Van Niekerk (2006) that sees the Olifantshoek Supergroup divided into two unconformity-bounded sequences (Fig. 2). The oldest of these sequences is named the Elim Group in accordance with Van Niekerk (2006). The formations of this group are interpreted by Van Niekerk (2006) and others (e.g., Beukes et al. 2002; Evans et al. 2002) as being part of the Transvaal Supergroup and not an integral part of the Olifanshoek Supergroup as proposed by Moen (2006). The placement by Moen (2006) seems justified by recent unpublished constraints from detrital zircon grains from the Mapedi Formation (Da Silva 2011). Placement of the Elim Group rocks either before (i.e., Transvaal Supergroup) or after (i.e., Olifantshoek Supergroup) the intrusion of the 2.05 Ga Bushveld Complex is crucial for how the Kaapvaal Craton's APW path is defined, as will be shown (Section 5.3). The Elim Group consists of the Mapedi and Lucknow formations (Moen 1999), an upward coarsening shale to quartzite succession with interbedded carbonate rocks.

As recognized by Van Niekerk (2006), the second sequence is taken from the regional unconformity at the base of the overlying Hartley Formation, which is composed of basal conglomerate and quartzite (i.e., the so-called Neylan Member of the Hartley Formation in the subdivision of Van Niekerk, 2006) followed by dominantly volcanic rocks (Fig. 2). The Hartley Formation is overlain conformably by light grey to white arenites (orthoquartzite), with minor shale and poorly exposed silty sandstone (Fig. 2). Opinions vary widely on the lithostratigraphic status of this sandstone-dominated unit at the top of the Volop Group (Moen 2006; Van Niekerk 2006).

2.3. Hartley volcanic rocks and equivalents

The Hartley Formation is formed by dominantly basaltic lava flows also encompassing pyroclastic and sedimentary rocks, with a total estimated thickness that ranges between 300 and 762 m (Cornell 1987). The conservative estimate is supported by reports of thrust duplication (Tinker et al. 2002). Rare quartz-feldspar porphyry also occurs as isolated outcrops in the predominantly Kalahari sand covered N–S trending valleys of the present topography south of Olifantshoek (Cornell 1987). The 1928 ± 4 Ma age of Cornell et al. (1998) is from such porphyry that outcrops on the farm Pramberg (Fig. 1). In this work, another porhyry intersected in a borehole north of Olifantshoek (MHK 1/86), was sampled for U–Pb geochronology.

Cornell et al. (1998) proposed that basalt and interbedded sedimentary units some 140 km south of Olifantshoek (Fig. 1) are Hartley Formation correlatives. This unit (the Boegoeberg Dam Formation) could, however, also represent a volcanic unit of the 2.64 Ga lower Transvaal Supergroup (Smit et al. 1991). Fine-grained quartzite (sample BOS 10), interbedded with the Boegoeberg Dam Formation was sampled to test the proposed correlation.

In addition, an undated ~120 m-thick unit of mafic lava preserved in the lower part of the Selika Formation near the base of the Palapye Group in Botswana (Ermanovics et al. 1978), must be older than 1604 Ma according to Mapeo et al. (2004), and could represent a Hartley Formation equivalent. Elsewhere, near Moshaneng, Hanson et al. (2004) reported a narrow range of ~1927 Ma $^{207}Pb/^{206}Pb$ baddeleyite ages for dolerite sills that intrude the Waterberg Group (Fig. 1). They further illustrated geochemical similarity between these sills and basalt of the Hartley Formation.

In South Africa, U–Pb geochronology of zircons from two gabbroic drill core samples of the unexposed Trompsburg Complex near the southwestern Kaapvaal Craton margin, beneath the Phanerozoic cover (Fig. 1), yielded an age of 1915 ± 6 Ma (Maier et al. 2003), which is comparable to the existing ages for the Hartley Formation (Cornell et al. 1998) and Moshaneng sills (Hanson et al. 2004). Finally, a distinct dyke swarm known as the Tsineng Dyke Swarm (TDS), in the western Kaapvaal Craton (Fig. 1), has been linked to the Hartley Formation volcanic rocks (Goldberg 2010). The TDS is evident on aeromagnetic maps, and displays a slight convergence towards the west, where it is truncated by the Kheis Province. This truncation led Goldberg (2010) to suggest a pre-1.8 Ga age for the TDS. The dyke swarm fans out very slightly towards the ENE, and its strike is ~0–70°, with a slight dextral curvature to ~0–60° in the west. According to Goldberg (2010), aeromagnetic data indicate that these dolerite dykes crosscut the ca. 2.4 Ga Ongeluk Formation of the Transvaal Supergroup (Fairey et al. 2013; Gumsley et al. 2015b), presenting a maximum constraint on TDS emplacement. One of the NE-trending TDS dykes intersected in drill core near the town of Tsineng (sample RP353) was collected for U–Pb geochronology.

3. Methodology

3.1. SHRIMP U–Pb geochronology of the Hartley volcanic rocks

Zircon grains were separated from a quartz porphyry found at 683 m depth within drill core of borehole MHK1/86 (Fig. 2), from the farm Mooihoek just north of Olifantshoek (Fig. 1), as well as from fine-grained quartzite (Sample BOS 10) interbedded with volcanic rocks of the Boegoeberg Dam Formation (Figs. 1 and 2). A heavy mineral fraction was extracted using Bromoform on a washed 250 micron sieve after crushing and milling at the University of Johannesburg, South Africa. Zircons were concentrated from this heavy mineral fraction by magnetic separation at 1.25 A, and then separated using methylene iodine in the heavy mineral separation facilities of the PRISE Research School of Earth Sciences at the Australian National University in Canberra, Australia.

For microbeam analysis, the zircon grains were hand-picked, mounted in epoxy resin, polished and gold-coated. Cathodoluminescence and backscatter electron images were obtained by scanning electron microscopy, which were used to identify xenocrysts through morphology, and to avoid inclusions, cracks and metamict zones in grains.

Sensitive high-resolution ion microprobe reverse geometry analyses were performed at PRISE at the Australian National Uuniversity. The FC-1 and SL3 zircon standards were used for calibration (Compston & Williams 1984; Paces & Miller 1993). Common Pb corrections were done using the Stacey & Kramers (1975) terrestrial Pb model composition. The analytical data were reduced according to the method described in Williams & Claesson (1987) and Compston et al. (1992). Only $^{207}Pb/^{206}Pb$ ages with a discordance of less than 10% were used to define detrital zircon age populations in sample BOS10. Uncertainties of ages are given at 2σ in the text, ignoring decay constant errors.

3.2. ID-TIMS U–Pb geochronology of the Tsineng Dyke Swarm

Baddeleyite grains were extracted from drillcore sample RP353, which intersects one of the NE–SW trending TDS dolerite dykes. The borehole is located on Smartt Mine in the Kalahari Manganese Field near Tsineng in the Northern Cape Province of South Africa (see Fig. 1). Here, a dyke intrudes Mn-rich rocks of the Transvaal Supergroup (Hotazel Formation). The RP353 dyke sample is an unfoliated coarse-grained dolerite with abundant plagioclase phenocrysts. Baddeleyite grains were extracted after crushing, milling and water-based separation at Lund University following the procedures described in Schütte (1992). The best-quality grains were hand-picked and transferred to Teflon capsules, where they were washed repeatedly in ultrapure water and dilute HNO_3. One drop of a $^{233-236}U-^{205}Pb$ tracer solution and 10 drops of HF–HNO_3 (10:1) solution were added into each capsule. The samples were then completely dissolved after three days in the oven. Isotope Dilution Thermal Ionization Mass Spectrometry (ID-TIMS) analysis was done using a Finnigan Triton Thermal Ionization Mass Spectrometer in the Department of Geosciences at the Swedish Museum of National History in Stockholm. Data were plotted using Isoplot after Ludwig (1991). U decay constants used were those published in Jaffey et al. (1971). The correction for initial common Pb was carried out using the isotopic model compositions of global common Pb (Stacey & Kramers 1975). Further details are given in Olsson et al. (2010).

3.3. Palaeomagnetism of the Hartley volcanic rocks

Ten individual magmatic cooling units of the Hartley Formation were drilled and sampled for palaeomagnetic study (Fig. 1). A total of 77 oriented samples, with between 8 and 9 samples per unit, were taken using a water-cooled portable drill. The majority of samples originate from the Hartley Hill quarry outside of the town of Olifantshoek, where a largely undeformed succession of Hartley Formation volcanic rocks are exposed as eight sub-horizontal flow units (Cornell 1987). This locality was also previously sampled for palaeomagnetism by Evans et al. (2002). Additional samples were taken from a more foliated mafic volcanic unit on the farm O'Doneghue, and from the dated porphyry of Cornell et al. (1998) outcropping on the farm Pramberg. Sample orientation was done using a magnetic and sun compass, and drilled samples were cut into one or more shorter cylindrical specimens.

In the palaeomagnetic laboratory at UJ, the cut specimens were measured on a vertical 2G Enterprises DC-4 K magnetometer equipped with an automatic sample changer (Kirschvink et al. 2008). After measuring the natural remanent magnetization (NRM) of all specimens, they were demagnetized stepwise. Specimens were pretreated with low-field strength alternating field (AF) demagnetization from 2 mT up to 10 mT. Specimens that showed a strong resistance to this initial low-field strength AF demagnetization were submerged in liquid nitrogen before demagnetization was continued. Specimens were then treated to high-field strength AF demagnetization in steps up to 100 mT. Magnetic components were identified and quantified via the least-squares (LSQ) principal component method of Kirschvink (1980) using Palaeomag 3.1b2 software of Jones (2002). Palaeopoles were plotted using GPlates 1.2.0 software of Williams et al. (2012).

4. Results

4.1. Zircon U–Pb geochronology

Summarized geochronological data are presented in Table 1 and Table 2, with concordia diagrams and detrital age populations illustrated in Fig. 3.

4.1.1. Mooihoek Porphyry (MHK1/86)

This quartz porphyry yielded clear euhedral zircons with consistent Th/U ratios of between 0.5 and 0.75 indicating their magmatic origin. Seventeen zircon crystals analysed by SHRIMP-RG in 18 spots produce a well-defined U–Pb concordia age of 1920 ± 4 Ma with MSWD of 0.04 (Fig. 3A).

4.1.2. Boegoeberg Dam Formation (BOS10)

Sample BOS10 yielded zircon grains of between 75 and 150 µm in length that varied from being euhedral to well rounded. Some grains were clearly broken during the milling process and could have been in excess of 250 µm originally. Most zircon grains were clear, but about 15% of grains were covered in a mottled red coating. About half of the grains were pitted and cracked, while a few grains had inclusions or growth of xenotime along grain boundaries. The zircon grains were concentrically zoned, and some had detrital cores with younger zircon rims.

SHRIMP analyses of 52 zircon grains produced 29 concordant to near concordant (within 10%) ages that define two major age populations (Fig. 3B). All concordant and near-concordant grains from this sample had high Th/U ratios and are considered magmatic in origin. Eleven grains define a prominent ca. 2000–2100 Ma age peak, and 6 grains define a prominent age population around ca. 2700 Ma. There is also a secondary peak consisting of 3 grains around ca. 3200 Ma. Most interesting for our study was one zircon grain with an age of 1931 ± 20 Ma (analysis 39.2). Another zircon grain produced an age of 1957 ± 18 Ma (analysis 33.2) and may fall in the same young group. The two grains are both euhedral and may be derived from the Boegoeberg Dam Formation volcanic eruptions (Table 1).

4.2. Baddeleyite U–Pb geochronology

Summarized geochronological data are presented in Table 2, with a concordia diagram shown in Fig. 3. Baddeleyite grains extracted from the dolerite dyke drillcore sample (RP353) are transparent, light brown crystals with no signs of mottled surfaces or alteration. Three grain fractions plot concordant, yielding a robust concordia age of 1923 ± 6 Ma (MSWD = 0.56) for the RP353 dyke of the TDS (Fig. 3C).

4.3. Palaeomagnetism

Palaeomagnetic results from the Hartley Formation are summarized in Table 3. Examples of demagnetization behaviour and summaries of the remanent magnetization components are shown in Fig. 4.

4.3.1. Hartley Hill Quarry

Our samples from Hartley Hill quarry overlap with, and extend, the limited sampling originally done by Evans et al. (2002), who only took three oriented samples per flow unit (Fig. 2). We repeated LSQ analyses on specimen data of Evans et al. (2002) and combined it with our own data-set to calculate component means (Table 3).

Random low-coercivity components and a present field-like viscous remanent magnetization were successfully removed in most samples during initial demagnetization steps. An intermediate coercivity component (INT component) was recognized in samples from three of the sites (i.e., two samples from site HAA, as well as all the samples from sites HAF and HAH). This component is generally poorly constrained, but displays shallow inclination and southward declination in present geographic coordinates. High coercivity components (HIG1 component) were removed by demagnetization steps between 35 and 100 mT, either as origin-seeking linear trajectories of demagnetization, or as stable endpoints of demagnetization. These define generally westerly and moderately steep to very steep downwards directed vectors in present geographic coordinates (Figs. 4 and 5C). This component was present in all of the sampled volcanic units at

Table 1. Summary of SHRIMP geochronological data on zircon.

Grain.Spot	U/Th	^{206}Pbc (%)	^{206}Pb* ppm^2	^{207}Pb/^{235}U	±2σ % err.	^{206}Pb/^{238}U	±2σ % err.	^{207}Pb/^{235}U	±2σ	^{206}Pb/^{238}U (Ma)	±2σ	^{207}Pb/^{206}Pb (Ma)	±2σ	Error correlation	Discordance (%)
								BOS 10							
1.1	4.12	0.11	61.4	12.80	1.5	0.5096	1.3	0.1822	0.66	2655	29	2673	11	0.895	1
2.1	2.57	0.08	104.0	30.07	2.3	0.6183	1.3	0.3528	1.90	3103	32	3719	29	0.556	17
3.1	1.44	0.08	63.0	7.13	1.6	0.3390	1.2	0.1330	0.95	2118	22	2138	17	0.794	1
4.1	1.11	0.41	78.6	6.84	1.4	0.2904	1.2	0.1709	0.78	1644	17	2566	13	0.830	36
5.1	3.93	0.47	94.0	4.30	1.4	0.2430	1.1	0.1283	0.84	1403	14	2075	15	0.800	32
5.1	1.70	0.15	64.7	6.43	1.4	0.3602	1.2	0.1293	0.78	1983	21	2089	14	0.842	5
7.1	1.98	0.20	58.6	7.21	1.5	0.4041	1.3	0.1293	0.75	2188	23	2089	13	0.860	−5
8.1	1.34	1.24	119.0	4.32	1.5	0.2038	1.1	0.1536	1.00	1196	12	2386	17	0.729	50
9.1	3.94	0.17	97.1	6.51	1.3	0.3724	1.2	0.1267	0.64	2041	20	2053	11	0.876	1
10.1	5.91	0.35	114.0	6.73	1.3	0.2992	1.1	0.1631	0.66	1687	17	2488	11	0.862	32
11.1	0.94	0.09	83.8	6.37	1.3	0.3743	1.2	0.1234	0.62	2050	20	2006	11	0.881	−2
12.1	1.54	0.11	61.6	6.61	1.4	0.3803	1.2	0.1261	0.75	2078	22	2044	13	0.856	−2
13.1	1.87	0.04	109.0	22.60	1.3	0.6491	1.2	0.2530	0.41	3225	31	3204	7	0.946	−1
14.1	0.83	0.16	56.5	11.70	1.5	0.4747	1.3	0.1788	0.68	2504	27	2642	11	0.886	5
15.1	2.49	0.14	60.9	13.22	1.5	0.5185	1.3	0.1849	0.69	2693	28	2698	11	0.882	0
16.1	2.61	0.36	84.7	5.46	1.5	0.3092	1.2	0.1281	0.86	1737	19	2072	15	0.818	16
17.1	1.54	0.47	163.0	9.26	1.3	0.3732	1.1	0.1800	0.69	2045	19	2653	11	0.843	23
18.1	1.53	1.54	94.6	2.72	1.8	0.1474	1.1	0.1337	1.40	886	9	2147	24	0.620	59
19.1	1.88	0.37	111.0	6.99	1.3	0.3261	1.1	0.1555	0.63	1819	18	2407	11	0.871	24
20.1	0.48	0.39	78.1	6.67	1.3	0.3040	1.2	0.1591	0.67	1711	17	2446	11	0.864	30
21.1	1.35	0.08	157.0	18.91	1.2	0.5883	1.1	0.2332	0.36	2982	27	3074	6	0.952	3
22.1	2.12	0.27	115.0	23.28	1.5	0.6515	1.4	0.2592	0.57	3234	35	3242	9	0.924	0
23.1	1.95	0.00	75.0	12.60	1.4	0.5147	1.2	0.1776	0.55	2677	27	2630	9	0.914	−2
26.1	2.10	0.13	56.7	13.49	1.5	0.5143	1.4	0.1903	0.71	2675	30	2745	12	0.886	3
27.1	2.39	0.35	122.0	13.11	1.2	0.3819	1.1	0.2490	0.44	2085	20	3178	7	0.931	34
28.1	4.43	2.14	127.0	5.51	2.1	0.3029	1.1	0.1320	1.80	1706	17	2124	32	0.521	20
29.1	0.72	0.55	73.5	7.90	1.6	0.3389	1.3	0.1691	0.98	1881	20	2548	16	0.788	26
30.1	2.78	0.46	76.7	5.40	1.4	0.3041	1.2	0.1287	0.86	1712	18	2080	15	0.806	18
31.1	0.81	1.10	88.8	6.54	1.6	0.2211	1.1	0.2146	1.10	1288	13	2941	18	0.714	56
32.2	1.62	0.48	82.0	5.69	1.4	0.2527	1.1	0.1632	0.81	1452	14	2489	14	0.809	42

33.2	1.56	0.07	22.6	5.80	1.7	0.3506	1.4	0.1200	10.00	1937	24	1957	18	0.820	1
34.1	19.90	0.35	93.5	4.46	1.6	0.2595	1.1	0.1247	1.10	1487	15	2024	20	0.706	27
35.2	0.94	0.43	45.7	4.71	1.5	0.1908	1.2	0.1700	0.83	1126	12	2557	14	0.823	56
36.2	1.31	0.10	31.7	6.06	1.8	0.3518	1.3	0.1249	1.20	1943	22	2028	22	0.727	4
37.1	1.94	0.44	71.4	4.61	1.5	0.2602	1.2	0.1284	0.89	1491	16	2076	16	0.807	28
38.1	1.63	0.16	71.9	9.78	1.5	0.4497	1.2	0.1577	0.81	2394	24	2431	14	0.833	2
39.2	1.30	0.10	16.2	5.40	1.9	0.3311	1.5	0.1183	1.10	1843	24	1931	20	0.797	5
40.1	1.67	0.07	30.2	12.84	1.6	0.5026	1.4	0.1852	0.71	2625	31	2700	12	0.894	3
41.1	1.72	0.15	54.2	6.38	1.5	0.3725	1.3	0.1241	0.76	2041	22	2017	13	0.857	–1
42.1	2.19	0.00	55.5	14.13	1.8	0.5492	1.4	0.1866	1.20	2822	31	2712	20	0.752	–4
43.1	2.10	0.53	94.6	8.75	1.3	0.3404	1.1	0.1865	0.63	1889	19	2711	10	0.875	30
44.1	3.44	0.24	27.9	6.58	2.0	0.3785	1.5	0.1261	1.30	2070	27	2044	22	0.769	–1
45.1	2.52	0.31	56.6	12.35	1.5	0.5016	1.3	0.1786	0.77	2620	29	2639	13	0.868	1
46.1	2.81	0.22	113.0	10.95	1.2	0.3963	1.1	0.2005	0.48	2152	21	2830	8	0.920	24
47.1	1.45	0.61	73.3	4.86	1.5	0.2711	1.2	0.1300	0.99	1546	16	2098	17	0.764	26
48.1	1.33	0.06	93.7	13.63	1.3	0.5298	1.2	0.1866	0.51	2741	27	2712	9	0.920	–1
49.1	2.38	0.32	137.0	6.71	1.2	0.2927	1.1	0.1662	0.50	1655	16	2520	8	0.905	34
50.1	1.38	0.07	96.1	11.57	1.3	0.4781	1.2	0.1755	0.50	2519	25	2610	8	0.920	3
51.1	2.64		66.9	6.62	1.4	0.3786	1.2	0.1267	0.65	2070	21	2053	12	0.880	–1
52.1	1.90	0.05	64.5	6.49	1.4	0.3757	1.2	0.1253	0.71	2056	22	2032	13	0.865	–1
53.1	1.55	0.06	97.6	20.37	1.4	0.6034	1.3	0.2448	0.43	3044	31	3152	7	0.947	3
54.1	1.58	0.06	86.9	6.85	1.3	0.3855	1.2	0.1288	0.60	2102	21	2082	11	0.889	–1
								BH MDK							
1.1	1.77	0.10	29.4	5.62	1.8	0.3452	1.4	0.1181	1.10	1912	23	1928	20	0.776	1
2.1	1.52	0.00	55.9	5.70	1.6	0.3510	1.2	0.1177	1.00	1939	21	1922	19	0.766	–1
3.1	1.33		135.0	5.62	1.2	0.3471	1.1	0.1174	0.42	1921	18	1917	8	0.935	0
4.1	1.47	0.00	24.0	5.43	1.7	0.3325	1.4	0.1185	0.93	1851	23	1933	17	0.834	4
5.1	1.45	0.04	87.4	5.65	1.3	0.3474	1.2	0.1180	0.53	1922	19	1927	9	0.910	0
5.2	1.25	0.06	79.2	5.62	1.3	0.3838	1.2	0.1173	0.47	1905	20	1916	9	0.929	1
6.1	1.66	0.00	36.2	5.66	1.5	0.3431	1.3	0.1196	0.79	1901	22	1949	14	0.858	2
7.1	1.31	0.00	88.9	5.60	1.4	0.3460	1.3	0.1175	0.52	1915	21	1918	9	0.925	0
8.1	1.93	0.00	133.0	5.61	1.2	0.3465	1.1	0.1174	0.43	1918	18	1917	8	0.932	0

Table 1. (*Continued*).

Grain.Spot	U/Th	^{206}Pbc	^{206}Pb*	^{207}Pb/	±2σ	^{206}Pb/	±2σ	^{207}Pb/	±2σ	^{206}Pb/	±2σ	^{207}Pb/	±2σ	Error	Discordance
		(%)	ppm^2	^{235}U	% err.	^{238}U	% err.	^{235}U		^{238}U (Ma)		^{206}Pb (Ma)		correlation	(%)
9.1	1.54	0.00	41.4	5.68	1.5	0.3473	1.3	0.1185	0.75	1922	22	1934	13	0.866	1
10.1	1.64	0.02	47.8	5.61	1.5	0.3449	1.3	0.1180	0.77	1910	21	1926	14	0.855	1
11.1	1.32	0.05	75.7	5.67	1.3	0.3499	1.2	0.1175	0.50	1934	19	1919	9	0.917	−1
12.1	1.17		78.2	5.71	1.3	0.3510	1.2	0.1180	0.40	1939	21	1925	7	0.950	−1
13.1	1.64	0.00	55.3	5.59	1.2	0.3441	1.2	0.1179	0.47	1906	19	1924	9	0.925	1
14.1	1.77	0.00	31.2	5.54	1.4	0.3420	1.3	0.1175	0.63	1896	21	1918	11	0.895	1
15.1	1.26	0.02	187.0	5.59	1.2	0.3454	1.2	0.1174	0.27	1912	19	1917	5	0.973	0
16.1	1.44	0.01	79.5	5.26	1.2	0.3234	1.1	0.1179	0.42	1806	18	1924	8	0.936	6
17.1	1.42	0.05	45.5	5.72	1.3	0.3536	1.2	0.1174	0.57	1952	20	1917	10	0.905	−2

Notes: Pbc is common Pb.
Pb* is radiogenic Pb.

Hartley Hill, but its resolution progressively deteriorated towards the top of the quarry perhaps as an effect of increased weathering. The HIG1 component in the unit HAE (α_{95} = 43.7° and k = 4.0) and in unit HAH (where it was only recorded by two samples) were not included in the component mean calculation. In other upper units from the quarry (i.e., HL04, HAF and HAG), the HIG1 component was present in 30–50% of samples, and α_{95} values range from 21.9° to 23.4°. A cut-off of $\alpha_{95} \leq 16°$ for inclusion of values in mean calculations is usual, but a higher cut-off of 25° was employed here. The HIG1 component in unit HL04 is distinct from the other sites (Fig. 5C), in that it is shallow and upwards directed, and was excluded from the mean HIG1 component calculation (Table 3).

4.3.2. O'Doneghue Farm

At O'Doneghue Farm, lava of the Hartley Formation is foliated and appears to be more altered (i.e., more greenish). Random lower coercivity components are removed in all specimens with demagnetization below 60–80 mT. At higher levels of demagnetization a consistent east-south-easterly and upward directed (in geographic coordinates) characteristic component was revealed, and is labelled HIG2 (Fig. 5D). The easterly and upward directed grouping of high coercivity components restores to a north-easterly and downward directed position upon structural correction. This component (viewed either in geographic or tilt-corrected coordinates) has not been identified at Hartley Hill.

4.3.3. Pramberg Farm

Quartz porphyry outcrops as low hills towards the southeast of Volop Group quartzite ridges on the Pramberg Farm. The quartzite dips steeply (at ~53°) towards the west, which is taken as the attitude of the porphyry as well. Demagnetization of nine specimens yielded disappointingly disparate results that were challenging to interpret. Apart from a couple present field-like components, a easterly upwards directed component (in geographic coordinates) emerges in three specimens, which is comparable to the HIG2 component identified at O'Doneghue (Fig. 5D). At both Pramberg and O'Doneghue, the HIG2 component is very poorly constrained and is excluded from further discussion.

5. Discussion

5.1. Age of the Hartley Formation volcanism and related magmatism

The dates obtained on zircons from the quartz porphyry in drillcore from Mooihoek (MHK1/86) demonstrate an age of 1920 ± 4 Ma, which is within error of a new SIMS age of 1915 ± 3 Ma from the Pramberg porphyry (Dave Cornell, pers. comm. 2015). Variability in ages is unsurprising for rift related volcanism, as often isolated graben systems each recorded a unique sedimentary and volcanic fill (e.g., de Kock et al. 2012). The TDS sample RP353 was here dated to 1923 ± 6 Ma, which is comparable to ca. 1927 Ma ages obtained for broadly coeval mafic sills in Botswana by Hanson et al. (2004). These ages are also comparable with those of the youngest concordant detrital zircon grains (1931 ± 20 and 1957 ± 18 Ma), from sample BOS10, which are considered to

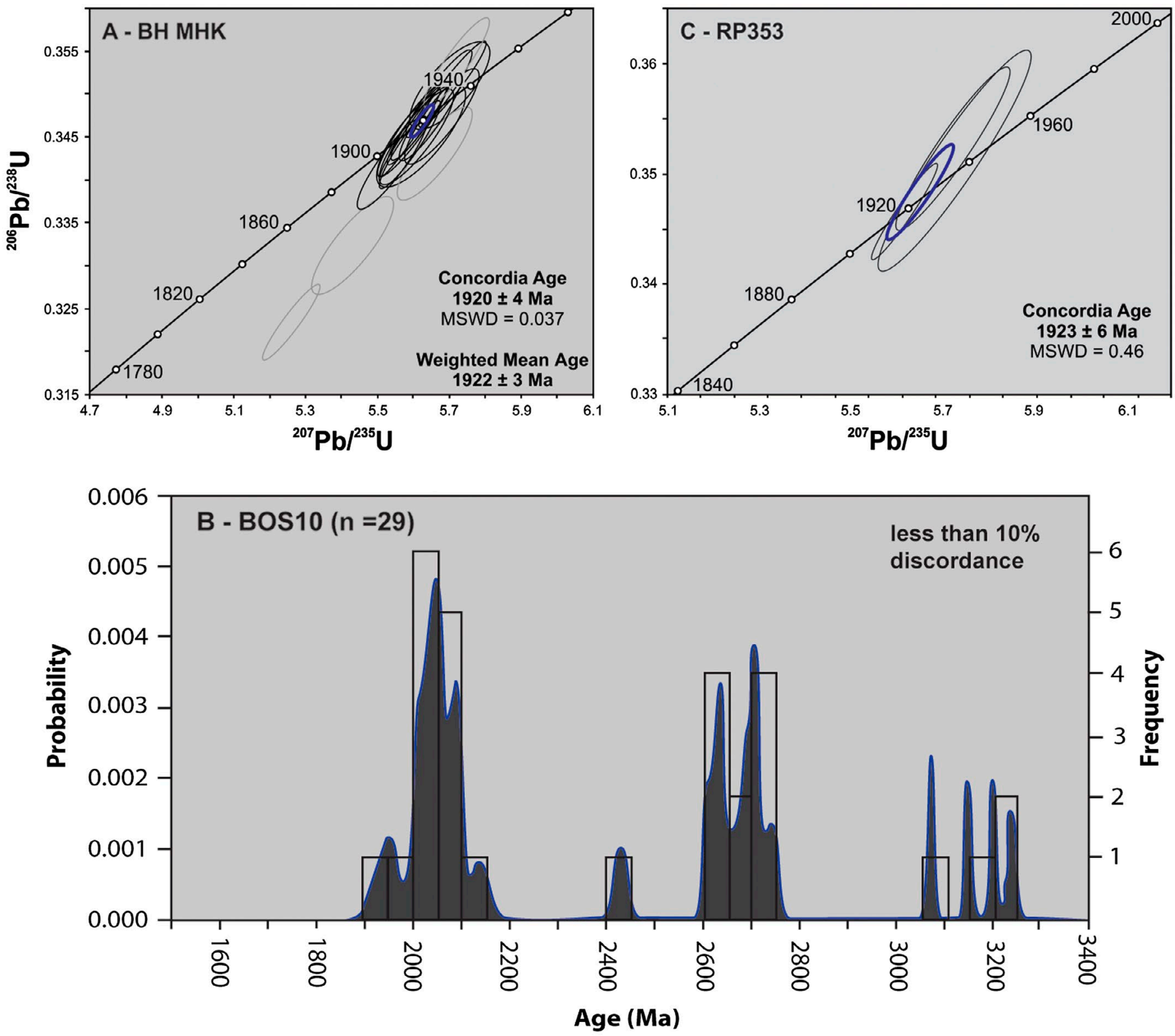

Fig. 3. U–Pb geochronological results from SHRIMP on zircon and ID-TIMS on baddeleyite. **A**. Concordia diagram illustrating ages of zircon grains from the Mooihoek quartz prophyry (sample BH-MHK) of the Hartley Formation. **B**. Spectrum of detrital populations of sample BOS10 from the Boegoeberg Dam Formation on the farm Bovenseekoebaard shown as an age histogram and as a relative probability curve. Included are $^{207}Pb/^{206}Pb$ ages of individual zircon grains that were less than 10% discordant. **C**. Concordia diagram for the analyses of baddeleyite fractions from a dyke of the Tsineng Dyke Swarm in drill core from borehole RP353 at Smartt Mine in the Kalahari Manganese Field near Tsineng.

Table 2. Summary of ID-TIMS geochronological data on baddeleyite.

Analysis No. (number of grains)	U/ Th	Pbc/ Pbtot[1]	$^{206}Pb/^{204}Pb$ raw[2]	$^{207}Pb/^{235}U$	±2σ % err.	$^{206}Pb/^{238}U$	±2σ % err.	$^{207}Pb/^{235}U$	$^{206}Pb/^{238}U$	$^{207}Pb/^{206}Pb$	±2σ	Concordance
				[corr.][3]				[age, Ma]				
Bd-1 (9)	4.1	0.384	121.5	5.7238	1.78	0.35232	1.73	1935.0	1945.6	1923.5	11.2	1.011
Bd-2 (12)	5.8	0.213	286.3	5.7280	2.41	0.35118	2.35	1935.6	1940.2	1930.6	14.2	1.005
Bd-3 (16)	4.6	0.075	828.4	5.6202	1.04	0.34661	1.03	1919.2	1918.4	1920.0	5.2	0.999

[1]Pbc = common Pb; Pbtot = total Pb (radiogenic + blank + initial).
[2]Measured ratio, corrected for fractionation and spike.
[3]Isotopic ratios corrected for fractionation (0.1% per amu for Pb), spike contribution, blank (1 pg Pb and 0.1 pg U) and initial common Pb. Initial common Pb corrected with isotopic compositions from the model of Stacey and Kramers (1975) at the age of the sample.

Table 3. Summary of palaeomagnetic results.

Location (Strike/Dip)	Site	n/N	Declination (in °)	Inclination (in °)	α_{95} (in °)	k	Latitude (in °N)	Longitude (in °E)	(dp, dm) or A95 (in °)
			Present field-like (geographic coordinates)						
Hartley Hill (89°/22°S)	HAA and HL01*	9/16	332.4	−52.4	7.4	48.9			
(60°/7°SE)	HAB and HL02*	10/15	50.2	−63.8	9.8	25.2			
(32°/7°E)	HAD	4/5	43.0	−65.4	40.4	4.2			
(90°/22°S)	HAC and HL03*	9/11	15.6	−64.3	17.2	9.9			
(120°/4°SW)	HL04*	3/4	346.4	−46.9	37.4	7.9	No poles calculated for present present field-like Component A		
(90°/22°S)	HAE and HL05*	12/14	348.4	−80.0	16	8.4			
(88°/22°S)	HAF and HL06*	5/14	40.9	−28.3	21.6	13.5			
(66°/10°SE)	HAG and HL07*	4/14	18.5	−43.5	18.5	25.6			
Pramberg (107°/53°W)	HBA	3/9	349.3	−61.2	14.2	51.2			
	A Mean	7/9	14.8	−59.2	17.4	13			
			Component INT (geographic coordinates)						
Hartley Hill (88°/22°S)	HAF and HL06*	7/7	199.7	−16.8	9.8	39.2	48.8	53.2	(5.2, 10.1)
(75°/6°SE)	HAH and HL08*	8/12	154.3	7.8	30.5	4.3	55.7	332.6	(15.5, 30.7)
	JP-11**	5/10	180.5	−28.1	5.8	69.2	50.1	26.1	(3.5, 6.4)
			Component HIG1						
Location (strike/dip)	Site	n/N	Declination and inclination (in °) (geographic coordinates)	Declination and Inclination (in °) (tilt-corrected coordinates)	α_{95} (in °)	k	Latitude (in °N)	Longitude (in °E)	(dp, dm) or A95 (in °)
Hartley Hill (89°/22°S)	HAA and HL01*	8/16	293.4, 28.0	289.1, 26.6	13.0	19.2	9.6	314.4	(7.7, 14.1)
(60°/7°SE)	HAB and HL02*	8/15	305.4, 35.0	304.9, 36.9	14.1	16.3	18.0	329.0	(9.7, 16.5)
(90°/22°S)	HAC and HL03*	3/11	318.4, 44.8	322.8, 50.6	18.6	30.1	21.0	349.2	(16.8, 25.0)
(32°/7°E)	HAD	3/5	291.7, 31.3	291.2, 34.6	15.5	42.6	8.6	319.8	(10.2, 17.8)
(90°/22°S)	HAE and HL05*	5/14	310.0, 26.6	310.9, 25.1	43.7	4.0	27.2	327.0	(25.3, 47.0)
(88°/22°S)	HAF	4/14	307.5, 36.1	306.4, 38.0	23.4	12.3	18.6	330.5	(16.3, 27.7)
(66°/10°SE)	HAG and HL07*	4/14	312.0, 40.7	312.2, 44.1	22.7	17.3	19.3	337.9	(17.8, 28.4)
(75°/6°SE)	HAH and HL08*	2/12	303.7, 36.1	302.7, 37.0	–	–	16.4	327.6	–
(120°/4°SW)	HL04*	4/4	274.9,-16.9	275.7, −15.2	21.9	13.9	6.9	257.7	(11.5, 22.5)

	Hartley Mean	6/9		303.3, 39.0	10.6	40.6	16.1	329.9	11.0
Moshaneng (*no correction*)	JP-9**	14/0	324.1, 7.2	324.1, 7.2	6.3	40.2	45	329.4	(3.2, 6.4)
(*no correction*)	JP-10**	13/1	315.0, 0.9	315.0, 0.9	7.5	31.6	39.6	318.5	(3.7, 7.5)
Hartley Hill + Moshaneng	Hartley Mean	8/12		308.2, 30.6	14.6	15.4	22.7	328.6	11.7
Component HIG2 (geographic coordinates)									
Pramberg (107°/53°W)	HBA	4/9	114	−66.4	27.5	9.1	16.5	345.3	(28.9, 39.3)
O'Doneghue (99°/62°SW)	HCA	5/8	120	−55.5	26	7.7	4.7	338.1	(26.5, 37.1)

Notes: *Italic font* = data excluded from mean calculation.
n/N = number of samples included incomponent site mean/total number of samples collected at site.
*Sampled by Evans et al. (2002).
**Sampled by Hanson et al. (2004).

represent the timing of eruption of the Boegoeberg Dam mafic lava unit. This unit may thus be considered the age equivalent to the Hartley Formation as suggested by Cornell et al. (1998). An age range of 1927–1915 Ma can thus be placed on the Hartley Formation bimodal igneous rocks from the work in this study combined with the work of Cornell et al. (1998) and Hanson et al. (2004).

5.2. *Identifying the potential Hartley LIP and dynamics of late Palaeoproterozoic rifting*

With the now well-dated 1.93–1.91 Ga magmatic units of the Hartley Formation, Boegoeberg Dam Formation, TDS, Moshaneng sills and Trompsburg Complex, a large scale bimodal magmatic event is be recognized. We propose that these magmatic units be incorporated into a LIP, the Hartley Event. Its size (footprint on the order 4×10^5 km^2) is compatible with the magnitude of known LIP dimensions (Coffin & Eldholm 1993; Ernst 2014), but the duration of emplacement for the Hartley igneous rocks is longer than most typical LIPs according to the LIP definition (Ernst 2014).

Tinker et al. (2002) reported on a seismic reflection profile spanning the western margin of the northern Kaapvaal Craton (see Fig. 6 for the exact locality), and presented insight into the dynamics and structure associated with the extensional event that culminated in the emplacement of the Hartley LIP. Late Palaeoproterozoic extension was initiated before, but continued during eruption of the Hartley volcanic rocks (Tinker et al. 2002). According to Tinker et al. (2002), an unknown amount of extension occurred along such deep crustal structures as the Moshaweng Normal Fault (Fig. 6.), a prominent N–S trending normal fault that was reactivated or initiated by late Palaeoproterozoic rifting. According to Moen (2006), early graben formation is not evident from surface exposures, but the predominance of rudites in drillcore north of Olifantshoek suggest that the basal parts of the Elim Group were deposited in grabens. Late Palaeoproterozoic deformation along structures like the Moshaweng Fault was associated with the development of a series of normal faults, and caused relative uplift of the Elim Group in the form of a rollover anticline (Tinker et al. 2002). Continued extension resulted in the formation of half-grabens bounded on their east side by structures like the Moshaweng Fault and an anticlinal structure to their west side (Fig. 6 inset). The half-grabens were then later filled by erosional products, such as the Elim Group (i.e., the conglomerates and quartzites at the base of the Hartley Formation), followed by volcanic products of the Hartley Formation. A system of similar half-graben structures probably punctuated by several volcanic centres extended towards the south along the western Kaapvaal margin, as evidenced by the ca. 1.93 Ga Boegoeberg Dam Formation (Fig. 6). Flexural analyses (Tinker et al. 2004) have shown that the elastic lithosphere along this western margin was significantly reduced (to as little as 7.5 km, compared to the present day 60–70 km thickness) between ca. 1.93 and 1.75 Ga, suggesting that a significant amount of crustal thinning took place during this extensional event.

Our 1923 ± 6 Ma age for the TDS, which is truncated by the Kheis Province and extends towards the east-north-east, with a strike length of ~500 km into the cratonic hinterland (Fig. 6), probably dates an arm of NW-SE extension associated with rift-

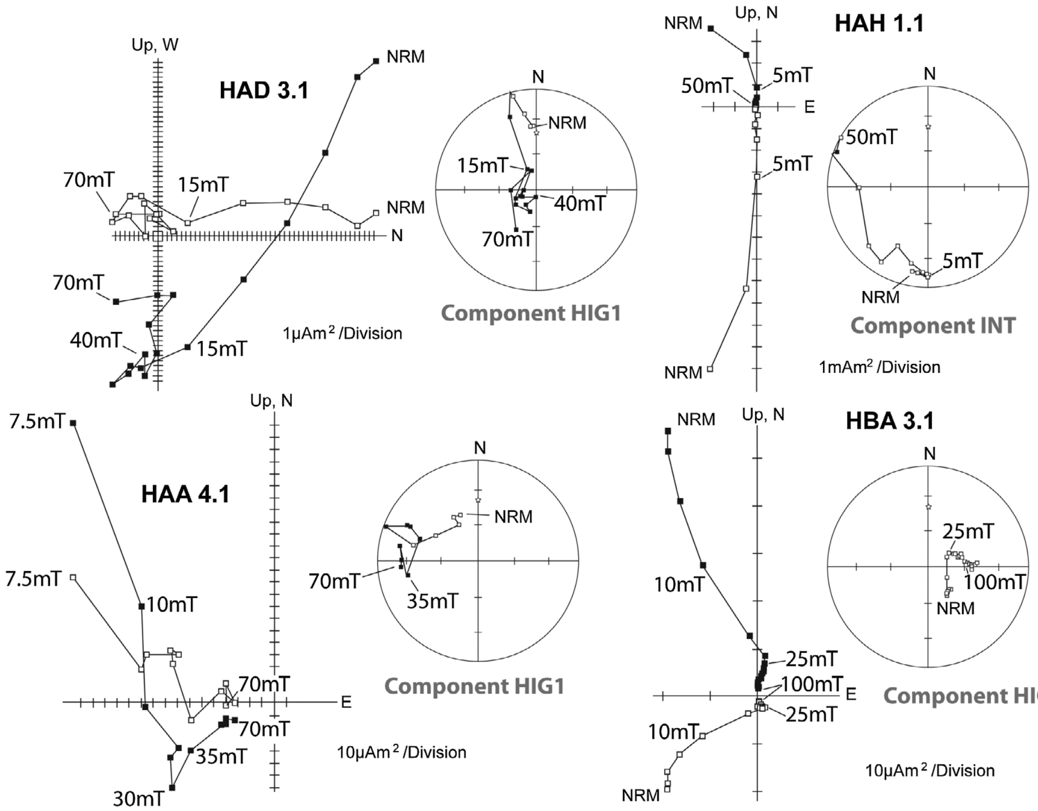

Fig. 4. Representative demagnetization behaviour for the Hartley volcanic rocks in geographic coordinates. Open symbols plot in the upper hemisphere of equal area plots, while solid symbols plot in the lower hemisphere. Open symbols on the orthogonal plots represent the projection of vector endpoints onto the horizontal plane, while closed symbols represents the projection of vector endpoints onto a vertical plane.

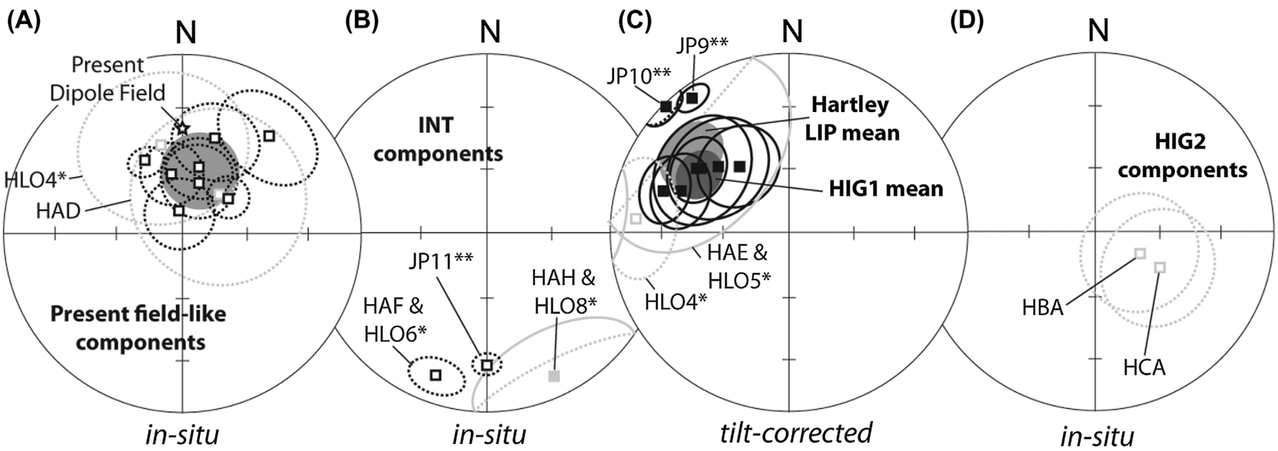

Fig. 5. Site and component means for magnetic components identified during this study. Ellipses are cones of 95% confidence (or α_{95}) about component means (shown as squares). Stippled ellipses and open squares plot in the upper hemisphere of the equal area diagrams, while solid ellipses and closed squares are in the lower hemisphere. Lighter shaded symbols and ellipses are from sites that were excluded from component mean calculations. Data from Evans et al. (2002) are identified by an *, whereas those from Hanson et al. (2004) by **. **A**. Low coercivity, present Earth field-like components (in geographic coordinates) with the present dipole field of the Earth shown as a star. **B**. Component INT site means compared to a similar component from a sill in Botswana (JP11), in geographic coordinates. **C**. Component HIG1 site means in tilt-corrected coordinates compared to similar components from sills in Botswana. **D**. Poorly constrained Component HIG2 site means in geographic coordinates.

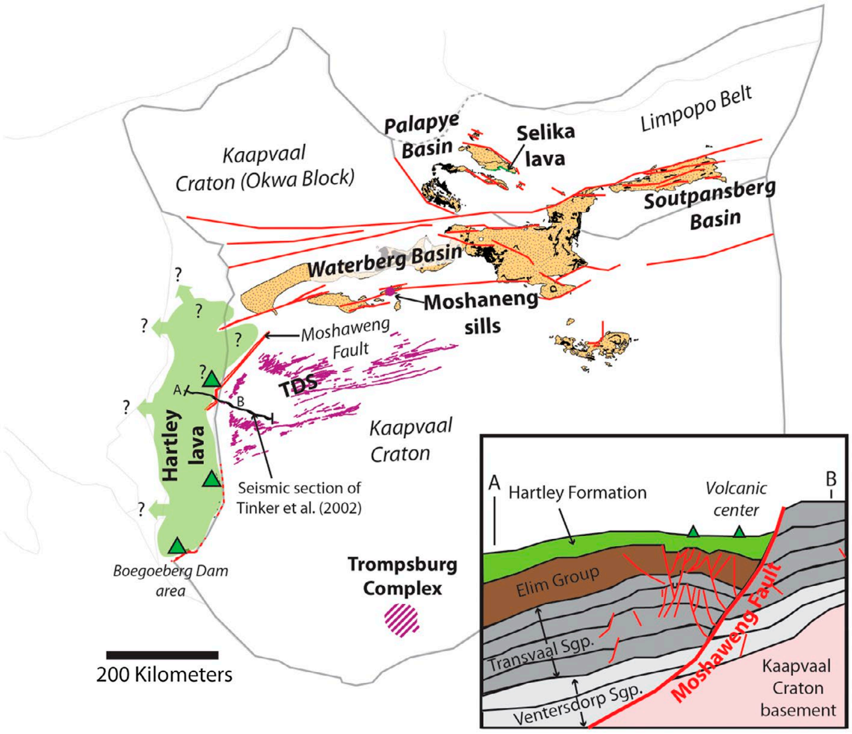

Fig. 6. Possible original extent and structural setting of the Hartley LIP event in relation to areas of red bed deposition across the Kaapvaal Craton and dominant volcanic centers (green triangles). Inset displays half-graben and rollover anticline structures west of the Moshaweng Fault (after Tinker et al. 2002).

ing. The Moshaweng Fault can be traced further towards the north where its trend swings towards the ENE–WSW (Fig. 6), becoming parallel to the trend of the TDS. Goldberg (2010) interpreted the TDS as part of a failed arm of the Palaeoproterozoic rifting along the western Kaapvaal Craton margin. In addition, the present day outcrop distribution of the Waterberg and Soutpansberg basins occur along a similar ENE–WSW axis as that of the TDS, and these basins have been proposed to occupy an aulocogen (Cornell 1987) or series of rifts (e.g., Barker 1983), and fault-bounded pull-apart basins (Eriksson et al. 2006), that acted as a long-lived (2.045 Ga to at least 1.83 Ga) areas of sediment accumulation.

The emplacement of the 1915 Ma Trompsburg Complex and ca. 1927 Ma Moshaneng Sills in the cratonic interior (Fig. 6), provide evidence for a larger volume of magma generation possibly associated with Palaeoproterozoic rifting. The exact relationship of the Trompsburg Complex to the Hartley LIP and rifting is not fully understood, although it is broadly coeval.

5.3. Hartley Formation palaeopole and the late Palaeoproterozoic APWP of the Kaapvaal Craton

The HIG1 component is a consistent characteristic remanent direction (Fig. 5C) for the Hartley Formation. A palaeopole at 16.1°N, 329.8°E with A_{95} = 11.0° can be calculated by combining six of our site virtual geomagnetic poles (VGPs) (Table 3, Fig. 7B, C). Like Evans et al. (2002), we too cannot be sure that our data effectively average out palaeosecular variation of the Earth's magnetic field. The averaging of secular variation can perhaps be addressed to some extent by adding the results from the ca. 1927 Ma Moshaneng sills (Hanson et al. 2004) to our data for the calculation of a 1927–1915 Ma mean palaeopole (Table 3). VGPs from the ca. 1927 Ma Moshaneng sills plot removed from, but in a generally similar region as our calculated site VGPs for the Hartley Formation. This might be expected given a possible age difference between the Moshaneng Sills and Hartley lava, but could also be due to unrecognized vertical axis rotation of about 15° during the development of the Kheis Province. The 1927–1915 Ma mean palaeopole is located at 22.7°N, 328.6°E with A_{95} = 11.7° (Fig. 7B, C), and rates as a 4 out of 7 on the Q-scale of reliability of Van der Voo (1990). By no means ideal (too few sample sites, lack of a field test and magnetic reversals), our new 1927–1915 Ga Hartley LIP palaeopole can still be considered a significant improvement on the existing VGP of Evans et al. (2002), given the significant increase in the number of samples per cooling unit, and the statistically sound palaeopole calculation.

The identified INT component yields a VGP at 48.8°N and 53.2°E (dp = 5.2, dm = 10.1) for site HAF, where it was best developed. Compared to palaeopoles from the Kaapvaal Craton (Table 4 and Fig. 7A), this VGP is very similar to the 1.2–1.1 Ga poles of the Kaapvaal Craton. A similar magnetic component was identified by Hanson et al. (2004) in a 1927 ± 1 Ma Moshaneng dolerite sill from Botswana (i.e., their JP11 sill, shown for comparison in Fig. 5B), where it was interpreted to be a 1.11 Ga magnetic overprint.

Several new palaeopoles and new age constraints (listed in Table 4) have been published since the last attempted reconstruc-

Table 4. Poles calculated during this study and a selection of published Late Palaeoproterozoic and Mesoproterozoic poles from the Kaapvaal Craton.

Rock Unit	Abbreviation	Age (Ma)	Age reference	Latitude (in °N)	Longitude (in °E)	(dp, dm) or A95 (in °)	Palaeopole reference
			Palaeoproterozoic palaeoples				
Ongeluk Lava	ONG	2222 ± 13	Cornell et al. (1996)	22	−0.5	5.3	Evans et al. (1997)
Basal Gamagara/Mapedi Formation	BGM	~2200 or	Evans et al. (2002)	2.2	81.9	(7.2, 11.5)	Evans et al. (2002)
Elim Group		~2000	Da Silva (2011)				
Phalaborwa Complex	PC	2061 ± 1	Reischmann (1995)	27.7	35.8	6.6	Letts et al. (2010)
Bushveld Complex	BC	2054 ± 1	Scoates & Friedman (2008)	19.2	30.8	5.8	Letts et al. (2009)
Bushveld B1 sills	B1	2058 ± 6	Wabo et al. (2015a)	13.1	44	14.3	Wabo et al. (2015a)
Uitkomst Complex	UC	2055 ± 7	Wabo et al. (2015b)	28.7	58.5	(6.2, 9.4)	Wabo et al. (2015b)
Waterberg unconformity	WUBS1	≤2054 ± 4	Dorland et al. (2006)	36.5	51.3	10.9	de Kock et al. (2006)
bounded sequence 1							
Vredefort Impact	VRED	2023 ± 4.0	Kamo et al. (1996)	21.8	44.5	(11.3, 15.4)	Carpozen et al. (2006)
Witwatersrand Supergroup	WITS	1945–2050	Layer et al. (1988)	26.1	22.3	(7.9, 10.3)	Layer et al. (1988)
Overprint							
Waterberg unconformity	WUBS2	>1930	de Kock et al. (2006)	−10.5	330.4	9.8	de Kock et al. (2006)
bounded sequence 2							
Hartley Formation VGP	HAR VGP	1928 ± 4	Cornell et al. (1998)	12.5	332.8	16	Evans et al. (2002)
Hartley Formation Palaeopole	HIG1	1921 ± 4	THIS STUDY	16.1	329.9	11	THIS STUDY
JP9 Mosheneng Sill	JP9	1928 ± 1	Hanson et al. (2004)	45	329.4	(3.2, 6.4)	Hanson et al. (2004)
JP10 Mosheneng Sill	JP10	1928 ± 1	Hanson et al. (2004)	39.6	318.5	(3.7, 7.5)	Hanson et al. (2004)
Hartley LIP	HAR LIP	1927–1915	THIS STUDY	22.7	328.6	11.7	THIS STUDY
							recalculated using Evans et al. (2002)
Sand River Dykes	SRD	1876 ± 73	Morgan and Briden (1981)	2.3	9.1	10.3	Morgan and Briden (1981)
Post-Waterberg Dolerites	PWD	1879–1872	Hanson et al. (2004)	15.6	17.1	8.9	Hanson et al. (2004)
Post-Phalaborwa Dykes	PPD	1857–1839	Olsson et al. (2015)	7.6	12.1	11.8	Letts et al. (2010)

(*Continued*)

Table 4. (*Continued*).

Rock Unit	Abbreviation	Age (Ma)	Age reference	Latitude	Longitude	(dp, dm) or A95	Palaeopole reference
				(in °N)	(in °E)	(in °)	
Post-Bushveld Dykes	PBD	1857–1839	Olsson et al. (2015)	12.6	24.1	10.8	Letts et al. (2010)
Black Hills Dyke Swarm	BHD	1857–1840	Olsson et al. (2015)	9.4	352	(4.3, 5.8)	Lubnina et al. (2010)
Mashonaland Sills	MASH	1886–1872	Hanson et al. (2011)	6.5	338.5	5	Hanson et al. (2011)
(Zimbabwe)			Söderlund et al. (2010)				
			Mesoproterozoic Palaeoploes				
Premier Kimberlite	P	~1200–1180	Hanson et al. (2006)	51.3	37.9	(4.0, 7.5)	Hargraves & Onstott (1980)
Kalkpunt Formation	KP	1093 ± 7	Pettersson et al. (2007)	57	183	(4.0, 7.0)	Briden et al. (1979)
Umkondo Dolerites	UMK	1108–1112	de Kock et al. (2014)	64	38.8	3.7	Gose et al. (2006)
Namaqua Eastern Zone	NEZ	<1165	Pettersson et al. (2007)	44.9	21.5	12.8	Evans et al. (2002)
Namaqua-Natal	NAM	~1000	Gose et al. (2013)	9.4	329.5	17.8	Gose et al. (2013)
Metamorphic Rocks							
Hartley Component INT	INT	~1100	THIS STUDY	48.8	53.2	(5.2, 10.1)	THIS STUDY

tion of the Palaeoproterozoic APW path of the Kaapvaal Craton (de Kock et al. 2006). In the proposed path of de Kock et al. (2006), a pre-Bushveld age for the Elim Group was assumed following the work of Evans et al. (2002). Recent indications by Da Silva (2011) suggest that the Elim Group may post-date emplacement of Bushveld Complex as proposed by Moen (2006), which may have significant implications for how the APW path is constructed, and paths for both age options of the Elim Group are presented (Fig. 7).

5.3.1. *A pre-Bushveld age for the Elim Group*

In the pre-Bushveld age option for the Elim Group, the late Palaeoproterozoic APW path of the Kaapvaal Craton (Fig. 7B) begins from the Gamagara-Mapedi Formation palaeopole of Evans et al. (2002) from the base of the Elim Group. From here the path is constrained by a 2060–2024 Ma cluster of palaeopoles (see Table 4 for details on individual poles and their age constraints). This cluster includes poles from the 2060 Ma Phalaborwa Complex (Letts et al. 2010), 2059–2054 Ma Bushveld LIP (Letts et al. 2009; Wabo et al. 2015a, b), the Bushveld Complex-induced magnetic overprint pole from the Mesoarchean Witwatersrand Supergroup (Layer et al. 1988), the younger than 2054 Ma first unconformity-bounded sequence of the Waterberg Group palaeopole or WUBS1 pole (de Kock et al. 2006), and the 2023 Ma Vredefort impact structure (Carpozen et al. 2006). From here the pre-1.9 Ga palaeopole from the second unconformity-bounded Waterberg Group sequence or WUBS2 palaeopole (de Kock et al. 2006) suggests a long southwesterly swath of the APW path (Fig. 7B). Our 1927–1915 Ma mean palaeopole from the Hartley LIP is located at a hairpin of the APW path (Fig. 7B), where the path loops back on itself towards ca. 1.8 Ga poles. The ca. 1.8 Ga cluster includes a palaeopole from the 1.88–1.84 Ga Post-Waterberg sills by Hanson et al. (2004), and palaeopoles from the NNE–SSW and NE–SW trending dykes of the Black Hills Dyke Swarm (Morgan 1985; Letts et al. 2010; Lubnina et al. 2010; Olsson et al. 2015). The Black Hills Dyke Swarm includes the so-called Sand River dykes and post-Bushveld dykes.

5.3.2. *A post-Bushveld age for the Elim Group*

In this option (Fig. 7C), the APW path starts with the 2.06–2.02 Ga palaeopole cluster as defined above (Section 5.3.1.), then moves a short distance to the ca. 2.0 Ga Elim Group Gamagara–Mapedi Formation palaeopole (Evans et al. 2002). Evans et al. (2002) also illustrated this possibility, but not as their preferred choice. The next youngest palaeopole is the WUBS2 palaeopole (de Kock et al. 2006), but instead of requiring a long southwesterly swath of the path as in Fig. 7B, by choosing an opposite polarity option for this pole, the APW path continues towards the east (Fig. 7C). Palaeopoles can be represented either as a North Pole or South Pole when defining APW paths, given the ambiguity of magnetic reversals in the past. However, the next younger palaeopole in a path is usually placed in the polarity option that minimizes the path length between successive poles. From the

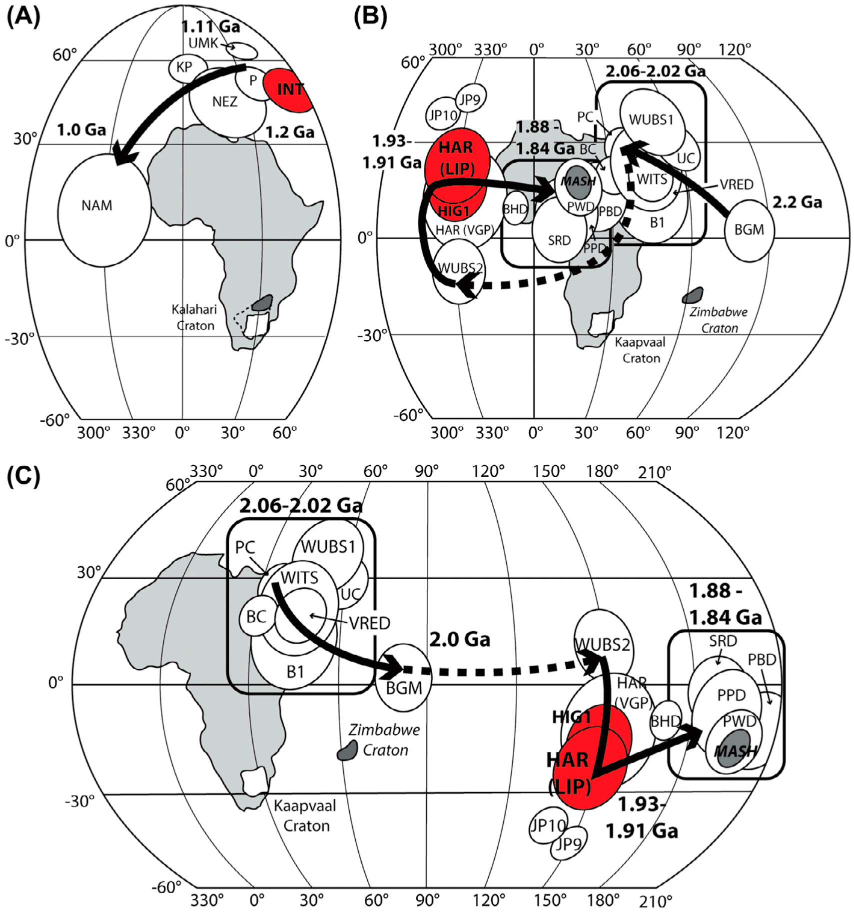

Fig. 7. **A**. Component INT this study (in red) compared with Mesoproterozoic poles from the Kaapvaal Craton. The 1.2–1.0 Ga segment of the Mesoproterozoic APW path is shown as a thick black arrow after Gose et al. (2013). For pole abbreviations and more details on their ages, see Table 3. **B**. Late Palaeoproterozoic APW path (thick black arrow) of the Kaapvaal Craton with a pre-Bushveld age for the Elim Group. **C**. Alternative late Palaeoproterozoic APW path (thick black arrow) for the Kaapvaal Craton with a post-Bushveld age for the Elim Group. The relative position of the Zimbabwe Craton with respect to the Kaapvaal Craton at 1.88 Ga (rotated −39° around an Euler pole at 69.4°S and 50.9°E; Hanson et al. 2004), is shown in both Late Palaeoproterozoic APW path options. The Zimbabwean Mashonaland sills pole (MASH) is shaded, while poles presented in this study are shown in red. APW path is stippled for times of poor data coverage.

WUBS2 palaeopole, the path swings slightly south towards our 1.93–1.91 Ma Hartley LIP palaeopole (opposite polarity option), and continues eastwards towards the opposite polarity option of the 1.88–1.84 Ga pole cluster (Fig. 7C). This radically different interpretation of the Kaapvaal Craton's late Palaeoproterozoic APW path segment eliminates the need for a loop in the APW path of the Kaapvaal Craton.

5.4. The late Palaeoproterozoic magmatic record of the Kaapvaal Craton and constraints on Kalahari Craton assembly

Within basal sections of the Waterberg Group, which is otherwise devoid of volcanic rocks, bimodal volcanic rocks are preserved (yielding 2054 ± 4 and 2021 ± 5 Ma ages; Dorland et al., 2006). The 1927–1915 Ma Hartley LIP (this study) represents the next record of volcanic and magmatic activity for the Kaapvaal Craton. This event may also include the undated mafic volcanic rocks of the lower Selika Formation of the Palapye Group of Botswana. It is followed by extensive 1.88–1.83 Ga intraplate magmatism. Sills that intrude the Waterberg Group (Fig. 1) were dated in the 1879–1872 Ma age range (Hanson et al. 2004), while the extensive NE–SW trending Black Hills Dyke Swarm (Fig. 1) have been shown to have ages ranging from 1857–1839 Ma (Olsson et al. 2015). The post-Waterberg dolerite sills were correlated with the basal volcanic units preserved in the Soutpansberg Group. However, recent dates by Geng et al. (2014) suggest that the Sibasa Formation of the Soutpansberg Group is younger. The 1831 ± 15 and 1832 ± 9 Ma detrital zircon ages from Sibasa Formation by Geng et al. (2014) are closer to the younger range of dolerite dyke ages found by Olsson et al. (2015) for the Black Hills Dyke Swarm. The Kaapvaal Craton likely experienced an extended period of intraplate magmatism starting with the 1879–1872 Ma post-Waterberg sills and ending with the extrusion of the Sibasa Formation at 1832 Ma. Younger, but less-well dated magmatic units are also found in the upper Soutpansberg Group, as well as within the Brulpan Group along the craton's western margin. The age of Palaeoproterozoic

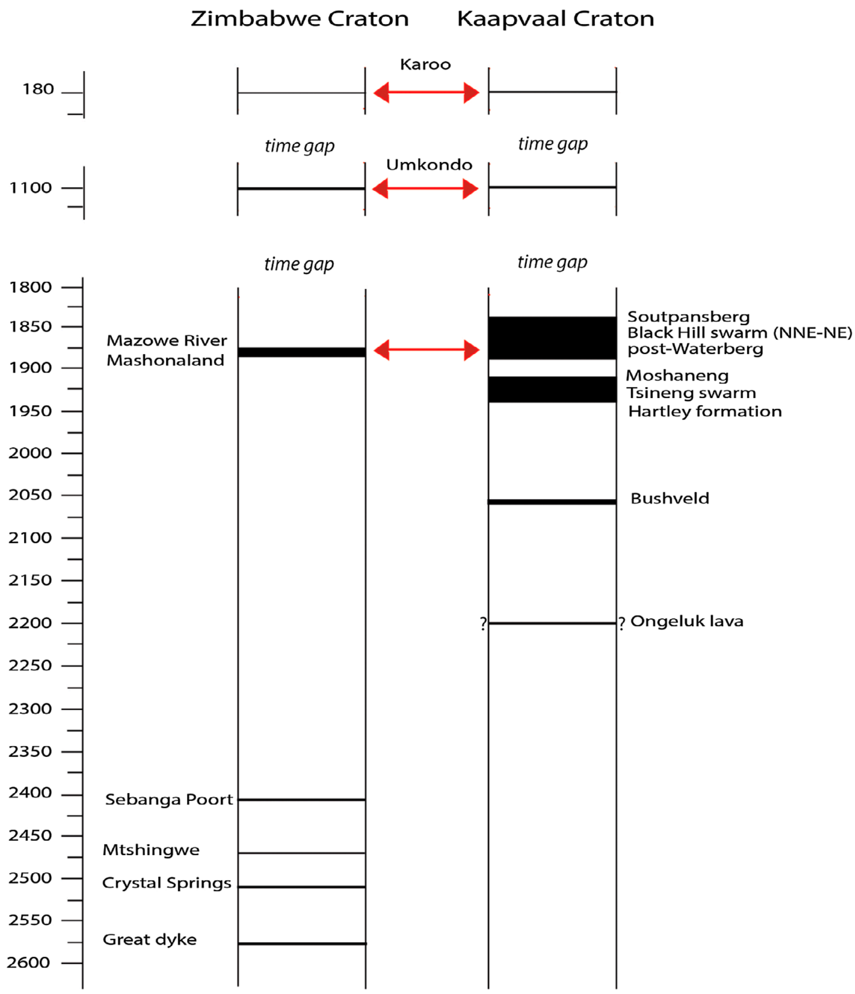

Fig. 8. Magmatic barcodes for the Kaapvaal and Zimbabwe cratons modified after Söderlund et al. (2010).

sills in the Soutpansberg Group are only constrained by a Rb–Sr isochron age of 1797 ± 104 Ma (Barton 1979; recalculated using λ^{87}Rb of Rotenberg et al. 2012). The Brulpan Group (i.e., the Skerpioenpunt Member) yielded a recalculated Rb–Sr whole rock errorchron age of 1095 ± 144 Ma (Barton & Burger 1983; Rotenberg et al. 2012), suggesting Sr-isotopic homogenization during the Namaqua–Natal Orogeny (Barton & Burger 1983). These volcanic rocks might be the equivalents of unaltered dolerite sills and dykes that intrude the Olifantshoek Supergroup within numerous borehole cores. One such dolerite sill crosscuts foliated Hartley Formation south of Olifantshoek on the farm Mamatlun (Fig. 1), and Cornell et al. (1998) reported a Rb–Sr biotite mineral age of 1797 ± 60 Ma (also adjusted using new decay constant value by Rotenberg et al. 2012). A possibility that this younger ca. 1.80 Ga igneous event may be more widespread so as to include the Skerpioenspunt volcanic rocks of the Groblerhoop Group and the Soutpansberg's Ngwanedzi volcanic rocks and sills was highlighted by Dorland et al. (2006), but remains untested.

It has been pointed out by Söderlund et al. (2010) that the 1927–1915 Ma magmatic event appears to be unique for the Kaapvaal Craton, which is in contrast to the 1.88–1.83 Ga event that can be identified in both the Kaapvaal and Zimbabwe cratons. In Zimbabwe, the intrusion of the Mashonaland sills has been dated to between 1886 and 1871 Ma (Söderlund et al. 2010; Hanson et al. 2011). This indicates that the two cratons might have been "nearest neighbours" as defined by Bleeker & Ernst (2006) at ca. 1.88 Ga. However, Hanson et al. (2011) argued for a greater than 2000 km displacement between the Kaapvaal and Zimbabwe cratons based on the difference between their ca. 1.88 Ga palaeopoles (Fig. 7B, C). The Zimbabwe Craton does not share a record of the Kaapvaal Craton Hartley LIP at 1.93–1.91 Ga (Fig. 8), which appears to have been emplaced during an early phase of Kalahari Craton assembly.

6. Conclusion

A SHRIMP U–Pb zircon age of 1920 ± 4 Ma for the Hartley Formation (Olifantshoek Supergroup) on the western margin of the Kaapvaal Craton of South Africa is presented. Together with a new maximum concordant detrital zircon age of 1931 ± 20 Ma for a coeval unit 140 km to the south, and a new 1923 ± 6 Ma U–Pb ID-TIMS baddeleyite date from the Hartley-related Tsineng Dyke Swarm, a potential LIP, herein named the "Hartley Event", is now recognized. Included in the potential Hartley LIP are previously dated 1.93–1.91 Ga magmatic units of the Kaapvaal Craton (i.e., Moshaneng sills and Trompsburg Complex). In addition, the new palaeomagnetic data presented in this paper from the Hartley Formation are combined with previously published results to define an improved 1.93–1.91 Ga palaeopole for the Hartley LIP that assists in refining the late Palaeoproterozoic APW path of the Kaapvaal Craton.

Acknowledgements – The authors wish to thank Ken Buchan, Don Davis and Henry Halls for their detailed reviews, and especially would like to thank the guest editor Wouter Bleeker for helping to improve this manuscript considerably. The authors also wish to thank David Cornell for mention of his new SIMS age from the Pramberg quartz porphyry. MDK thanks the NRF (through incentive funding), and Jim and Gladys Taylor Trust for financial support. MDK further aknowledges additional funding from CIMERA (DST-NRF Centre of Excellence for Integrated Mineral and Energy Resource Analysis). This is publication No. 56 of the International Government-Industry-Academia Program "Reconstruction of Supercontinents Back To 2.7 Ga Using The Large Igneous Province (LIP) Record, With Implications For Mineral Deposit Targeting, Hydrocarbon Resource Exploration, and Earth System Evolution" (www.supercontinent.org).

Disclosure statement No potential conflict of interest was reported by the authors.

References

Armstrong, R.A., 1987: *Geochronological Studies on Archaean and Proterozoic Formations of the Foreland of the Namaqua Front and Possible Correlates on the Kaapvaal Craton*. Unpublished Ph. D thesis. University of the Witwatersrand, Johannesburg, South Africa. 273 pp.

Barker, O.B., 1983: A proposed geotectonic model for the Soutpansberg Group within the Limpopo Mobile Belt, South Africa. *In* W.J. Van Biljon & J.H. Legg (eds.): *The Limpopo Belt. Special Publications of the Geological Society of South Africa, No. 8*, 181–190. The Geological Society of South Africa, Johannesburg, South Africa.

Barton, E.S. & Burger, A.J., 1983: Reconnaissance isotope investigations in the Namaqua Mobile Belt and implications for Proterozoic crustal evolution – Uppington geotraverse. *In* B.J.V. Botha (ed.): *Namaqualand Metamorphic Complex. Special Publication of the Geological Society of South Africa, No. 10*, 173–191. The Geological Society of South Africa, Johannesburg.

Barton, J.M., 1979: The chemical compositions, Rb-Sr isotopic systematics and tectonic setting of certain post-kinematic mafic igneous rocks, Limpopo Mobile Belt, Southern Africa. *Precambrian Research 9*, 57–80.

Beukes, N.J., Dorland, H.C., Gutzmer, J., Nedachi, M. & Ohmoto, H., 2002: Tropical laterites, life on land, and the history of atmospheric oxygen in the Paleoproterozoic. *Geology 30*, 491–494.

Bleeker, W. & Ernst, R.E., 2006: Short-lived mantle generated magmatic events and theri dike swarms: the key unlocking Earth's paleogeographic record back to 2.6 Ga *In:* E. Hanski, S. Mertanen, T. Rämö & J. Vuollo (eds.): *Dike Swarms: Time Markers of Crustal Evolution*, 3–26. Taylor & Francis/Balkema, Leiden.

Briden, J.C., Duff, B.A. & Kröner, A., 1979: Palaeomagnetism of the Koras group, Northern Cape province, South Africa. *Precambrian Research 10*, 43–57.

Carpozen, L., Gilder, S.A. & Hart, R.J., 2006: Origin and implications of two Verwey transitions in the basement rocks of the Vredefort meteorite crater, South Africa. *Earth and Planetary Science Letters 251*, 305–317.

Coffin, M.F. & Eldholm, O., 1993: Scratching the surface: estimating dimensions of large igneous provinces. *Geology 21*, 515–518.

Compston, W. & Williams, I.S., 1984: U–Pb geochronology of zircons form lunar Breccia 73217 using a sensitive high mass-resolution ion microprobe. *Journal of Geophysical Research 89*, B525–B534.

Compston, W., Williams, I.S., Kirschvink, J.L., Zang, Z. & Ma, G., 1992: Zircon U–Pb ages for the Early Cambrian timescale. *Journal of the Royal Geological Society, London 149*, 171–184.

Corcoran, P.L., Bumby, A.J. & Davis, D.W., 2013: The Paleoproterozoic Waterberg Group, South Africa: provenance and its relation to the timing of the Limpopo orogeny. *Precambrian Research 230*, 45–60.

Cornell, D.H., 1987: A field and petrographic study of the Hartley Basalt Formation, Northern Cape Province of South Africa. *Transactions Geological Society South Africa 90*, 5–27.

Cornell, D.H., Armstrong, R.A. & Walraven, F., 1998: Geochronology of the Proterozoic Hartley Basalt formation, South Africa: constraints on the Kheis tectogenesis and the Kaapvaal Craton's earliest Wilson Cycle. *Journal of African Earth Sciences 26*, 5–27.

Cornell, D.H., Thomas, R.J. & Moen, H.F.G., 2006: The Namaqua-Natal Province. *In* M.R. Johnson, C.R. Anhaeusser & R.J. Thomas (eds.): *The Geology of South Africa*, 325–379. Geological Society of South Africa/Council of Geoscience, Johannesburg/Pretoria.

Da Silva, R., 2011: *Distribution and Geochronology of Unconformity-bounded Sequences in Paleoproterozoic Elim-Olifansthoek Red Beds: Implications for Timing of Formation of Shishen-type Iron Ore and Heavy Carbonate Carbon Isotope Excursion*. Unpublished MSc thesis. University of Johannesburg. 103 pp.

de Kock, M.O., Beukes, N.J. & Armstrong, R.A., 2012: New SHRIMP U–Pb zircon ages from the Hartswater Group, South Africa: implications for correlations of the Neoarchean Ventersdorp Supergroup on the Kaapvaal craton and with the Fortesque Group on the Pilbara craton. *Precambrian Research 204–205*, 66–74.

de Kock, M.O., Ernst, R.E., Söderlund, U., Jourdan, F., Hofmann, A., Le Gall, B., Bertrand, H., Chisonga, B.C., Beukes, N.J., Rajesh, H.M., Moseki, L.M. & Fuchs, R., 2014: Dykes of the 1.11 Ga Umkondo LIP, Southern Africa: clues to a complex plumbing system. *Precambrian Research 249*, 129–143.

de Kock, M.O., Evans, D.A.D., Dorland, H.C., Beukes, N.J. & Gutzmer, J., 2006: Paleomagnetism of the lower two unconformity-bounded sequences of the Waterberg Group, South Africa: towards a better-defined apparent polar wander path for the Paleoproterozoic Kaapvaal Craton. *South African Journal of Geology 109*, 157–182.

Dorland, H.C., Beukes, N.J., Gutzmer, J., Evans, D.A.D. & Armstrong, R.A., 2006: Precise SHRIMP U–Pb zircon age constraints on the lower Waterberg and Soutpansberg Groups, South Africa. *South African Journal of Geology 109*, 139–156.

Eglington, B.M., 2006: Evolution of the Namaqua-Natal Belt, southern Africa – a geochronological and isotope geochemical review. *Journal of African Earth Sciences 46*, 93–111.

Eglington, B.M. & Armstrong, R.A., 2004: The Kaapvaal Craton and adjacent orogens, southern Africa: a geochronological database and overview of the geological development of the craton. *South African Journal of Geology 107*, 13–32.

Eriksson, P.G., Bumby, A.J., Brümer, J.J. & van der Neut, M., 2006: Precambrian fluvial deposits: enigmatic palaeohydrological data from the c. 2–1.9 Ga Waterberg Group, South Africa. *Sedimentary Geology 190*, 25–46.

Ermanovics, I., Key, R.M. & Jones, M.T., 1978: The Palapye Group, central-eastern Botswana. *Transactions of the Geological Society of South Africa 81*, 61–73.

Ernst, R.E., 2014: *Large Igneous Provinces*. Cambridge University Press, Cambridge.

Evans, D.A., Beukes, N.J. & Kirschvink, J.L. 1997: Low-latitude glaciation in the Palaeoproterozoic era. *Nature* 386, 262–266.

Evans, D.A.D., Beukes, N.J. & Kirschvink, J.L., 2002: Palaeomagnetism of a lateritic paleoweathering horizon and overlying Paleoproterozoic red beds from South Africa: implications for the Kaapvaal apparent polar wander path and a confirmation of atmospheric oxygen enrichment. *Journal of Geophysical Research-Solid Earth and Planets 107*, 1–22.

Fairey, B., Tsikos, H., Corfu, F. & Polteau, S., 2013: U–Pb systematics in carbonates of the Postmasburg Group, Transvaal Supergroup, South Africa: primary versus metasomatic controls. *Precambrian Research 231*, 194–205.

Geng, H., Brandl, G., Sun, M., Wong, J. & Kröner, A., 2014: Zircon ages defining deposition of the Palaeoproterozoic Soutpansberg Group and further evidence for Eoarchaean crust in South Africa. *Precambrian Research 249*, 247–262.

Goldberg, A.S., 2010: Dyke swarms as indicators of major extensional events in the 1.9–1.2 Ga Columbia supercontinent. *Journal of Geodynamics 50*, 176–190.

Gose, G.A., Hanson, R.E., Dalziel, I.W.D., Pancake, J.A. & Seidel, E.K., 2006: Paleomagnetism of the 1.1 Ga Umkondo large igneous province in southern africa. *Journal of Geophysical Research 111*, 1–18.

Gose, W.A., Hanson, R.E., Harmer, R.E. & Seidel, E.K., 2013: Reconnaissance paleomagnetic studies of Mesoproterozoic alkaline igneous complexes in the Kaapvaal craton, South Africa. *Journal of African Earth Sciences 85*, 22–30.

Gose, W.A., Johnston, S.T. & Thomas, R.J., 2004: Age of magnetization of Mesoproterozoic rocks from the Natal sector of the Namaqua-Natal belt, South Africa. *Journal of African Earth Sciences 40*, 137–145.

Gumsley, A.P., Bleeker, W., Chamberlain, K., Söderlund, U., de Kock, M.O., Kampmann, T. & Larsson, E., 2015: U–Pb TIMS and *in situ* SIMS dating of baddeleyite and zircon from sub-volcanic sills of the Ongeluk Formation (Transvaal SupergroupP in the Griqualand West sub-basin, Kaapvaal Craton, with implications for Snowball Earth and the Great Oxygenation Event. *Joint Assembly of the AGU, GAC-MAC-CGU*, 378–379. 3–7 May 2015, Montreal, Canada.

Gumsley, A.P., de Kock, M.O., Rajesh, H.M., Knoper, M.W., Söderlund, U. & Ernst, R.E., 2013: The Hlagothi Complex: the identification of fragments from a Mesoarchean large igneous province on the Kaapvaal Craton. *Lithos 174*, 333–348.

Gumsley, A.P., Olsson, J.R., Söderlund, U., de Kock, M.O., Hofmann, A. & Klausen, M., 2015: Precise U–Pb baddeleyite age dating of the Ushushwana Complex, southern Africa – implications for the Mesoarchaean magmatic and sedimentological evolution of the Pongola Supergroup, Kaapvaal Craton. *Precambrian Research 257*, 174–185.

Hanson, R.E., Gose, W.A., Crowley, J.L., Ramezani, J., Bowring, S.A., Bullen, D.S., Hall, R.P., Pancake, J.A. & Mukwakwami, J., 2004: Paleoproterozoic intraplate magmatism and basin development on the Kaapvaal Craton: age, paleomagnetism and geochemistry of ~1.93 to ~1.87 Ga post-Waterberg dolerites. *South African Journal of Geology 107*, 233–254.

Hanson, R.E., Harmer, R.E., Blenkinsop, T.G., Bullen, D.S., Dalziel, I.W.D., Gose, W.A., Hall, R.P., Kampunzu, A.B., Key, R.M., Mukwakwami, J., Munyanyiwa, H., Pancake, J.A., Seidel, E.K. & Ward, S.E., 2006: Mesoproterozoic intraplate magmatism in the Kalahari Craton: a review. *Journal of African Earth Sciences 46*, 141–167.

Hanson, R.E., Rioux, M., Gose, W.A., Blackburn, T.J., Bowring, S.A., Mukwakwami, J. & Jones, D.L., 2011: Paleomagnetic and geochronological evidence for large-scale post 1.88 Ga displacement between the Zimbabwe and Kaapvaal cratons along the Limpopo belt. *Geology 39*, 487–490.

Hargraves, R.B. & Onstott, T.C., 1980: Paleomagnetic results from some southern African kimberlites, and their tectonic significance. *Journal of Geophysical Research 85*, 3587–3596.

Jaffey, A.H., Flynn, K.F., Glendenin, L.E., Bently, W.C. & Essling, A.M., 1971: Precision measurement of half-lives and specific activities of U235 and U238. *Physical Review C 4*, 1889–1906.

Jones, C.H., 2002: User-driven integrated software lives: "Paleomag" paleomagnetic analysis on the Macintosh. *Computers & Geosciences 28*, 1145–1115.

Kamo, S.L., Reimold, W.U., Krogh, T.E. & Colliston, W.P., 1996: A 2.023 Ga age for the Vredefort impact event and a first report of shock metmorphosed zircons in pseudotachylitic breccias and granophyre. *Earth and Planetary Science Letters 144*, 369–387.

Kampmann, T., Gumsley, A.P., de Kock, M.O. & Söderlund, U., 2015: U–Pb geochronology and paleomagnetism of the Westerberg Sill Suite, Kaapvaal Craton – support for a coherent Kaapvaal–Pilbara Block (Vaalbara) into the Paleoproterozoic? *Precambrian Research 269*, 58–72.

Kirschvink, J.L., 1980: The least-squares line and plane and the analysis of palaeomagnetic data. *Geophysical Jounral of the Royal Astronomical Society 62*, 699–718.

Kirschvink, J.L., Kopp, R.E., Raub, T.D., Baumgartner, C.T. & Holt, J.W., 2008: Rapid, precise, and high-sensitivity acquisition of paleomagnetic and rock-magnetic data: development of a low-noise automatic sample changing system for superconducting rock magnetometers. *Geochemistry Geophysics Geosystems 9*, 1–18.

Kramers, J.D. & Mouri, H., 2011: The geochronology of the Limpopo Complex: a controversy solved. *In* D.D. Van Reenen, J.D. Kramers, S. McCourt & L.L. Perchuk (eds.): *Origin and Evolution of Precambrian High-Grade Gneiss Terranes, with Special Emphasis on the Limpopo Complex of South Africa: Geological Society of America Memoir 207*, 85–106. The Geological Society of America.

Layer, P.W., Kröner, A., McWilliams, M. & Clauer, N., 1988: Regional magnetic overprinting of Witwatersrand Supergroup Sediments, South Africa. *Journal of Geophysical Research 93*, 2191–2200.

Letts, S., Torsvik, T.H., Webb, S.J. & Ashwal, L.D., 2009: Palaeomagnetism of the 2054 Ma Bushveld Complex (South Africa): implications for emplacement and cooling. *Geophysical Journal International 179*, 850–872.

Letts, S., Torsvik, T.H., Webb, S.J. & Ashwal, L.D., 2010: New Palaeoproterozoic palaeomagnetic data from the Kaapvaal Craton, South Africa. *Geological Society, London, Special Publications 357*, 9–26.

Lubnina, N., Ernst, R.E., Klausen, M. & Söderlund, U., 2010: Paleomagnetic study of NeoArchean–Paleoproterozoic dykes in the Kaapvaal Craton. *Precambrian Research 183*, 523–552.

Ludwig, K.R., 1991: Isoplot – a plotting and regression program for radiogenic isotopic data. *Open File Report*. USGS. 445 pp.

Maier, W.D., Peltonen, P., Grantham, G. & Mänttäri, I., 2003: A new 1.9 Ga age for the Trompsburg intrusion, South Africa. *Earth and Planetary Science Letters 212*, 351–360.

Mapeo, R.B.M., Ramokate, L.V., Armstrong, R.A. & Kampunzu, A.B., 2004: U–Pb zircon age of the upper Palapye group (Botswana) and regional implications. *Journal of African Earth Sciences 40*, 1–16.

Moen, H.F.G., 1999: The Kheis Tectonic Subprovince, southern Africa: a lithostratigraphic perspective. *South African Journal of Geology 102*, 27–42.

Moen, H.F.G., 2006: The Olifantshoek Supergroup. *In* M.R. Johnston, C.R. Anhaeusser & R.J. Thomas (eds.): *The Geology of South Africa*, 319–324. The Geological Society of South Africa and Council for Geoscience, Johannesburg and Pretoria.

Morgan, G.E., 1985: The paleomagnetism and cooling history of metamorphic and igneous rocks from the Limpopo Mobile Belt, southern Africa. *Geological Society of America Bulletin 96*, 663–675.

Morgan, G.E. & Briden, J.C., 1981: Aspects of Precambrian palaeomagnetism, with new data from the Limpopo Mobile Belt and Kaapvaal Craton in soouthern Africa. *Physics of the Earth and Planetary Interiors 24*, 142–168.

Mukasa, S.B., Wilson, A.H. & Young, K.R., 2013: Geochronological constraints on the magmatic and tectonic development of the Pongola Supergroup (Central Region), South Africa. *Precambrian Research 224*, 268–286.

Olsson, J.R., Klausen, M., Hamilton, M., März, N., Söderlund, U. & Roberts, R.J. 2015: Baddeleyite U-Pb ages and geochemistry of the 1875-1835 Ma Black Hills Dyke Swarm across north-eastern South Africa: part of a trans-Kalahari Craton back-arc setting? *GFF*. doi: http://dx.doi.org/10.1080/11035897.2015.1103781.

Olsson, J.R., Söderlund, U., Hamilton, M.A., Klausen, M.B. & Helffrich, G.R., 2011: A late Archean radiating dyke swarm as possible clue to the origin of the Bushveld Complex. *Nature Geoscience 4*, 865–869.

Olsson, J.R., Söderlund, U., Klausen, M.B. & Ernst, R.E., 2010: U–Pb baddeleyite ages linking major Archean dyke swarms to volcanic-rift forming events in the Kaapvaal craton (South Africa), and a precise age for the Bushveld Complex. *Precambrian Research 183*, 490–500.

Paces, J.B. & Miller, Jr, J.D., 1993: Precise U–Pb ages of Duluth Complex and related mafic intrusions, northeastern Minnesota: geochronological insights to physical, petrogenetic, paleomagnetic, and tectonomagmatic processes associated with the 1.1 Ga Midcontinent Rift System. *Journal of Geophysical Research 98*, 13997–14013.

Pettersson, Å., Cornell, D.H., Moen, H.F.G., Reddy, S. & Evans, D., 2007: Ion-probe dating of 1.2 Ga collision and crustal architecture in the Namaqua-Natal Province of southern Africa. *Precambrian Research 158*, 79–92.

Reischmann, T., 1995: Precise U/Pb age determination with baddeleyite (ZrO_2), a case study from the Palaborwa Igneous Complex, South Africa. *South African Journal of Geology 98*, 1–4.

Rotenberg, E., Davis, D.W., Amelin, Y., Gosh, S. & Bergquist, B.A., 2012: Determination of the decay-constant of ^{87}Rb by laboratory accumulation of ^{87}Sr. *Geochimica et Cosmochimica Acta 85*, 41–57.

Schütte, S.S., 1992: *Ongeluk Volcanism in Relation to the Kalahari Manganese Deposits*. Unpublished Ph. D. University of Natal. 262 pp.

Scoates, J.S. & Friedman, R.M., 2008: Presice age of the platineferous Merensky Reef, Bushveld Complex, South Africa, by the U–Pb zircon chemical abrasion ID-TIMS technique. *Economic Geology 103*, 465–471.

Smit, C.A., Beukes, N.J., Johnson, M.R., Malherbe, S.J. & Visser, J.N.J., 1991: *Lithostratigraphy of the Vryburg Formtion (Including the Kalkput, Geelbeksdam, Rosendal, Waterloo and Oceola Members). South African Committee for Stratigraphy Lithostratigraphic Series, No. 14*, Council for Geoscience, Pretoria.

Söderlund, U., Hofmann, A., Klausen, M.B., Olsson, J.R., Ernst, R.E. & Persson, P.-O., 2010: Towards a complete magmatic barcode for the Zimbabwe craton: Baddeleyite U–Pb dating of regional dolerite dyke swarms and sill complexes. *Precambrian Research 183*, 388–398.

Stacey, J.S. & Kramers, J.D., 1975: Approximation of terrestrial lead isotope evolution by a two-stage model. *Earth and Planetary Science Letters 26*, 207–221.

Tinker, J., De Wit, M.J. & Grotzinger, J., 2002: Seismic stratigraphic constraints on Neoarchean–Paleoproterozoic evolution of the western margin of the Kaapvaal Craton, South Africa. *South African Journal of Geology 105*, 107–134.

Tinker, J.H., De Wit, M.J. & Royden, L.H., 2004: Old, strong continental lithosphere with weak Archean margin at ~1.8 Ga, Kaapvaal Craton, South Africa. *South African Journal of Geology 107*, 255–260.

Van der Voo, R., 1990: The reliability of paleomagnetic data. *Tectonophysics 184*, 1–9.

Van Niekerk, H.S., 2006: *The Origin of the Kheis Terrane and its Relationship with the Archean Kaapvaal Craton and the Grenvillian Namaqua Province in Southern Africa*. Unpublished Ph. D thesis. University of Johannesburg. 241 pp.

Wabo, H., de Kock, M.O., Klausen, M., Söderlund, U. & Beukes, N.J. 2015a: *Paleomagnetism and chronology of B-1 marginal sills of the Bushveld Complex from the eastern Kaapvaal Craton*. South Africa, *GFF*. doi: http://dx.doi.org/10.1080/11035897.2015.1099566.

Wabo, H., Olsson, J.R., De Kock, M.O., Humbert, F., Söderlund, U. & Klausen, M. 2015b: New U-Pb age and paleomagnetic constraints from the UItkomst Complex. *South Africa: clues to the timing of intrusion. GFF.*. doi: http://dx.doi.org/10.1080/11035897.2015.1098726.

Williams, I.S. & Claesson, S., 1987: Isotopic evidence for the Precambrian provenance Caledonian metamorphism of high grade paragneisses from the Seve Nappes, Scandinavian Caledonides. II ion microbrobe zircon U–Th–Pb. *Contributions to Mineralogy and Petrology 97*, 205–217.

Williams, S.E., Müller, R.D., Landgrebe, T.C.W. & Whittaker, J.M., 2012: An open-source software environment for visualizing and refining plate tectonic reconstructions using high-resolution geological and geophysical data sets. *GSA Today 22*, 4–9.

PAPER V

Timing and tempo of the Great Oxidation Event

Ashley P. Gumsley[a,1], Kevin R. Chamberlain[b,c], Wouter Bleeker[d], Ulf Söderlund[a,e], Michiel O. de Kock[f], Emilie R. Larsson[a], and Andrey Bekker[g,f]

[a]Department of Geology, Lund University, Lund 223 62, Sweden; [b]Department of Geology and Geophysics, University of Wyoming, Laramie, WY 82071; [c]Faculty of Geology and Geography, Tomsk State University, Tomsk 634050, Russia; [d]Geological Survey of Canada, Ottawa, ON K1A 0E8, Canada; [e]Department of Geosciences, Swedish Museum of Natural History, Stockholm 104 05, Sweden; [f]Department of Geology, University of Johannesburg, Auckland Park 2006, South Africa; and [g]Department of Earth Sciences, University of California, Riverside, CA 92521

Edited by Mark H. Thiemens, University of California, San Diego, La Jolla, CA, and approved December 27, 2016 (received for review June 11, 2016)

The first significant buildup in atmospheric oxygen, the Great Oxidation Event (GOE), began in the early Paleoproterozoic in association with global glaciations and continued until the end of the Lomagundi carbon isotope excursion ca. 2,060 Ma. The exact timing of and relationships among these events are debated because of poor age constraints and contradictory stratigraphic correlations. Here, we show that the first Paleoproterozoic global glaciation and the onset of the GOE occurred between ca. 2,460 and 2,426 Ma, ~100 My earlier than previously estimated, based on an age of 2,426 ± 3 Ma for Ongeluk Formation magmatism from the Kaapvaal Craton of southern Africa. This age helps define a key paleomagnetic pole that positions the Kaapvaal Craton at equatorial latitudes of 11° ± 6° at this time. Furthermore, the rise of atmospheric oxygen was not monotonic, but was instead characterized by oscillations, which together with climatic instabilities may have continued over the next ~200 My until ≤2,250–2,240 Ma. Ongeluk Formation volcanism at ca. 2,426 Ma was part of a large igneous province (LIP) and represents a waning stage in the emplacement of several temporally discrete LIPs across a large low-latitude continental landmass. These LIPs played critical, albeit complex, roles in the rise of oxygen and in both initiating and terminating global glaciations. This series of events invites comparison with the Neoproterozoic oxygen increase and Sturtian Snowball Earth glaciation, which accompanied emplacement of LIPs across supercontinent Rodinia, also positioned at low latitude.

Great Oxidation Event | Snowball Earth | Paleoproterozoic | Kaapvaal Craton | Transvaal Supergroup

The early Paleoproterozoic is characterized by dramatic changes in Earth's atmosphere and oceans, with the transition from anoxic to oxic conditions commonly referred to as the Great Oxidation Event (GOE) (1). It is generally thought that the onset of the GOE was a singular event (2), an assumption rooted in the perceived bistability of atmospheric oxygen (3). However, this inferred bistability in oxygen was challenged through additional modeling (4), allowing for multiple oscillations in atmospheric oxygen during the onset of the GOE. Geological evidence has also established that this transition was broadly coincident with emplacement of numerous large igneous provinces (LIPs) (5) on extensive continental landmasses positioned at low latitudes (6) and glaciations interpreted to reflect global Snowball Earth conditions (7). Models linking these events have been hampered, however, by uncertainties in local and global stratigraphic correlations and age constraints (2). Evidence from the Huronian Supergroup on the Superior Craton in Canada, which hosts three Paleoproterozoic glacial intervals, indicates that the GOE is bracketed in age between ca. 2,460 and 2,308 Ma (8–10). New observations from the critical Transvaal Supergroup in southern Africa indicate that the GOE may have occurred by ca. 2,310 Ma (9) but requires a fourth glaciation at ≤2,250–2,240 Ma (9, 11) before the development of the oldest widely accepted oxygenated paleosols (12) and red-bed sandstones (13). Discrepancies in correlations between these glacially influenced stratigraphic successions and the age of the GOE hinge on a disputed age for the Ongeluk Formation basalts (14–16). By using high-resolution in situ secondary ion mass spectrometry (SIMS) on microbaddeleyite grains coupled with precise isotope dilution thermal ionization mass spectrometry (ID-TIMS) and paleomagnetic studies, we resolve these uncertainties by obtaining accurate and precise ages for the volcanic Ongeluk Formation and related intrusions in South Africa. These ages lead to a more coherent global perspective on the timing and tempo of the GOE and associated global glaciations and LIPs.

Transvaal Supergroup

The Neoarchean to Paleoproterozoic Transvaal Supergroup overlies the Kaapvaal Craton and is preserved in two main subbasins. In the Griqualand West subbasin, the Makganyene Formation consists of a series of glaciomarine diamictites (Fig. 1) (17). Paleomagnetic data for the Ongeluk Formation, which conformably overlies and interfingers with the Makganyene Formation, indicate that these glacial sedimentary rocks were deposited at low latitude, implying a glacial event of global extent (6, 7). The age of the Ongeluk Formation basalts has long been accepted at 2,222 ± 13 Ma based on a whole-rock Pb-Pb isochron date (14) and correlation with the noncontiguous basalts of the ≤2,250–2,240 Ma Hekpoort Formation in the Transvaal subbasin (11, 12, 14, 18), although this correlation has been questioned recently (15, 16, 19). The Ongeluk Formation is overlain by banded iron and manganese deposits of the Hotazel Formation, which in turn, are followed by carbonate rocks of the Mooidraai Formation (Fig. 1). Pb-Pb and U-Pb dating of the Mooidraai Formation carbonates has yielded dates of 2,394 ± 26 and 2,392 ± 23 Ma (15, 20), respectively, in conflict with the 2,222 ± 13 Ma Pb-Pb date on the stratigraphically

Significance

We present U-Pb ages for the extensive Ongeluk large igneous province, a large-scale magmatic event that took place near the equator in the Paleoproterozoic Transvaal basin of southern Africa at ca. 2,426 Ma. This magmatism also dates the oldest Paleoproterozoic global glaciation and the onset of significant atmospheric oxygenation. This result forces a significant reinterpretation of the iconic Transvaal basin stratigraphy and implies that the oxygenation involved several oscillations in oxygen levels across 10^{-5} present atmospheric levels before the irreversible oxygenation of the atmosphere. Data also indicate that the Paleoproterozoic glaciations and oxygenation were ushered in by assembly of a large continental mass, extensive magmatism, and continental migration to near-equatorial latitudes, mirroring a similar chain of events in the Neoproterozoic.

Author contributions: A.P.G., U.S., and M.O.d.K. designed research; A.P.G., K.R.C., W.B., U.S., M.O.d.K., and E.R.L. performed research; K.R.C., W.B., U.S., and M.O.d.K. contributed new reagents/analytic tools; A.P.G., K.R.C., W.B., U.S., M.O.d.K., E.R.L., and A.B. analyzed data; and A.P.G., K.R.C., W.B., U.S., M.O.d.K., E.R.L., and A.B. wrote the paper.

The authors declare no conflict of interest.

This article is a PNAS Direct Submission.

Freely available online through the PNAS open access option.

[1]To whom correspondence should be addressed. Email: ashley.gumsley@geol.lu.se.

This article contains supporting information online at www.pnas.org/lookup/suppl/doi:10.1073/pnas.1608824114/-/DCSupplemental.

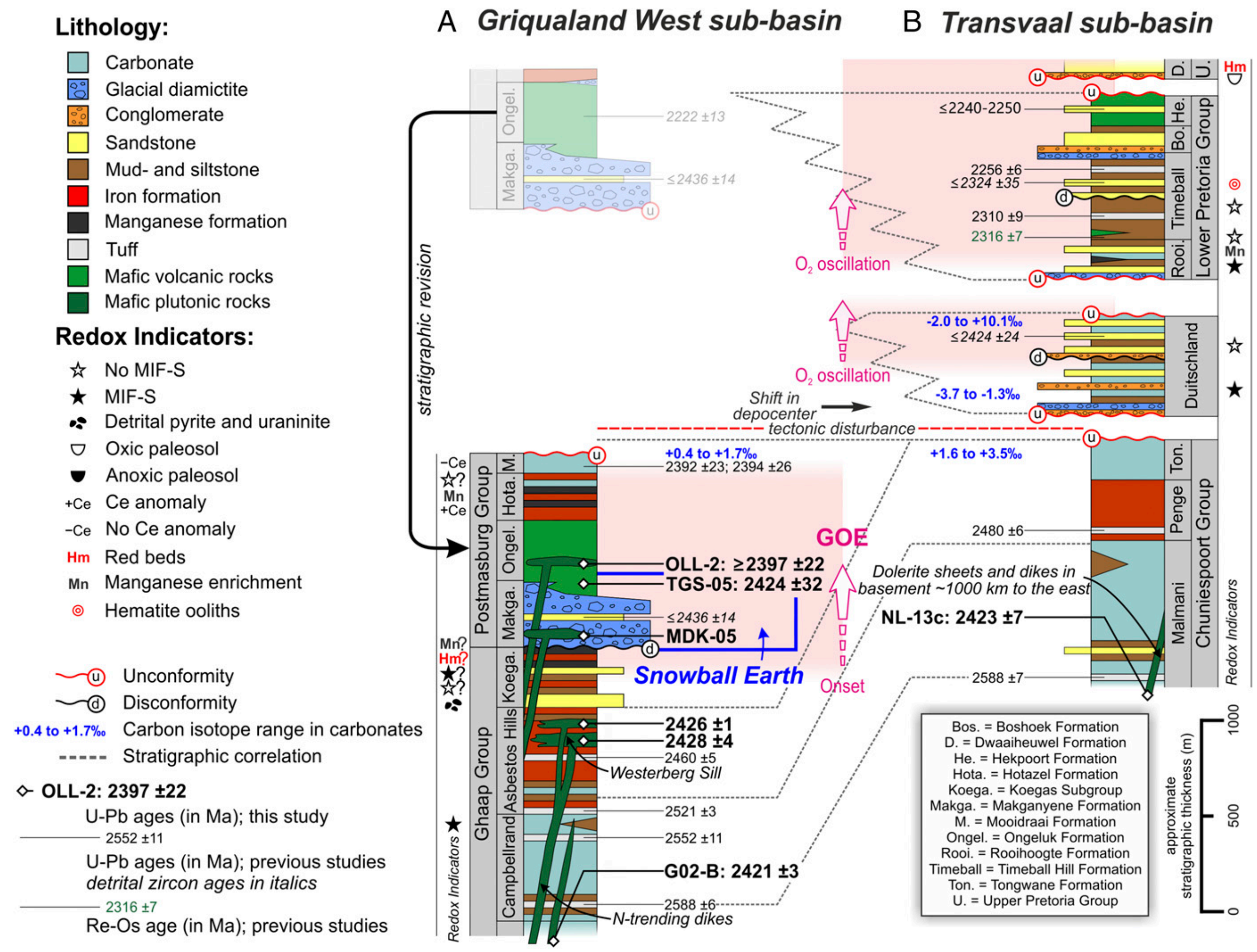

Fig. 1. Stratigraphic synthesis (*SI Methods*, *Stratigraphic Synthesis*) of the Transvaal Supergroup as preserved in its two main subbasins: (*A*) Griqualand West in the southwest and (*B*) Transvaal in the northeast. Dated samples and results (bold) are shown in stratigraphic context and collectively, unlock the long-held correlation between the basalts of the Ongeluk and Hekpoort formations (12, 14, 18). A selection of previously published ages is schematically shown (Table S1) along with redox indicators and ranges of carbon isotope values in carbonates (Table S2). The redox records within the two subbasins tracks the rhythm of GOE and reflects at least two O_2 oscillations back through 10^{-5} PAL after the onset of GOE (bold pink arrows and variable intensity pink background shading). Redox indicators requiring more detailed studies are denoted with question marks. All ages are quoted at 2σ uncertainty.

lower Ongeluk Formation (14). The Hotazel Formation hosts giant Mn deposits with a negative Ce anomaly that are unequivocally interpreted to reflect deposition after the onset of the GOE (7, 21), whereas the Koegas Subgroup underlying the Makganyene Formation contains detrital pyrite and uraninite grains signifying deposition before the GOE (22). In the Transvaal subbasin (Fig. 1), the start of the GOE has been placed in the middle of either the Duitschland Formation or the Rooihoogte Formation by different authors (23, 24), with the age of the upper Duitschland Formation constrained by detrital zircon to ≤2,424 ± 24 Ma (11). A 2,316 ± 7 Ma Re-Os age for diagenetic pyrite (25) and a 2,309 ± 9 Ma U-Pb age for tuff in the lower Timeball Hill Formation (9), which conformably overlies the Rooihoogte Formation, suggest that the GOE began by ca. 2,309 Ma (24). All chronological and redox records for the Transvaal Supergroup are provided in Tables S1 and S2.

Sampling

To test and resolve some of these critical correlations, we have dated by U-Pb isotopic methods a number of dolerite and basalt samples that are linked geologically and paleomagnetically to the Ongeluk Formation basalts (*SI Methods*, *Sampling*, Fig. S1, and Table S3). An N-trending dolerite dike from the Griqualand West subbasin (G02-B) (Fig. 1) (26) as well as an intrusive dolerite sheet from the southeastern Kaapvaal Craton (NL-13c) (Fig. 1) (27) were dated using U-Pb ID-TIMS on baddeleyite. Samples TGS-05 and OLL-2, a coarse-grained, thick basalt flow and a dolerite sill, respectively, from near the base of the Ongeluk Formation basalts (Fig. 1) (6) were dated by in situ U-Pb SIMS on microbaddeleyite grains. To couple geochronological and paleomagnetic records for these mafic units, complementary paleomagnetic studies were conducted on specimens from the TGS-05 and MDK-05 sample sites (Fig. 1) using conventional demagnetization techniques.

Results

Samples G02-B and NL-13c produce upper intercept baddeleyite dates of 2,421 ± 3 and 2,423 ± 7 Ma, respectively (Fig. 2, *SI Methods*, *Geochronology—ID-TIMS Analysis*, Fig. S2, and Table S4), whereas samples TGS-05 and OLL-2 yield upper intercept dates of 2,424 ± 32 and 2,397 ± 22 Ma, respectively (Fig. 2, *SI Methods*, *Geochronology—SIMS Analysis*, Fig. S2, and Table S5). The upper intercept dates of 2,424 ± 32, 2,423 ± 7, and 2,421 ± 3 Ma are interpreted as reliable crystallization ages and overlap within 2σ uncertainty, whereas the date obtained from OLL-2 is likely affected by a minor contribution of secondary zircon as

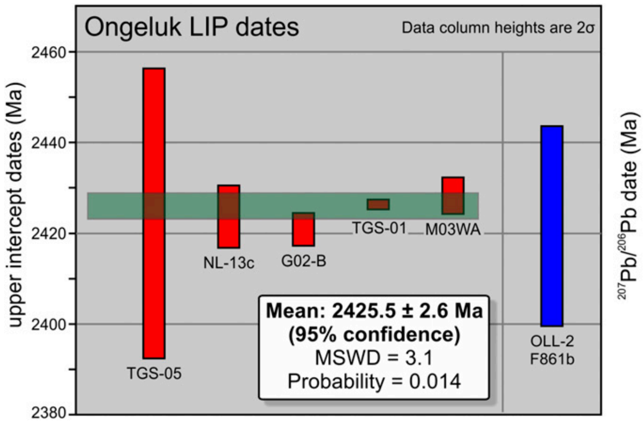

Fig. 2. Weighted mean age of the Ongeluk LIP. Shown is a comparison of upper intercept dates with 2σ uncertainties (red columns) from five samples of the Ongeluk LIP, including the Westerberg Sill Province (samples TGS-01 and M03WA) (28), with a calculated weighted mean age of 2,425.5 ± 2.6 Ma (green bar). The result from a single analysis spot (F861b in OLL-2) is shown for comparison (blue column) (Fig. S2).

indicated by SEM imaging. We, therefore, interpret the 2,397 ± 22 Ma date of OLL-2 as a minimum age. In support of this interpretation, one baddeleyite grain (spot F861b) (Fig. 2) yielded a $^{207}Pb/^{206}Pb$ date of 2,421 ± 22 Ma.

A structurally corrected virtual geomagnetic pole (VGP) for the dated sample TGS-05 is located at −0.7° N and 288.2° E, whereas the VGP of sample MDK-05 is located at −0.9° N and 283.7° E (*SI Methods*, *Paleomagnetism*, Fig. S3, and Table S6). Samples OLL-2, G02-B, and NL-13c already have published shallow magnetization directions similar to those reported for the Ongeluk Formation (6, 26, 27).

Discussion

The Ongeluk LIP. All samples were collected stratigraphically from within or below the lower Ongeluk Formation (Fig. 1) and represent either the feeder system of dolerite dikes and sills to the Ongeluk Formation basalts or coarse-grained interiors of thicker basalt flows. We interpret the Westerberg Sill Province and the N-trending dolerite dike swarm (Fig. 1), both intruding into the Griqualand West subbasin stratigraphy, as parts of the same short-lived magmatic event based on their temporal, spatial, and stratigraphic proximities and similar paleomagnetic results. The age of the Westerberg Sill itself was defined by an upper intercept date of 2,441 ± 6 Ma composed of five discordant baddeleyite analyses (28). However, excluding the most discordant analysis from this result yields a more probable upper intercept date of 2,428 ± 4 Ma. This reinterpretation is supported by concordant baddeleyite analyses from a second sill dated at 2,426 ± 1 Ma as part of the same study (28). Combining all of these dates, we calculate a weighted mean date of 2,425.5 ± 2.6 Ma (Fig. 2) as the age of a single relatively short-lived magmatic event, which is now clearly distinguished from ≤2,250–2,240 Ma Hekpoort Formation volcanism with which it was previously correlated. Because sample NL-13c is located ∼1,000 km to the east of the other sample sites, our results indicate a defined craton-scale LIP, the Ongeluk LIP.

The Ongeluk Key Paleomagnetic Pole. The VGPs presented in this study overlap with previously published paleopoles for the Ongeluk Formation and associated intrusions (6, 26–28). Collectively, the combined VGPs from all of these studies for the basalts from the Ongeluk Formation (6) and their intrusive feeders (26–28) define a grand key paleomagnetic pole for the Ongeluk LIP that is near-equatorial (29) at 4.1° N, 282.9° E (Table S7), with an A_{95} of 5.3° that achieves five of seven on the quality scale by Van der Voo (30).

Revising the Transvaal Supergroup Stratigraphy. The age for Ongeluk Formation volcanism demands the revision of stratigraphic correlations between the successions of the Griqualand West and Transvaal subbasins of the Transvaal Supergroup (Fig. 1). Previous studies have correlated the Postmasburg and Pretoria Groups using the 2,222 ± 13 Ma Ongeluk Formation and the ≤2,250–2,240 Ma Hekpoort Formation volcanic rocks (11, 12, 14, 18). This correlation is now shown to be incorrect based on the 2,426 ± 3 Ma age constraint provided by the Ongeluk Formation volcanic rocks and associated intrusions. In addition, lithologic and chemostratigraphic data for the Duitschland and Rooihoogte formations (15, 18, 23, 24, 31) coupled with recent age constraints (9, 11, 25) and arguments relying on basin architecture (16) indicate that the Duitschland and Rooihoogte formations are younger than the Postmasburg Group (Fig. 1). A more complete discussion on the Transvaal Supergroup stratigraphy and the proposed revisions is provided in the stratigraphic synthesis (*SI Methods*, *Stratigraphic Synthesis*).

Atmospheric Oxygen Oscillations. This stratigraphic interpretation indicates a dynamic state of atmospheric oxygen levels during the early Paleoproterozoic glacial period. The onset of the GOE occurred in the immediate aftermath of the Makganyene Formation glaciation with deposition of the world's largest manganese deposit, the Hotazel Formation, with a negative Ce anomaly, both indicative of oxygenation (7, 21). This oxygenation was followed by a return to anoxic atmospheric conditions as indicated by the lack of a Ce anomaly in foreslope carbonates of the Mooidraai Formation (Fig. 1) (21, 32) and a mass-independent fractionation of sulfur (MIF-S) signal recorded by early diagenetic sulfides from the lower Duitschland Formation (Fig. 1) (23). Subsequent oxygenation events occurred during deposition of the upper Duitschland Formation (23) and once again, in the middle of the Rooihoogte Formation (24) as indicated by the reappearance and disappearance of the MIF-S signal (Fig. 1).

Detrital pyrite grains persist above the oldest glacial diamictite in the Mississagi Formation in the Huronian Supergroup of the Superior Craton, Canada (33) and support oscillations in atmospheric oxygen herein inferred from the records of the Transvaal Supergroup (Fig. 3). Our geochronologic and stratigraphic framework argues against a simple, monotonic rise of atmospheric oxygen in the early Paleoproterozoic, a time period further characterized by four glaciations. Instead, the onset of the GOE was followed by oscillations in atmospheric oxygen content across the 10^{-5} present atmospheric level (PAL) threshold over an ∼200-My interval, adding empirical evidence to atmospheric modeling predictions (4).

Linking Snowball Earth and the GOE. The Makganyene Formation, deposited in the tropics (6), records the oldest known Snowball Earth event (7). Makganyene Formation diamictites are now constrained to be slightly older than ca. 2,426 Ma and likely correlate with glacial units of the Ramsay Lake Formation in the Huronian Supergroup, Canada and the Campbell Lake Formation from the Snowy Pass Supergroup on the Wyoming Craton in the United States. Other correlative glacial units worldwide include the ca. 2,435 Ma Polisarka Formation on the Kola–Karelia Craton in Fennoscandia (34) as well as possibly, the Meteorite Bore Member on the Pilbara Craton in Australia, defining the wide extent of the oldest Paleoproterozoic glaciation (Fig. 3). This early Paleoproterozoic glaciation is broadly coeval with the onset of the GOE; both events are now tightly bracketed between ca. 2,460 Ma, the age of volcanic rocks near the base of the Huronian Supergroup (8, 10), and ca. 2,426 Ma, the approximate age of the Makganyene Formation glaciation and near-coeval Ongeluk Formation volcanic rocks in the Transvaal Supergroup. In addition, the 2,442 ± 2 Ma Seidorechka Formation and the overlying 2,435 ± 2 Ma Polisarka formations (34, 35) overlying the Kola–Karelia Craton may tightly bracket the oldest Paleoproterozoic glacial event between ca. 2,442 Ma and 2,435 Ma, respectively, implying that it lasted less than 7 My (Fig. 3).

Our results add to the growing evidence for large low-latitude continental landmasses in the early Paleoproterozoic, including

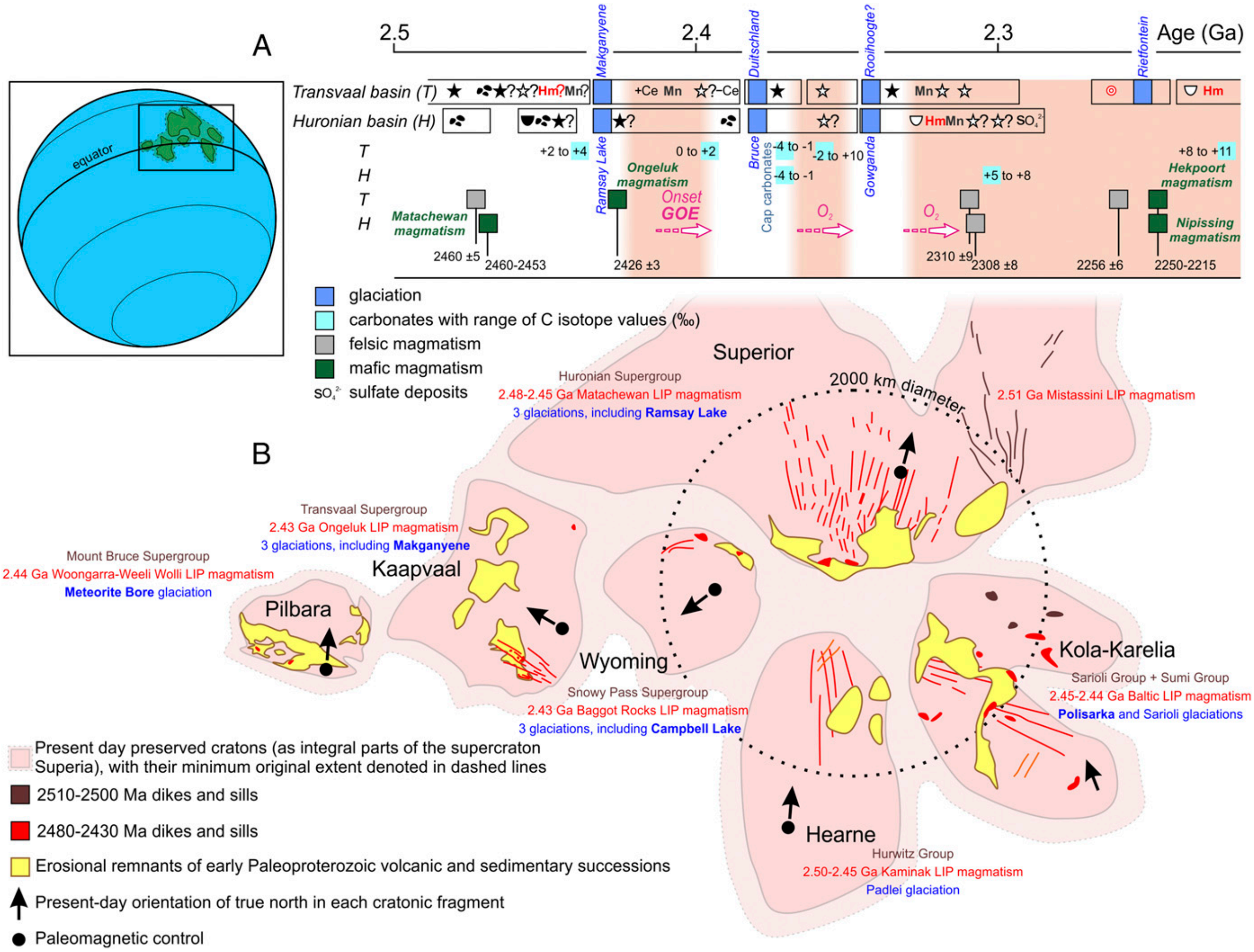

Fig. 3. *A* is a graph illustrating the approximate chronology (Table S1) of the glaciations and atmospheric oxygen oscillations according to the related redox indicators in the Huronian and Transvaal basins (Table S2) using the same symbols as used in Fig. 1. Also shown are dated mafic and felsic magmatic events as well as $\delta^{13}C$ ranges for carbonates (Tables S1 and S2) and the extent of stratigraphic records in each basin denoting gaps in records at unconformities and disconformities. (*B*) The early Paleoproterozoic geography of the Superior, Kola–Karelia, Hearne, and Wyoming cratons as integral parts of the supercraton Superia (5, 36)* with the addition of the Kaapvaal and Pilbara cratons in the supercraton Vaalbara configuration (52). The early Paleoproterozoic basins developed on these cratonic fragments include both ca. 2.51–2.43 Ga volcanic rocks and glacial units, which can be correlated across the cratons. The glacial units in bold denote the glacial deposits likely recording the first glaciation. All of the cratonic fragments also contain dolerite dikes and sills emplaced between ca. 2.51 Ga and 2.43 Ga, showing the extent of the LIPs formed during this time. Available paleomagnetic studies indicate that the majority of the cratonic fragments (as part of supercraton Superia) were positioned near the paleoequator. The arrows denoting present-day true north in the crustal blocks illustrate the rotations necessary to make the reconstruction. (*Inset*) The hypothesized paleolatitude of these Archean cratons in the early Paleoproterozoic.

the Kaapvaal Craton (6) and the clan of cratons that defines supercraton Superia (5, 36, 37): Superior, Wyoming, Hearne, and Karelia–Kola. These landmasses, at least in part contiguous, record a series of LIP events between 2,510 Ma and 2,440 Ma and include the Mistassini, Kaminak, Baltic, Baggot Rocks, and Matachewan LIPs (Fig. 3) (5) before the ca. 2,426 Ma Ongeluk LIP of the Kaapvaal Craton. Cumulatively, these large juvenile volcanic provinces on extensive low-latitude continental landmasses are likely to have triggered near-equatorial glaciations via enhanced chemical weathering of aerially extensive, nutrient-rich continental flood basalts. This weathering resulted in increased carbon dioxide drawdown (38, 39) and an enhanced flux of phosphorus and other essential nutrients (40) onto extensive continental margins and into intracratonic basins. An enhanced nutrient flux would have greatly increased photosynthetic activity and oxygen production, temporally linked to higher net burial of organic carbon in accumulating sediments, as reflected by $\delta^{13}C$ values of carbonates in the upper Tongwane Formation of the Transvaal Supergroup (31). The Tongwane Formation is locally preserved above the ca. 2,480–2,460 Ma iron formations (41) but below the major unconformity documented in the entire Transvaal basin (Fig. 1) (18). Thus, even an incipient rise of free atmospheric oxygen would have led to rapid oxidation of atmospheric methane (42), forcing catastrophic climate change and plunging Earth into a global glaciation (43). Importantly, the dated near-equatorial Ongeluk LIP, conformably overlying and interfingering with the uppermost Makganyene Formation glacial diamictites (Fig. 1), illustrates the dual role of LIPs in these global events, in that they would also have contributed carbon dioxide to rebuilding the greenhouse atmosphere that led to abrupt termination of the first Snowball Earth state of the early Paleoproterozoic.

*Bleeker W, Chamberlain K, Kamo S, Kilian T, Buchan K (2016) Kaapvaal, Superior and Wyoming: Nearest neighbours in supercraton Superia. Proceedings of the 35th International Geological Congress.

Comparing the Paleoproterozoic with the Neoproterozoic. In the Neoproterozoic, a remarkably similar sequence of events occurred, involving successive emplacement of multiple LIPs on the supercontinent Rodinia, a low-latitude position of this supercontinent, and incipient rifting and breakup (44). The massive Franklin LIP at ca. 717 Ma (45) immediately preceded the most dramatic and longest global glaciation of the Neoproterozoic, the Sturtian (46). This overall period is characterized by the second most dramatic change in surface redox conditions linked with Snowball Earth glaciations (47) and accompanied high rates of organic carbon burial (48, 49). Although substantial differences between the Paleo- and Neoproterozoic glacial periods might be expected, for instance, in the triggering mechanisms for the initial global glaciations, because methane was probably a more important greenhouse gas before the Makganyene glaciation (42, 43) than before the Sturtian glaciation (38, 39), there are also uncanny parallels. Examples include supercraton- or supercontinent-size continental landmasses that were capped by continental flood basalts, incipient rifting and/or breakup, and rapid transit to low latitudes. All of these factors enhanced chemical weathering of juvenile basaltic material and greatly increased the flux of bio-limiting nutrients to depositional basins, thus leading to a biotic response of higher organic carbon burial (40, 50) as well as deposition of giant iron and manganese deposits. It seems likely that these similar scenarios are not coincidental but that the critical factors (assembly of large landmasses, LIPs, incipient rifting, and relief enhancement—all resulting in a lithospheric mass anomaly and movement to low latitudes, high rates of organic carbon burial, surface oxygenation, and Snowball Earth glaciations) are mechanistically linked. In this case, a critical link might be true polar wander caused by the lithospheric mass anomaly that nudged the basalt-covered and rifting supercontinental landmasses to the equator (51), where chemical weathering and nutrient fluxes kicked into high gear and triggered the biotic, redox, and climatic responses.

Methods

Sampling. Samples in this study were taken from dolerite intrusions that intruded into the basement of the Kaapvaal Craton and the overlying cover succession of the Transvaal Supergroup in the Griqualand West subbasin, South Africa, except for one sample taken ~1,000 km to the east (Fig. 1, *SI Methods*, Fig. S1, and Table S3). One sample is tentatively interpreted as a coarse-grained basalt from the base of the Ongeluk Formation.

Geochronology—ID-TIMS Analysis. Water-based separation of baddeleyite was attempted for all rock samples at Lund University. Samples NL-13c and G02-B yielded baddeleyite grains using this method. Grains were selected and analyzed using U-Pb ID-TIMS on a Thermo Finnigan Triton Mass Spectrometer at the Department of Geosciences at the Swedish Museum of Natural History. Additional details of the operating procedures for the ID-TIMS analyses at the Swedish Museum of Natural History and results are given in *SI Methods*, Fig. S2, and Table S4.

Geochronology—SIMS Analysis. Zr-bearing phases were imaged, mapped using SEM in conjunction with energy-dispersive spectrometry in samples TGS-05 and OLL-2, and then, ranked (*SI Methods* and Fig. S2). U-Pb isotopic data using SIMS were determined in situ on the microbaddeleyite grains in the mapped thin sections using the CAMECA ims1270 Mass Spectrometer at the University of California, Los Angeles (UCLA). Additional details of the operating procedures for the SIMS at UCLA and results are given in *SI Methods*, Fig. S2, and Table S5.

Paleomagnetism. Measurements of magnetic remanence from samples TGS-05 and MDK-05 were made using the superconducting vertical 2G Enterprises DC-4K Rock Magnetometer at the University of Johannesburg (UJ). All specimens were exposed to stepwise alternating-field demagnetization. Additional details of the sampling and operating procedures for the magnetometer at the UJ and results are given in *SI Methods*, Fig. S3, and Table S6.

ACKNOWLEDGMENTS. We thank the staff of the SIMS and the TIMS laboratories at UCLA and the Department of Geosciences, Swedish Museum of Natural History, respectively, for all of the assistance during analyses. We thank N. Beukes for providing sample TGS-05. Funding was provided by grants from the Royal Physiographic Society in Lund (A.P.G.) and the Swedish Research Council (U.S.); M.O.d.K. and A.B. acknowledge support from the South African Department of Science and Technology and the National Research Foundation (DST-NRF)–funded Centre of Excellence for Integrated Mineral and Energy Resource Analysis (CIMERA). This article is a contribution to International Geoscience Programme (IGCP) 648: Supercontinents and Global Geodynamics.

1. Holland HD (2002) Volcanic gases, black smokers, and the Great Oxidation Event. *Geochim Cosmochim Acta* 66(21):3811–3826.
2. Hoffman PF (2013) The Great Oxidation and a Siderian snowball Earth: MIF-S based correlation of Paleoproterozoic glacial epochs. *Chem Geol* 362:143–156.
3. Goldblatt C, Lenton TM, Watson AJ (2006) Bistability of atmospheric oxygen and the Great Oxidation. *Nature* 443(7112):683–686.
4. Daines SJ, Lenton TM (2016) The effect of widespread early aerobic marine ecosystems on methane cycling and the Great Oxidation. *Earth Planet Sci Lett* 434:42–51.
5. Ernst R, Bleeker W (2010) Large igneous provinces (LIPs), giant dyke swarms, and mantle plumes: Significance for breakup events within Canada and adjacent regions from 2.5 Ga to the Present. *Can J Earth Sci* 47(5):695–739.
6. Evans DA, Beukes NJ, Kirschvink JL (1997) Low-latitude glaciation in the Palaeoproterozoic era. *Nature* 386(6622):262–266.
7. Kirschvink JL, et al. (2000) Paleoproterozoic snowball earth: Extreme climatic and geochemical global change and its biological consequences. *Proc Natl Acad Sci USA* 97(4):1400–1405.
8. Ketchum KY, Heaman LM, Bennett G, Hughes DJ (2013) Age, petrogenesis and tectonic setting of the Thessalon volcanic rocks, Huronian Supergroup, Canada. *Precambrian Res* 233:144–172.
9. Rasmussen B, Bekker A, Fletcher IR (2013) Correlation of Paleoproterozoic glaciations based on U-Pb zircon ages for tuff beds in the Transvaal and Huronian Supergroups. *Earth Planet Sci Lett* 382:173–180.
10. Bleeker W, Kamo SL, Ames DE, Davis D (2015) New field observations and U-Pb ages in the Sudbury area: Toward a detailed cross-section through the deformed Sudbury Structure. *Geol Surv Canada Open File* 7856:151–166.
11. Schröder S, Beukes NJ, Armstrong RA (2016) Detrital zircon constraints on the tectonostratigraphy of the Paleoproterozoic Pretoria Group, South Africa. *Precambrian Res* 278:362–393.
12. Beukes NJ, Dorland H, Gutzmer J, Nedachi M, Ohmoto H (2002) Tropical laterites, life on land, and the history of atmospheric oxygen in the Paleoproterozoic. *Geology* 30(6):491–494.
13. Eriksson PG, Cheney ES (1992) Evidence for the transition to an oxygen-rich atmosphere during the evolution of red beds in the lower Proterozoic sequences of southern Africa. *Precambrian Res* 54(2-4):257–269.
14. Cornell DH, Schütte SS, Eglington BL (1996) The Ongeluk basaltic andesite formation in Griqualand West, South Africa: Submarine alteration in a 2222 Ma Proterozoic sea. *Precambrian Res* 79(1-2):101–123.
15. Bau M, Romer RL, Lüders V, Beukes NJ (1999) Pb, O, and C isotopes in silicified Mooidraai dolomite (Transvaal Supergroup, South Africa): Implications for the composition of Paleoproterozoic seawater and "dating" the increase of oxygen in the Precambrian atmosphere. *Earth Planet Sci Lett* 174(1-2):43–57.
16. Moore JM, Tsikos H, Polteau S (2001) Deconstructing the Transvaal Supergroup, South Africa: Implications for Palaeoproterozoic palaeoclimate models. *J Afr Earth Sci* 33(3-4):437–444.
17. Polteau S, Moore JM, Tsikos H (2006) The geology and geochemistry of the Palaeoproterozoic Makganyene diamictite. *Precambrian Res* 148(3-4):257–274.
18. Eriksson PG, Altermann W, Hartzer FJ (2006) The Transvaal Supergroup. *The Geology of South Africa*, eds Johnson MJ, Anhaeusser CR, Thomas RJ (Geological Society of South Africa/Council for Geoscience, Johannesburg), pp 237–260.
19. Moore JM, Polteau S, Armstrong RA, Corfu F, Tsikos H (2012) The age and correlation of the Postmasburg Group, southern Africa: Constraints from detrital zircon grains. *J Afr Earth Sci* 64:9–19.
20. Fairey B, Tsikos H, Corfu F, Polteau S (2013) U-Pb systematics in carbonates of the Postmasburg Group, Transvaal Supergroup, South Africa: Primary versus metasomatic controls. *Precambrian Res* 231:194–205.
21. Bau M, Alexander B (2006) Preservation of primary REE patterns without Ce anomaly during dolomitization of Mid-Paleoproterozoic limestone and the potential re-establishment of marine anoxia immediately after the "Great Oxidation Event." *South Afr J Geol* 109(1-2):81–86.
22. Johnson JE, Gerpheide A, Lamb MP, Fischer WW (2014) O_2 constraints from Paleoproterozoic detrital pyrite and uraninite. *Geol Soc Am Bull* 126(5-6):813–830.
23. Guo Q, et al. (2009) Reconstructing Earth's surface oxidation across the Archean-Proterozoic transition. *Geology* 37(5):399–402.
24. Luo G, et al. (2016) Rapid oxygenation of Earth's atmosphere 2.33 billion years ago. *Sci Adv* 2(5):e1600134.
25. Hannah JL, Bekker A, Stein HJ, Markey RJ, Holland HD (2004) Primitive Os and 2316 Ma age for marine shale: Implications for Paleoproterozoic glacial events and the rise of atmospheric oxygen. *Earth Planet Sci Lett* 225:43–52.
26. de Kock MO, et al. (2009) Paleomagnetism of a Neoarchean-Paleoproterozoic carbonate ramp and carbonate platform succession (Transvaal Supergroup) from surface outcrop and drill core, Griqualand West region, South Africa. *Precambrian Res* 169(1-2):80–99.
27. Lubnina N, Ernst R, Klausen M, Söderlund U (2010) Paleomagnetic study of NeoArchean-Paleoproterozoic dykes in the Kaapvaal Craton. *Precambrian Res* 183(3):523–552.
28. Kampmann TC, Gumsley AP, de Kock MO, Söderlund U (2015) U-Pb geochronology and paleomagnetism of the Westerberg Sill Suite, Kaapvaal Craton - Support for a

coherent Kaapvaal-Pilbara Block (Vaalbara) into the Paleoproterozoic? *Precambrian Res* 269:58–72.
29. Buchan KL (2013) Key paleomagnetic poles and their use in Proterozoic continent and supercontinent reconstructions: A review. *Precambrian Res* 238:93–110.
30. Van der Voo R (1990) The reliability of paleomagnetic data. *Tectonophysics* 184(1):1–9.
31. Bekker A, et al. (2001) Chemostratigraphy of the Paleoproterozoic Duitschland Formation, South Africa: Implications for coupled climate change and carbon cycling. *Am J Sci* 301(3):261–285.
32. Kunzmann M, Gutzmer J, Beukes NJ, Halverson GP (2014) Depositional environment and lithostratigraphy of the Paleoproterozoic Mooidraai Formation, Kalahari Manganese Field, South Africa. *South Afr J Geol* 117(2):173–192.
33. Ulrich T, Long DGF, Kamber BS, Whitehouse MJ (2011) In situ trace element and sulfur isotope analysis of pyrite in a Paleoproterozoic Gold Placer Deposit, Pardo and Clement Townships, Ontario, Canada. *Econ Geol* 106(4):667–686.
34. Brasier AT, et al. (2013) Earth's earliest global glaciation? Carbonate geochemistry and geochronology of the Polisarka Sedimentary Formation, Kola Peninsula, Russia. *Precambrian Res* 235:278–294.
35. Amelin YV, Heaman LM, Semenov VS (1995) U-Pb geochronology of layered mafic intrusions in the eastern Baltic Shield: Implications for the timing and duration of Paleoproterozoic continental rifting. *Precambrian Res* 75(1-2):31–46.
36. Bleeker W, Ernst R (2006) Short-lived mantle generated magmatic events and their dyke swarms: The key unlocking Earth's paleogeographic record back to 2.6 Ga. *Dyke Swarms—Time Markers of Crustal Evolution*, eds Hanski E, Mertanen S, Rämö T, Vuollo J (Taylor and Francis, London), pp 3–26.
37. Bleeker W (2003) The late Archean record: A puzzle in ca. 35 pieces. *Lithos* 71(2-4):99–134.
38. Marshall HG, Walker JCG, Kuhn WR (1988) Long-term climate change and the geochemical cycle of carbon. *J Geophys Res Atmos* 93(D1):791–801.
39. Donnadieu Y, Goddéris Y, Ramstein G, Nédélec A, Meert J (2004) A 'snowball Earth' climate triggered by continental break-up through changes in runoff. *Nature* 428(6980):303–306.
40. Horton F (2015) Did phosphorus derived from the weathering of large igneous provinces fertilize the Neoproterozoic ocean? *Geochem Geophys Geosyst* 16(6):1723–1738.
41. Schröder S, Warke MR (2016) Termination of BIF deposition in the Paleoproterozoic: The Tongwane Formation, South Africa. *South Afr J Geol* 119(2):329–346.
42. Pavlov AA, Kasting JF (2002) Mass-independent fractionation of sulfur isotopes in Archean sediments: Strong evidence for an anoxic Archean atmosphere. *Astrobiology* 2(1):27–41.
43. Bekker A, Kaufman AJ (2007) Oxidative forcing of global climate change: A biogeochemical record across the oldest Paleoproterozoic ice age in North America. *Earth Planet Sci Lett* 258(3-4):486–499.
44. Li ZX, et al. (2008) Assembly, configuration, and break-up history of Rodinia: A synthesis. *Precambrian Res* 160(1-2):179–210.
45. Macdonald FA, et al. (2010) Calibrating the Cryogenian. *Science* 327(5970):1241–1243.
46. Rooney AD, Strauss JV, Brandon AD, Macdonald FA (2015) A Cryogenian chronology: Two long-lasting synchronous Neoproterozoic glaciations. *Geology* 43(5):459–462.
47. Pogge von Strandmann PAE, et al. (2015) Selenium isotope evidence for progressive oxidation of the Neoproterozoic biosphere. *Nat Commun* 6:10157.
48. Thomson D, Rainbird RH, Planavsky NJ, Lyons TW, Bekker A (2015) Chemostratigraphy of the Shaler Supergroup, Victoria Island, NW Canada: A record of ocean composition prior to the Cryogenian glaciations. *Precambrian Res* 263:232–245.
49. Turner EC, Bekker A (2016) Thick sulfate evaporite accumulations marking a mid-Neoproterozoic oxygenation event (Ten Stone Formation, Northwest Territories, Canada). *Geol Soc Am Bull* 128(1-2):203–222.
50. Cox GM, et al. (2016) Continental flood basalt weathering as a trigger for Neoproterozoic Snowball Earth. *Earth Planet Sci Lett* 446:89–99.
51. Li Z-X, Zhong S (2009) Supercontinent-superplume coupling, true polar wander and plume mobility: Plate dominance in whole-mantle tectonics. *Phys Earth Planet Inter* 176(3-4):143–156.
52. de Kock MO, Evans DAD, Beukes NJ (2009) Validating the existence of Vaalbara in the Neoarchean. *Precambrian Res* 174(1-2):145–154.
53. Gumsley A, et al. (2015) Precise U-Pb baddeleyite age dating of the Usushwana Complex, southern Africa: Implications for the Mesoarchaean magmatic and sedimentological evolution of the Pongola Supergroup, Kaapvaal Craton. *Precambrian Res* 267:174–185.
54. Stacey JS, Kramers JD (1975) Approximation of terrestrial lead isotope evolution by a two-stage model. *Earth Planet Sci Lett* 26(2):207–221.
55. Jaffey AH, Flynn KF, Glendenin LE, Bentley WC, Essling AM (1971) Precision measurement of half-lives and specific activities of U235 and U238. *Phys Rev C Nucl Phys* 4:1889–1906.
56. Steiger RH, Jäger E (1977) Subcommission on geochronology: Convention on the use of decay constants in geo- and cosmochronology. *Earth Planet Sci Lett* 36(3):359–362.
57. Ludwig KR (2003) *User's Manual for Isoplot 3.00—A Geochronological Toolkit for Microsoft Excel* (Berkeley Geochronology Center, Berkeley, CA), Special Publ 4.
58. Chamberlain KR, et al. (2010) In situ U-Pb SIMS (IN-SIMS) micro-baddeleyite dating of mafic rocks: Method with examples. *Precambrian Res* 183(3):379–387.
59. Compston W, Williams IS, Meyer C (1984) U-Pb geochronology of zircons form lunar Breccia 73217 using a sensitive high mass-resolution ion microprobe. *J Geophys Res Solid Earth* 89(S02):B525–B534.
60. Ireland TR, Williams IS (2003) Considerations in zircon geochronology by SIMS. *Rev Miner Geochem* 53(1):215–241.
61. Kirschvink JL (1980) The least-squares line and plane and the analysis of paleomagnetic data. *Geophys J Int* 62(3):699–718.
62. Jones CH (2002) User-driven integrated software lives: "Paleomag" paleomagnetics analysis on the Macintosh. *Comput Geosci* 28(10):1145–1151.
63. Williams SE, Müller RD, Landgrebe TCW, Whittaker JM (2012) An open-source software environment for visualizing and refining plate tectonic reconstructions using high-resolution geological and geophysical data sets. *GSA Today* 22(4):4–9.
64. Evans DAD, Beukes NJ, Kirschvink JL (2002) Paleomagnetism of a lateritic paleoweathering horizon and overlying Paleoproterozoic red beds from South Africa: Implications for the Kaapvaal apparent polar wander path and a confirmation of atmospheric oxygen enrichment. *J Geophys Res Solid Earth* 107(B12):EPM 2-1–EPM 2-22.
65. Schröder S, Bedorf D, Beukes NJ, Gutzmer J (2011) From BIF to red beds: Sedimentology and sequence stratigraphy of the Paleoproterozoic Koegas Subgroup (South Africa). *Sediment Geol* 236(1-2):25–44.
66. Beukes NJ (1984) Sedimentology of the Kuruman and Griquatown iron-formations, Transvaal Supergroup, Griqualand West, South Africa. *Precambrian Res* 24(1):47–84.
67. Bekker A, et al. (2008) Fractionation between inorganic and organic carbon during the Lomagundi (2.22–2.1 Ga) carbon isotope excursion. *Earth Planet Sci Lett* 271(1-4):278–291.
68. Coetzee LL, Beukes NJ, Gutzmer J, Kakegawa T (2006) Links of organic carbon cycling and burial to depositional depth gradients and establishment of a snowball Earth at 2.3 Ga. Evidence from the Timeball Hill Formation,Transvaal Supergroup, South Africa. *South Afr J Geol* 109(1-2):109–122.
69. Farquhar J, Bao H, Thiemens M (2000) Atmospheric influence of Earth's earliest sulfur cycle. *Science* 289(5480):756–759.
70. Bekker A, et al. (2004) Dating the rise of atmospheric oxygen. *Nature* 427(6970):117–120.
71. Johnson JE, et al. (2013) Manganese-oxidizing photosynthesis before the rise of cyanobacteria. *Proc Natl Acad Sci USA* 110(28):11238–11243.
72. Pickard AL (2003) SHRIMP U-Pb zircon ages for the Palaeoproterozoic Kuruman Iron Formation, northern Cape Province, South Africa: Evidence for simultaneous BIF deposition on Kaapvaal and Pilbara cratons. *Precambrian Res* 125(3-4):275–315.
73. Sumner DY, Bowring SA (1996) U-Pb geochronologic constraints on deposition of the Campbellrand Subgroup, Transvaal Supergroup, South Africa. *Precambrian Res* 79(1-2): 25–35.
74. Barton ES, Altermann W, Williams IS, Smith CB (1994) U-Pb zircon age for a tuff in the Campbell Group, Griqualand West sequence, South Africa: Implications for early Proterozoic rock accumulation rates. *Geology* 22(4):343–346.
75. Altermann W, Nelson DR (1998) Sedimentation rates, basin analysis and regional correlations of three Neoarchaean and Palaeoproterozoic sub-basins of the Kaapvaal craton as inferred from precise U-Pb zircon ages from volcaniclastic sediments. *Sediment Geol* 120(1-4):225–256.
76. Nelson DR, Trendall AF, Altermann W (1999) Chronological correlations between the Pilbara and Kaapvaal cratons. *Precambrian Res* 97(3-4):165–189.
77. Swart QD (1999) *Carbonate Rocks of the Paleoproterozoic Pretoria and Postmasburg Groups, Transvaal Supergroup* (Rand Afrikaans Univ, Johannesburg).
78. Bekker A, Karhu JA, Kaufman AJ (2006) Carbon isotope record for the onset of the Lomagundi carbon isotope excursion in the Great Lakes area, North America. *Precambrian Res* 148(1-2):145–180.
79. Sekine Y, et al. (2011) Manganese enrichment in the Gowganda Formation of the Huronian Supergroup: A highly oxidizing shallow-marine environment after the last Huronian glaciation. *Earth Planet Sci Lett* 307(1-2):201–210.
80. Chandler FW (1988) Diagenesis of sabkha-related, sulphate nodules in the early Proterozoic Gordon Lake formation, Ontario, Canada. *Carbonates Evaporites* 3(1):75–94.
81. Fedo CM, Nesbitt HW, Young GM (1995) Unraveling the effects of potassium metasomatism in sedimentary rocks and paleosols, with implications for paleoweathering conditions and provenance. *Geology* 23(10):921–924.
82. Papineau D, Mojzsis SJ, Schmitt AK (2007) Multiple sulfur isotopes from Paleoproterozoic Huronian interglacial sediments and the rise of atmospheric oxygen. *Earth Planet Sci Lett* 255(1-2):188–212.
83. Bekker A, Kaufman AJ, Karhu JA, Eriksson KA (2005) Evidence for Paleoproterozoic cap carbonates in North America. *Precambrian Res* 137(3-4):167–206.
84. Murakami T, Utsunomiya S, Imazu Y, Prasad N (2001) Direct evidence of late Archean to early Proterozoic anoxic atmosphere from a product of 2.5 Ga old weathering. *Earth Planet Sci Lett* 184(2):523–528.
85. Roscoe SM (1969) Huronian rocks and uraniferous conglomerates in the Canadian Shield. *Geol Surv Canada Open File* 68:1–205.
86. Gumsley A, Rådman J, Söderlund U, Klausen M (2016) U–Pb baddeleyite geochronology and geochemistry of the White Mfolozi Dyke Swarm: Unravelling the complexities of 2.70–2.66 Ga dyke swarms across the eastern Kaapvaal Craton, South Africa. *GFF* 138(1):115–132.
87. Reischmann T (1995) Precise U/Pb age determination with baddeleyite (ZrO2), a case study from the Phalaborwa igneous complex, South Africa. *South Afr J Geol* 98(1):1–14.
88. Letts S, Torsvik TH, Webb SJ, Ashwal LD (2011) New Palaeoproterozoic palaeomagnetic data from the Kaapvaal Craton, South Africa. *Geol Soc Lond Spec Publ* 357:9–26.
89. Zeh A, Ovtcharova M, Wilson AH, Schaltegger U (2015) The Bushveld Complex was emplaced and cooled in less than one million years—results of zirconology, and geotectonic implications. *Earth Planet Sci Lett* 418:103–114.
90. Letts S, Torsvik TH, Webb SJ, Ashwal LD (2009) Palaeomagnetism of the 2054 Ma Bushveld Complex (South Africa): Implications for emplacement and cooling. *Geophys J Int* 179(2):850–872.
91. Dorland HC, Beukes NJ, Gutzmer J, Evans DAD, Armstrong RA (2006) Precise SHRIMP U-Pb zircon age constraints on the lower Waterberg and Soutpansberg Groups, South Africa. *South Afr J Geol* 109(1-2):139–156.
92. de Kock MO, Evans DAD, Dorland HC, Beukes NJ, Gutzmer J (2006) Paleomagnetism of the lower two unconformity-bounded sequences of the Waterberg Group, South Africa: Towards a better-defined apparent polar wander path for the Paleoproterozoic Kaapvaal Craton. *South Afr J Geol* 109(1-2):157–182.
93. Kamo SL, Reimold WU, Krogh TE, Colliston WP (1996) A 2.023 Ga age for the Vredefort impact event and a first report of shock metamorphosed zircons in pseudotachylitic breccias and Granophyre. *Earth Planet Sci Lett* 144(3-4):369–387.
94. Carporzen L, Gilder SA, Hart RJ (2005) Palaeomagnetism of the Vredefort meteorite crater and implications for craters on Mars. *Nature* 435(7039):198–201.

PAPER VI

AUSTRALIAN JOURNAL OF EARTH SCIENCES, 2017
VOL. 64, NO. 2, 225–237
http://dx.doi.org/10.1080/08120099.2017.1289981

Paleomagnetism and U–Pb geochronology of the Black Range dykes, Pilbara Craton, Western Australia: a Neoarchean crossing of the polar circle

D. A. D. Evans [a], A.V. Smirnov [b] and A. P. Gumsley [c]

[a]Department of Geology & Geophysics, Yale University, New Haven, CT 06520-8109, USA; [b]Department of Geological & Mining Engineering & Sciences, Michigan Technological University, Houghton, MI 49931-1295, USA; [c]Department of Geology, Lund University, Lund 223 62, Sweden

ABSTRACT
We report a new paleomagnetic pole for the Black Range Dolerite Suite of dykes, Pilbara craton, Western Australia. We replicate previous paleomagnetic results from the Black Range Dyke itself, but find that its magnetic remanence direction lies at the margin of a distribution of nine dyke mean directions. We also report two new minimum ID-TIMS $^{207}Pb/^{206}Pb$ baddeleyite ages from the swarm, one from the Black Range Dyke itself (>2769 ± 1 Ma) and another from a parallel dyke whose remanence direction lies near the centre of the dataset (>2764 ± 3 Ma). Both ages are slightly younger than a previous combined SHRIMP $^{207}Pb/^{206}Pb$ baddeleyite weighted mean date from the same swarm, with slight discordance interpreted as being caused by thin metamorphic zircon overgrowths. The updated Black Range suite mean remanence direction ($D = 031.5°$, $I = 78.7°$, $k = 40$, $\alpha_{95} = 8.3°$) corresponds to a paleomagnetic pole calculated from the mean of nine virtual geomagnetic poles at 03.8°S, 130.4°E, $K = 13$ and $A_{95} = 15.0°$. The pole's reliability is bolstered by a positive inverse baked-contact test on a younger Round Hummock dyke, a tentatively positive phreatomagmatic conglomerate test, and dissimilarity to all younger paleomagnetic poles from the Pilbara region and contiguous portions of Australia. The Black Range pole is distinct from that of the Mt Roe Basalt (or so-called 'Package 1' of the Fortescue Group), which had previously been correlated with the Black Range dykes based on regional stratigraphy and imprecise SHRIMP U–Pb ages. We suggest that the Mt Roe Basalt is penecontemporaneous to the Black Range dykes, but with a slight age difference resolvable by paleomagnetic directions through a time of rapid drift of the Pilbara craton across the Neoarchean polar circle.

ARTICLE HISTORY
Received 10 December 2016
Accepted 29 January 2017

KEYWORDS
paleomagnetism; U–Pb geochronology; Black Range Dolerite Suite; Pilbara craton; Western Australia; Neoarchean

Introduction

Precambrian craton reconstructions require high-quality paleomagnetic poles from well-dated and well-preserved rocks. The question of whether Earth's supercontinent cycle began in Archean or Proterozoic time (Bleeker, 2003; Evans, 2013; Van Kranendonk & Kirkland, 2016) hinges on identifying former 'supercraton' connections and assessing whether those connections amalgamated into a single Neoarchean supercontinent, named Kenorland (Williams, Hoffman, Lewry, Monger, & Rivers, 1991), or whether instead they were embedded within continent-sized blocks (Bleeker, 2003). One classic supercraton is Vaalbara, the hypothesised conjunction of Kaapvaal craton, in southern Africa, with the Pilbara craton in Western Australia (Cheney, 1996). Different alternative reconstruction models (ibid., de Kock, Evans, & Beukes, 2009; Zegers, de Wit, Dann, & White, 1998) place the two cratons adjacent to each other in various relative locations and orientations.

The constituent cratons of Vaalbara have yielded a uniquely comprehensive dataset of Archean paleomagnetic directions, owing to their equally unique preservation of low-grade volcano-sedimentary rocks. On the Pilbara, initial success in obtaining coherent remanence directions from Fortescue lavas (Irving & Green, 1958) inspired further investigations of those rocks with similar results (Schmidt & Embleton, 1985). The most recent published paleomagnetic study documented Earth's oldest recorded stratabound magnetic reversal and quantified cratonic drift velocities comparable with those of the last few hundred million years (Strik, Blake, Zegers, White, & Langereis, 2003). Further data also led to a revised reconstruction of Vaalbara that demarcates a simple pattern of depositional facies across the supercraton, in conjunction with paleomagnetic studies (de Kock *et al.*, 2009).

Pre-Fortescue basement in the Pilbara craton has good potential for extending the paleomagnetic record before *ca* 2770 Ma, in order to determine whether geodynamo records and tests of plate velocities can be extended back further into Archean time (e.g. Bradley, Weiss, & Buick, 2015). The purpose of the present study is to begin such efforts by refining the Black Range suite of dykes paleomagnetic pole, using paleomagnetism integrated with U–Pb baddeleyite geochronology. Our results have important implications for stratigraphic correlations in the north-central Pilbara region.

CONTACT D. A. D. Evans david.evans@yale.edu

Stratigraphic context

Archean stratigraphy of the Pilbara craton can be divided into two temporally and structurally defined successions (Figure 1). The older succession generally has granitoid–greenstone dome-trough crustal architecture with ages between *ca* 3500 and 2800 Ma, and is divided into the Pilbara and De Grey Supergroups in the East Pilbara Terrane or their lateral equivalents in the West Pilbara Terrane (Hickman, 2012; Van Kranendonk *et al.*, 2006a). Following a large-scale regional unconformity, the second succession begins with the volcanic-dominated Fortescue Group and related intrusions within the time interval *ca* 2800–2700 Ma (Thorne & Trendall, 2001), followed conformably by the largely sedimentary Hamersley Group that extends into Paleoproterozoic time (Trendall, 1983). The Fortescue–Hamersley succession has been interpreted to record a plate-tectonic evolution from rifting to development of a passive margin (Blake, 1993; Thorne & Trendall, 2001), perhaps initially with the aid of a mantle plume (Arndt, Bruzak, & Reischmann, 2001; Rainbird & Ernst, 2001).

Fortescue Group strata are variable across the craton (Figure 1), but generally include a lowest mafic volcanic unit (Mount Roe Basalt), followed by a sandstone-dominated interval (Hardey Formation), more dominantly mafic volcanic units (variable names), and an uppermost shale-dominated unit (Jeerinah Formation). Felsic igneous rocks (Bamboo Creek and Spinaway porphyries) locally occur within or adjacent to the Hardey Formation. Around the northern part of the craton, variability can be observed along strike from the west near the Roebourne/Pyramid area, to the east near the Nullagine region and beyond to the Gregory Range. Near the centre of the northern outcrop belt, where the metamorphic grade is lowest (Smith, Perdrix, & Parks, 1982), the Marble Bar Sub-basin (an erosional outlier) exposes several alternations of basaltic lava and siliciclastic sedimentary rock that are disconnected from other Fortescue Group exposures. In that region, the stratigraphically lowest package was moderately to steeply folded prior to deposition of the overlying succession (Blake, 1993).

The Mount Roe Basalt, referred to as Fortescue Group 'Package 1' in the sequence-stratigraphic framework of Blake (1993) and Blake, Buick, Brown, and Barley (2004), has been dated by U–Pb methods in three localities: 2763 ± 13 Ma (SHRIMP on zircon) near the type locality at Roebourne (Arndt, Nelson, Compston, Trendall, & Thorne, 1991), 2775 ± 10 Ma (SHRIMP on zircon) in the far southwest area of the craton (ibid.), and 2767 ± 3 (TIMS on air-abraded zircon; ~1.4% discordant) in an isolated exposure near the southern edge of the Marble Bar outlier (Van Kranendonk, Bleeker, & Ketchum, 2006b). Ages from the overlying Hardey Formation interval include a volcanic member in the easternmost Pilbara (2764 ± 8 Ma, SHRIMP on zircon; Arndt *et al.*, 1991); two

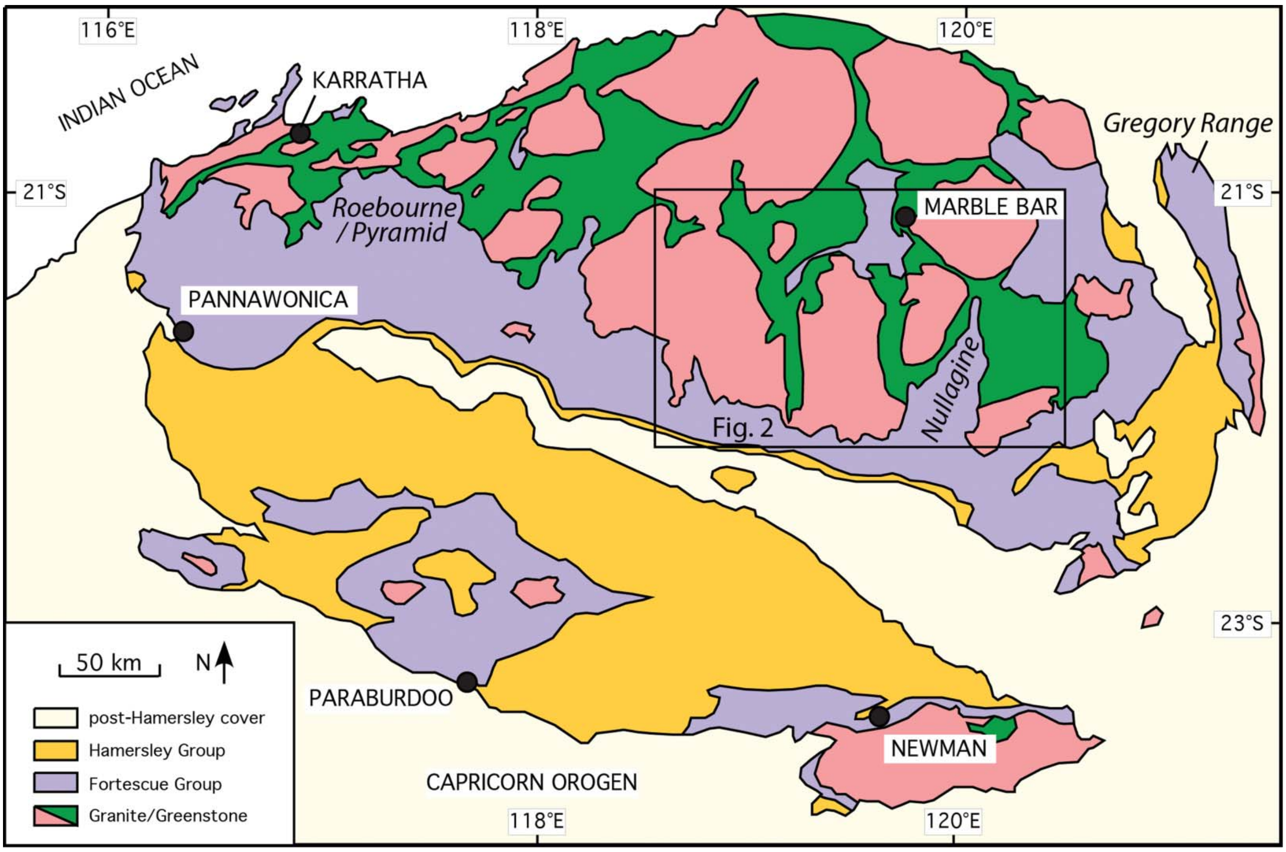

Figure 1. Simplified map of the Pilbara cratonic region, showing the sampling area relative to other exposures of Fortescue Group and related intrusive rocks.

porphyries in east-central part of the craton, Spinaway (2768 ± 16 Ma conventional U–Pb on zircon, Pidgeon, 1984; 2766 ± 2 Ma, SHRIMP U–Pb on zircon, Blake *et al.*, 2004) and Bamboo Creek (2756 ± 8 Ma, SHRIMP on zircon; Arndt *et al.*, 1991); a lower rhyolite unit (2766 ± 3 Ma; Blake *et al.*, 2004); a felsic tuff near the top of the sequence (2752 ± 5 Ma; Blake *et al.*, 2004); and a volcanic unit within the sandstone in the southern region (2750 ± 5 Ma; Hall, 2005). The latter three ages were all obtained by U–Pb SHRIMP methods on zircon.

For many years, it has been considered that eruption of the Mount Roe Basalt was coincident with emplacement of the Black Range Dolerite Suite of NNE-trending mafic dykes, which include both the Black Range Dyke itself and the Cajuput Dyke farther to the east (Figure 2)—the latter of which is nonconformably overlain by Hardey Formation sandstone (Hickman, 1983; Lewis, Rosman, & de Laeter, 1975). The correlation of Mount Roe Basalt and the Black Range dyke swarm was strengthened by an integrated ^{207}Pb–^{206}Pb SHRIMP baddeleyite age of 2772 ± 2 Ma for the dykes (Wingate, 1999), which was within uncertainty of the previous Mount Roe Basalt ages (Arndt *et al.*, 1991). The Black Range and Cajuput dykes also share a paleomagnetic remanence direction (Embleton, 1978) with that of the Mount Roe Basalt (Schmidt & Embleton, 1985; Strik *et al.*, 2003), thus appearing to reinforce the correlation even further.

Nonetheless, near the southwestern edge of the Marble Bar Sub-basin (Figure 2), at least one dyke of the Black Range suite (herein referred to as the Pilga dyke, with new U–Pb geochronology presented below) intrudes the lowermost lava package—moderately tilted as noted above, and shown on published Geological Survey of Western Australia (GSWA) quadrangle maps as Mount Roe Basalt (Hickman, 2010, 2013; Hickman & Lipple, 1978; Van Kranendonk, 2000). What might be a northward, right-stepping en echelon offset of that dyke also appears to intrude lavas correlated with the Kylena basalt, which would be surprising, as the Kylena Formation (in its type locality) is definitively younger than Hardey Formation sandstone and has yielded ages in the range of *ca* 2760–2740 Ma (Blake *et al.*, 2004). Such stratigraphic relationships prompted Van Kranendonk (2000) to conclude that the Pilga dyke 'must belong to a younger set.' Not all Fortescue stratigraphers agree, however, with the mapped correlations by GSWA in the Marble Bar Sub-basin. Blake (1993) maintained correlation of the lowest Marble Bar Sub-basin basalt package, which attains steep dips, with the subhorizontal Mount Roe Basalt of the Nullagine area, but correlated the overlying, subhorizontal lavas of his 'Glen Herring Creek Sequence' to the Hardey Formation rather than Kylena Formation (Figure 3). With further modification, Strik (2004) discovered that the lowest Marble Bar Sub-basin lava succession (with locally

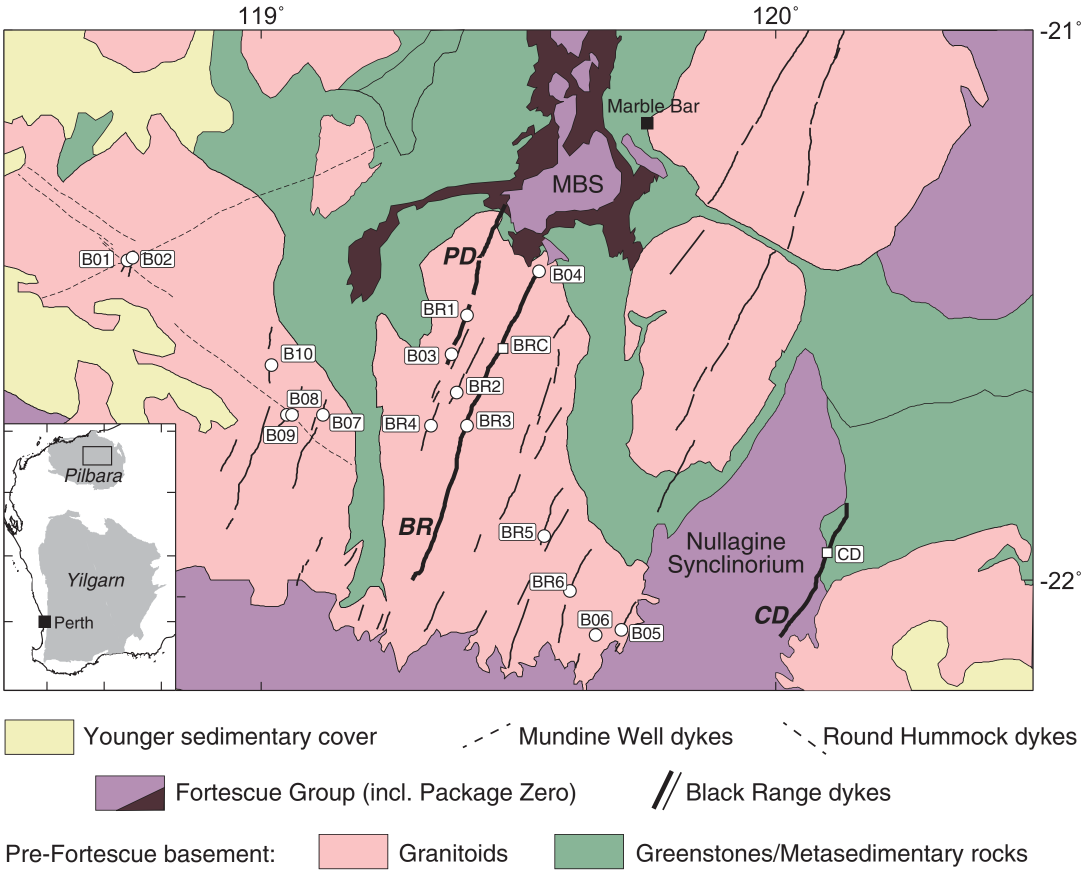

Figure 2. Location of sampling sites (circles, this study; squares, Embleton, 1978) and simplified geology of the sampling area. The Black Range Dolerite Suite of mafic dykes includes the Pilga dyke (PD), Black Range Dyke (BR) and Cajuput Dyke (CD). MBS, Marble Bar Sub-basin. Inset map shows the location of our sampling area within the Pilbara cratonic area (box) in Western Australia.

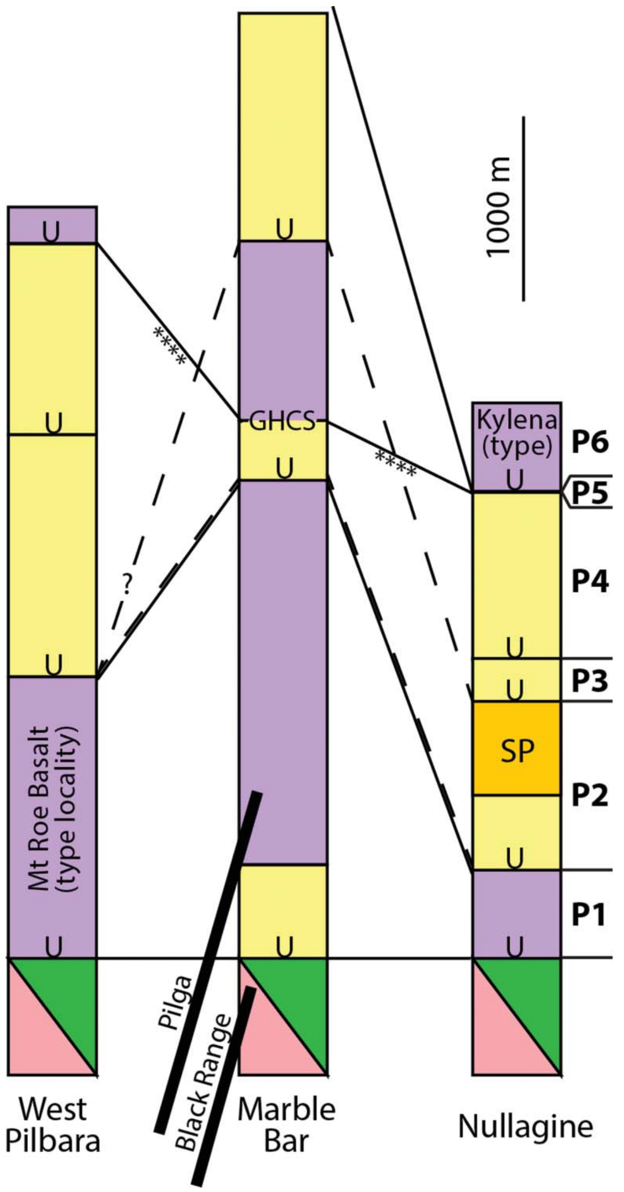

Figure 3. Alternative published stratigraphic correlations across the northern Pilbara craton, as of 2003, modified after Blake (1984). Unconformities are denoted by 'U.' Dashed lines: correlations of Blake (1984). Undecorated solid lines: correlations of Blake (1993) including GHCS, Glen Herring Creek Sequence. Solid lines marked with '****' are correlations from published editions of the Marble Bar geological maps at 1:250 000 scale (Hickman, 2010, 2013; Hickman & Lipple, 1978) and 1:100 000 scale (Hickman & Van Kranendonk, 2008). Nullagine synclinorium stratigraphic sequence 'packages' P1–P6 follow Blake et al. (2004); the stratigraphy continues higher than shown. SP, Spinaway felsic porphyry of Lipple (1975), included within the Bamboo Creek Member of the Hardey Formation by Thorne and Trendall (2001) and Hickman (2007).

steep dips) has a distinct paleomagnetic remanence from Mount Roe Basalt in other regions of the northern Pilbara. According to paleomagnetic correlations by Strik (2004), the lowest lavas in the Marble Bar Sub-basin were named 'Package 0,' and the overlying Glen Herring Creek Sequence lavas would more appropriately correlate to 'Package 1' of the Mount Roe Basalt (Strik *et al.*, 2003). These alternative correlations could allow the entire Black Range suite of dykes, including the Pilga dyke, to occupy a single stratigraphic position consistent with available geochronology: penecontemporaneous to 'Package 1.'

The present paper describes new geochronological and paleomagnetic data from the Black Range dyke swarm, and discusses how the new data can be interpreted in a new, integrated litho- and chronostratigraphy for the northern Pilbara region in Neoarchean times.

Methods

Geochronological processing was made at the Department of Geology in Lund University, where dolerite dyke sample C09B03 (Pilga dyke) and C08BR3 (Black Range Dyke at Hillside) were crushed and milled in order to extract baddeleyite. Extraction was carried out using the water-based separation technique of Söderlund and Johansson (2002) with a Wilfley Table. The best-quality baddeleyite crystals were hand-picked and combined into fractions comprising between one to five crystals each, and placed in separate pre-cleaned Teflon capsules in a fume hood within the clean laboratory at Lund University. The baddeleyite grain fractions in the capsules were then washed thoroughly in steps with small quantities of ultrapure HNO_3 and H_2O. After washing the Teflon capsules containing the cleaned baddeleyite grains, a spike solution consisting of ^{205}Pb, ^{233}U and ^{236}U was added to every capsule together with concentrated ultrapure HF. The capsules were then placed in an oven at 200°C for three days in order to dissolve the baddeleyite grains and homogenise the initial and spike U and Pb solutions together. In the clean laboratory at the Department of Geosciences in the Museum of Natural History (Stockholm), the Teflon capsules containing the sample solutions were then placed on a hot plate at 100°C until the combined solution evaporated in a fume hood. Ultrapure 6 M HCl and 0.25 M H_3PO_4 was then added to each capsule before being dried down once again on the hotplate at 100°C, leaving a small sample droplet. These droplets in the capsules consist of the dissolved sample fraction and spike in H_3PO_4 that was then further redissolved in 2 μL of Si-gel prepared using a recipe of Gerstenberger and Haase (1997) before being loaded on outgassed Re filaments.

The analyses were made on the Finnigan Triton mass spectrometer at the Department of Geosciences, Swedish Museum of Natural History in Stockholm following the same procedure as that employed by Gumsley *et al.* (2015). The Re filaments with the samples were loaded onto a carousel and mounted, and then heated, in the high vacuum chamber in the mass spectrometer. The Pb isotopes were measured after being heated and emitted in a temperature range of approximately 1210–1250°C. The isotopes ^{204}Pb, ^{205}Pb, ^{206}Pb, ^{207}Pb and ^{208}Pb were measured in either static mode with Faraday detectors, or in peak-switching mode with a Secondary Electron Multiplier amplifier. Age, size and quantity of grains could be linked to whether static or peak-switching mode was used. Large samples with high ^{206}Pb/^{205}Pb ratios and strong and stable signals were preferentially measured in static mode. Upon completion of the Pb isotopic analyses, the filament temperatures were increased to

Table 1. ID-TIMS baddeleyite isotopic data from the Pilga and Black Range dykes.

Analysis no. (no. of grains)	U/Th	Pb_{bc}/Pb_{tot}raw[b]	$^{206}Pb/^{204}Pb$	$^{207}Pb/^{235}U$ (corr.)[c]	$\pm 2\sigma$ % error	$^{206}Pb/^{238}U$	$\pm 2\sigma$ % error	$^{207}Pb/^{235}U$ (age, Ma)	$^{206}Pb/^{238}U$	$^{207}Pb/^{206}Pb$	$\pm 2\sigma$	Concordance (%)
Pilga (C09B03): 2763.9 ± 3.3 Ma, 1/6 point $^{207}Pb/^{206}Pb$ minimum date												
a (4)	4.6	0.015	3905.0	13.965	0.337	0.527	0.314	2747.3	2728.0	2761.6	2.2	98.8
b (3)	3.0	0.021	2770.9	13.826	0.568	0.524	0.553	2737.9	2716.8	2753.5	3.5	98.7
c (5)	9.0	0.054	1175.8	13.988	0.845	0.527	0.844	2748.9	2728.5	2763.9	3.4	98.7
d (1)	15.5	0.093	693.5	14.185	1.458	0.536	1.459	2762.1	2766.8	2758.7	5.7	100.3
e (2)	2.2	0.047	1337.5	13.971	0.745	0.528	0.739	2747.7	2735.1	2757.0	3.2	99.2
f (4)	4.6	0.034	1771.7	13.554	0.589	0.515	0.570	2719.0	2678.9	2749.1	3.3	97.4
Black Range (C08BR3): 2769.4 ± 1.0 Ma, 1/5 point $^{207}Pb/^{206}Pb$ minimum date												
a (1)	43.6	0.019	3223.1	12.451	0.453	0.488	0.448	2639.0	2563.9	2697.2	1.6	95.1
b (1)	74.4	0.042	1476.7	13.374	0.905	0.506	0.888	2706.4	2640.7	2755.9	3.9	95.8
c (1)	43.1	0.010	6281.7	13.981	0.217	0.527	0.202	2748.4	2730.3	2761.8	1.4	98.9
d (1)	52.5	0.057	1092.7	14.085	1.068	0.532	1.057	2755.4	2748.8	2760.3	4.4	99.6
e (1)	49.4	0.005	11955.1	14.185	0.242	0.533	0.236	2762.1	2752.3	2769.4	1.0	99.4

[a]P_{bc} = common Pb; Pb_{tot} = total Pb (radiogenic + blank + initial). [b] Measured ratio, corrected for mass fractionation and spike. [c] Isotopic ratios corrected for mass fractionation (0.1% per amu for Pb, determined by replicate analyses of NBS standard SRM. 981 and SRM 983), spike contribution (^{205}Pb–^{233}U–^{236}U tracer solution), blank (1 pg Pb and <0.1 pg U), and initial common Pb. Initial common Pb corrected with isotopic compositions from the model of Stacey and Kramers (1975) at the age of the sample. corr. = corrected

between 1310–1320°C, where ^{235}U and ^{238}U isotopes were emitted and measured. An 'in-house' program made by Per-Olof Persson (Department of Geosciences, Natural History Museum, Stockholm) with calculations following Ludwig (2001) was used for data handling, and final age calculations were made using Isoplot (Ludwig, 2001).

For paleomagnetic studies, we sampled 16 sites representing 14 separate dykes in the northeastern part of the Pilbara craton (Figure 2). Seven to 17 field-drilled, oriented, 2.5 cm-diameter core samples were collected from each site. Orientation was done with both solar and magnetic compasses. Although outcrops were screened with a compass for notable magnetic deflections by lightning, at some sites minor deflections were unavoidable owing to limited outcrop.

Magnetic remanence measurements were conducted at Michigan Technological University using an automated three-axis DC-SQuID 2G rock magnetometer housed in a magnetically shielded room. After measurement of the natural remanent magnetisation (NRM), the samples were cycled through the Verwey transition at ~120 K (Verwey, 1939) by immersing them into liquid nitrogen for about 2 h in order to reduce a viscous component carried by larger magnetite grains (Schmidt, 1993). The low-temperature treatment was followed by 15–20 thermal demagnetisation steps performed in an inert (nitrogen) atmosphere. Progressive demagnetisation was carried out until the magnetic intensity of the samples dropped below system noise level or until the measured directions became erratic and unstable (typically at 580–590°C).

The characteristic remanent magnetisation (ChRM) for samples displaying near-linear demagnetisation trajectories was isolated using principal-component analysis (Kirschvink, 1980). The best-fit line was used if defined by at least five consecutive demagnetisation steps that trended toward the origin and had a maximum angle of deviation less than 10°. The mean directions were calculated using Fisher statistics (Fisher, 1953). A site mean was accepted for further calculations if it was obtained from three or more samples, and the confidence circle radius (α_{95}) was smaller than 10°.

Results and discussion

Geochronology

Both mafic dyke samples yielded abundant fragments of euhedral baddeleyite with thin surface coatings, frosty in appearance, which are interpreted as zircon overgrowths (cf. Heaman & LeCheminant, 1993). Such overgrowths are well documented in mafic rocks of high metamorphic grade, but the north-central Pilbara has experienced only prehnite–pumpellyite metamorphism (Smith *et al.*, 1982), dated by monazite at *ca* 2160 Ma (Rasmussen, Fletcher, & Sheppard, 2005). If zirconium mobilisation during that episode (or some other secondary event) caused the minor zircon overgrowth, then each analysis would measure a mixture of the primary baddeleyite cores, and a small contribution from secondary zircon rims, and thus underestimate the age of baddeleyite crystallisation. Our choices for calculating the data of the subsets (Table 1) are made with these factors under consideration.

From the Pilga sample C09B03 (Figure 4), six fractions were analysed, each combining between one and five grains. Fraction (d) was the only single-grain baddeleyite analysed. $^{207}Pb/^{206}Pb$ dates from the six analyses ranged between 2764 Ma and 2749 Ma, with concordance varying from 97% to 100%. The oldest $^{207}Pb/^{206}Pb$ date of 2763.9 ± 3.4 Ma (fraction c), at 99% concordance, is interpreted to provide a minimum age for the Pilga dyke emplacement.

From the Black Range Dyke sample C08BR3, five single grains were analysed. Two grains (fractions a, b), had variable concordance between 95 and 96% (Figure 4) and are not considered further. Fractions (c, d, e), however, were between 99 and 100% concordant and yielded variable $^{207}Pb/^{206}Pb$ dates between 2769 Ma and 2760 Ma. As such, the oldest $^{207}Pb/^{206}Pb$ date of 2769.4 ± 1.0 Ma on fraction (e) likely represents the best minimum estimate for the age of baddeleyite crystallisation.

These new two $^{207}Pb/^{206}Pb$ TIMS ages are comparable with the previously published weighted mean $^{207}Pb/^{206}Pb$ SHRIMP baddeleyite age of 2772 ± 2 Ma for the Black Range Dolerite Suite (Wingate, 1999), as shown in Figure 4b. The oldest TIMS analysis on our Black Range sample (fraction e) has a

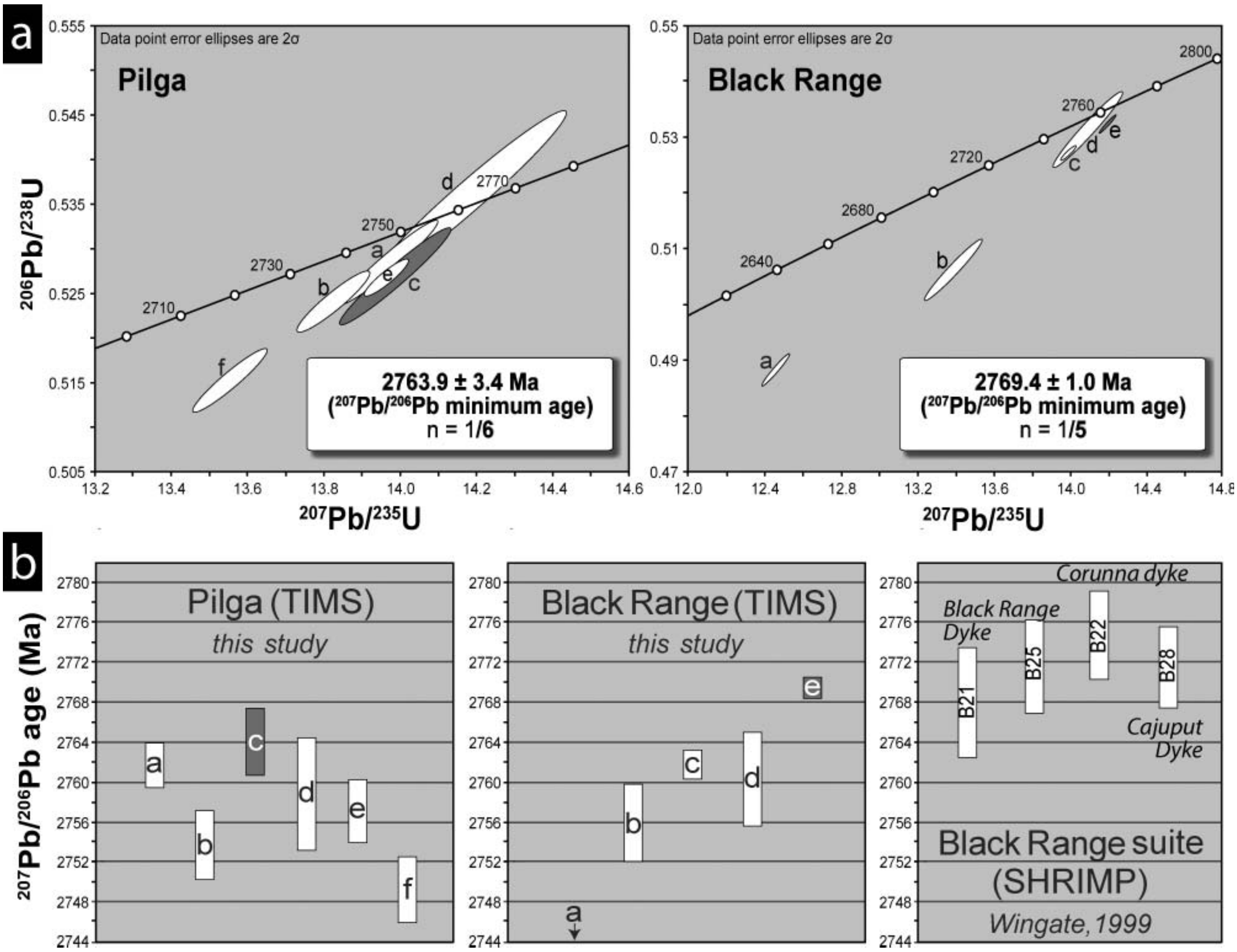

Figure 4. (a) Wetherill U–Pb ID-TIMS concordia diagrams for the analysed baddeleyite from the Pilga and Black Range dykes, with the error ellipses demarcating individual fractions analysed, for details see Table 1. (b) $^{207}Pb/^{206}Pb$ plots of the individual baddeleyite fractions analysed in this study for the Pilga and Black Range dykes at left, with a comparison of complete $^{207}Pb/^{207}Pb$ ages by SHRIMP also shown of the Black Range Dolerite Suite by Wingate (1999) at right, which were combined into the 2772 ± 2 Ma mean age in that study.

$^{207}Pb/^{206}Pb$ age within error of the mean SHRIMP result from the same dyke and suggests that our preferred method of selecting the oldest-age fraction is the most accurate assessment of the variable TIMS data, at least in this instance. SHRIMP analyses on the interior domains of baddeleyite grains are better placed to avoid zircon overgrowths and generate unbiased ages of crystallisation, despite being less precise.

Interpretation of the Pilga dyke data is hindered by the absence of a SHRIMP result on the same intrusion as a reference. The preferred 2764 ± 3 Ma result provides a minimum date for dyke emplacement, but it remains unclear whether the Pilga and Black Range dykes are strictly coeval, or whether the Pilga dyke could have intruded several million years after the other dykes in the Black Range suite. Regardless, the Pilga data are clearly more similar to the SHRIMP results from the Mount Roe Basalt, rather than the Kylena Formation, with implications for Fortescue Group correlations between Marble Bar Sub-basin and other outcrop areas.

Paleomagnetism

Most sites exhibited one or two components of remanent magnetisation (Figure 5). Most samples showed a consistent high unblocking temperature (~500–580°C) ChRM with steep downward directions, generally N to E in declination. Low–moderate-temperature components were generally scattered or had a weak tendency toward low inclinations to the WNW or ENE; in only two sites were such overprints coherent enough to produce a clustered mean direction (site BR4, $D = 299°$, $I = 10°$, $\alpha_{95} = 8°$, $N = 6/7$; and site B05, $D = 305°$, $I = -35°$, $\alpha_{95} = 10°$, $N = 8/12$), which could possibly date from the regional low-grade metamorphic event at *ca* 2160 Ma (Rasmussen *et al.*, 2005). Exceptions to these general trends were observed in samples with anomalously high values of NRM intensity and parallel components removed by both liquid nitrogen treatment and moderate levels (300–500°C) of thermal demagnetisation. We strongly suspect such sites to be affected by lightning; some sites with consistent and anomalous moderate-temperature components (e.g. BR1,

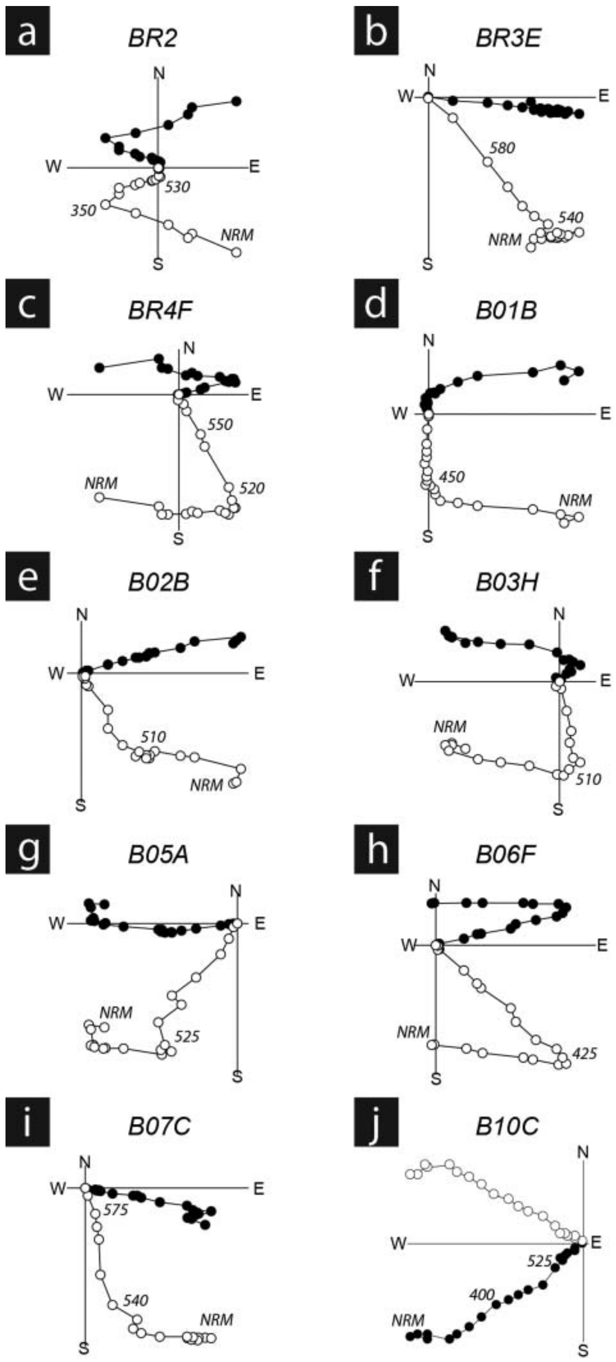

Figure 5. Typical orthogonal vector plots of thermal demagnetisation (vertical/horizontal projections shown by open/filled symbols) from the Black Range dykes. Panels (a–i) show sites used to calculate the grand mean; panel (j) shows an anomalous site that was excluded (Table 2). Numbers indicate temperature steps (in°C).

BR5) are interpreted to represent the distal tangential magnetic field about the point of lightning impact. The other two sites with coherent, non-modal ChRM directions (BR6, B10; both toward the SW but with opposing signs of inclination) did not have the same demagnetisation behaviour as the modal sites: rather than sharp unblocking spectra restricted to >500°C, those two sites' ChRM vectors had distributed unblocking through ~250–570°C (Figure 5j). The origin of their remanence vectors is uncertain, but they are clearly anomalous relative to the Black Range suite as a whole (Table 2).

Figure 6 summarises data from each of the nine sites that are included in the mean Black Range suite paleomagnetic direction. We replicate the SE-down ChRM direction for the Black Range Dyke itself at the Hillside locality (Embleton, 1978), but we find that such a direction lies, together with that of the Cajuput Dyke (ibid.) and its easterly satellite dyke (Strik *et al.*, 2003), at the outer edge of the modal distribution of NE-down remanence directions (Figure 7). We attribute the differences in remanence of the various Black Range suite dykes to paleosecular variation of the Neoarchean geodynamo. An alternative interpretation might be that the Black Range and Cajuput dykes are older than other dykes in the swarm; the Pilga and other dykes bearing the mean NE-down ChRM could be a few million years younger as allowed by our new ^{207}Pb/^{206}Pb age constraints (Figure 4). That model, however, would require a complex pattern of ChRM oscillations in stratigraphic sequence: from NW-down of Package 0 (Strik, 2004), to SE-down of the Black Range and Cajuput dykes (Embleton, 1978; this study), to NE-down of the Pilga and other dykes (this study), and back to SE-down in the higher Fortescue basalt packages (Schmidt & Embleton, 1985; Strik *et al.*, 2003). We prefer the simpler model of a single age for the Black Range Dolerite Suite, with its NE-down ChRM falling neatly between those of Package 0 and Package 1 basalts (Strik, 2004). In local coordinates, the mean Black Range suite direction (Table 2) is parameterised by $D = 031.5°$, $I = 78.7°$, $k = 40$, and $\alpha_{95} = 8.3°$, and the corresponding paleomagnetic pole, calculated from the mean of nine virtual geomagnetic poles, is at 03.8°S, 130.4°E, $K = 13$, and $A_{95} = 15.0°$.

Reliability of our new Black Range dykes pole is affirmed by an inverse baked-contact test with a Round Hummock dyke in the western part of our study area, near Obstinate Creek. Site C09B02, from a N- to NNE-striking dyke, yields a steep NE-downward ChRM typical of the Black Range suite. About 1.5 km to the south, the same Black Range dyke is cross-cut by a NW-striking dyke of the Round Hummock swarm (site I09R4). In that locality, the younger Round Hummock dyke carries a NW-down remanence direction (Figure 8) that is typical for the Round Hummock swarm, which has a preliminary ID-TIMS U–Pb baddeleyite date of *ca* 1070 Ma (D. Evans and A. Gumsley, unpublished; details to presented in a forthcoming manuscript). The Black Range dyke samples from that site, all within 5 m of the Round Hummock dyke, carry a ChRM at moderate unblocking temperatures between 300 and 375°C, likely held by contact-metamorphic pyrrhotite generated at the time of Round Hummock intrusion. Although the baked Black Range dyke remanence is likely a crystallisation-remanent magnetisation rather than a thermal-remanent magnetisation, effects from the time of Round Hummock intrusion are clearly apparent. For the purposes of the present contribution, this positive inverse baked-contact test demonstrates that the Black Range suite characteristic remanence is older than *ca* 1070 Ma. A second baked-contact test was attempted at site C09B08, where a member of the Black Range suite is

Table 2. Summary of ChRM results from the Black Range dykes.

Site ID	λ_s (°S)	Φ_s (°E)	N	B	D (°)	I (°)	k	α_{95} (°)	λ_p (°N)	Φ_P (°E)	K	A_{95} (°)
C08 BR1[a] ('Pilga dyke')	21.520	119.400	7		174.1	18.2		15.5	–	–		
C08 BR2	21.662	119.381	7	√	038.5	65.5		8.9	12.5	144.8		
C08 BR3 Black Range Dyke	21.720	119.404	7	√	099.5	77.9		6.2	−23.6	144.3		
C08 BR4	21.716	119.334	7	√	059.2	78.7		2.7	−09.6	138.2		
C08 BR5[a]	21.923	119.549	7		004.6	00.8		8.6	–	–		
C08 BR6[a]	22.015	119.603	8		236.0	50.4		8.0	–	–		
C09 B01	21.421	118.743	7	√	005.8	73.0		3.3	09.9	121.8		
C09 B02	21.415	118.748	6	√	045.2	71.8		3.2	03.2	141.7		
B02 baked by I09R4[a]	21.429	118.747	12		341.8	51.9		4.2	–	–		
I09R4[a] (Round Hummock)	21.429	118.747	4		308.2	52.2		4.7	–	–		
C09 B03 'Pilga dyke'	21.585	119.370	10	√	033.9	75.1		4.3	02.2	134.6		
C09 B04[a,b]	21.441	119.541	6		287.4	−30.1		79.5	–	–		
C09 B05	22.086	119.703	9	√	314.9	82.6		7.7	−11.5	109.2		
C09 B06	22.096	119.645	7	√	348.6	65.1		8.0	20.0	111.4		
C09 B07	21.699	119.118	8	√	161.6	81.2		3.0	−37.9	125.9		
C09 B08 baked by I09R5[a]	21.703	119.065	7		323.4	68.7		1.5	–	–		
I09R5[a] (Round Hummock dyke)	21.703	119.065	12		332.8	47.5		3.3	–	–		
C09 B09[a,c]	21.703	119.065	–		–	–		–	–	–		
C09 B10[a]	21.606	119.020	8		245.5	−25.6		15.3	–	–		
Black Range Dyke at Hillside[a,d,e]	21.72	119.40	9		093.0	76.0		8.0	–	–		
Black Range Dyke at Cooglegong Creek[a,d]	21.58	119.47	7		131.2	64.8		4.5	–	–		
Cajuput Dyke[a,d]	21.95	120.10	9		145.0	71.0		13	−47.6	149.0		
Total mean—This study only				**9**	**31.5**	**78.7**	**40**	**8.3**	**−3.8**	**130.4**	**13**	**15.0**

[a]Site is not used for calculation of the mean direction. [b] Conglomerate/breccia test. [c] Significantly scattered within-site directions. [d] Data from Embleton (1978). [e] Equivalent to Site C08BR3.

λ_s, Φ_s are the site latitude and longitude. *N* is the number of samples used to calculate the paleomagnetic declination (*D*) and inclination (*I*); α_{95} and k are the 95% confidence circle and the concentration parameter for paleomagnetic directions. *B* is the number of sites used for a between-site mean direction. λ_p and Φ_P are the latitude and longitude of the virtual geomagnetic pole (VGP). A_{95} and K are the 95% confidence circle and the concentration parameter for VGP distribution.

intruded by another Round Hummock dyke, which is 23 m wide at the intersection. Round Hummock dyke samples there (site I09R5) yield a typical NW-moderate-down ChRM direction from that swarm, but Black Range dyke rocks within 2 m of the contact have a steeper NW-down direction that is intermediate between the Round Hummock remanence and other Black Range directions (Table 2). As no more distant rocks were sampled from that particular Black Range intrusion, the test remains inconclusive.

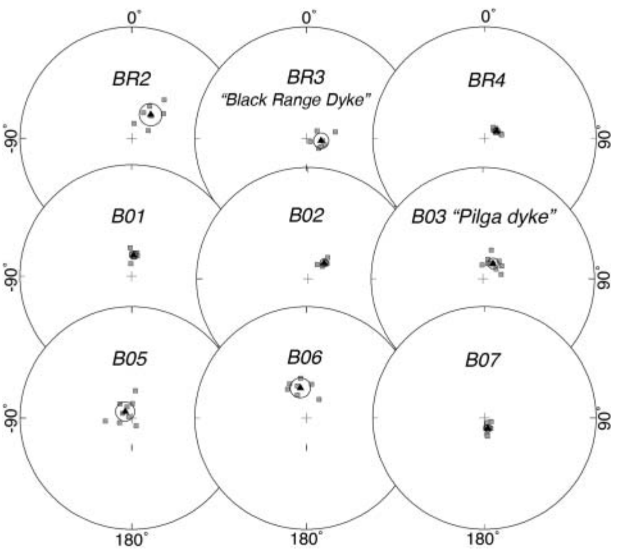

Figure 6. Site-mean paleomagnetic remanence directions from the Black Range dykes used to calculate the mean (Table 2). Equal-area plots show the accepted paleomagnetic directions (grey squares) and their means (solid triangle) with the 95% confidence circle (α_{95}) for each site.

As a final attempted test on the age of Black Range dykes' remanence, fine-grained mafic pebbles ('basalt droplets') in the granite boulder volcanic conglomerate unit of Van Kranendonk *et al.* (2006b) were individually sampled from a locality within a few hectometres of the exposed tip of the Black Range Dyke. Low-temperature components are generally directed north and upward, parallel to Earth's present magnetic field at the sampling site (Figure 9a); some samples exhibited only this presumably recent component. Other samples, collected from one side of the outcrop, show a univectorial, west-horizontal magnetisation that unblocks at temperatures generally below 500°C (Figure 9b); that direction is dissimilar to all previously documented paleomagnetic results from the northern Pilbara cratonic region and must represent a very localised overprint of unknown age. Among clasts located at the other side of the outcrop, six out of eight specimens carry a distinct ChRM after removal of the low-temperature present-field component; these higher-temperature directions, retaining stability as demagnetisation end-points from about 500 to 540°C, are quite dispersed (labelled 'SEP' in Figure 9c). The six stable end-point (SEP) vectors have a resultant mean length of 3.01; a test for uniformity against a unimodal alternative (Fisher, Lewis, & Embleton, 1987, p. 110) indicates that a uniform ('random') distribution on the sphere cannot be rejected at the 95% confidence level, a positive statistical test. The unblocking temperatures from the suite of

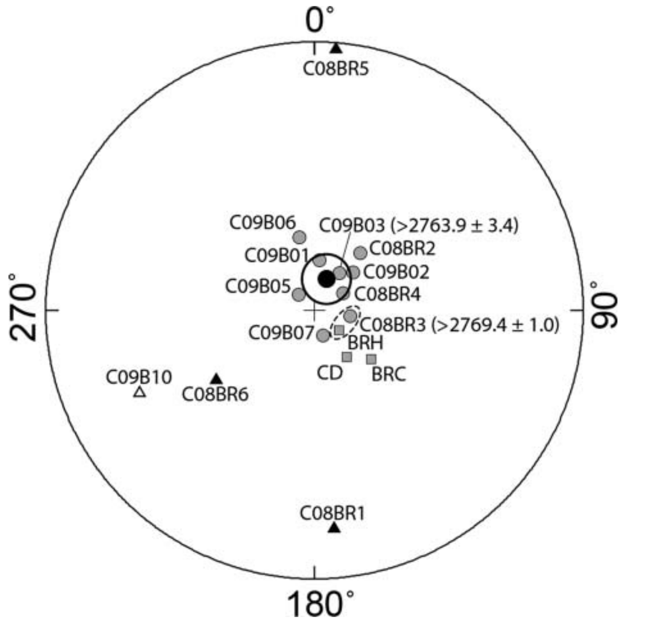

Figure 7. Summary of paleomagnetic results from the Black Range dykes. Grey circles show the accepted directions from this study; grey squares show the site-means from Embleton (1978): BRC, Black Range Dyke at Cooglegong Creek; BRH, Black Range Dyke at Hillside; CD, Cajuput Dyke (Table 1). Dashed ellipse encloses the data from Hillside locality of the Black Range Dyke, sampled by both Embleton (1978) and this study. Solid circle is the grand mean calculated from this study, with associated cone of 95% confidence (Table 2). Upright triangles show the Black Range Suite site-means from this study that are not used in the mean calculation.

'basalt droplet' clasts, however, are lower than either Black Range dykes (this study) or Mount Roe Basalt (Strik, 2004; Strik *et al.*, 2003), so the test must be considered only tentatively positive. The data are consistent with a low-temperature phreatomagmatic recrystallisation or solid-state remagnetisation of the basalt droplets prior to their incorporation into the conglomerate, which was formed penecontemporaneously to the Black Range Dyke intrusion (Van Kranendonk *et al.*, 2006b). Most definitively, the steep NE-down mean ChRM observed in the Black Range Dolerite Suite is not observed as a consistent overprint at the conglomerate site. The Shipunov, Muraviev, and Bazhenov (1998) test on that Black Range mean direction and the six conglomerate clast end-points also indicates consistency of their being drawn from a uniform ('random') distribution at the 95% confidence level.

In addition to the field tests described above, including the positive inverse baked-contact test at Obstinate Creek, an additional consideration on the age of the Black Range suite mean magnetic remanence, is the fact that its pole is distinct from all younger poles derived from Western Australia, and also all Precambrian poles generated in rocks of the North Australian craton after the latter has been restored to the West+South Australian reference frame according to Li and Evans (2011). There is broad similarity of our new Black Range suite pole to that of the first paleomagnetic analysis on the Ediacaran–Cambrian Arumbera Sandstone in central Australia (Embleton,

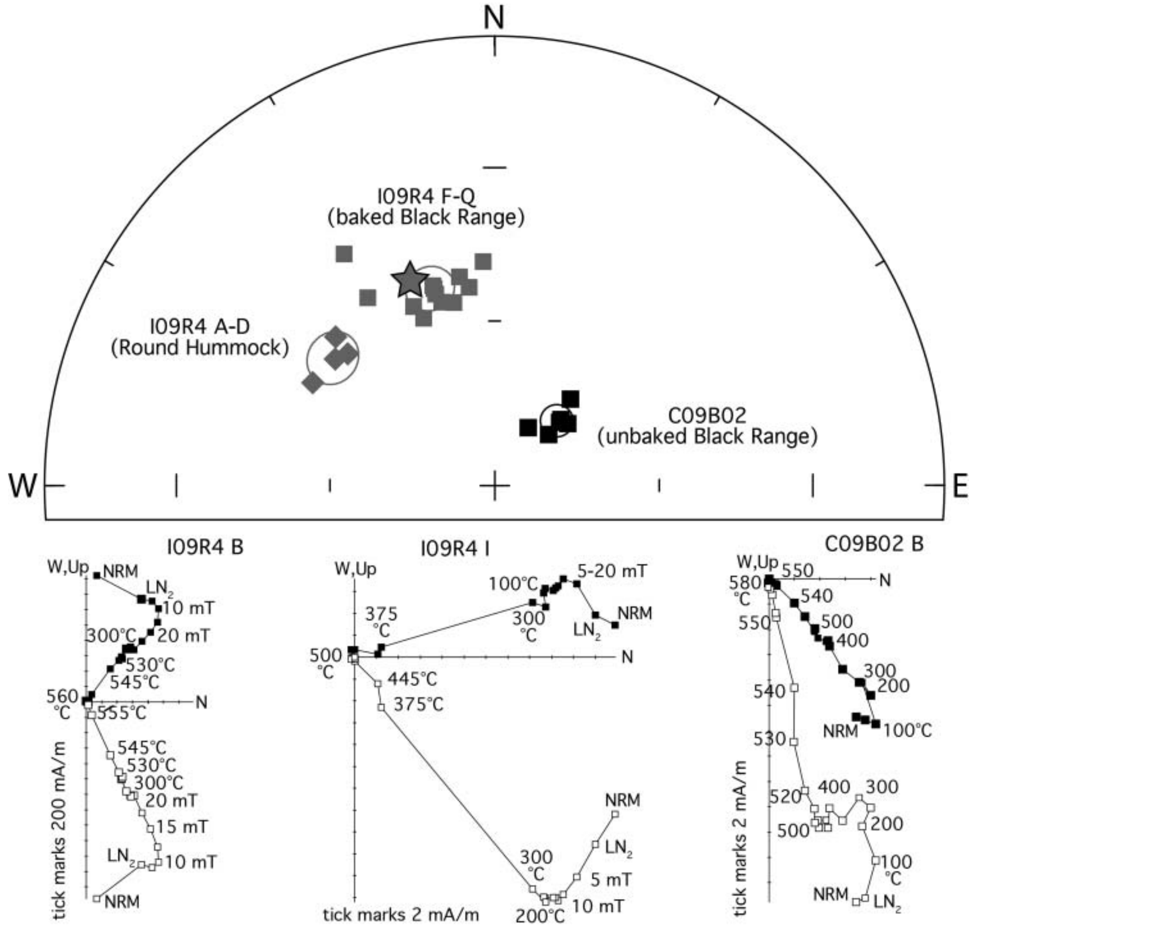

Figure 8. Inverse baked-contact test of a Black Range suite dyke (C09B02) intruded by a *ca* 1070 Ma Round Hummock dyke (I09R4) near Obstinate Creek in the western part of the study area. All stereonet vector end-points are in the lower hemisphere; squares, Black Range dyke; diamonds, Round Hummock dyke; star, expected magnetic direction from the Warakurna large igneous province mean pole (Wingate, Pisarevsky, & Evans, 2002). Orthogonal projection symbols as in Figure 5.

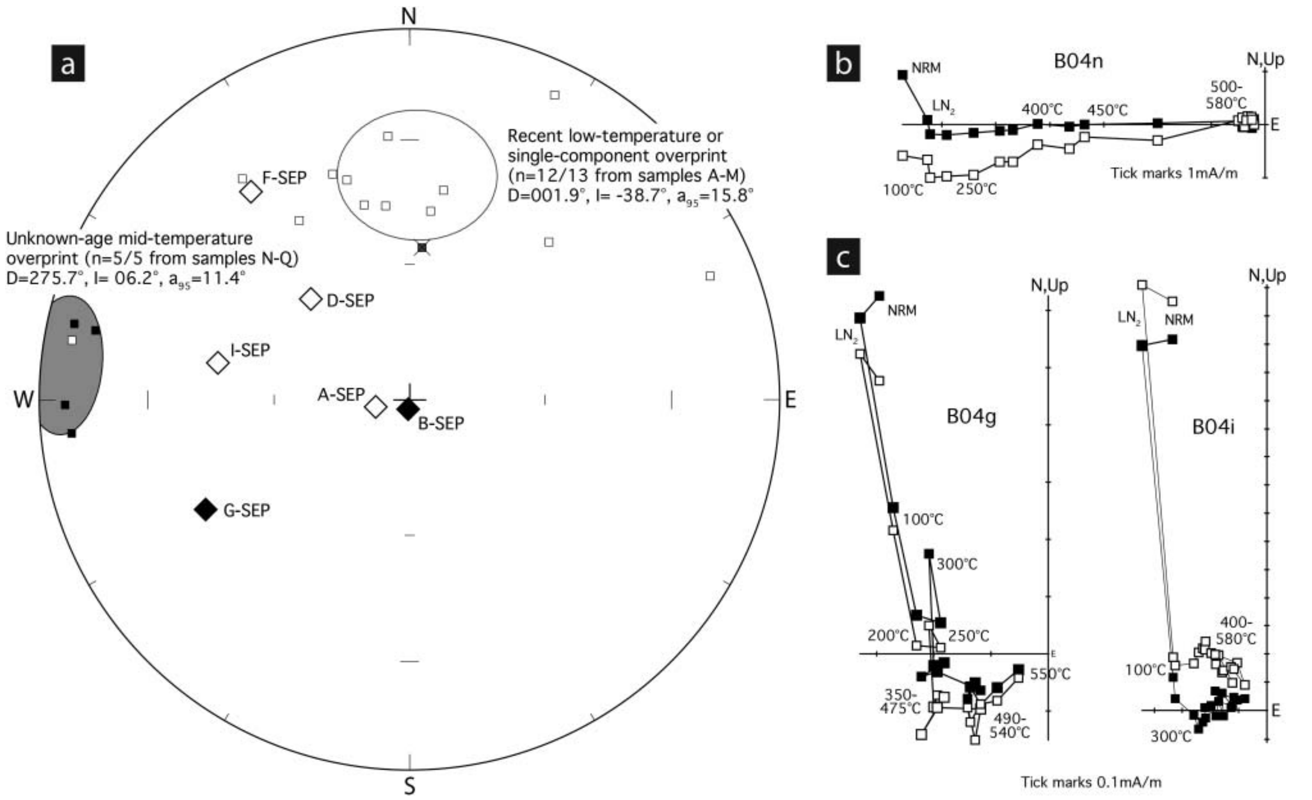

Figure 9. Phreatomagmatic breccia test from the tip of the Black Range Dyke. (a) Equal-area projection of vector component directions. Squares, low- and mid-temperature components of magnetisation; diamonds, stable end-point (SEP) vectors from samples in the outcrop area less affected by the localised mid-temperature overprint. (b) Orthogonal projection diagram of a sample with a mid-temperature overprint. (c) Orthogonal projection diagrams of samples with both low- and high-temperature components.

1972). However, that younger direction is likely a mid-Carboniferous overprint related to the Alice Springs Orogeny (Li, Powell, & Thrupp, 1990), and Paleozoic overprinting of the Black Range suite is precluded by our field stability tests. To summarise the quality of the new Black Range suite pole: on the seven-point reliability scale (Q) of Van der Voo (1990), it scores six out of seven points, lacking only dual polarity of the remanence. That criterion is met, however, by the Nullagine succession in the same region (Strik *et al.*, 2003; Table 3).

Our new paleomagnetic pole for the Black Range dyke suite (Figure 10) lies midway between poles from two unconformity-bounded sequences in the lowermost Fortescue Group: the informally named Package 1, which is generally correlated with the Mount Roe Basalt (Strik *et al.*, 2003), and the stratigraphically lower Package 0 (Strik, 2004) that is restricted to the Marble Bar Sub-basin and also generally mapped as Mount Roe Basalt (e.g. Hickman, 2010, 2013). Because ages from the rocks mapped as Mount Roe Basalt are either imprecise (Arndt *et al.*, 1991) or of uncertain correlation to the type locality (Van Kranendonk *et al.*, 2006b), the progression of paleomagnetic poles among the Mount Roe Basalt and related units may provide an independent chronometer for magmatism and sedimentation across the northern Pilbara. The poles (Table 3) sweep across the craton in rough

Table 3. Late Archean (*ca* 2800–2700 Ma) paleomagnetic poles from Pilbara craton, Western Australia.

Paleomagnetic pole	Code	Age (Ma)	Method	Pole (°N, °E)	A_{95} (°)	1234567 (Q)	Test	References
Fortescue Package 0	P0	>2772 ± 2	SHRIMP-b	−01, 093	8	0111101 (5)	F	Strik, 2004; Wingate, 1999
Black Range suite	BRS	2772 ± 2	SHRIMP-b	−04, 130	15	1111101 (6)	c, G	Wingate, 1999; this study
Fortescue Package 1	P1	*ca* 2770	(Strat, APW)	−41, 160	4	1111100 (5)	G, M	Strik et al., 2003; Van Kranendonk et al., 2006b
Fortescue Package 2	P2	2766 ± 2	SHRIMP-z	−47, 153	15	1011100 (4)	G, M	Blake et al., 2004; Strik et al., 2003
Mt Jope volcanics pre-fold	MJV	>2750 ± 5	SHRIMP-z	−41, 129	20	1011100 (4)	f	Hall, 2005; Schmidt & Embleton, 1985
Fortescue Package 4–7	P4–7	*ca* 2730	SHRIMP-z	−50, 138	13	1110100 (4)	M	Blake et al., 2004; Strik et al., 2003
Fortescue Package 8–10	P8–10	*ca* 2715	SHRIMP-z	−59, 186	6	1110100 (4)	M	Blake et al., 2004; Strik et al., 2003
Southern Hamersley VH	SVH	2717 ± 2	SHRIMP-z	−65, 204	12	1010100 (3)	–	Blake et al., 2004; Sumita, Hatakeyama, Yoshihara, & Hamano, 2001

Code, abbreviation shown in Figure 10. (Strat, APW), age estimate from stratigraphic correlation and simple interpolation along a paleomagnetic apparent polar wander path. A_{95}, Fisher's (1953) confidence cone radius. Q, reliability from Van der Voo (1990). The fourth criterion of a field stability test, if positive, is abbreviated as follows: c, inverse baked-contact test; F, intrasuccessional fold test; f, tectonic fold test; G, intrasuccessional conglomerate test; M, magnetostratigraphy test of stratabound reversals in sequence. In these abbreviations, upper-case symbols indicate primary paleomagnetic remanence; lower-case symbols indicate ancient remanence that might be primary but not demonstrated conclusively by the test.

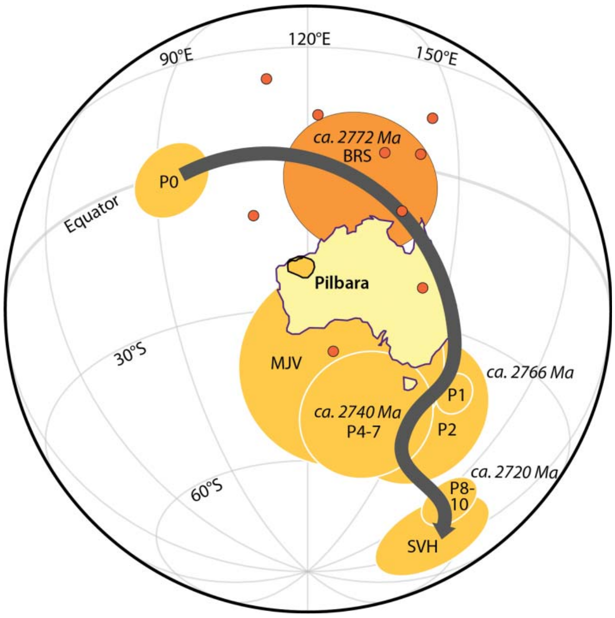

Figure 10. Apparent polar wander path for Pilbara craton during Fortescue Group deposition. Pole abbreviations given in Table 3. Darker shading denotes the mean Black Range suite (BRS) pole and its nine-constituent site-mean virtual geomagnetic poles.

stratigraphic order from NW to SE, and in the absence of a more complex oscillatory apparent polar wander (as in the alternative model of variable Black Range suite ages discussed above), the ages of remanence acquisition should decrease monotonically in that direction. The most parsimonious interpretation of apparent polar wander progression begins with Package 0 sedimentation and basaltic volcanism being restricted to the Marble Bar Sub-basin, followed by folding of that sequence, then intrusion of the Black Range dykes at *ca* 2772 Ma, and followed further by deposition of the Package 1 sequence and younger clastic and volcanic strata across a much larger area of the craton. During that succession of events, the Pilbara craton crossed polar areas of Earth's surface. Although Strik (2004) expressed concern about the tectonic feasibility of an approximately 180° change in magnetic remanence declination between Package 0 and Package 1, such a shift in declination naturally arises from simple translation by a rigid tectonic block across the geographic pole.

The above model of a simple polar crossing at *ca* 2772 Ma generates specific correlations of unconformity-bounded sequences in the lower Fortescue Group, especially in the Marble Bar Sub-basin (Figure 11). The correlations adopted herein are identical to those suggested by Strik (2004) and would require revision to geological quadrangle maps published by the GSWA (e.g. Hickman, 2010, 2013; Hickman & Van Kranendonk, 2008). On those maps that include the Marble Bar Sub-basin, the 'Kylena Formation' (correlated paleomagnetically to Package 1 of Strik *et al.*, 2003) would need to be reassigned to the Mount Roe Basalt. If new lithostratigraphic designations for the immediately underlying 'Hardey Formation' sandstone unit and lower Package 0 lavas are desired, then local names

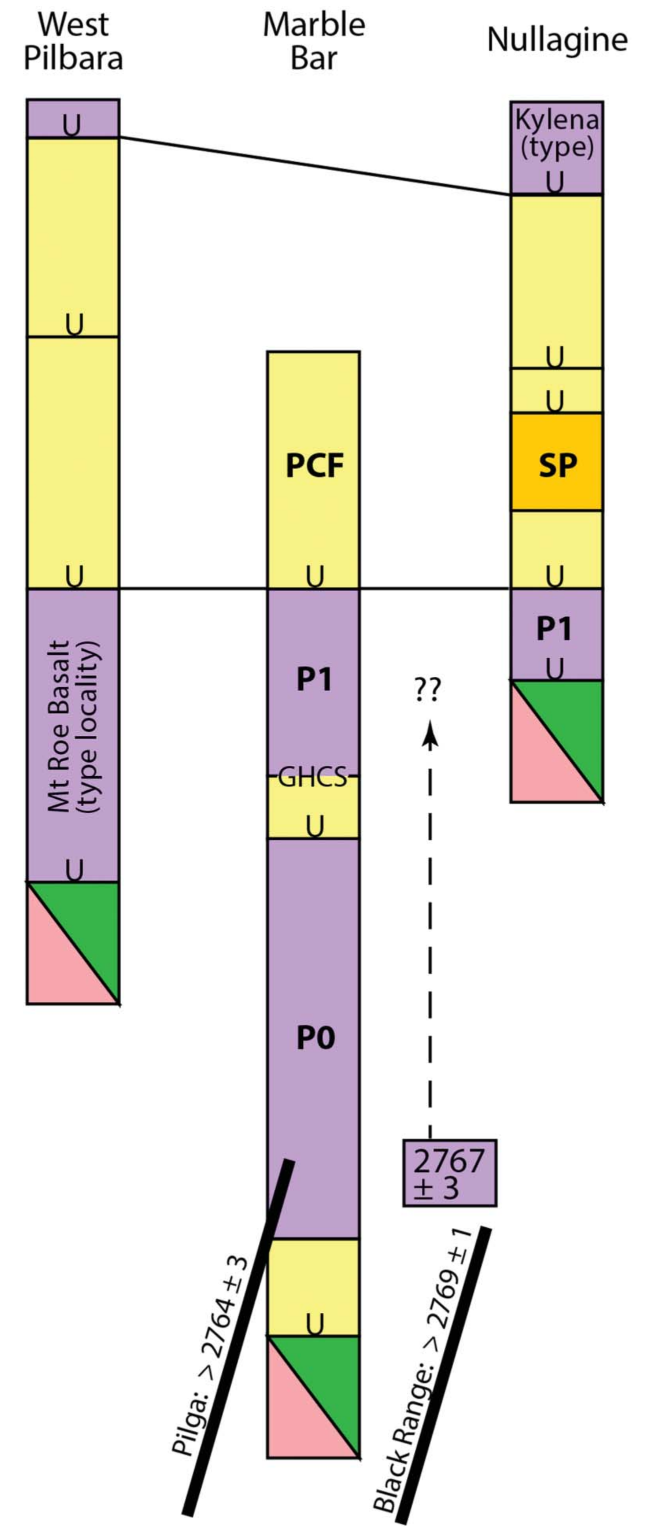

Figure 11. Revised correlations of lower Fortescue Group strata across northern Pilbara craton, according to paleomagnetic and ID-TIMS $^{207}Pb/^{206}Pb$ geochronologic data. Abbreviations as in Figure 3, plus the following: P0, Package 0 of Strik (2004); PCF, Pear Creek Formation.

from the Marble Bar Sub-basin would need to replace 'Mount Roe Basalt' as currently mapped in that area. The U–Pb TIMS age of 2767 ± 3 Ma from an isolated outcrop of shallowly dipping strata near the tip of the Black Range

Dyke (Van Kranendonk *et al.*, 2006b) could reasonably apply to either of the two lowest volcanic packages of the Fortescue Group, although paleomagnetic analysis on those particular-dated strata could help resolve the issue. At stratigraphically higher levels, the conglomeratic 'Pear Creek Formation' could retain its unique name in the Marble Bar Sub-basin, or it might eventually be incorporated within the Hardey Formation if age constraints permit. As summarised above, the Spinaway porphyry lies within sedimentary rocks of the Hardey Formation in the Nullagine region and has been dated by U–Pb SHRIMP on zircon at 2766 ± 2 Ma (Blake *et al.*, 2004). Our preferred correlations are consistent with that date and younger ages from the Fortescue Group (ibid.).

Conclusions

The present study has produced a revised, high-quality paleomagnetic pole from the Black Range suite of mafic dykes, constrained by minimum ^{207}Pb–^{206}Pb ages on baddeleyite from two intrusions at 2769 ± 1 Ma (the Black Range Dyke itself) and 2764 ± 3 Ma (the Pilga dyke). The best estimate for the crystallisation age of the Black Range Dolerite Suite remains 2772 ± 2 from an earlier study (Wingate, 1999), but our data include the Pilga dyke as a likely member of that swarm—contrary to earlier suggestions. The new paleomagnetic data indicate a polar crossing by the Pilbara craton during initial development of rifting and volcanism as manifested by lowermost strata in the Fortescue Group. New correlations of those strata indicate that rifting began in the localised region of the Marble Bar Sub-basin and was followed by Black Range suite dyke emplacement at 2772 ± 2 Ma and subsequent development of craton-wide magmatism and sedimentation.

Acknowledgements

We thank D. Chad Moore, Ian Rose and Taylor Kilian for field assistance; Martin Van Kranendonk for logistical advice; and Jennifer Kasbohm, Blair Schoene and Michael Wingate for discussions during preparation of the manuscript. Michael Wingate and Sergei Pisarevsky are also thanked for their constructive reviews of the manuscript. Funding was provided by the U.S. National Science Foundation, Swedish Research Council, Royal Physiographic Society in Lund, and Yale University.

Disclosure statement

No potential conflict of interest was reported by the authors.

ORCID

D. A. D. Evans http://orcid.org/0000-0001-8952-5273
A. P. Gumsley http://orcid.org/0000-0003-1395-3065

References

Arndt, N. T., Bruzak, G., & Reischmann, T. (2001). The oldest continental and oceanic plateaus: Geochemistry of basalts and komatiites of the Pilbara Craton, Australia. In R. E. Ernst & K. L. Buchan (Eds.), *Mantle plumes: Their identification through time* (pp. 359–387). 359–387. Boulder, Co: Geological Society of America Special Paper, 352.

Arndt, N. T., Nelson, D. R., Compston, W., Trendall, A. F., & Thorne, A. M. (1991). The age of the Fortescue Group, Hamersley Basin, Western Australia, from ion microprobe zircon U–Pb results. *Australian Journal of Earth Sciences*, *38*, 261–281.

Blake, T. S. (1984). Evidence for stabilization of the Pilbara Block, Australia. *Nature*, *307*, 721–723.

Blake, T. S. (1993). Late Archaean crustal extension, sedimentary basin formation, flood basalt volcanism and continental rifting: The Nullagine and Mount Jope Supersequences, Western Australia. *Precambrian Research*, *60*, 185–241.

Blake, T. S., Buick, R., Brown, S. J. A., & Barley, M. E. (2004). Geochronology of a Late Archaean flood basalt province in the Pilbara Craton, Australia: Constraints on basin evolution, volcanic and sedimentary accumulation, and continental drift rates. *Precambrian Research*, *133*, 143–173.

Bleeker, W. (2003). The late Archean record: A puzzle in ca. 35 pieces. *Lithos*, *71*, 99–134.

Bradley, K., Weiss, B. P., & Buick, R. (2015). Records of geomagnetism, climate, and tectonics across a Paleoarchean erosion surface. *Earth and Planetary Science Letters*, *419*, 1–13.

Cheney, E. S. (1996). Sequence stratigraphy and plate tectonic significance of the Transvaal succession of southern Africa and its equivalent in Western Australia. *Precambrian Research*, *79*, 3–24.

de Kock, M. O., Evans, D. A. D., & Beukes, N. J. (2009). Validating the existence of Vaalbara in the Neoarchean. *Precambrian Research*, *174*, 145–154.

Embleton, B. J. J. (1972). The palaeomagnetism of some Proterozoic–Cambrian sediments from the Amadeus Basin, central Australia. *Earth and Planetary Science Letters*, *17*, 217–226.

Embleton, B. J. J. (1978). The palaeomagnetism of 2400 m.y. old rocks from the Australian Pilbara craton and its relation to Archaean–Proterozoic tectonics. *Precambrian Research*, *6*, 275–291.

Evans, D. A. D. (2013). Reconstructing pre-Pangean supercontinents. *Geological Society of America Bulletin*, *125*, 1735–1751.

Fisher, R. A. (1953). Dispersion on a sphere. *Proceedings Royal Society A*, *217*, 295–305.

Fisher, N. I., Lewis, T., & Embleton, B. J. J. (1987). *Statistical analysis of spherical data*. Cambridge, UK: Cambridge University Press, 313 pp.

Gerstenberger, H., & Haase, G. (1997). A highly effective emitter substance for mass spectrometric Pb isotope ratio determinations. *Chemical Geology*, *136*, 309–312.

Gumsley, A., Olsson, J., Söderlund, U., de Kock, M., Hofmann, A., & Klausen, M. (2015). Precise U–Pb baddeleyite age dating of the Usushwana Complex, southern Africa—Implications for the Mesoarchaean magmatic and sedimentological evolution of the Pongola Supergroup, Kaapvaal Craton. *Precambrian Research*, *267*, 174–185.

Hall, C. E. (2005). SHRIMP U–Pb depositional age for the lower Hardey Formation: Evidence for diachronous deposition of the lower Fortescue Group in the southern Pilbara region, Western Australia. *Australian Journal of Earth Sciences*, *52*, 403–410.

Heaman, L. M., & LeCheminant, A. N. (1993). Paragenesis and U–Pb systematics of baddeleyite (ZrO_2). *Chemical Geology*, *110*, 95–126.

Hickman, A. H. (1983). *Geology of the Pilbara Block and its environs. Western Australia Geological Survey, Bulletin 127*, Perth, WA: Western Australia Geological Survey, 268 p.

Hickman, A. H. (compiler) (2007). Nullagine. *Western Australia Geological Survey 1:250 000 Geological Map Sheet SF 51-05* (3rd ed.). Perth, WA: Western Australia Geological Survey.

Hickman, A. H. (compiler) (2010). Marble Bar. *Western Australia Geological Survey 1:250 000 Geological Map Sheet SF 50-8* (3rd ed.). Perth, WA: Western Australia Geological Survey.

Hickman, A. H. (2012). Review of the Pilbara Craton and Fortescue Basin, Western Australia: Crustal evolution providing environments for early life. *Island Arc*, *21*, 1–31.

Hickman, A. H. (compiler) (2013). North Shaw. *Western Australia Geological Survey 1:100 000 Geological Map Sheet 2755* (2nd ed.). Perth, WA: Western Australia Geological Survey.

Hickman, A. H., & Lipple, S. L. (1978). Marble Bar. *Western Australia Geological Survey 1:250 000 Geological Series Explanatory Notes*. Perth, WA: Western Australia Geological Survey, 24 pp.

Hickman, A. H., & Van Kranendonk, M. V. (compilers) (2008). Marble Bar. *Western Australia Geological Survey 1:100 000 Geological Map Sheet 2855* (1st ed.). Perth, WA: Western Australia Geological Survey.

Irving, E., & Green, R. (1958). Polar movement relative to Australia. *Geophysical Journal of the Royal Astronomical Society*, *1*, 64–72.

Kirschvink, J. L. (1980). The least squares line and plane and the analysis of paleomagnetic data. *Geophysical Journal of the Royal Astronomical Society*, *62*, 699–718.

Lewis, J. D., Rosman, K. J. R., & de Laeter, J. R. (1975). The age and metamorphic effects of the Black Range dolerite dyke. Western Australia Geological Survey, Annual Report for the Year 1974 (pp. 80–88). Perth, WA: Western Australia Geological Survey.

Li, Z.-X., & Evans, D. A. D. (2011). Late Neoproterozoic 40° intraplate rotation within Australia allows for a tighter-fitting and longer-lasting Rodinia. *Geology*, *39*, 39–42.

Li, Z. X., Powell, C. McA., & Thrupp, G. A. (1990). Australian Palaeozoic palaeomagnetism and tectonics–II. A revised apparent polar wander path and palaeogeography. *Journal of Structural Geology*, *12*, 567–575.

Lipple, S. L. (1975). Definitions of new and revised stratigraphic units of the Eastern Pilbara Region. *Western Australia Geological Survey, Annual Report for the Year 1974* (pp. 58–63). Perth, WA: Western Australia Geological Survey.

Ludwig, K. R. (2001). Isoplot: A Geochronological Toolkit for Microsoft Excel, Berkeley Geochronology Center, USA, Special Publication No. 1a. Berkeley, Cal: University of California.

Pidgeon, R. T. (1984). Geochronological constraints on early volcanic evolution of the Pilbara Block, Western Australia. *Australian Journal of Earth Sciences*, *31*, 237–242.

Rainbird, R. H., & Ernst, R. E. (2001). The sedimentary record of mantle-plume uplift. In R. E. Ernst & K. L. Buchan (Eds.), *Mantle plumes: Their identification through time* (pp. 227–245). Boulder, Co: Geological Society of America Special Paper, 352.

Rasmussen, B., Fletcher, I. R., & Sheppard, S. (2005). Isotopic dating of the migration of a low-grade metamorphic front during orogenesis. *Geology*, *33*, 773–776.

Schmidt, P. W. (1993). Paleomagnetic cleaning strategies. *Physics of the Earth and Planetary Interiors*, *76*, 169–178.

Schmidt, P. W., & Embleton, B. J. J. (1985). Prefolding and overprint magnetic signatures in Precambrian (~2.9–2.7 Ga) igneous rocks from the Pilbara Craton and Hamersley Basin, NW Australia. *Journal of Geophysical Research*, *90*, 2967–2984.

Shipunov, S. V., Muraviev, A. A., & Bazhenov, M. L. (1998). A new conglomerate test in palaeomagnetism. *Geophysical Journal International*, *133*, 721–725.

Smith, R. E., Perdrix, J. L., & Parks, T. C. (1982). Burial metamorphism in the Hamersley Basin, Western Australia. *Journal of Petrology*, *23*, 75–102.

Söderlund, U., & Johansson, L. (2002). A simple way to extract baddeleyite (ZrO_2). *Geochemistry Geophysics Geosystems*, *3*, 1–7.

Stacey, J. S., & Kramers, J. D. (1975). Approximation of terrestrial lead isotope evolution by a two stage model. *Earth and Planetary Science Letters, 26*, 207–221.

Strik, G. H. M. A. (2004). *Palaeomagnetism of late Archaean flood basalt terrains: Implications for early Earth geodynamics and geomagnetism* (PhD thesis). Geologica Ultraiectina, Mededelingen van de Faculteit Geowetenschappen Universiteit Utrecht, Utrecht, Netherlands, 242, 160 pp.

Strik, G., Blake, T. S., Zegers, T. E., White, S. H., & Langereis, C. G. (2003). Palaeomagnetism of flood basalts in the Pilbara Craton, Western Australia: Late Archaean continental drift and the oldest known reversal of the geomagnetic field. *Journal of Geophysical Research*, *108*, doi:10.1029/2003JB002475

Sumita, I., Hatakeyama, T., Yoshihara, A., & Hamano, Y. (2001). Paleomagnetism of late Archean rocks of Hamersley basin, Western Australia and the paleointensity at early Proterozoic. *Physics of the Earth and Planetary Interiors, 128*, 223–241.

Thorne, A. M., & Trendall, A. F. (2001). *Geology of the Fortescue Group, Pilbara Craton, Western Australia*. Perth, WA: Western Australia Geological Survey, Bulletin, 144, 249 pp.

Trendall, A. F. (1983). The Hamersley Basin. In A. F. Trendall & R. C. Morris (Eds.), *Iron-formation: Facts and problems* (pp. 69–129). Amsterdam: Elsevier.

Van der Voo, R. (1990). The reliability of paleomagnetic data. *Tectonophysics*, *184*, 1–9.

Van Kranendonk, M. J. (2000). Geology of the North Shaw 1:100 000 Sheet. Western Australia Geological Survey 1:100 000 Geological Series Explanatory Notes. Perth, WA: Western Australia Geological Survey, 86 pp.

Van Kranendonk, M. J., Bleeker, W., & Ketchum, J. (2006b). Phreatomagmatic boulder conglomerates at the tip of the *ca* 2772 Ma Black Range dolerite dyke, Pilbara Craton, Western Australia. *Australian Journal of Earth Sciences*, *53*, 617–630.

Van Kranendonk, M. J., Hickman, A. H., Smithies, R. H., Williams, I. R., Bagas, L., & Farrell, T. R. (2006a). Revised lithostratigraphy of Archean supracrustal and intrusive rocks in the northern Pilbara Craton, Western Australia. *Western Australia Geological Survey, Record, 2006/15*. Perth, WA: Western Australia Geological Survey, 57 pp.

Van Kranendonk, M. J., & Kirkland, C. L. (2016). Conditioned duality of the Earth system: Geochemical tracing of the supercontinent cycle through Earth history. *Earth-Science Reviews*, *160*, 171–187.

Verwey, E. J. W. (1939). Electronic conduction of magnetite (Fe_3O_4) and its transition point at low-temperature. *Nature*, *44*, 327–328.

Williams, H., Hoffman, P. F., Lewry, J. F., Monger, J. W. H., & Rivers, T. (1991). Anatomy of North America: Thematic geologic portrayals of the continent. *Tectonophysics*, *187*, 117–134.

Wingate, M. T. D. (1999). Ion microprobe baddeleyite and zircon ages for Late Archaean mafic dykes of the Pilbara Craton, Western Australia. *Australian Journal of Earth Sciences*, *46*, 493–500.

Wingate, M. T. D., Pisarevsky, S. A., & Evans, D. A. D. (2002). Rodinia connections between Australia and Laurentia: No SWEAT, no AUSWUS? *Terra Nova*, *14*, 121–128.

Zegers, T. E., de Wit, M. J., Dann, J., & White, S. H. (1998). Vaalbara, Earth's oldest assembled continent? A combined structural, geochronological, and palaeomagnetic test. *Terra Nova*, *10*, 250–259.

Litholund Theses

Dissertations

1. *Emma F. Rehnström, 2003:* Geography and geometry of pre-Caledonian western Baltica : U-Pb geochronology and palaeomagnetism.

2. *Oskar Paulsson, 2003:* U-Pb geochronology of tectonothermal events related to the Rodinia and Gondwana supercontinents : observations from Antarctica and Baltica.

3. *Ingela Olsson-Borell, 2003:* Thermal history of the Phanerozoic sedimentary succession of Skåne, southern Sweden, and implications for applied geology.

4. *Johan Lindgren, 2004:* Early Campanian mosasaurs (Reptilia; Mosasauridae) from the Kristianstad Basin, southern Sweden.

5. *Audrius Cecys, 2004:* Tectonic implications of the ca. 1.45 Ga granitoid magmatism at the southwestern margin of the East European Craton.

6. *Peter Dahlqvist, 2005:* Late Ordovician-Early Silurian facies development and stratigraphy of Jämtland, central Sweden.

7. *Mårten Eriksson, 2005:* Silurian carbonate platform and unconformity development, Gotland, Sweden.

8. *Jane Wigforss-Lange, 2005:* The effects of Late Silurian (mid-Ludfordian) sea-level change : a case study of the Öved-Ramsåsa Group in Skåne, Sweden.

9. *Erik Eneroth, 2006:* Nanomagnetic and micromagnetic properties of rocks, minerals and sulphide-oxidation products.

10. *Niklas Axheimer, 2006:* The lower and middle Cambrian of Sweden : trilobites, biostratigraphy and intercontinental correlation.

11. *Fredrik Terfelt, 2006:* Upper middle Cambrian through Furongian of Scandinavia with focus on trilobites, paleoenvironments and correlations.

12. *Andrius Rimsa, 2007:* Understanding zircon geochronology : constraints from imaging and trace elements.

13. *Mårten Eriksson 2007:* Silurian carbonate platforms of Gotland, Sweden : archives of local, regional and global environmental changes.

14. *Jane Wigforss-Lange, 2007:* Geochemical and sedimentary signatures of Phanerozoic events.

15. *Tobias Hermansson, 2007:* The tectonic evolution of the western part of the Svecofennian orogen, central Sweden : Insight from U/Pb and $^{40}Ar/^{39}Ar$ geochronology at Forsmark.

16. *Pia Söderlund,* 2008: ^{40}Ar-^{39}Ar, AFT and (U-Th)/He thermochronologic implications for the low-temperature geological evolution in SE Sweden.

17. *Anders Cronholm,* 2009: The flux of extraterrestrial matter to Earth as recorded in Paleogene and Middle Ordovician marine sediments.

18. *Carl Alwmark,* 2009: Traces in Earth's geological record of the break-up of the L-chondrite parent body 470 Ma.

19. *Linda Larsson-Lindgren,* 2009: Climate and vegetation during the Miocene : evidence from Danish palynological assemblages.

20. *Ingemar Bergelin,* 2010: $^{40}Ar/^{39}Ar$ whole-rock geochronology of Mesozoic basalts in Scania : evidence for episodic volcanism over an extended period of ca. 80 Myr.

21. *Johanna Mellgren,* 2011: Conodont biostratigraphy, taxonomy and palaeoecology in the Darriwilian (Middle Ordovician) of Baltoscandia : with focus on meteorite and extraterrestrial chromite-rich strata.

22. *Johan Olsson,* 2012: U-Pb baddeleyite geochronology of Precambrian mafic dyke swarms and complexes in southern Africa : regional-scale extensional events and the origin of the Bushveld complex.

23. *Kristina Mehlqvist,* 2013: Early land plant spores from the Paleozoic of Sweden : taxonomy, stratigraphy and paleoenvironments.

24. *Andreas Petersson,* 2015: Evolution of continental crust in the Proterozoic : growth and reworking in orogenic systems.

25. *Karolina Bjärnborg,* 2015: Origin of the Kleva Ni-Cu sulphide mineralisation in Småland, southeast Sweden.

26. *Lorraine Tual,* 2016: P–T evolution and high-temperature deformation of Precambrian eclogite, Sveconorwegian orogen.

27. *Mimmi Nilsson,* 2016: New constraints on paleoreconstructions through geochronology of mafic dyke swarms in North Atlantic Craton.

28. *Sanna Alwmark,* 2016: Terrestrial consequences of hypervelocity impact : shock metamorphism, shock barometry, and newly discovered impact structures.

29. *Anders Lindskog,* 2017: Early–Middle Ordovician biotic and sedimentary dynamics in the Baltoscandian paleobasin.

30. *Ashley Gumsley*, 2017: Validating the existence of the supercraton Vaalbara in the Mesoarchaean to Palaeoproterozoic.

Printed by Media-Tryck, Lund 2017 NORDIC ECOLABEL, 3041 0903

Validating the existence of the supercraton Vaalbara in the Mesoarchaean to Palaeoproterozoic

One of the earliest known potential crustal configurations is that of Vaalbara, which incorporates ancient crust in southern Africa and Western Australia. In this thesis, six papers are presented that have tested the validity of the existence of Vaalbara using new temporal and spatial constraints from the geological record of anonymously large, short-lived volcanic provinces. We achieved this by sampling many of these ancient volcanic units in South Africa and Australia, and made age determinations which were complemented by paleomagnetic studies. The principle conclusion is that these data provide little support for a direct connection between these two ancient pieces of crust from 3 to 2. billion years ago. Instead, it is proposed that these pieces of crust that formed Vaalbara was part of a much larger continent in the middle Archean to early Proterozoic. This continent or supercontinent included pieces of ancient crust in the U.S.A., Canada, Finland, Russia, Ukraine, as well as in India, and to which herein is referred to as ‘Supervaalbara’.

The author, Ashley Gumsley, is a geologist trained at both Lund University in Sweden and the University of Johannesburg in South Africa. He has worked as an exploration geologist looking for economic deposits of copper and gold in Botswana and Tanzania before deciding to pursue a career in research. Ashley’s academic interests are in Precambrian geology, utilizing mostly geochronologic and paleomagnetic tools to solve fundamental problems in our knowledge (or lack thereof) of the history Earth, its origin and evolution.

LUND UNIVERSITY

Lithosphere and Biosphere Science
Department of Geology
Lund University
Sölvegatan 12
SE-223 62 Lund, Sweden
Telephone +46 46 222 78 80

ISSN 1651-6648
ISBN 978-91-87847-32-5